

# Re-engineering of a Haem Protein A Spectroscopic and Functional Analysis of Leghaemoglobin

Thesis submitted for the degree of  
Doctor of Philosophy  
at the University of Leicester

by

Neesha Patel MChem Chemistry, University of Leicester  
Department of Chemistry  
Faculty of Science  
University of Leicester  
October 2002

UMI Number: U601353

All rights reserved

INFORMATION TO ALL USERS

The quality of this reproduction is dependent upon the quality of the copy submitted.

In the unlikely event that the author did not send a complete manuscript and there are missing pages, these will be noted. Also, if material had to be removed, a note will indicate the deletion.



UMI U601353

Published by ProQuest LLC 2013. Copyright in the Dissertation held by the Author.  
Microform Edition © ProQuest LLC.

All rights reserved. This work is protected against  
unauthorized copying under Title 17, United States Code.



ProQuest LLC  
789 East Eisenhower Parkway  
P.O. Box 1346  
Ann Arbor, MI 48106-1346

*To Dad, Mum,  
Bharat and Vickesh*

# Statement

Unless otherwise acknowledged, the experimental work described in this thesis has been carried out by the author in the Department of Chemistry at the University of Leicester between October 1999 to September 2002. The work has not been submitted, and is not presently being submitted for any other degree at this or any other university.

Signed: 

Date: 9/02

Department of Chemistry  
University of Leicester  
University Road  
Leicester  
United Kingdom  
LE1 7RH

# **Re-engineering of a Haem Protein: A Spectroscopic and Functional Analysis of Leghaemoglobin**

**Neesha Patel**

## **Abstract**

Site directed mutagenic replacement, of key active site residues, in recombinant leghaemoglobin (rLb) has been performed to probe structure/function relationships in this and other haem proteins.

The role of the active site residues, in nicotinate binding was investigated. Replacement of the tyrosine 30 and histidine 61 residues with alanine, essentially removing the hydrogen-bond stabilisation to the haem-bound nicotinate, resulted in a ~ 20-fold decrease in affinity for nicotinate. A pH-dependent nicotinate binding study was also conducted on rLb ( $pK_a$  of 5.2) and Glu63Leu (pH-independent), using electronic (through determination of  $K_d$ s) and NMR spectroscopy, and identified glutamate 63 as the residue regulating nicotinate binding under acidic conditions.

A His61Ala variant was constructed to determine the origin of the low-spin haem species evident in leghaemoglobin. The absence of the low-spin signals in the variant, as determined using a range of spectroscopic techniques, confirmed the origin of the low-spin haem species as arising from coordination of the mobile His61 residue to the haem.

The mobility of the His61 residue was further exploited to incorporate new haem axial ligation into rLb. Spectroscopic analysis (using electronic absorption, MCD and EPR spectroscopy) of the His61Tyr and His61Lys variants confirmed haem ligation of the new amino acids and revealed similar spectroscopic characteristics to other haem proteins containing similar haem ligation. Characterisation of the His61Arg variant revealed bis-nitrogenous haem ligation, however, only a tentative assignment for the haem axial ligation could be made.

New reactivity was incorporated by replacement of His61 with alanine. The His61Ala variant exhibited haem oxygenase reactivity, as evidenced (using a combination of electronic absorption, HPLC and MS techniques) by the degradation of haem to Fe(III)-biliverdin, via the Fe(II)-O<sub>2</sub> and unstable verdohaem intermediates, in the presence of a reducing agent (ascorbate). However, the haem degradation of His61Ala proceeded with non-regiospecificity, in contrast to the  $\alpha$ -regiospecificity observed for HO and Mb.

# Contents

<b>Statement</b>	<b>i</b>
<b>Abstract</b>	<b>ii</b>
<b>Table of Contents</b>	<b>iii</b>
<b>Table of Figures</b>	<b>ix</b>
<b>Table of Tables</b>	<b>xiii</b>
<b>Table of Schemes</b>	<b>xv</b>
<b>Acknowledgements</b>	<b>xvi</b>
<b>Abbreviations</b>	<b>xvii</b>

## Table of Contents

<b>1</b>	<b>Structure/Function Relationship in Haem Proteins: An Introduction to Leghaemoglobin</b>	<b>1</b>
1.1	The Role of Metal Ions in Biological System	2
1.2	Haem Prosthetic Group	2
1.3	Haem Proteins	5
1.4	Electron Transfer Haem Proteins	7
1.5	Monooxygenases	9
1.6	Haem Peroxidases	10
1.7	Globins	13
1.7.1	Myoglobin	13
1.7.2	Leghaemoglobin	16
1.7.2.1	Biological Background	17
1.7.2.2	Soybean Leghaemoglobin	17
1.7.2.3	Nicotinate-The Physiological Ligand of Leghaemoglobin	20
1.7.2.4	The Flexible Active Site Structure of Soybean Leghaemoglobin	22
1.7.3	cDNA and Recombinant Expression Systems	23
1.7.4	Recent Developments	23
1.7.5	The Unresolved Questions	25
1.8	References	26

<b>2</b>	<b>Investigation of the Nicotinate Binding Process in Leghaemoglobin:</b>	
	<b>Role of the Active Site Residues</b>	<b>33</b>
2.1	Introduction	34
2.2	Mutagenesis of rLb, Protein Expression, Isolation and Purification	37
2.3	Results	37
2.3.1	Hydrogen-Bonding Investigations	37
2.3.1.1	Electronic Absorption Spectra of rLb and His61Ala/Tyr30Ala	37
2.3.1.2	Binding of Anionic Ligands to rLb and His61Ala/Tyr30Ala	39
2.3.1.3	Acid-Alkaline Transition of rLb and His61Ala/Tyr30Ala	39
2.3.1	Investigation of Nicotinate Binding	42
2.3.2	pH-Dependent Nicotinate Binding	42
2.3.2.1	Mutagenesis, Isolation and Purification of Glu63Leu	45
2.3.2.2	Characterisation of Glu63Leu	45
	<i>Electronic Absorption Spectra of Glu63Leu</i>	45
	<i>Anionic Ligand Binding</i>	45
	<i>pH Titration</i>	48
	<i>Spectroelectrochemistry</i>	49
2.3.2.3	pH-Dependent Nicotinate Binding	49
	<i>Nuclear Magnetic Resonance (NMR) Spectroscopy</i>	51
	<i>Nicotinate Binding in rLb in the Acidic Region</i>	53
2.4	Discussion	59
2.4.1	Influence of Distal Histidine and Tyrosine in Stabilisation of Nicotinate	59
2.4.1.1	Haem Electronic Structure	59
2.4.1.2	Nicotinate Binding to His61Ala/Tyr30Ala	60
2.4.2	pH-Dependent Nicotinate Binding (Glu63Leu)	61
2.4.2.1	Haem Electronic Structure	61
2.4.2.2	Determination of the Mid-Point Potential	62
2.4.2.3	pH-Dependent Nicotinate Binding	62
2.5	Summary	65
2.6	References	66
<b>3</b>	<b>Determination of the Haem Axial Ligation in Leghaemoglobin:</b>	
	<b>Does the Origin of the Low-Spin Haem Arise from Ligation of His61?</b>	<b>68</b>
3.1	Introduction	69
3.2	Mutagenesis, Protein Expression and Isolation	71
3.3	Results	71

3.3.1	Preliminary Characterisation of His61Ala	71
3.3.1.1	Electronic Absorption Spectroscopy	71
3.3.1.2	Ligand binding	72
3.3.1.3	Spectrometric pH Titrations	75
3.3.1.4	Spectroelectrochemistry	75
3.3.2	Spectroscopic Analysis Of His61Ala	76
3.3.2.1	Electronic Absorption spectroscop	76
3.3.2.2	Resonance Raman Spectroscopy	77
3.3.2.4	Magnetic Circular Dichroism (MCD) Spectroscopy	79
	<i>Room Temperature MCD</i>	79
	<i>Low Temperature- MCD</i>	82
3.3.2.5	Electron Paramagnetic Resonance (EPR) Spectroscopy	84
3.4	Discussion	87
3.4.1	Preliminary Characterisation of His61Ala	87
3.4.1.1	Spectroelectrochemistry	88
3.4.2	Spectroscopic Correlations	89
3.5	Summary	92
3.6	References	93
<b>4</b>	<b>Incorporation of New Haem Axial Ligation into Leghaemoglobin: Spectroscopic, Electrochemical and Ligand Binding Analysis of the His61Tyr Variant</b>	<b>95</b>
4.1	Introduction	96
4.2	Mutagenesis, Protein Expression and Isolation	97
4.3	Characterisation of His61Tyr	98
4.3.1	Electronic Absorption Spectroscopy	98
4.3.2	Ligand Binding	99
4.3.3	Determination of the $pK_a$ of His61Tyr	101
4.3.4	Spectroelectrochemistry	104
4.3.5	Extended X-ray Absorption Fine Structure (EXAFS)	104
4.3.6	Magnetic Circular Dichroism (MCD) Spectroscopy	108
4.3.7	Electron Paramagnetic Resonance (EPR) Spectroscopy	108
4.4	Discussion	113
4.5	Summary	122
4.6	References	123

<b>5</b>	<b>Alteration of the Haem Axial Ligation in Leghaemoglobin: Spectroscopic, Electrochemical and Ligand Binding Analysis of the His61Lys and His61Arg Variants</b>	<b>128</b>
5.1	Introduction	129
5.2	Mutagenesis, Expression, Isolation and Purification	130
5.3	Results	131
5.3.1	Electronic Absorption Spectra	132
5.3.2	Ligand Binding	132
5.3.3	Determination of the haem $pK_a$ of His61Lys and His61Arg	134
5.3.4	Spectroelectrochemistry	138
5.3.5	Electronic X-ray Absorption Fine Structure (EXAFS)	138
5.3.6	Magnetic Circular Dichroism (MCD) Spectroscopy	141
5.3.6.1	His61Lys	141
	<i>Room Temperature MCD</i>	141
	<i>Low Temperature MCD</i>	143
5.3.6.2	His61Arg	145
	<i>MCD at Acidic pH (pH 4.4)</i>	145
	<i>MCD at Alkaline pH (pH 8.8)</i>	146
5.3.7	Electronic Paramagnetic Resonance (EPR) Spectroscopy	147
5.3.7.1	His61Lys	147
5.3.7.2	His61Arg	148
5.4	Discussion	149
5.4.1	Spectroscopic Characterisation of His6Lys and His61Arg	149
5.5	Summary	158
5.6	References	159
<b>6</b>	<b>Introducing New Haem Functionality into Leghaemoglobin: A Functional Analysis of the Haem Oxygenase Reactivity of the His61Ala Variant</b>	<b>163</b>
6.1	Introduction	164
6.2	Results	166
6.2.1	Aerobic Coupled Oxidation of His61Ala	166
6.2.2	Aerobic Coupled Oxidation of rLb	166
6.2.3	Analysis of Haem Degradation Products	167
6.2.4	Dependence of Oxygen in the Coupled Oxidation Reaction	172
6.2.4.1	Anaerobic Coupled Oxidation of His61Ala and rLb	172

6.2.4.2	One Equivalent of Oxygen	174
6.2.4.3	Two Equivalents of Oxygen	174
6.2.4.4	Three Equivalents of Oxygen	177
6.2.5	Ascorbate as a Reducing Agent	177
6.2.6	Regiospecificity of the Coupled Oxidation Reaction	178
6.2.7	$^{18}\text{O}_2$ Labelled Coupled Oxidation	179
6.2.8	Extended X-ray Absorption Fine Structure (EXAFS) Spectroscopy	181
6.3	Discussion	185
6.4	Summary	192
6.5	References	193
<b>7</b>	<b>Experimental</b>	<b>195</b>
7.1	Leghaemoglobin	196
7.1.1	Oligonucleotides	196
7.1.2	Mutagenesis	196
7.1.3	Isolation of DNA	198
7.1.4	Agarose Gel Electrophoresis	198
7.1.5	DNA Sequencing	199
7.1.6	Transformation of the Recombinant DNA into Competent <i>E. Coli</i> Cells	199
7.1.7	Expression of rLb and Variants in <i>E. Coli</i>	199
7.1.8	Isolation and Purification of rLb and Variants	200
7.1.9	SDS/Polyacrylamide Gel Electrophoresis of Proteins	201
7.1.10	Preparation of Protein Samples for Analysis	201
7.2	Spectroscopic and Analytical Techniques	203
7.2.1	Electronic Absorption Spectroscopy	203
7.2.2	Determination of the Absorption Coefficient	204
7.2.3	Ligand Binding Equilibria	205
7.2.4	Haem Extraction from rLb, Glu63Leu and His61Ala and Reconstitution of the Apo-Proteins with Protoporphyrin IX Dimethyl Ester.	207
7.2.5	pH Titrations of rLb and Variants	208
7.2.6	Paramagnetic $^1\text{H}$ NMR Spectroscopy	209
7.2.6.1	$^1\text{H}$ -NMR of Nicotinate Derivatives	209
7.2.7	Spectroelectrochemistry	209
7.2.7.1	Preparation of Protein Samples	210
7.2.7.2	Data Collection and Analysis	211
7.2.8	Extended X-ray Absorption Fine Structure (EXAFS)	213

7.2.9	Resonance Raman Spectroscopy	214
7.2.10	Magnetic Circular Dichroism Spectroscopy	215
7.2.11	EPR Spectroscopy	215
7.2.12	Haem Oxygenase Activity of rLb and His61Ala	216
7.2.12.1	Coupled Oxidation Assay	216
	<i>Aerobic Coupled Oxidation</i>	216
	Anaerobic Coupled Oxidation	216
	<i>Stoichiometric Addition of O<sub>2</sub> to the Coupled Oxidation Reaction</i>	216
7.2.12.2	Kinetics of the Coupled Oxidation Reaction	217
7.2.12.3	Biliverdin Extraction	217
7.2.12.4	Verdohaem Extraction	218
7.2.12.5	HPLC Analysis of Haem Degradation Products	218
7.2.12.6	Reduction of Ferric His61Ala with Ascorbate	219
7.2.12.7	Analysis of Regiospecificity of Coupled Oxidation	219
7.2.12.8	Mass Spectrometry	219
7.2.12.9	<sup>18</sup> O <sub>2</sub> Labelling	220
7.3	References	221
<b>Appendix</b>		<b>I</b>
Appendix A Solutions and Buffers		II

# Table of Figures

1.1	Structure of iron protoporphyrin IX, protoporphyrin IX, haem <i>a</i> , haem <i>c</i> and haem <i>d</i> .	4
1.2	Schematic haem pocket architecture	5
1.3	The structure of yeast cytochrome <i>c</i>	9
1.4	The structure of cytochrome P450 <sub>cam</sub>	11
1.5	Peroxidase mechanism, crystal structure and active site of yeast cytochrome <i>c</i>	14
1.6	Crystal structure of oxymyoglobin	16
1.7	Sequence alignment of horse heart and sperm whale myoglobin and soybean leghaemoglobin	19
1.8	The crystal structure of soybean leghaemoglobin <i>a</i>	21
1.9	Pyridine-3-carboxylic acid anion (nicotinate)	21
2.1	Active site structure of nicotinate-bound Lb	36
2.2	Electronic absorption spectra of ferric rLb and ferric His61Ala/Tyr30Ala	38
2.3	Electronic absorption spectra of ferric, ferrous and the ferric anionic ligand-bound derivatives His61Ala/Tyr30Ala	40
2.4	Spectrometric pH titration of ferric rLb and ferric His61Ala/Tyr30Ala	43
2.5	Electronic absorption spectra of the nicotinate titration of His61Ala/Tyr30Ala	44
2.6	Electronic absorption spectra of ferric rLb and ferric Glu63Leu	46
2.7	Electronic absorption spectra of ferric, ferrous and the ferric anionic ligand-bound derivatives Glu63Leu	46
2.8	Spectrometric pH titration of ferric Glu63Leu	48
2.9	Thin-layer spectroelectrochemical spectra for rLb and Glu63Leu	50
2.10	300 MHz <sup>1</sup> H-NMR spectra of rLb and Glu63Leu	51
2.11	300 MHz <sup>1</sup> H-NMR spectra of rLb-nicotinate and Glu63Leu-nicotinate	54
2.12	Variation of chemical shift resonances of rLb-nicotinate and Glu63Leu-nicotinate with pH	55
2.13	Variation of $K_d$ with pH for binding of nicotinate to rLb and Glu63Leu	56
2.14	Variation of $K_d$ with pH for the binding of nicotinate to rLb, His61Ala and Glu63Leu containing protoporphyrin IX dimethyl ester	57
2.15	Active site of nicotinate-bound Lb <i>a</i>	58

3.1	Active site structure of nicotinate-bound Lb	70
3.2	Electronic absorption spectra of ferric rLb and ferric His61Ala	72
3.3	Electronic absorption spectra of ferric, ferrous and various anionic ligand-bound derivatives His61Ala	73
3.4	Spectrometric pH titration of ferric His61Ala	76
3.5	Thin-layer spectroelectrochemical spectra for His61Ala at various applied potentials	77
3.6	High frequency region of the resonance Raman spectra of rLb and His61Ala	80
3.7	Electronic absorption of His61Ala and UV-visible MCD spectra	83
3.8	Near-infrared MCD spectra of His61Ala	85
3.9	X-band EPR spectra of His61Ala	86
4.1	rLb and His61Tyr	98
4.2	Electronic absorption spectra of ferric and ferrous His61Tyr	99
4.3	Electronic absorption spectra of His61Tyr and phenol derivative of rLb	100
4.4	Electronic absorption spectra of anionic ligand-bound derivatives of ferric His61Tyr	101
4.5	Spectrometric titration of His61Tyr with cyanide and azide	103
4.6	Spectrometric pH titration of His61Tyr	105
4.7	Spectrometric pH titration of rLb	106
4.8	Thin-layer spectroelectrochemical spectra for His61Tyr at various applied potentials	107
4.9	EXAFS and Fourier transform amplitude of EXAFS of rLb and His61Tyr	108
4.10	UV-visible MCD spectrum of His61Tyr	111
4.11	X-band EPR spectrum of His61Tyr	112
5.1	Electronic absorption spectra of ferric and ferrous His61Lys and His61Arg	132
5.2	Electronic absorption spectra of the ferric and ferrous methylamine derivative of rLb	133
5.3	Electronic absorption spectra of anionic ligand-bound derivatives of His61Lys and His61Arg	134
5.4	Spectrometric titration of His61Lys and His61Arg with cyanide	137
5.5	Spectrometric pH titration of His61Lys and His61Arg	138
5.6	Thin-layer spectroelectrochemical spectra for His61Lys and His61Arg at various applied potentials	140

5.7	The EXAFS spectra and Fourier transform amplitude of EXAFS of His61Lys and His61Arg	141
5.8	UV-visible MCD spectrum of His61Lys	145
5.9	Near-IR MCD of His61Lys	146
5.10	UV-visible MCD spectrum of His61Arg	147
5.11	X-band EPR spectrum of His61Lys	148
5.12	X-band EPR spectrum of His61Arg	149
5.13	A comparison of torsional geometries of histidine and arginine	153
6.1	Changes in the electronic absorption spectra during the coupled oxidation of His61Ala	167
6.2	Electronic absorption spectra of Fe(II)-dioxy rLb and Fe(II)-dioxy His61Ala	168
6.3	Changes in the electronic absorption spectra during the coupled oxidation of rLb	169
6.4	Electronic absorption spectra of authentic biliverdin and the chloroform extract of the His61Ala coupled oxidation product	170
6.5	HPLC analysis of the products isolated from the coupled oxidation reaction of rLb and His61Ala	170
6.6	ESI-MS analysis of product isolated from the coupled oxidation reaction of His61Ala and rLb	171
6.7	Changes in the electronic absorption spectra during the anaerobic coupled oxidation of His61Ala	173
6.8	Changes in the electronic absorption spectra during the coupled oxidation of His61Ala in the presence of one equivalent and two equivalent of oxygen	175
6.9	Electronic absorption spectra of authentic verdohaem and the pyridine/chloroform extract of the His61Ala coupled oxidation product and ESI-MS analysis of the product isolated from the coupled oxidation reaction of His61Ala following addition of two equivalents of oxygen	176
6.10	Reduction of His61Ala by ascorbate	178
6.11	HPLC analysis of the dimethyl ester derivatives isolated from authentic biliverdin IXa and biliverdin obtained from the coupled oxidation of His61Ala	179
6.12	ESI-MS of <sup>18</sup> O <sub>2</sub> -labelled Fe(III)-biliverdin and <sup>18</sup> O <sub>2</sub> -labelled biliverdin	180
6.13	The EXAFS spectra and Fourier transform amplitude of EXAFS of His61Ala	182

7.1	SDS-PAGE gel showing purification stages of rLb	202
7.2	SDS-PAGE gel showing purified rLb and variants	202
7.3	Electronic absorption spectrum of the reduced pyridine haemochromagen of rLb	205
7.4	OTTLE cell used for spectroelectrochemistry and experimental set up of the OTTLE cell	212

# Table of Tables

1.1	The diversity of haem protein structure and function	6
1.2	Comparison of association ( $k_{on}$ ) and dissociation ( $k_{off}$ ) rate constants, and association binding constant ( $K$ ) for oxygen binding to Lb, human Hb and horse-heart Mb.	18
2.1	Wavelength maxima and absorption coefficients for the ferric and ferrous derivatives of rLb and His61Ala/Tyr30Ala	41
2.2	Wavelength maxima and absorption coefficients for the ferric and ferrous derivatives of rLb and Glue63Leu	47
3.1	Wavelength maxima and absorption coefficients for the ferric and ferrous derivatives of rLb and His61Ala	74
3.2	Characteristic RR spin marker bands ( $\text{cm}^{-1}$ ) for ferric derivatives of His61Ala and rLb	79
4.1	Wavelength maxima and absorption coefficients for the ferric and ferrous derivatives of rLb and His61Tyr	102
4.2	Structural results obtained by fitting the EXAFS spectra from met-Mb, rLb and the His61Tyr variant of rLb	110
4.3	Summary of spectroscopic data for haem proteins and variants in which the distal ligand to the haem is provided by a tyrosine	115
4.4	Summary of spectroscopic data for haem proteins and variants in which the proximal ligand to the haem is provided by a tyrosine	116
4.5	The charge transfer transitions (from the MCD) and low-spin g-values (from the EPR) of haem hydroxy-, water- and phenolate-haem ligated proteins	121
5.1	Wavelength maxima and absorption coefficients for the ferric and ferrous derivatives of His61Lys and His61Arg	136
5.2	Structural results obtained by fitting the EXAFS spectra from rLb and the His61Arg and His61Lys variants of rLb	143
5.3	Summary of spectroscopic data for haem proteins and variants in which the distal ligand to the haem is provided by a lysine	151
5.4	EPR and Near-IR MCD properties of Lys/His ligand low-spin ferric haems	157

6.1	Structural results obtained by fitting data from the EXAFS spectra, from rLb and His61Ala	183
6.2	Comparison of the EXAFS determined haem bond distances of His61Ala, horse heart Mb and haem oxygenase	184
7.1	The forward and reverse oligonucleotides used to generate the variants of rLb	197

# Table of Schemes

1.1	Catalytic cycle of cytochrome P450	11
1.2	Temperature-dependent change in co-ordination geometry in Lb. The 298K species contains high-spin haem, 77K species is entirely low spin	22
1.3	Scheme indicating the protonation states of His 61 and their effects on the binding of nicotinate	24
4.1	The Brookhaven haem nomenclature	111
4.2	Predicted ligations of rLb and His61Tyr at neutral and acidic pH as envisaged through	122
6.1	The reaction sequence catalysed by haem oxygenase	165
6.2	The haem degradation pathway of His61Ala	189

# Acknowledgements

I would like to thank Dr. E. L. Raven for her guidance in writing this thesis and encouragement throughout my Ph.D. research. I gratefully acknowledge the EPSRC without whose financial support none of this would have been possible.

I am grateful to Drs S. Gurman and A. Svensson for their help with the EXAFS experiments; Dr. P. Moënné Loccoz for the RR spectra; Dr. M. Cheesman for the long awaited EPR and MCD data. Thanks should also be extended to Dr. G. Eaton for ESI-mass spectrometry and Dr. G. Griffith for help in recording NMR spectra; Prof. N. S. Scrutton and Dr. J. Basran for their assistance with the anaerobic experiments and use of equipment and Dr. S. Baker and Dr. M. Sutcliffe for help in producing high quality active site pictures.

My appreciation goes to members of the department for making my time at Leicester University enjoyable, of whom there are too many to mention. In particular I would like to thank the friendship and patience exhibited by Drs. M. Mewies, L. Lad and C. Metcalf; Ms. K. Sharp and Mr. K. Singh (to whom I also give thanks for excellent technical assistance) without whom I may well have become increasingly insane. Finally, I wish to thank Mr. R. Dedi for his continued support during the past three years and patience in dealing with a very “stressed postgraduate”!

# Abbreviations

## *Amino Acids*

Ala	Alanine (A)
Arg	Arginine (R)
Asp	Aspartic acid (D)
Cys	Cysteine (C)
Glu	Glutamic acid (E)
His	Histidine (H)
Leu	Leucine (L)
Lys	Lysine (K)
Met	Methionine (M)
Trp	Tryptophan (W)
Tyr	Tyrosine (Y)
Val	Valine (V)

## *Buffers*

NaPi	Sodium phosphate
CHES	2-(cyclohexylamino)ethanesulphonic acid
MOPS	3-(N-morpholino)propanesulphonic acid
MES	2-(N- morpholino)ethanesulphonic acid
HEPES	N-2-hydroxyethylpiperazine-N'-2-ethanesulphonic acid
TAPS	N-tris[hydroxymethyl]methyl-3-aminopropanesulphonic acid
TRIS	Tris(hydroxymethyl)aminomethane

## *Chemicals*

DTT	dithiothreitol
IPTG	Isopropyl- $\beta$ -D thiogalactopyranoside
SDS	Sodium dodecyl sulphate

## ***Enzymes***

CcP	Cytochrome <i>c</i> peroxidase
EPO	Eosinophil peroxidase
FHb	Flavohaemoproteins
Hb	Haemoglobin
HRP	Horse radish peroxidase
Lb	Native soybean leghaemoglobin
Lba	Leghaemoglobin <i>a</i>
rLb	Recombinant leghaemoglobin <i>a</i>
LPO	Lactoperoxidase
Mb	Myoglobin
MPO	Myeloperoxidase

## ***Experimental***

cDNA	complementary DNA
dH <sub>2</sub> O	deionised water
LB	Luria-Bertani broth
PAGE	Polyacrylimide gel electrophoresis
Rz	Reinheitzahl

## ***Techniques***

EPR	Electron Paramagnetic Resonance
ESI-MS	Electrospray ionisation mass spectrometry
EXAFS	Extended X-Ray Absorption Fine Structure
HPLC	High pressure liquid chromatography
IR	Infra-red
MCD	Magnetic circular Dichroism
NMR	Nuclear magnetic resonance
OTTLE	Optically transparent thin-layer electrode
PCR	Polymerase Chain Reaction
RR	Resonance Raman
SCE	Saturated calomel electrode
SHE	Saturated hydrogen electrode
UV	Ultraviolet

### ***Units/symbols***

$\epsilon$	absorption coefficient
$K_a$	association constant
kb	kilo bases
$K_d$	dissociation constant
kDa	kilo Dalton
$\mu$	ionic strength
ppm	parts per million
m/z	mass/charge ratio
T	Tesla

**Chapter 1**  
**Structure/Function**  
**Relationship in Haem**  
**Proteins: An Introduction to**  
**Leghaemoglobin**

# 1 Structure/Function Relationship in Haem Proteins: An Introduction to Leghaemoglobin

## 1.1 The Role of Metal Ions in Biological Systems

Nature uses metal ions extensively in functional as well as structural roles within a protein. In biological systems, metal ions are of crucial importance in a range of reactions. Iron has been selected in molecular evolution to carry out a wide range of biological functions due to its rich and subtle chemical properties and also because of its abundance in the earth's crust. In appropriately tailored macromolecular environments, iron is responsible for the transport of oxygen (haemoglobin, myoglobin and haemerythrin), the activation of molecular oxygen (oxygenases, peroxidases, monooxygenases and oxidases) and for electron transport (cytochromes and iron-sulphur proteins). In addition, because of the tendency of iron to hydrolyse and precipitate in aqueous solution, special molecules have been designed for its transport (ferrichromes and transferrin) and storage (ferritin).

There are two major factors that control the properties of iron and other metal ions in biological systems: (a) the structure of the metal centre, including the geometry and structure of the metal complex and the nature of the ligands attached to the metal and (b) the environment of the metal complex, including the polarity of the immediate surroundings and steric constraints on the accessibility of substrates to the metal and of the metal to the solvent. In order to partially address how these factors can influence the reactivity at a metal centre, this Chapter focuses on the diverse reactions displayed by haem-containing proteins. Accordingly, the following section will give an introduction to the haem macromolecular structure followed by a brief overview of the diverse range of reactivities exhibited by haem proteins and the factors believed to govern their particular function.

## 1.2 Haem Prosthetic Group

The majority of haem proteins (haemoglobins, myoglobins, catalase, most peroxidases, the *b*-type cytochromes and the cytochromes P450) contain the same prosthetic group at their active site, namely that of an iron protoporphyrin IX, Figure 1.1(A). This group, also known as haem *b*, can be described as a partially unsaturated tetradentate macrocyclic ligand, which in its deprotonated form can bind to metal ions. In this thesis, the term 'haem' will be used to describe iron protoporphyrin IX. The haem group consists of an organic

component and an iron atom. The organic component, protoporphyrin, is made up of four pyrrole rings linked by methene bridges to form the tetrapyrrole ring. Four methyl (at positions 1, 3, 5 and 8), two vinyl (at positions 2 and 4) and two propionate side chains (at positions 6 and 7) are attached, Figure 1.1(B). The iron atom binds to the four pyrrole nitrogens in the centre of the protoporphyrin ring, giving rise to a square planar structure; the net charge on the haem with four coordinate iron (III) is +1, Figure 1.1(A). The iron can form two additional bonds, one on either side of the haem plane and are termed as fifth (or proximal) and sixth (or distal) coordination sites, Figure 1.2. The nature of coordination at these sites varies between haem proteins, although in many cases the proximal ligand is histidine.

Modifications to the basic porphyrin structure, Figure 1.1(B), are also known, however.<sup>[1]</sup> For example cytochrome *c* oxidase, which is responsible for the reduction of oxygen to water during the terminal electron transfer step in mitochondrial respiratory chains, contains a haem *a* prosthetic group, Figure 1.1(C). This haem group has a hydroxyethylfarnesyl side chain at position 2 and a formyl group at position 8 of the porphyrin ring. Cytochromes *c*, the electron transfer proteins, contain a type *c* haem group, Figure 1.1(D), in which the porphyrin is covalently linked to the surrounding protein matrix via two thioether linkages at positions 2 and 4. A final example is the haem *d<sub>1</sub>* group, Figure 1.1(E), which is present in cytochrome *cd<sub>1</sub>* nitrite reductase, a bifunctional enzyme that catalyses both the one electron reduction of nitrite to nitric oxide and four electron reduction of oxygen to water. This haem group has two acetate groups at positions 1 and 3 and two carbonyl groups at positions 2 and 4 of the porphyrin ring.

As is evident from the above discussion, the haem complex is clearly one of the most versatile redox centres in biology<sup>[2]</sup> and is a ubiquitous prosthetic group found in many haem proteins and enzymes. However, although these proteins share a common or very similar porphyrin structure, they display a very wide range of biological functions, which will be highlighted in the following section.

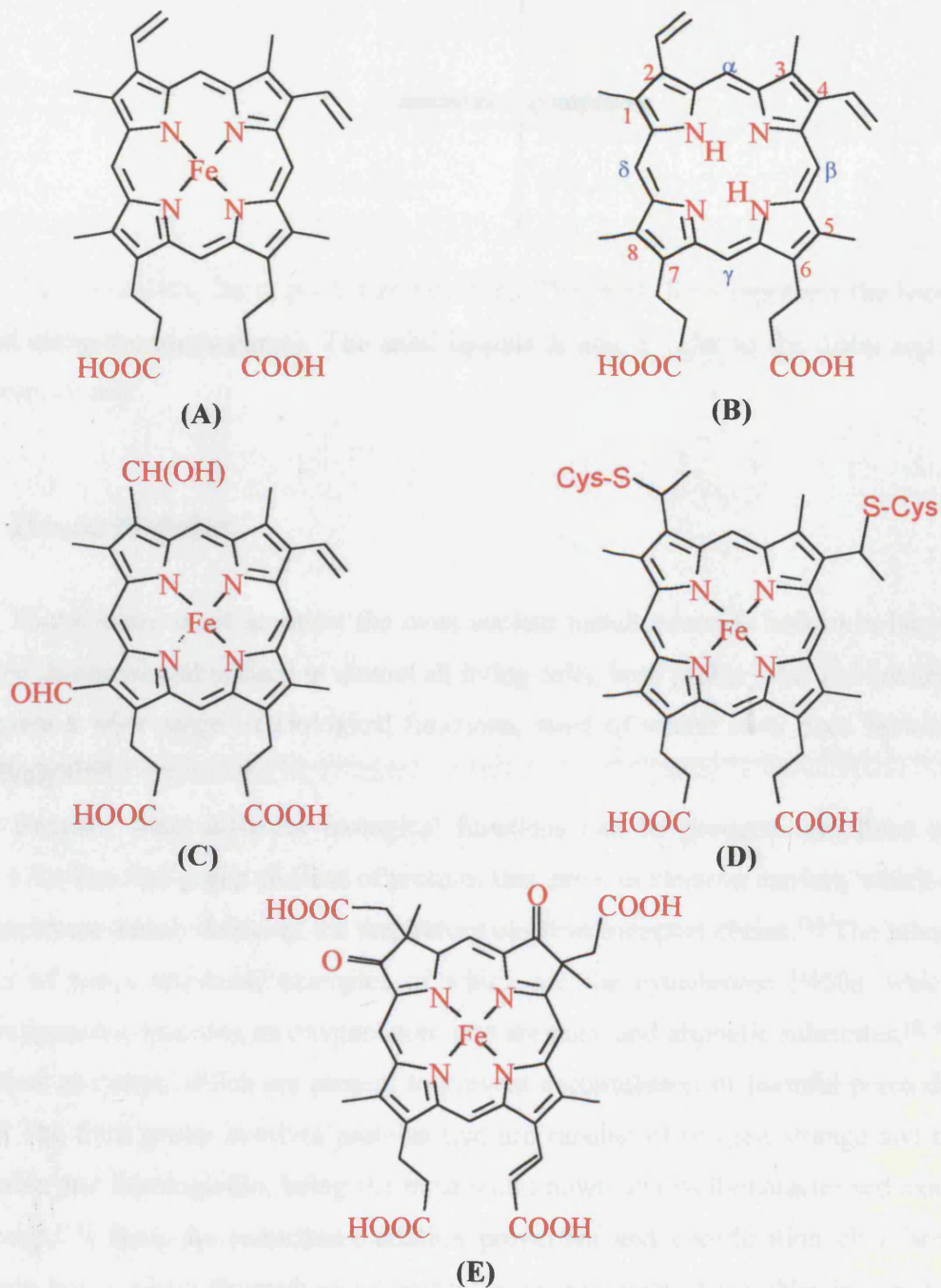


**Figure 1.1.** The structures of (A) iron protoporphyrin IX, as found in the cytochromes *b*, globins, monooxygenases and some peroxidases, (B) protoporphyrin IX, (C) haem *a*, where  $R = [(CH_2)_2CH=C(CH_3)]_3CH_3$ , found in cytochrome *c* oxidase, (D) haem *c*, as found in the cytochromes *c*, and (E) haem *d*<sub>1</sub>, as found in cytochrome *cd*<sub>1</sub> nitrite reductase.

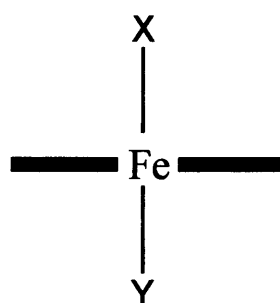


**Figure 1.2.** Schematic haem pocket architecture. The block lines represent the haem moiety (viewed along the haem plane). The axial ligands X and Y refer to the distal and proximal sites, respectively.

### 1.3 Haem Proteins

Haem proteins are amongst the most ancient metalloproteins known in biochemistry. They are contained and utilised in almost all living cells, both prokaryotic and eukaryotic, and encompass a wide range of biological functions, most of which have been reviewed fairly extensively.<sup>[3-7]</sup>

Broadly, these different biological functions can be grouped into three categories (Table 1.1). The first group consists of proteins that serve as electron carriers, which comprise the cytochrome family found in the respiratory electron transport chains.<sup>[6]</sup> The second group consists of redox enzymes, examples of which are the cytochrome P450s, which act as monooxygenases, inserting an oxygen atom into aromatic and aliphatic substrates,<sup>[8, 9]</sup> and the peroxidase enzymes, which are present to prevent accumulation of harmful peroxides in the cell.<sup>[10]</sup> The third group involves proteins that are capable of oxygen storage and transport, myoglobin and haemoglobin, being the most well-known and well-characterised examples of this group.<sup>[11]</sup> Both the reduction-oxidation properties and coordination chemistry of the porphyrin iron – which themselves are controlled by a number of variables imposed upon the molecule by the surrounding protein structure – can influence the function of the metalloprotein. The various functions of some haem proteins are outlined in Table 1.1.

**Table 1.1.**

The diversity of haem protein structure and function

Protein	Coordination Number	Coordinating Ligand(s) (X/Y)	Function
Cytochrome <i>c</i>	6	His/Met	Electron transfer
Cytochrome P450	6	H <sub>2</sub> O/Cys	Monooxygenase
Cytochrome <i>c</i> peroxidase	5	-/His	Peroxidase
Haemoglobin	6	H <sub>2</sub> O/His	Oxygen binding
Myoglobin	6	H <sub>2</sub> O/His	Oxygen storage

The flexibility in function, more than likely, arises from a combination of differences in both the polypeptide and haem constituents of the various haem proteins. Cytochromes, mostly found in the respiratory pathways, act as one-electron carrier proteins by shuttling between iron (II) and iron (III) at their active site.<sup>[6, 12]</sup> These haem proteins, which are involved in such simple electron transfer reactions, need to avoid substantial reorganisation at the haem iron upon electron transfer and, as a consequence, are predominantly six-coordinate. The ligation of two strong ligands at the proximal and distal sites, Figure 1.2, of the haem iron results in a low-spin species being maintained in both oxidation states. In contrast, the availability of a coordination site to bind exogenous ligands is important for haem proteins that bind or are activated by oxygen. The haem iron of the P450 haem enzymes, which act as monooxygenases by using dioxygen (*via* oxygen insertion) to catalyse aromatic and aliphatic hydroxylations,<sup>[8, 9]</sup> possess weakly ligated ligands at the sixth site that can be easily replaced with substrates. The haem group of peroxidases is known to have a vacant sixth site and therefore can easily bind substrates such as peroxides. Peroxidases are able to reduce peroxides and, as a consequence, are utilised to prevent the accumulation of potentially toxic H<sub>2</sub>O<sub>2</sub> in cells.<sup>[6]</sup> Haemoglobin and myoglobin also contain haem with weakly ligated sixth coordination site so that other exogenous ligands, such as oxygen, can easily bind to the haem. Hence, haemoglobin and myoglobin are able to maintain a balanced supply of oxygen by functioning as oxygen transport and binding proteins.<sup>[11]</sup>

Identification of the ways in which protein structure is able to modulate the chemistry of the haem (or any other) prosthetic group is one of the most significant challenges in bio-

inorganic chemistry. The acquisition of such fundamental knowledge is of more than academic interest: it is central to developing our understanding of the way proteins operate and ought to establish a firm foundation upon which the rational design of new enzymes and proteins for potential industrial or medical uses can be based. Accordingly, given the diversity in function that is displayed by haem proteins, an understanding of the mechanism by which the chemical reactivity of the haem iron is controlled by the polypeptide structure of haem protein is of tremendous importance to the advancement of our current ideas on structure-function relationships. The availability of crystallographic data for these haem proteins makes them highly attractive targets in this context as the availability of recombinant DNA technology has revolutionised the way in which haem structure/function studies in general are conducted. Hence, it is now possible to introduce systematic perturbations into the protein architecture by site-directed mutagenesis which, when combined with detailed structural, spectroscopic and functional analysis, can provide very specific information on the role of individual residues. In addition, it has been possible to introduce structural and functional aspects of one haem protein into another, which further assists towards rationalising structure/function relationships that exist between the different classes of haem proteins.<sup>[13]</sup>

The following sections aim to summarise how the versatility in function of different haem proteins is made possible. A brief introduction to the different classes of haem proteins and the fundamental issues that govern protein function - haem axial ligation (cytochromes, globins and peroxidases) and haem environment (peroxidases and globins) will be outlined. The main focus of the rest of this Chapter will be based on leghaemoglobin, the haem protein extensively investigated in this thesis.

## 1.4 Electron Transfer Haem Proteins

The ability of a variety of proteins to undergo reversible oxidation-reduction is especially important in photosynthesis and respiration. The ability of proteins (and other electron transfer systems in general) to carry out electron transfer reactions is dependent on a number of factors. First, the distance between redox centres during the transfer process and the nature of the intervening medium, *i.e.* whether the electron travels through bond or through space, is vitally important. Second, the rates of electron transfer within physiological systems are influenced by the differences in reduction (mid-point) potential between the electron donor and acceptor. This factor contributes to the driving force for the reaction. In

addition, the re-organisation energy associated within the protein also affects the efficiency of electron transfer.

Haem groups are ideally suited for electron transfer reactions. The use of the extended porphyrin  $\pi$ -system allows delocalisation of the electron/electrons over an extended area. This minimises the re-ordering of the local atomic structure and the surrounding environment when the electron transfer occurs. Cytochromes, one of the electron transfer haem proteins found in Nature, capitalise on these advantages by minimising the required re-organisation energy associated with the electron transfer within the rigid hydrophobic haem environment. The protein achieves this through its six-coordinate, low-spin haem for cytochrome *c*, methionine and histidine act as the fifth and sixth ligands, respectively, Figure 1.3, which are encapsulated within a hydrophobic pocket.<sup>[14]</sup> Therefore, delocalisation of the electron can be easily achieved over the porphyrin ring  $\pi$ -system. Cytochromes possess a wide range of properties and function in a large number of different redox processes.<sup>[15, 16]</sup> Four classes of cytochrome *c* have been recognised.<sup>[17]</sup> Class I includes low-spin soluble cytochrome *c* of mitochondria and bacteria. Class II<sup>[18]</sup> includes high-spin cytochrome *c* and a number of low-spin cytochromes, *e.g.* cytochrome *c*<sub>556</sub>. Class III<sup>[19]</sup> comprises the low redox potential multihaem cytochromes: cytochrome *c*<sub>7</sub> (trahaem), *c*<sub>3</sub> (tetrahaem) and high molecular weight cytochrome *c* (HMC; hexadecahaem). Class IV includes flavocytochrome *c* and cytochrome *cd*<sub>1</sub>.

As mentioned above, the reduction potential of electron donor and electron acceptors influence the rate of electron transfer. The reduction potential of the haem can be modulated over a wide range (-400 to +400 mV) by the surrounding protein environment. Site-directed mutagenesis has facilitated quantification of the effect that haem-iron ligation has upon haem protein reduction potentials.<sup>[13, 20-23]</sup> Factors that are known to also affect reduction potential include orientation of the haem,<sup>[24]</sup> the identity of the haem ligands,<sup>[25]</sup> the orientation of the haem vinyl groups<sup>[26]</sup> and hydrogen bonding to the proximal and distal ligands.<sup>[27, 28]</sup> Unfortunately, the isolation of only one of these variables, whilst keeping all others constant, has proved to be quite difficult. As a result, the exact structural factors controlling reduction potential are still not clearly defined.

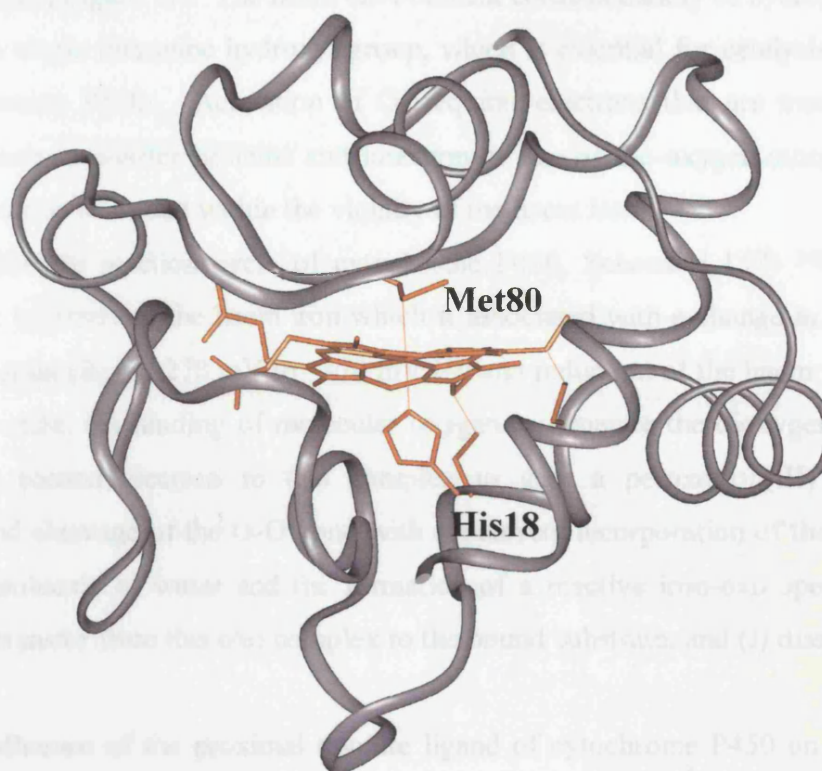


**Figure 1.3.** The structure of yeast cytochrome *c*.<sup>[14]</sup> The haem group is shown in orange together with the cysteine thiolate linkages to the vinyl groups and the methionine (Met80) and histidine (His18) axial ligands are indicated.

## 1.5 Monooxygenases

Haem-containing monooxygenases<sup>[8]</sup> activate molecular oxygen and catalyse the incorporation of one of the two oxygen atoms of an  $O_2$  molecule into a broad variety of substrates with concomitant reduction of the other oxygen by two electrons to water,<sup>[29, 30]</sup> Equation [1.1].



A well-known example of this group of haem proteins are the cytochrome P450s,<sup>[31, 32]</sup> which have been isolated from numerous mammalian tissues, insects, plants, yeasts and bacteria.<sup>[33]</sup> The reactive site of cytochrome P450 is remarkably simple, containing only haem *b* with cysteine as the fifth ligand, leaving the sixth coordination site to bind and activate

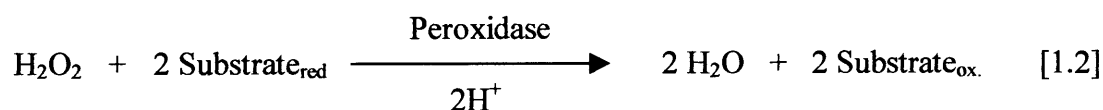
molecular oxygen, Figure 1.4. The haem environment consists mainly of hydrophobic protein residues and a single threonine hydroxyl group, which is essential for catalysis for some but not all cytochrome P450s. Activation of O<sub>2</sub> requires electrons that are transferred to the enzyme by electron transfer proteins and insertion of one of the oxygen atoms necessitates that the substrate to be bound within the vicinity of the haem iron.

The catalytic reaction cycle of cytochrome P450, Scheme 1.1,<sup>[30, 34]</sup> involves: (a) binding of the substrate to the haem iron which is associated with a change in the haem-iron reduction potential (from -270 mV to -170 mV)<sup>[35]</sup> and reduction of the haem from the ferric to the ferrous state; (b) binding of molecular oxygen to generate the dioxygen complex; (c) transfer of a second electron to this complex to give a peroxoiron(III) complex; (d) protonation and cleavage of the O-O bond with concurrent incorporation of the distal oxygen atom into a molecule of water and the formation of a reactive iron-oxo species;<sup>[36, 37]</sup> (e) oxygen atom transfer from this oxo complex to the bound substrate; and (f) dissociation of the product.

The influence of the proximal thiolate ligand of cytochrome P450 on the haem-iron chemistry has been examined in a number of ways.<sup>[8, 13]</sup> Comparisons between the anionic ligand binding properties of ferric P450 and met-myoglobin has provided indirect confirmation that the monooxygenases have a much lower affinity for anionic ligands, which is most probably due to the electron-releasing character of the proximal thiolate. Mutagenic substitution of the proximal histidine of human myoglobin with cysteine has been shown to enhance the heterolytic O-O cleavage of peroxide (oxidant) in comparison with native myoglobin. The axial thiolate apparently stabilises the oxy ferryl (oxo) haem iron species formed.<sup>[38-40]</sup>

## 1.6 Haem Peroxidases

Haem-containing peroxidases comprise of a family of metalloenzymes that catalyse the H<sub>2</sub>O<sub>2</sub>-dependant oxidation of a plethora of organic and inorganic substrates,<sup>[42, 43]</sup> Equation [1.2].



Peroxidases can be categorised into two superfamilies based on sequence similarity:

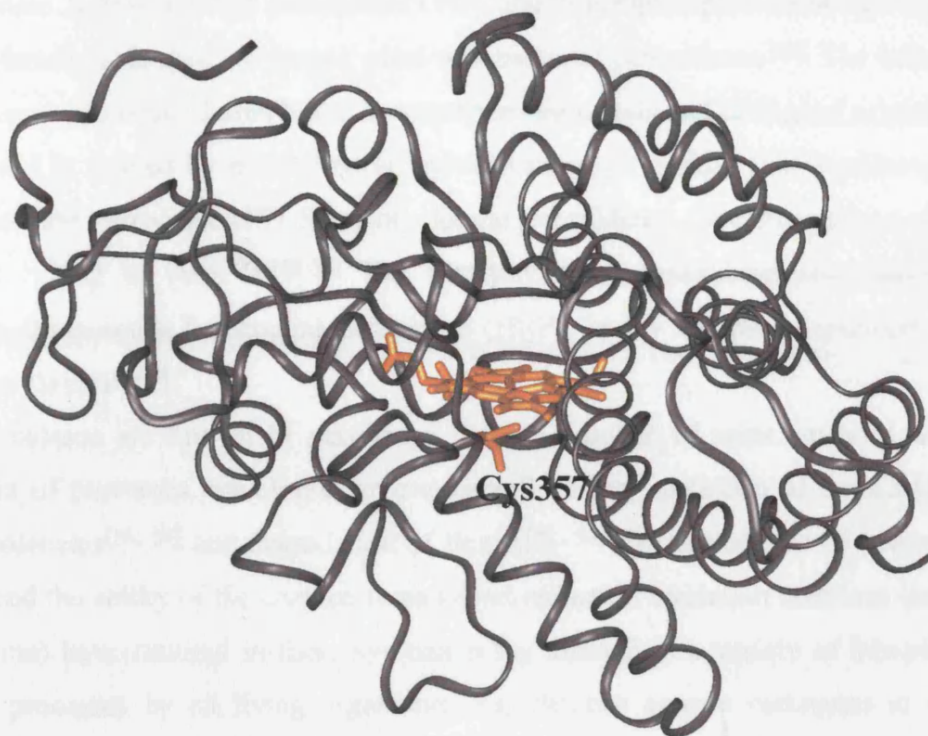
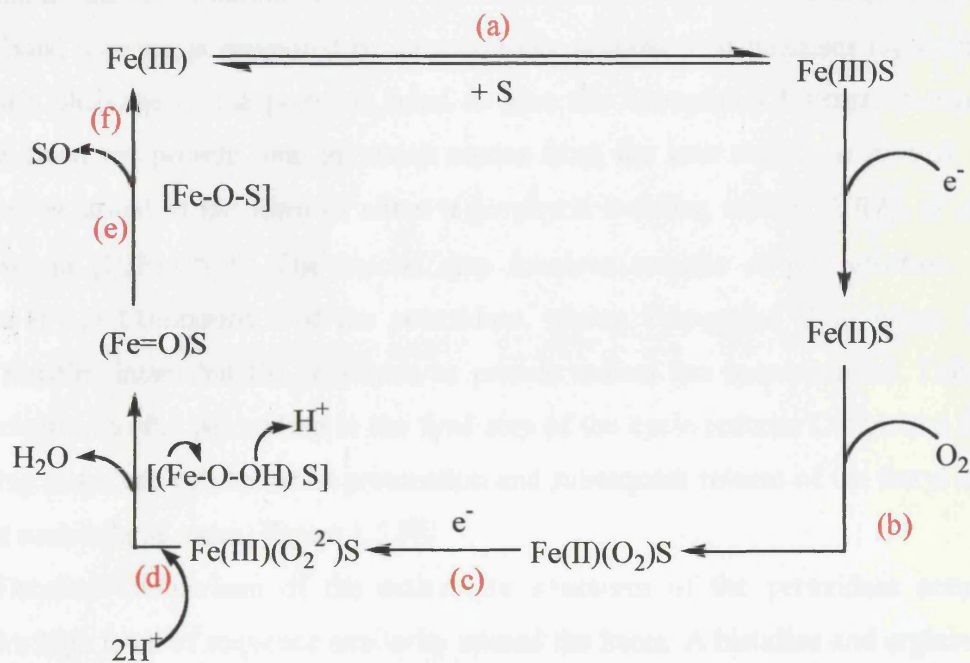


**Figure 1.4.** The crystal structure of cytochrome P450cam,<sup>[41]</sup> illustrating the haem group and thiolate ligand (orange).



**Scheme 1.1.** Catalytic cycle of cytochrome P450.<sup>[30]</sup> S = substrate.

animal peroxidases form one of the superfamilies, examples include myeloperoxidase (MPO), lactoperoxidase (LPO), thyroid peroxidase (TPO) and eosinophil peroxidase (EPO).<sup>[44]</sup> The other superfamily is formed by fungal, plant and bacterial peroxidases.<sup>[45]</sup> The latter can be further grouped into three classes based on sequence alignments and biological origin.<sup>[45, 46]</sup>

Class I is formed by mitochondrial cytochrome *c* peroxidase (CcP), chloroplast and cytosol ascorbate peroxidases.<sup>[47]</sup> Secretory fungal peroxidases (like manganese and lignin peroxidase) belong to class II.<sup>[48-50]</sup> The secretory plant peroxidases, or classical plant peroxidases, for example horseradish peroxidase (HRP), barley and peanut peroxidase,<sup>[46, 51, 52]</sup> belong to class III.<sup>[45]</sup>

Peroxidases are known to perform a diverse number of roles, such as aiding the development of processes, which are environmentally clean, oxidation of dyes and/or toxic phenolic molecules<sup>[53, 54]</sup> and degradation of lignin.<sup>[55, 56]</sup> The abundance of peroxidases in Nature<sup>[57]</sup> and the ability of the enzyme to carry out reduction-oxidation reactions (acting as a redox enzyme) have resulted in these systems being utilised in a variety of biosynthetic or degradable processes by all living organisms, *e.g.* defence against pathogens or oxidative pressure.<sup>[51, 53]</sup>

Most haem peroxidases follow the reaction mechanism summarised in Figure 1.5 (the mechanism shown in Figure 1.5 is that of cytochrome *c* peroxidase).<sup>[58]</sup> Peroxidase catalysis is initiated by the coordination of neutral hydrogen peroxide to the ferric haem iron. Oxygen-oxygen bond scission is promoted by an active site arginine that polarises the double bond. Heterolytic cleavage of the peroxide bond to give this Compound I structure requires two electrons from the protein, one of which comes from the iron atom, the second oxidising equivalent is stored in the form of either a porphyrin  $\pi$ -cation radical (HRP), or a protein-based radical (CcP).<sup>[59, 60]</sup> The second step involves transfer of one electron from the substrate (S) to Compound I of the peroxidase, giving Compound II in which the ferryl species remains intact but the porphyrin or protein radical has been reduced. Transfer of a second electron to the peroxidase in the final step of the cycle reduces Compound II back to the resting state, and results in the protonation and subsequent release of the ferryl oxygen as a second molecule of water, Figure 1.5.<sup>[61]</sup>

Detailed comparison of the active site structures of the peroxidase enzymes has revealed a high level of sequence similarity around the haem. A histidine and arginine residue on the distal side of the haem form the peroxide binding pocket. On the proximal side of the haem, the proximal histidine residue hydrogen bonds with a buried aspartate residue. Figure

1.5 outlines the general structure of the peroxidase active site and summarises the roles of the active site residues in governing enzyme activity as elucidated from mutagenesis experiments of recombinant CcP and HRP.[42, 60, 62, 63]

## 1.7 Globins

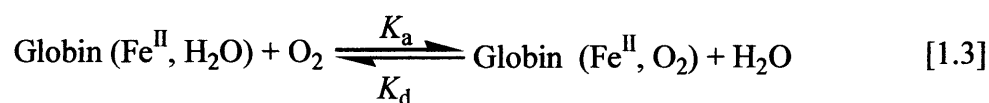
Globins are a class of haem proteins that are used by Nature to maintain and regulate oxygen supply within biological systems. The globin superfamily includes vertebrate haemoglobins (Hb), vertebrate myoglobins (Mb), invertebrate globins, fungal and bacterial flavohaemoproteins (FHb) and plant globins. Three-dimensional structures are known for a number of globins and all share the highly conserved 'globin fold'.<sup>[64-67]</sup>

The field of globin chemistry has been an ongoing area of research. The increasing availability of crystallographic data and the availability of recombinant cDNA technology and site-directed mutagenesis for these proteins still makes them highly attractive to ongoing research into protein structure/function relationships. Characterisation of the new variant proteins using a range of techniques helps towards dissecting the structure/function relationships that exist within a protein.

The following section summarises some of the current knowledge that has been gained from ongoing research on mammalian myoglobins. Following on from this, an introduction to soybean leghaemoglobin, a plant haemoglobin, which is the main subject of the research presented in this thesis, will be discussed.

### 1.7.1 Myoglobin

Myoglobin plays a role in oxygen storage,<sup>[68, 69]</sup> although the role in the diffusion of dioxygen through muscle tissue to mitochondria has also been postulated.<sup>[70-73]</sup> The protein functions by reversibly binding oxygen. This equilibrium, Equation [1.3],



requires that the haem iron be maintained in its ferrous oxidation state under physiological conditions. The hydrophobic distal haem pocket of myoglobin, Figure 1.6, (and globins in

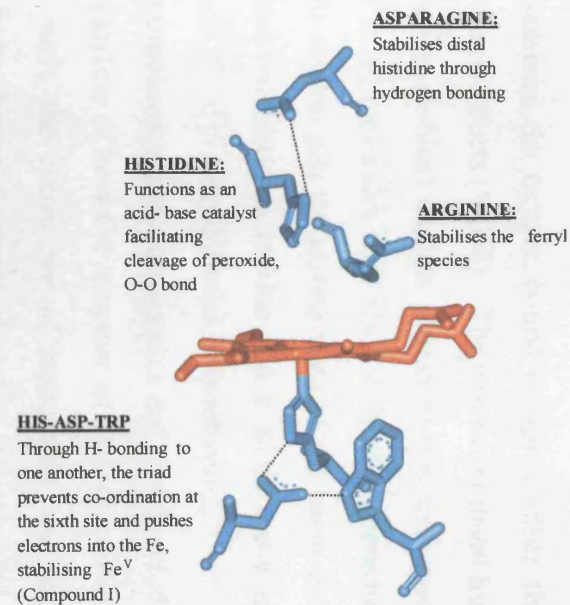
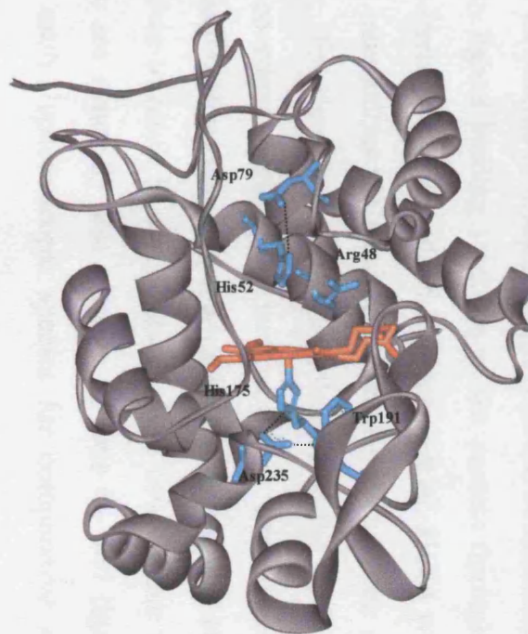
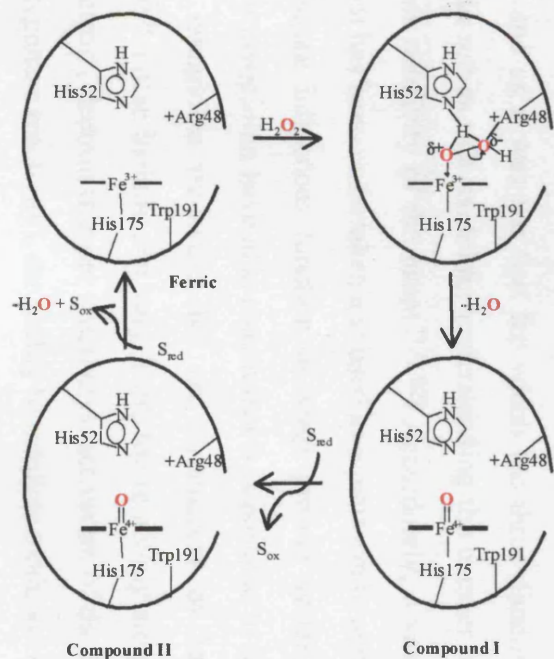


**Figure 1.5. Left:** General peroxidase mechanism showing ferric enzyme, Compound I and Compound II. S<sub>ox</sub> and S<sub>red</sub> refer to the oxidised and reduced forms of the substrate, respectively. The key active site residues have been labelled according to the residues numbering of cytochrome *c* peroxidase. **Middle:** The crystal structure of yeast cytochrome *c* peroxidase showing the haem (orange) and key active site residues (cyan).<sup>[58]</sup> **Right:** The active site structure of cytochrome *c* peroxidase showing key active site residues and hydrogen bonding (dashed lines).

general) stabilises the oxygen bound complex either through hydrogen bond stabilisation (His64) or steric effects (Val68). The conserved distal histidine and valine residues (found in all mammalian globins) hinders access to the sixth coordination site so that a controlled binding of small molecules may result only as a consequence of side chain dynamics of the protein. At neutral pH, the resting state of the haem iron of myoglobin is coordinated to a highly conserved histidine residue and a labile water molecule, which are located on the proximal and distal protein domains, respectively.

Recombinant expression systems and site-directed mutagenesis have greatly enhanced our understanding of how the structure of globins controls haem coordination geometry.<sup>[2, 5, 40, 74]</sup> As such, the active site of myoglobin, and the effect of active site amino acid substitutions has been the subject of intense experimental scrutiny.<sup>[40, 74]</sup> The role of the distal histidine 64 residue of myoglobin has received considerable interest and has been shown to be crucial in ligand binding reactions of the protein through its hydrogen-bonding interactions with the haem-bound ligand.<sup>[74]</sup> Replacement of His64 with residues incapable of hydrogen-bonding interactions has resulted in the alteration of the coordination state of the haem. For example, His64 stabilises water coordination at the sixth site, removal of this residue results in five-coordinate, high-spin metmyoglobin derivatives<sup>[75]</sup> with altered ligand binding properties.<sup>[74]</sup> However, in a few cases, substitution of His64 with appropriate residues has been shown to result in coordination of the new residue to the haem iron.<sup>[76-81]</sup> Variants of this type are generally less reactive in their O<sub>2</sub> and ligand binding, but they nevertheless provide useful spectroscopic species for comparative studies with other types of haem proteins.

As the structure of myoglobin is relatively simple compared to the other haem proteins, and as it was the first for which the three-dimensional structure was determined, myoglobin serves as a model for understanding the manner in which the protein environment determines reactivity of the haem.<sup>[13, 82]</sup> Accordingly, a vast range of mutagenic studies on myoglobin has been undertaken and used as a platform to address the fundamental question of how structure influences function in haem protein systems.<sup>[40]</sup> Site-directed mutagenesis studies on myoglobin have also shown that it is possible to incorporate new haem reactivities into the myoglobin molecule that are reminiscent of haem reactivities of other haem proteins.<sup>[13]</sup> These include and vary from, the relatively simple process of reversible binding of an electron (electron transfer reactivity), activation of dioxygen for substrate hydroxylation (monooxygenase reactivity), the ability to catalyse oxidation of substrates by H<sub>2</sub>O<sub>2</sub>

(peroxidase activity), oxidation of unsaturated fatty acids (lipoxygenase activity), and haem degradation (haem oxygenase reactivity).[40]

Myoglobin will be used as a basis for comparisons for the work carried out on leghaemoglobin throughout this thesis.

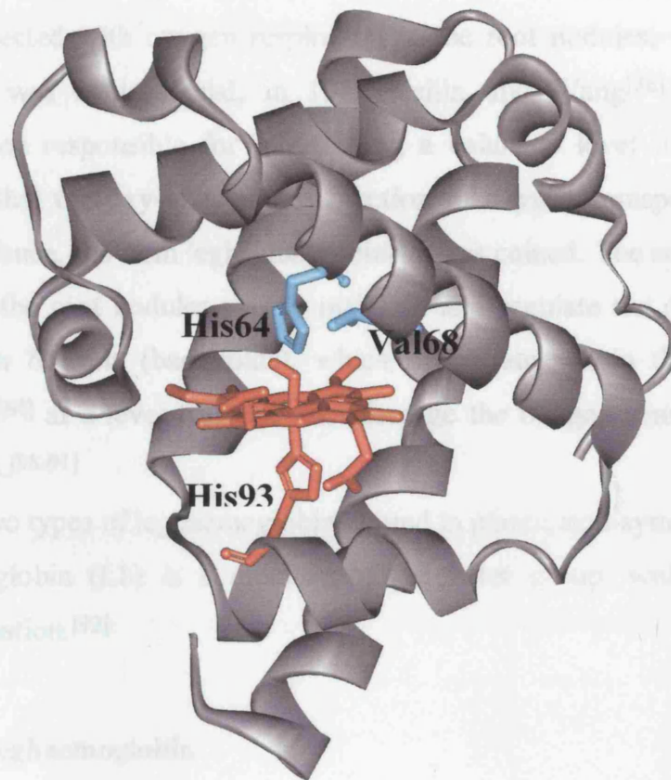


**Figure 1.6.** The crystal structure of oxymyoglobin, pH 8.4,[64] illustrating the His64, Val68 and His93 residues and the hydrogen bond between His64 and the bound oxygen.

### 1.7.2 Leghaemoglobin

Although mammalian globins have been identified since the late half of the 19<sup>th</sup> century,[40, 83] the existence of globins in the plant kingdom (leguminous plants) has also been recognised.[84] The following sections aim to present the current knowledge on these proteins, in particular on soybean leghaemoglobin, and highlight some of the limitations faced in this area of research. The way in which these limitations have been recently overcome, and the key questions that remain to be answered, will be highlighted.

### 1.7.2.1 Biological Background

The classical definition of haemoglobin<sup>[85]</sup> required haem to be combined with a globin in such a way that dioxygen could form a reversible complex in which the iron remained in the ferrous state. In 1939, Kubo<sup>[84]</sup> recognised this property in a red pigment isolated from the nodules of soybean. It was concluded that this haemoglobin-like pigment was therefore connected with oxygen respiration in the root nodules. Although the initial proposed function was controversial, in 1945 Keilin and Wang<sup>[86]</sup> confirmed that the molecule was indeed responsible for maintaining a balanced level of oxygen within the legume plant and that the oxy-form might function in oxygen transport during symbiotic nitrogen fixation. Hence, the term leghaemoglobin<sup>[87]</sup> was coined. The suggested main role of leghaemoglobin in the root nodules was to maintain and regulate the oxygen supply to the vigorous *Rhizobium* bacteria (bacteroids), which proliferate within the plant cells of the developing nodule,<sup>[84]</sup> at a level that does not damage the oxygen sensitive nitrogen fixing nitrogenase enzyme.<sup>[88-91]</sup>

There are two types of leghaemoglobins found in plants, non-symbiotic and symbiotic: soybean leghaemoglobin (Lb) is a member of the latter group, with protein expression induced upon nodulation.<sup>[92]</sup>

### 1.7.2.2 Soybean Leghaemoglobin

Soybean leghaemoglobin can be isolated in good yields from root nodules, 25-28 days after *Rhizobium* infection. From isolation and isoelectric focussing experiments, the protein was found to contain four major components (*a*, *c*<sub>1</sub>, *c*<sub>2</sub>, *c*<sub>3</sub>) and four minor components (*b*, *d*<sub>1</sub>, *d*<sub>2</sub>, *d*<sub>3</sub>),<sup>[93]</sup> (the minor components are N-terminal acetylation products of the major components). This is not unusual: most leghaemoglobin species have been found to contain a number of components, lupin,<sup>[94]</sup> cowpea,<sup>[95]</sup> broad bean,<sup>[96]</sup> kidney bean<sup>[97]</sup> and *alfalfa*<sup>[98]</sup> are good examples. Peptide sequencing of components from different leghaemoglobins shows that there are relatively few differences observed between different components of a particular species and comparison of soybean leghaemoglobins *a* and *c* show only an 8% difference in sequence.<sup>[88, 99]</sup> Leghaemoglobins show conserved regions as in most protein 'families'- only two histidine residues are present, on the proximal and distal side of the haem, and no cysteine residues are present, thereby favouring a monomeric species.

Soybean leghaemoglobin *a* (Lb) is a monomeric protein of 144 amino acids and has a mass of 15.9 kDa similar to that of vertebrate myoglobin. However, although the masses of the two proteins are similar, there are quite a few differences between the two proteins. The amino acid sequence of soybean leghaemoglobin, when aligned with vertebrate myoglobins, (*e.g.* sperm whale and horse heart, Figure 1.7), shows that between residues 68 and 143 of soybean Lb (highlighted in green), there is only 28% and 31% sequence identity, respectively, and 17% and 13% sequence similarity, respectively, to sperm whale and horse heart myoglobins. Although the amino acid sequences of leghaemoglobin differ, common features between soybean leghaemoglobins and myoglobin appear in the nature of the globin fold.

The elucidation of the crystal structure of soybean Lb<sup>[100, 101]</sup> provided further insight into understanding this protein. The crystal structures revealed that, whilst the haem coordination geometry on the proximal side is similar to that present in the mammalian globins, the distal side of leghaemoglobin is slightly larger, which allows passage of ligands into and out of the active site.<sup>[100-104]</sup> Additionally, the crystal structures also showed that there is no obvious channel by which oxygen or any other exogenous ligands may gain access to the haem group, so fluctuations in the protein as well as conformational changes are implicated for these ligand-binding processes.<sup>[105]</sup> This may explain the extremely high oxygen affinity observed for soybean Lb when compared to myoglobin and haemoglobin equivalents, Table 1.2, which is known to arise from a very fast rate constant for association of oxygen, together with a moderately slow rate of dissociation,<sup>[103]</sup> Equation [1.4].

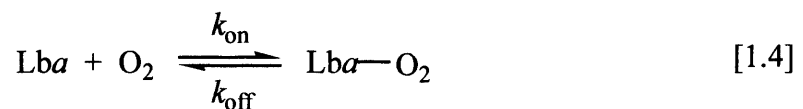


**Table 1.2.**

Comparison of association ( $k_{\text{on}}$ ) and dissociation ( $k_{\text{off}}$ ) rate constants, and association binding constant ( $K$ ) for oxygen binding to Lb, human Hb and horse heart Mb.<sup>[103]</sup>

Globin	$k_{\text{on}}$ ( $\mu\text{M}^{-1}\text{s}^{-1}$ )	$k_{\text{off}}$ ( $\text{s}^{-1}$ )	$K$ ( $\mu\text{M}^{-1}$ )
Leghaemoglobin(Lb)	118	4.4	27
Human Hb $\beta$ -chain	71	16	4.4
Horse heart Mb	14	11	1.3



### 1.7.2.3 Nicotinate-The Physiological Ligand of Leghaemoglobin

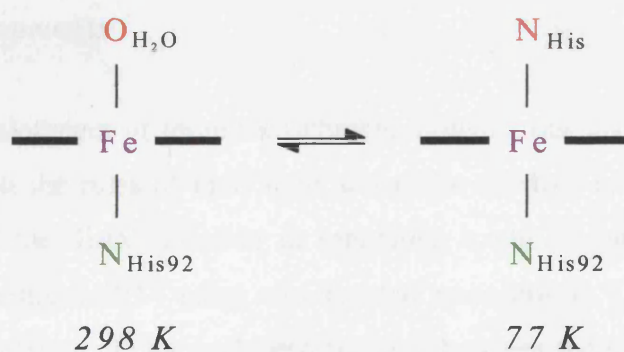
The crystallographic data for the nicotinate derivatives of soybean Lb,<sup>[100, 101]</sup> Figure 1.8, and lupin<sup>[106]</sup> have revealed that a deprotonated pyridine nitrogen ( $pK_a = 4.87$ )<sup>[107]</sup> replaces water as the sixth axial ligand to the haem in both ferric and ferrous oxidation states, Figure 1.8. This observation supported earlier work where chromatographically pure samples of Lb had shown a non-homogeneity when examined spectroscopically, and were found to contain a low-spin haem protein contaminant.<sup>[108, 109]</sup> Early work focussed on the origin of this low-spin contaminant and, in 1973, the low-spin haem derivative was identified and was found to arise from the interaction of a pyridine 3-carboxylic acid anion (nicotinate), Figure 1.9, which is found in the root nodules of the plant, with the haem iron. Spectroscopic data<sup>[110, 111]</sup> for the nicotinate derivatives have subsequently emerged and also confirmed this haem ligation. The nicotinate binds most strongly at a pH of 5.2,<sup>[107]</sup> where a protonated distal histidine residue stabilises the complex, Figure 1.8. The existence of an additional hydrogen bond in Lb between the carboxyl group of nicotinate and phenolic O atom of 'Tyr B9' (distal tyrosine 30)<sup>[100, 101]</sup> has also been predicted by Arutyunyan,<sup>[112]</sup> and additional stabilisation of the complex, Figure 1.8. However, the exact quantitative contribution of these residues in stabilising nicotinate in the active site has not been established.

The presence of nicotinic acid in soybean Lb has been shown to decrease the affinity of the protein for oxygen at low oxygen pressures.<sup>[107]</sup> The stabilisation of the Lb-nicotinate complex in the active site by endogenous residues is thought to have direct implications towards this decrease in affinity for oxygen. Therefore, there must be stringent physiological control within the plant to prevent elevated oxygen pressure, whilst maintaining adequate levels of nicotinate-free protein. One physiological factor believed to regulate this control was pH. The change of nodule pH, perhaps in a local domain within the cell or under metabolic stress conditions, could have the effect of affecting Lb oxygen affinity since nicotinate binding is affected by change in pH.<sup>[107, 113]</sup> However, little is known about this pH-dependent nicotinate binding process. Earlier work on the native protein has only predicted that active site amino acid residues may be involved in controlling this binding process, but no clear or direct evidence has been published.<sup>[107, 114-116]</sup> Hence, although the presence of nicotinate in Lb has been established, very little work has been undertaken in order to establish its true function.

### 1.7.2.4 The Flexible Active Site Structure of Soybean Leghaemoglobin

The larger and flexible active site architecture of leghaemoglobin, shown by crystallographic<sup>[88, 100, 101, 103, 104]</sup> and proton relaxation technique studies,<sup>[102]</sup> gives rise to some rather unusual features. First, and in contrast to the mammalian globins, leghaemoglobins are able to bind very bulky ligands (*e.g.* nicotinate) at the distal site,<sup>[107]</sup> which has been proposed to involve a mechanism involving the distal histidine ‘swinging’ away from the haem pocket.<sup>[88]</sup> It is believed that the movement of the histidine occurs by rotation about the C( $\alpha$ ) – C( $\beta$ ), such that the imidazole ring swings out of the hydrophobic pocket and away from the haem iron, thereby allowing access of a ligand into the active site pocket to the buried haem.

Further early evidence for the mobility of histidine in leghaemoglobin was provided by the magnetic susceptibility and EPR experiments of Ehrenberg and Ellfolk.<sup>[117]</sup> These studies have established that soybean ferric leghaemoglobin exists as an equilibrium mixture of high- and low-spin haem species (pH 6.1) at room temperature. However at low temperature, a temperature-dependent alteration in spin state and coordination geometry was detected, Scheme 1.2, which resulted in formation of a low-spin species and has been interpreted<sup>[88]</sup> in terms of a flexible haem pocket, involving coordination of a mobile distal histidine residue to the haem iron (Section 1.7.2.5).<sup>[118]</sup> It is believed that the distal histidine approaches close enough to the haem iron (at a distance of 2-2.4 Å) to become the sixth ligand and hence form a bis-histidine, low-spin form.<sup>[88]</sup> However, direct evidence for the true origin of the low-spin species detected at both room and low temperature has not yet been established.



**Scheme 1.2.** Temperature-dependent change in coordination geometry in Lb. The 298K species contains high-spin haem, 77K species is entirely low spin.

### 1.7.3 cDNA and Recombinant Expression Systems

Leghaemoglobins from soybean and other species, such as lupin<sup>[119]</sup> and kidney bean,<sup>[114]</sup> have been isolated and characterised, although the soybean protein is by far the most-well characterized, with extensive availability of spectroscopic data<sup>[90, 91, 120]</sup> and crystal structures for the free and nicotinate-bound derivative.<sup>[100, 101]</sup> Despite the number of investigative studies, many of the unique functional aspects remain unexplained at the molecular level, and the exact role of protein structure in the control of function is relatively ill-defined. A prerequisite for structure/function studies is the ready availability of efficient bacterial expression systems for generation of recombinant protein from *E.coli*. The absence of cDNA and recombinant technology, site-directed mutagenesis and expression systems hindered progress in this case and the roles of individual amino acids on protein function and spectroscopic properties therefore could not be established.

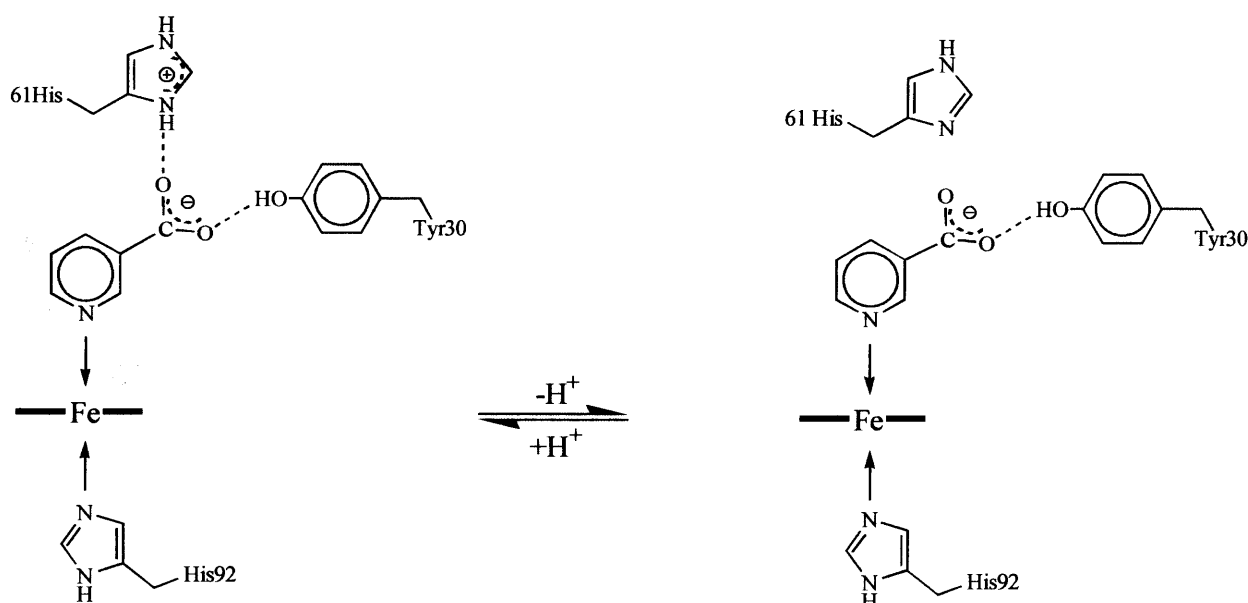
Recently, cDNA sequences for a number of leghaemoglobins (Lbs) have emerged, including *Medicago sativa* (alfafa),<sup>[121-123]</sup> *Sesbania rostrata*,<sup>[124]</sup> *Vigna unguiculata* (cowpea),<sup>[95]</sup> *Lupinus luteus* (lupin)<sup>[125, 126]</sup> and *Glycine max* (soybean).<sup>[127, 128]</sup> Expression systems have been developed as a result of the available sequence information for lupin Lb<sup>[129]</sup> and cowpea LbII,<sup>[95]</sup> but until 1996,<sup>[130]</sup> no bacterial expression system was available for soybean Lb. Unfortunately, the early systems generated insoluble inclusion bodies, which meant that large quantities of soluble protein were not readily obtained.<sup>[130, 131]</sup> Subsequently, an alternative vector was used for the expression of this gene,<sup>[132]</sup> which has recently been shown, by a number of spectroscopic methods, to generate protein that is identical to the native protein. Hence, structure/function studies on recombinant Lb are now possible.

### 1.7.4 Recent Developments

Since the development of these recombinant systems, our knowledge of soybean Lb has been extended and the roles of individual active site residues have been examined. For example, the role of the distal histidine in regulating oxygen binding<sup>[131]</sup> and nicotinate binding has been investigated<sup>[133]</sup> using site-directed mutagenesis. Oxygen binding studies have revealed that at neutral pH the hydrogen bonding between the haem bound oxygen and the distal histidine 61 is less important in regulating O<sub>2</sub> binding to the soybean protein when compared to the analogous binding interaction in myoglobin.<sup>[4, 134]</sup> Redox effects have been

investigated through electrostatic substitution of the proximal leucine residue with aspartic acid (Leu88Asp): this mutation has been established to weaken the ligand binding properties of the protein and enhance the stability of the ferric form.<sup>[135]</sup>

Nicotinate binding studies in soybean Lb have revealed that the hydrogen bonds formed between the distal histidine and distal tyrosine to the 3-carboxylic anion of nicotinate<sup>[101]</sup> are important in stabilising the Lb-nicotinate complex. The removal of the hydrogen bond donors (His61Ala and Tyr30Ala variants) resulted in a ~10-fold decrease in the binding affinity of the protein for nicotinate.<sup>[133]</sup> This work also established that the distal histidine participates in regulating nicotinate binding under neutral to alkaline pH conditions, with nicotinate binding being disfavoured at alkaline pH<sup>[133]</sup>, Scheme 1.3. This was explained through protonation of His61, which occurs below the  $pK_a$  of histidine 61 ( $pK_a$  of 6.9)<sup>[133]</sup> and facilitates binding of the nicotinate ligand through formation of a hydrogen bond; above the  $pK_a$  of histidine 61, hydrogen bond formation is not possible and hence the binding interaction is disfavoured.<sup>[133]</sup> A possible regulatory role for nicotinate, which naturally occurs in the root nodules of the soybean has also been proposed<sup>[133]</sup> on the basis of these results. The presence of nicotinate was also shown to decrease the reduction potential of the protein by ~ 100 mV, stabilising the ferric form of the protein, thereby inhibiting oxygen binding.



**Scheme 1.3.** Scheme indicating the protonation states of His61 and their effects on the binding of nicotinate.<sup>[133]</sup>

### 1.7.5 The Unresolved Questions

Although there has been some progress towards understanding the roles of some key residues in the function of soybean Lb, there are still a number of questions that yet remain to be answered. These include:

1. How would nicotinate binding be affected if both of the hydrogen-bond interactions between the protein and the ligand were removed? (Chapter 2)
2. How is nicotinate binding regulated by pH in the acidic region and which groups or residues are involved in this process? (Chapter 2)
3. Does the origin of the low-spin haem species in soybean Lb arise from ligation of the distal histidine 61? (Chapter 3)
4. Can new haem coordination structure (Chapters 4 and 5) and reactivities (Chapter 6) be incorporated into the Lb molecule?

The availability of an adequate expression system for recombinant soybean Lb<sup>[132]</sup> allow these questions to be addressed and provides the rationale for the experiments presented in this thesis.

## 1.8 References

1. R. Timkovich and L. L. Bondoc, *Adv. Biophys. Chem* (1990) **1**, 203.
2. S. K. Chapman, S. Daff and A. W. Munro, *Struc. Bond.* (1997) **88**, 40.
3. A. G. Sykes, in *Advances in Inorganic Chemistry*, A. G. Sykes, G. Mauk, Eds. (Academic Press, London) 2001, vol. 51.
4. B. A. Springer, S. G. Sligar, J. S. Olson and G. N. Phillips, *Chem. Rev.* (1994) **94**, 699.
5. P. R. Ortiz de Montellano, *Acc. Chem. Res.* (1987) **20**, 289.
6. H. B. Gray and J. R. Winkler, *Ann. Rev. Biochem.* (1996) **65**, 537.
7. J. H. Dawson, *Science* (1988) **240**, 433.
8. M. Sono, M. P. Roach, E. D. Coulter and J. H. Dawson, *Chem. Rev.* (1996) **96**, 2841.
9. L. L. Wang, *Curr. Opin. Chem. Biol.* (1988) **2**, 263.
10. H. R. Bosshard, H. Anni and T. Yonetani, in *Peroxidases in Chemistry and Biology*, J. Everse, K. E. Everse, M. B. Grisham, Eds. (CRC Press, Boca Raton, Florida) 1991, vol. 2, pp. 51.
11. E. Antonini and M. Brunori, in *Hemoglobin and Myoglobin in Their Reactions with Ligands*, (North Holland, Amsterdam) 1971, pp. 10.
12. D. E. Fenton, in *Biocoordination Chemistry*, (Oxford University Press, London) 1995, pp. 48.
13. Y. Lu, S. M. Berry and T. D. Pfister, *Chem. Rev.* (2001) **101**, 3047.
14. A. M. Berghius and G. D. Brayer, *J. Mol. Biol.* (1992) **223**, 259.
15. G. R. Moore and G. W. Moore, in *Cytochromes c. Evolutionary, Structural and Physiochemical Aspects*, G. W. Ed. (SpringerVerlag, Berlin-Heidelberg-New York) 1990.
16. G. W. Pettigrew and G. R. Moore, in *Cytochromes c. Biological Aspects*, (SpringerVerlag, Berlin-Heidelberg-New York) 1987.
17. R. P. Ambler, *Biochim. Biophys. Acta* (1991) **1058**, 42.
18. G. R. Moore, *Biochim. Biophys. Acta* (1991) **1058**, 38.
19. I. B. Coutinho and A. V. Xavier, *Methods Enzymol* (1994) **243**, 119.
20. P. Turano and Y. Lu, in *Handbook on MetalloProteins*, I. Bertini, H. Sigel, A. Sigel, Eds. (Marcel Decker, New York) 2001, pp. 269.
21. R. A. Scott and A. G. Mauk, in *Cytochrome c. A Multidisciplinary Approach*, (University Science Books, Sausalito, CA) 1996.

22. G. R. Moore and G. W. Pettigrew, in *Cytochromes c*, G. W. Eds. (Springer-Verlag, Berlin) 1990.
23. A. G. Mauk, *Struct. Bond.* (1991) **75**, 131.
24. J. S. Valentine, R. P. Sheridan, L. C. Allen and P. C. Kahn, *Proc. Natl. Acad. Sci. USA* (1979) **76**, 1009.
25. F. A. Walker, D. Emrick, J. E. Rivera, B. J. Hanquet and D. H. Buttlaire, *J. Am. Chem. Soc.* (1988) **110**, 6234.
26. L. S. Reid, A. R. Lim and A. G. Mauk, *J. Am. Chem. Soc.* (1986) **108**, 8917.
27. G. Garau, S. Geremia and L. Randaccio, *FEBS Lett.* (2002) **516**, 285.
28. F. Walker, B. H. Huynh, W. R. Scheidt and S. R. Osvath, *J. Am. Chem. Soc.* (1986) **108**, 5288.
29. D. F. V. Lewis, in *Cytochromes P450*, T. A. Francis, Ed. (London) 1996).
30. P. R. Ortiz de Montellano, in *Cytochrome P450: Structure, Mechanism and Biochemistry*, (Plenum Press, New York, London) 1995.
31. R. E. White and M. J. Coon, *Am. Rev. Biochem.* (1980) **49**, 315.
32. G. H. Loew and D. L. Harris, *Chem. Rev.* (2000) **100**, 407.
33. J. H. Dawson and K. S. Eble, *Adv. Inorg. Bioinorg. Mech.* (1986) **4**, 1.
34. R. Benhardt, *Rev. Physiol. Biochem. Pharmacol.* (1995) **127**, 137.
35. S. G. Sligar, *Biochemistry* (1976) **15**, 5399.
36. I. Schlichting, J. Berendzen, K. Chu, A. M. Stock, S. A. Maves, D. E. Benson, R. M. Sweet, D. Ringe, G. A. Petsko and S. G. Sligar, *Science* (2000) **287**, 1615.
37. J. J. Wilker, I. J. Dmochowski, J. H. Dawson, J. R. Winkler and H. B. Gray, *Angew. Chem. Int. Ed.* (1999) **38**, 90.
38. S. Adachi, S. Nagano, Y. Watanabe and I. Morishima, *Biochem. Biophys. Res. Commun.* (1991) **180**, 138.
39. S. Adachi, S. Nagano, K. Ishimori, Y. Watanabe, I. Morishima, T. Egawa, T. Kitagawa and R. Makino, *Biochemistry* (1993) **32**, 241.
40. E. L. Raven and A. G. Mauk, *Adv. Inorg. Chem.* (2001) **51**, 1.
41. T. L. Poulos, B. C. Finzel, I. C. Gunsalus, G. C. Wagner and J. Kraut, *J. Biol. Chem.* (1985) **260**, 16122.
42. H. B. Dunford, in *Heme Peroxidase*, (Wiley & Sons Inc.) 1999.
43. I. S. Isaac and J. H. Dawson, in *Essays in Biochemistry*, 1999, vol. 34.
44. S. Kimura and M. Ikeda-Saito, *Proteins* (1988) **3**, 113.

45. K. G. Welinder, *Curr. Opin. Struct. Biol.* (1992) **31**, 307.
46. D. J. Schuller, N. Ban, R. B. Van Huystee, A. McPherson and T. L. Poulos, *Structure* (1996) **4**, 311.
47. W. R. Patterson and T. L. Poulos, *Biochemistry* (1995) **34**, 4331.
48. N. Kunishima, K. Fukuyama and H. Matsubara, *J. Mol. Biol.* (1994) **235**, 331.
49. S. L. Edwards, R. Raag, H. Wariishi, H. M. Gold and T. L. Poulos, *Proc. Natl. Acad. Sci. USA* (1993) **90**, 750.
50. M. Sundaramoorthy, K. Kishi, M. H. Gold and T. L. Poulos, *J. Biol. Chem.* (1994) **235**, 331.
51. A. Henriksen, K. G. Welinder and M. Gajhede, *J. Biol. Chem.* (1998) **273**, 2241.
52. M. Gajhede, D. J. Schuller, A. Henriksen, A. T. Smith and T. L. Poulos, *Nature Struct. Biol.* (1997) **4**, 1032.
53. M. A. Ator and P. R. Ortiz de Montellano, *J. Biol. Chem.* (1987) **263**, 1542.
54. P. R. Ortiz de Montellano, *Ann. Rev. Pharm. Toxicol.* (1992) **32**, 89.
55. H. Wariishi, *J. Biol. Chem.* (1990) **265**, 11137.
56. T. K. Kirk and R. L. Farrell, *Ann. Rev. Microbiol.* (1987) **41**, 465.
57. P. J. Van Deurien, *Tetrahedron* (1997) **53**, 13183.
58. B. C. Finzel and T. L. Poulos, *J. Biol. Chem.* (1984) **259**, 13027.
59. B. C. Finzel, T. L. Poulos and J. Kraut, *J. Biol. Chem.* (1984) **259**, 3027.
60. M. Sivaraja, D. B. Goodin, M. Smith and B. M. Hoffman, *Science* (1989) **245**, 738.
61. T. L. Poulos, S. T. Freer, R. A. Alden, S. L. Edwards, U. Skogland, K. Takio, B. Eriksson, N. H. Xuong, T. Yonetani and J. Kraut, *Biochemistry* (1980) **255**, 575.
62. J. E. Erman and L. B. Vitello, *J. Biochem. Mol. Biol.* (1998) **31**, 307.
63. A. M. English and G. Tsapraili, *Adv. Inorg. Chem.* (1995) **43**, 79.
64. G. S. Kachalova, A. N. Popov and H. D. Bartunik, *Science* (1999) **284**, 473.
65. A. Ostermann, R. Waschipky, F. G. Parak and G. U. Neinhaus, *Nature* (2000) **404**, 205.
66. I. Schlichting, J. Berendzen, G. N. P. Jr and R. M. Sweet, *Nature* (1994) **371**, 808.
67. H. E. Aronson, W. E. Royer and W. A. Henrickson, *Protein Science* (1994) **3**, 1706.
68. G. A. Millikan, *Proc. R. Soc. London* (1937) **B123**, 218.
69. H. Theorell, *Biochem. Z* (1934) **268**, 73.
70. K. E. Conley and C. Jones, *Am. J. Physiol.* (1996) **271**, C2027.
71. B. A. Wittenberg, J. B. Wittenberg and P. R. Caldwell, *J. Biol. Chem.* (1975) **250**, 9038.

72. J. B. Wittenberg, *Physiol. Rev.* (1970) **50**, 559.
73. B. A. Wittenberg and J. B. Wittenberg, *Proc. Natl. Acad. Sci. USA* (1987) **84**, 7503.
74. S. G. Sligar, J. S. Olson and G. N. Phillips, *Chem. Rev.* (1994) **94**, 699.
75. M. L. Quillin, R. M. Arduini, J. S. Olson and G. N. Phillips, *J. Mol. Biol.* (1993) **234**, 140.
76. K. D. Egeberg, B. A. Springer, S. A. Martinis, S. G. Sligar, D. Morikis and P. M. Champion, *Biochemistry* (1990) **29**, 9783.
77. J. R. Christian, M. Unno, J. T. Sage, P. M. Champion, E. Chien and S. G. Sligar, *Biochemistry* (1997) **36**, 11198.
78. M. S. Hargrove, E. W. Singleton, M. L. Quillin, L. A. Ortiz, G. N. Phillips, J. S. Olson and A. J. Mathews, *J. Biol. Chem* (1994) **269**, 4207.
79. D. Morikis, P. M. Champion, B. A. Springer, K. D. Egeberg and S. G. Sligar, *J. Biol. Chem.* (1990) **265**, 12143.
80. S. Pin, B. Alpert, R. Cortes, I. Ascone, M. L. Chiu and S. G. Sligar, *Biochemistry* (1994) **33**, 11618.
81. R. Maurus, R. Bogumil, Y. Luo, H.-L. Tang, M. Smith, A. G. Mauk and G. D. Brayer, *J. Biol. Chem.* (1994) **269**, 12606.
82. S. V. Evans and G. D. Brayer, *J. Biol. Chem.* (1988) **263**, 4263.
83. L. J. Kagen, in *Myoglobin. Biochemical, Physiological and Clinical Aspects*, (Columbia Univ. Press) 1973, pp. 151.
84. H. Kubo, *Acta Phytochim.* (1939) **11**, 195.
85. R. Lemberg and J. W. Legge, in *Hematin Compounds and Bile Pigments*, (Interscience Publishers, New York) 1949, pp. 207.
86. D. Keilin and Y. L. Wang, *Nature* (1945) **155**, 227.
87. A. I. Virtanen, J. Jorma and T. Laine, *Suom. Kemisstil* (1945) **B18**, 49.
88. C. A. Appleby, J. Trewhella and P. E. Wright, *Biochim. Biophys. Acta* (1982) **700**, 171.
89. M. J. Davies, C. Mathieu and A. Puppo, *Adv. Inorg. Chem.* (1999) **46**, 495.
90. C. A. Appleby, in *The Biology of Nitrogen Fixation*, A. Quispel, Ed. (Elsevier, North Holland, Amsterdam) 1974, pp. 521.
91. M. J. Dilworth, *Meth. Enzymol.* (1980) **69**, 812.
92. C. A. Appleby, *Annual Review of Plant Physiology and Plant Molecular Biology* (1984) **35**, 443.

93. C. A. Appleby, N. A. Nicola, J. G. R. Hurrell and S. J. Leach, *Biochemistry* (1975) **14**, 4444.
94. W. J. Broughton, M. J. Dilworth and C. A. Goodfrey, *Biochem. J.* (1972) **127**, 309.
95. R. Arrendo-Peter, J. R. Moran, G. Sarath, P. Luan and R. V. Klucas, *Plant Physiol.* (1997) **114**, 493.
96. M. Richardson, M. J. Dilworth and M. J. Scawan, *FEBS Lett.* (1975) **51**, 33.
97. P. Lehtovaara and N. Ellfolk, *FEBS Lett.* (1974) **43**, 239.
98. Y. Jing, A. S. Paa and W. J. Brill, *Plant Sci. Lett.* (1982) **25**, 119.
99. G. G. Brown, J. S. Lee, N. Brisson and D. P. S. Verma, *J. Mol. Evol.* (1984) **21**, 19.
100. P. J. Ellis, C. A. Appleby, J. M. Guss, W. N. Hunter, D. L. Ollis and H. C. Freeman, *Acta Crystallographica Section D* (1997) **53**, 302.
101. D. L. Ollis, C. A. Appleby, P. M. Colman, A. E. Cutten, J. M. Guss, M. P. Venkatappa and H. C. Freeman, *Aust. J. Chem.* (1983) **36**, 451.
102. D. L. Ollis, P. E. Wright, J. M. Pope and C. A. Appleby, *Biochemistry* (1981) **20**, 587.
103. J. B. Wittenberg, C. A. Appleby and B. A. Wittenberg, *J. Biol. Chem.* (1971) **247**, 527.
104. E. H. Harutyunyan, T. N. Safonova, I. P. Kuranova, A. N. Popov, A. V. Teplyakov, G. V. Obmolova, A. A. Rusakov, B. K. Vainshtein, G. G. Dodson, J. C. Wilson and M. F. Perutz, *J. Mol. Biol.* (1995) **251**, 104.
105. C. A. Appleby, W. E. Blumberg, J. H. Bradbury, W. H. Fushman, J. Peisach, B. A. Wittenberg, J. B. Wittenberg and P. E. Wright, in *Hemoglobin and Oxygen Binding*, C. Ho, Ed. (Elsevier, North Holland, Amsterdam) 1982, pp. 435.
106. E. G. Arutyunyan, I. P. Kuranova, A. B. Tovbis, A. I. Grebenko, A. Voronova, Y. V. Nekrasov and B. K. Vainshtein, *Sov. Phys. Crystallogr.* (1980) **25**, 302.
107. C. A. Appleby, B. A. Wittenberg and J. B. Wittenberg, *Proc. Natl. Acad. Sci. USA* (1973) **70**, 564.
108. C. A. Appleby, B. A. Wittenberg and J. B. Wittenberg, *J. Biol. Chem.* (1973) **243**, 3183.
109. N. Ellfolk and G. Sievers, *Acta Chem. Scand.* (1967) **21**, 1457.
110. C. A. Appleby, W. E. Blumberg, J. Peisach, B. A. Wittenberg and J. B. Wittenberg, *J. Biol. Chem.* (1976) **251**, 6090.
111. R. N. Johnson, J. H. Bradbury and C. A. Appleby, *J. Biol. Chem.* (1978) **253**, 2148.
112. E. G. Arutyunyan, I. P. Kuranova, A. B. Tovbis, A. I. Grebenko, A. A. Voronova, Y. V. Nekrasov and B. K. Vainshtein, *Mol. Biol. (Moscow)* (1981) **15**, 27.

113. C. A. Appleby, J. H. Bradbury, M. R. J., B. A. Wittenberg, J. B. Wittenberg and P. E. Wright, *J. Biol. Chem.* (1983) **258**, 2254.
114. B. P. Atanasov, E. A. Dimitrova, N. N. Kudryavtseva, G. Y. Zhiznevskaya and C. A. Appleby, *Biochim. Biophys. Acta* (1989) **998**, 80.
115. J. Trewhella, P. E. Wright and C. A. Appleby, *Nature* (1979) **280**, 87.
116. J. Trewhella and P. E. Wright, *Biochim. Biophys. Acta* (1980) **625**, 202.
117. A. Ehrenberg and N. Ellfolk, *Acta Chem. Scand.* (1963) **17**, S343.
118. G. Sievers, P. M. A. Gadsby, J. Peterson and A. J. Thomson, *Biochim. Biophys. Acta* (1983) **742**, 637.
119. I. P. Kuranova, A. I. Grebenko, N. V. Konareva, I. F. Syromyatnikova and V. V. Barynin, *Biokhimiya* (1976) **1**, 1603.
120. C. A. Appleby and M. J. Dilworth, in *A Treatise on Dinitrogen Fixation*, A. Quispel, Ed. (Wiley, New York) 1979 and references therein.
121. E. J. Davidowitz, G. Creissen, E. Vincze, G. B. Kiss and N. Lang-Unnasch, *Plant Mol. Biol.* (1991) **16**, 161.
122. G. B. Kiss, Z. Vegh and E. Vincze, *Nucl. Acids. Res.* (1987) **15**, 3620.
123. M. Lobler and A. M. Hirsch, *Plant Mol. Biol.* (1992) **20**, 733.
124. P. Welters, B. A. Metz, J. Schell and F. J. De Bruijn, *Nucl. Acids Res.* (1989) **17**, 1253.
125. A. Konieczny, E. O. Jensen, K. A. Marcker and A. B. Legocki, *Mol. Biol. Reports* (1987) **12**, 61.
126. A. Konieczny, *Nucl. Acids Res.* (1987) **15**, 6742.
127. O. Wiborg, J. J. Hyldig-Nielson, E. O. Jensen, K. Paludan and K. A. Marcker, *Nucl. Acids. Res.* (1982) **10**, 3487.
128. J. J. Hyldig-Nielson, E. O. Jensen, K. Paludan, O. Wiborg, R. Garrett, P. Jorgensen and K. A. Marcker, *Nucl. Acids Res.* (1982) **10**, 689.
129. M. M. Sikorski, A. F. Topunov, P. M. Strozycki, C. E. Vorgias, K. S. Wilson and A. B. Legocki, *Plant Science* (1995) **108**, 109.
130. S. Prytulla, H. J. Dyson and P. E. Wright, *FEBS Lett.* (1996) **399**, 283.
131. M. S. Hargrove, J. K. Barry, E. A. Brucker, M. B. Berry, G. N. Phillips, J. S. Olson, P. R. Arredondo, J. M. Dean, R. V. Klucas and G. Sarath, *J. Mol. Biol.* (1997) **266**, 1032.
132. D. K. Jones, R. Badii, F. I. Rosell and E. Lloyd, *Biochem. J.* (1998) **330**, 983.
133. N. Patel, D. K. Jones and E. L. Raven, *Eur. J. Biochem.* (2000) **267**, 2581.

134. B. A. Springer, K. D. Egeberg, S. G. Sligar, R. J. Rohlfs, A. J. Mathews and J. S. Olson, *J. Biol. Chem.* (1989) **264**, 3057.
135. D. K. Jones, N. Patel and E. L. Raven, *Arch. Biochem. Biophys.* (2002) **400**, 111.

# **Chapter 2**

## **Investigation of the Nicotinate Binding Process in Leghaemoglobin: Role of the Active Site Residues**

## 2 Investigation of the Nicotinate Binding Process in Leghaemoglobin: Role of the Active Site Residues

### 2.1 Introduction

The physiologically significant ligand-binding interaction between nicotinate and the haem of leghaemoglobin (Lb), Figure 2.1, was first identified in 1973.<sup>[1]</sup> The high affinity that the protein displayed for the nicotinate ligand was particularly interesting and had attracted increasing attention, since the interaction of a strong ligand with the haem was likely to affect the ability of the molecule to bind dioxygen in an efficient manner. As a result, the binding interaction between the protein and nicotinate was believed to have direct functional consequences. The strong nicotinate-Lb interaction lowered the overall affinity of the protein<sup>[1]</sup> for oxygen and as a consequence a physiological role for nicotinate as an oxygen-regulator within the root nodules of the plant was predicted.

X-ray crystallographic (for soybean<sup>[2-3]</sup> and lupin<sup>[4]</sup>) and spectroscopic<sup>[5]</sup> data have since confirmed that the deprotonated pyridine nitrogen of nicotinic acid provides the sixth axial ligand to the haem of Lb. In addition, data for Lb have implicated the participation of the carboxylic anion of the bound ligand in hydrogen-bonding interactions with the active site residues histidine 61 and tyrosine 30, Figure 2.1. Structural identification of the hydrogen-bonding interactions within the active site provided important information since these hydrogen-bonding residues were likely to be influential in controlling the ability of the protein to bind nicotinate. Complementary *quantitative* evidence from other sources on the exact thermodynamic contribution of each residue to the binding process has not been forthcoming until recently.

The availability of an efficient expression system for recombinant Lb (rLb)<sup>[6]</sup> for the generation of site-directed variants has allowed the dissection of the Lb-nicotinate binding interaction in more detail than has been previously possible. The relative contributions of the protein-ligand interactions<sup>[7]</sup> that provide hydrogen-bonding stabilisation to nicotinate have previously been examined by mutagenic replacement of the distal histidine 61 and tyrosine 30 residues with alanine (His61Ala and Tyr30Ala, respectively). These alterations effectively removed consecutive hydrogen-bonding interaction to the bound nicotinate and thermodynamic data for the two variants revealed that both hydrogen bonds from histidine 61 and tyrosine 30 are important in the binding process.<sup>[7]</sup>

An additional feature of the nicotinate-Lb interaction was the influence of pH.<sup>[8]</sup> The residues thought to govern the pH-dependent nicotinate binding process have been the subject

of great interest.<sup>[8-12]</sup> Although the distal histidine 61 was assigned as controlling the pH-dependent nicotinate binding process in Lb under neutral to alkaline conditions, the exact value of the  $pK_a$  for the distal histidine had been a matter of continuing confusion in literature.<sup>[8-12]</sup> The definitive assignment of the distal histidine 61 as controlling the pH-dependent nicotinate binding process in Lb under neutral to alkaline conditions was later confirmed through equilibrium binding studies of rLb, His61Ala and Tyr30Ala with unambiguous assignment for the  $pK_a$  of His61 (6.9 and 6.7 for rLb and Tyr30Ala, respectively).<sup>[7]</sup>

An additional titration process, in the acidic region, has also been reported to affect nicotinate binding.<sup>[1, 8]</sup> This process has been variously assigned as arising from titration of the ring nitrogen of nicotinate itself,<sup>[1]</sup> either of the haem propionate groups<sup>[5, 12, 13]</sup> or a glutamic acid residue located close to the haem.<sup>[8]</sup> A clue to the likely identity of the titrating residue in Lb, which has been proposed to act as an electrostatic ‘gate’ for ligand binding,<sup>[1, 13]</sup> was provided by comparisons with the nicotinate binding interaction in kidney bean Lb, which is pH-dependent,<sup>[8]</sup> and in lupin Lb, which is pH-independent.<sup>[14]</sup> Examination of the crystal structure of Lb<sup>[2]</sup> identifies a glutamic acid residue at position 63 which, from sequence comparisons, is also known to be present in kidney bean Lb<sup>[15]</sup> but which is replaced by a non-titratable glycine residue in lupin Lb.<sup>[4, 16, 17]</sup>

This Chapter focuses on extending the pH-dependent analysis of the binding process of nicotinate in rLb. Two separate approaches have been employed. The first aim was to address the hydrogen-bonding stabilisation of nicotinate in the active site of Lb by examining the combined roles played by the active site residues, histidine 61 and tyrosine 30. The objective here was to replace the two residues with alanine to generate the double variant His61Ala/Tyr30Ala, effectively removing the hydrogen-bonding network to the haem-bound nicotinate. The second aim was to address the pH-dependent binding of nicotinate in rLb, in the acidic region, in order to identify the exact role of glutamic acid 63, Figure 2.1. A site-directed variant of rLb has been generated in which the glutamic acid 63 residue has been replaced with the isostructural and non-titratable leucine residue (Glu63Leu). Taken together with previous pH-dependent binding data in the neutral to alkaline region (see above),<sup>[7]</sup> the aim of this work is to fully describe the pH-dependent interaction between Lb and nicotinate.



## 2.2 Mutagenesis of rLb, Protein Expression, Isolation and Purification

The rLb DNA was obtained from Dr D K Jones (University of Leicester) and was the starting point for mutagenesis and protein isolation. Generation of His61Ala/Tyr30Ala was achieved by site-directed mutagenesis according to the QuikChange protocol, using the recombinant His61Ala rLb DNA and the Tyr30Ala mutagenic oligonucleotide (See Chapter 7, Section 7.2). Expression and purification of rLb and His61Ala/Tyr30Ala were conducted as described in Chapter 7, Section 7.1.7. The rLb protein was obtained as a haem-containing protein; however, His61Ala/Tyr30Ala was acquired in the apo-form. Reconstitution of apo-His61Ala/Tyr30Ala and rLb, to form holoprotein, was achieved by addition of a small excess of exogenous haem (Sigma) to both proteins and the excess haem removed by gel filtration (Sephadex G50). Samples of rLb and His61Ala/Tyr30Ala were obtained with  $R_z$  values of  $> 4$  and were comparable to those observed for Lb ( $R_z$  values of  $> 4$ ).<sup>[18]</sup> The samples obtained in this work were considered pure and migrated as a single band on the SDS PAGE gel (Chapter 7, Figure 7.2). Yields of  $\sim 10$  mg and  $\sim 8$  mg of purified protein per litre were obtained for rLb and His61Ala/Tyr30Ala, respectively.

## 2.3 Results

### 2.3.1 Hydrogen-Bonding Investigations

#### 2.3.1.1 Electronic Absorption Spectra of rLb and His61Ala/Tyr30Ala

The electronic absorption spectra of rLb and His61Ala/Tyr30Ala were recorded, Figure 2.2, following purification. Comparison with previously published spectra for rLb and Lb revealed that the spectroscopic features of rLb isolated in this work were in agreement with published data.<sup>[6, 18, 19]</sup> Characteristic six-coordinate, high-spin transitions ( $\lambda_{\max} = 403, 495$  and  $626$  nm) and six-coordinate, low-spin transitions ( $\lambda_{\max} = 530$  and  $560$  nm) were apparent and analogous to those previously published for rLb ( $\lambda_{\max} = 403, 495, 530, 560$  and  $626$  nm).<sup>[6]</sup> For Lb and rLb, the high- and low-spin species were assigned as arising from a six-coordinate, water-bound haem derivative and from coordination of the distal histidine 61 residue to the haem,<sup>[6, 18, 19]</sup> respectively.

Analysis of the electronic absorption spectrum of His61Ala/Tyr30Ala, Figure 2.2, revealed characteristic six-coordinate, high-spin transitions ( $\lambda_{\max} = 402, 499$  and  $631$  nm)

analogous to those found for His61Ala (Chapter 3) and rLb. These transitions dominated the electronic spectrum for His61Ala/Tyr30Ala in contrast to rLb, which also show significant low-spin character. A minority contribution from a low-spin haem species was also apparent in His61Ala/Tyr30Ala ( $\lambda_{\text{max}} = \sim 536$  and  $\sim 574.5$  nm). The high-spin transitions for His61Ala/Tyr30Ala were assigned to six-coordinate, water-bound haem, as for rLb. The minority low-spin transitions observed for His61Ala/Tyr30Ala were assigned to hydroxide-bound haem.

Molar absorption coefficients for rLb and His61Ala/Tyr30Ala were determined as an average of two haem contents using the pyridine haemochromagen method<sup>[20]</sup> (Chapter 7, Section 7.2.2). Values of  $\epsilon_{403} = 157 \text{ mM}^{-1}\text{cm}^{-1}$ <sup>[6]</sup> and  $\epsilon_{402} = 137 \text{ mM}^{-1}\text{cm}^{-1}$  were determined for rLb and His61Ala/Tyr30Ala, respectively. The calculated molar absorption coefficient for rLb in this work was consistent with previously published values<sup>[6]</sup> and has been used to calculate the haem-based concentrations reported throughout this thesis.

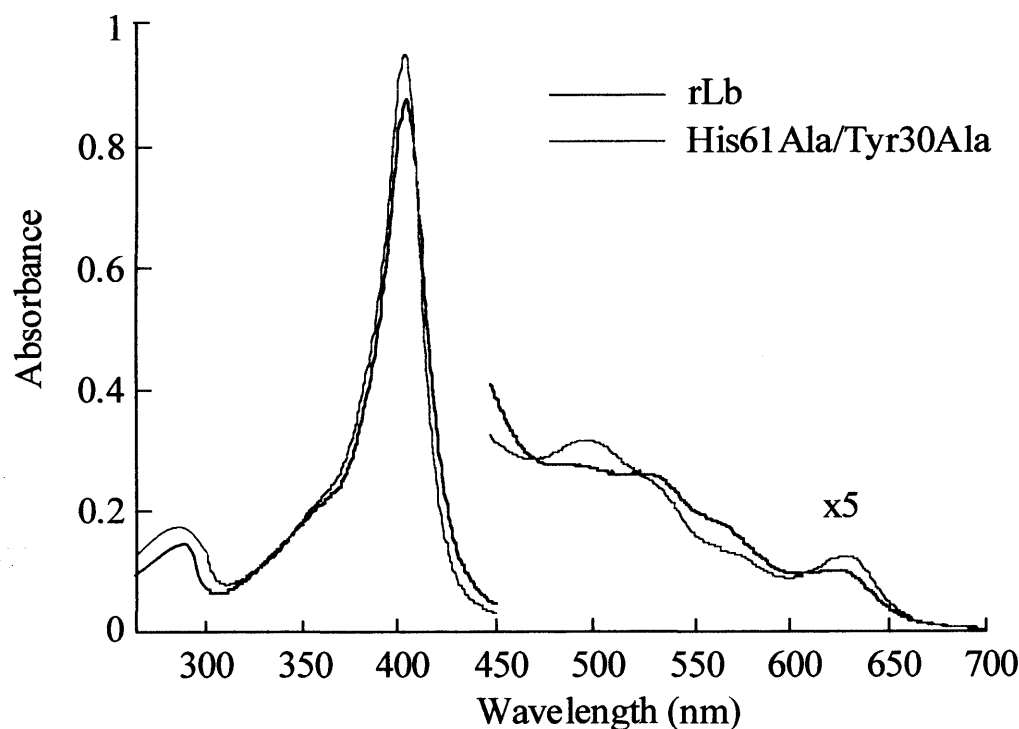


**Figure 2.2.** Electronic absorption spectra of ferric rLb and ferric His61Ala/Tyr30Ala. Absorbance values in the visible region (450-700 nm) have been multiplied by a factor of five. Conditions: sodium phosphate, pH 7.0,  $\mu = 0.10 \text{ M}$ ,  $25.0 \text{ }^\circ\text{C}$ .

### 2.3.1.2 Binding of Anionic Ligands to rLb and His61Ala/Tyr30Ala

The simplest of all haem protein reactions are those involving iron-centred ligand (X) binding, Equation [2.1].



Figure 2.3 shows a series of ferric anionic ligand-bound derivatives of rLb and His61Ala/Tyr30Ala. Absorption maxima and corresponding millimolar absorption coefficients for the various ferric and ferrous anionic derivatives of rLb and His61Ala/Tyr30Ala are presented in Table 2.1. Wavelength maxima for rLb found in this work were consistent with those previously published for rLb and Lb.<sup>[6, 18, 19]</sup> The spectra for the cyanide derivatives of rLb and His61Ala/Tyr30Ala were consistent with the formation of a six-coordinate, low-spin species with apparent red-shift of the Soret band and disappearance of the CT<sub>1</sub> band in the visible region. Binding of fluoride resulted in the formation of a six-coordinate, high-spin species with a slight blue-shift of the Soret band and the appearance of the CT<sub>1</sub> band (~600 nm) indicative of high-spin haem.

### 2.3.1.3 Acid-Alkaline Transition of rLb and His61Ala/Tyr30Ala

A series of spectrophotometric pH titrations were conducted on rLb and His61Ala/Tyr30Ala, with the aim of establishing the pK<sub>a</sub> of the distal water molecule. Titrations were conducted as described in Chapter 7, Section 7.2.5. Data for His61Ala/Tyr30Ala were acquired between pH 5.1 and pH 9.0<sup>a</sup>, Figure 2.4(A). Data for rLb were recorded between pH 6.2 and 9.9, Figure 2.4(B). Isobestic points at λ = 406, 470, 539 and 615 nm for rLb and λ = 410, 470, 535 and 610 nm for His61Ala/Tyr30Ala, dominated the pH-dependent equilibrium, indicating titration of one species.

The titration behaviour of rLb was similar to that previously reported for Lb and rLb,<sup>[6, 21, 22]</sup> Figure 2.4(B). A similar trend was also observed for His61Ala/Tyr30Ala, Figure 2.4(A). As the pH was raised, titration of the distal water molecule and subsequent formation of a hydroxide-bound derivative (λ = 408.5, 539 and 570 nm for rLb and λ = 406, 537 and 574 nm for His61Ala/Tyr30Ala) was observed, Equation [2.2].

<sup>a</sup> (acid denaturation below pH 5 and alkaline denaturation above pH 9 only permitted readings between pHs 5-9)

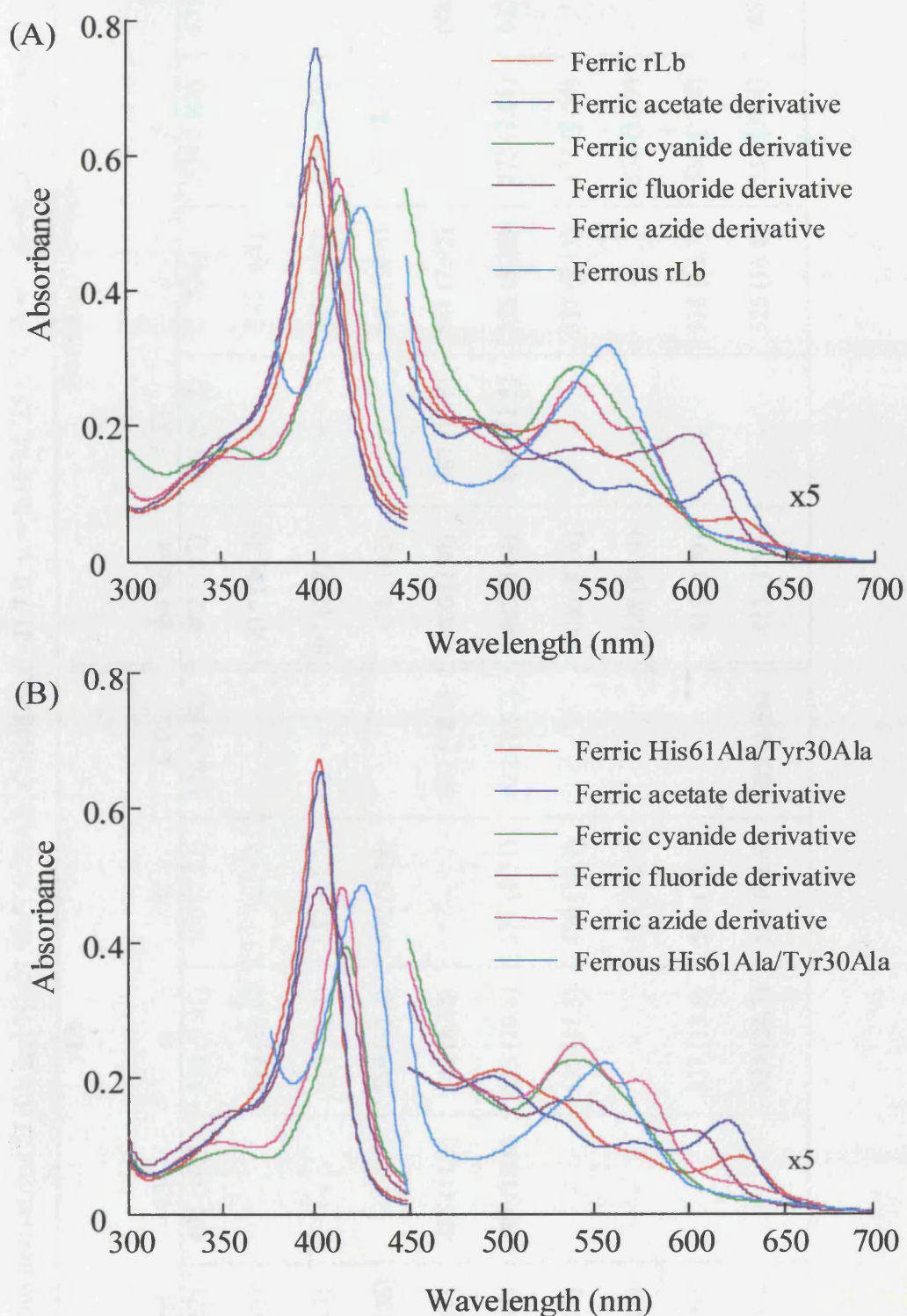


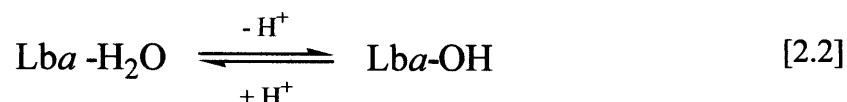
**Figure 2.3.** Electronic absorption spectra of ferric, ferrous and the ferric anionic ligand-bound derivatives of (A) rLb and (B) His61Ala/Tyr30Ala at 298 K. Conditions: sodium phosphate, pH 7.0,  $\mu = 0.10$  M, 25.0 °C

**Table 2.1.**

Wavelength maxima (nm) and, in parentheses, absorption coefficients ( $\text{mM}^{-1}\text{cm}^{-1}$ ) for the ferric and ferrous derivatives of rLb and His61Ala/Tyr30Ala. Conditions: pH 7.0,  $\mu = 0.10$  M, 25.0 °C. Nic = nicotinate, sh = shoulder.

Derivative	rLb					His61Ala/Tyr30Ala				
	( $\gamma$ ) Soret	CT <sub>2</sub>	$\alpha$	$\beta$	CT <sub>1</sub>	( $\gamma$ ) Soret	CT <sub>2</sub>	$\alpha$	$\beta$	CT <sub>1</sub>
Fe(III)	403 (157)	495 (10.7)	530 (9.91)	560 (7.13)	626 (4.92)	402 (137)	499 (9.12)	536	574.5 (sh)	631 (3.91)
Fe(III)-CN <sup>-</sup>	415 (117)	-	539 (11.9)	-	-	417 (84.4)	-	540 (9.8)	-	-
Fe(III)-Nic	407 (123)	-	529 (13.4)	557 (11.2)	-	407 (117)	-	530 (6.20)	562 (4.43)	-
Fe(III)-N <sub>3</sub> <sup>-</sup>	413.5 (126)	-	549 (12.4)	572 (9.36)	-	415 (102)	-	542 (10.6)	574 (8.1)	-
Fe(III)-F <sup>-</sup>	401 (149)	484 (11.1)	540 (8.88)	-	601 (10.0)	400 (150)	487 (13.2)	541 (7.92)	-	606 (9.86)
<sup>1</sup> Fe(III)-OAc <sup>-</sup>	403 (236)	497 (13.9)	533 (10.8)	571 (8.71)	622 (9.02)	403 (169)	494 (11.5)	535 (8.28)	572 (7.05)	622 (8.02)
Fe(III)-OH <sup>-</sup>	409 (117)	-	539 (11.3)	570 (10.1)	-	406 (83.6)	-	537 (7.11)	574 (6.54)	-
Fe(II)	427 (111)	-	-	555 (13.3)	-	428 (90.4)	-	-	558 (12.9)	-
Fe(II)-CO	415 (199)	-	537 (13.6)	561 (12.7)	-	419 (170)	-	538 (12.7)	567 (11.8)	-
Fe(II)-Nic	418 (230)	-	524 (24.7)	554 (44.6)	685 (2.56)	417 (170)	-	525 (16.4)	554 (39.4)	687 (2.3)

<sup>1</sup> Fe(III)-OAc<sup>-</sup> for Lb  $\lambda_{\text{max}} = 403, 496, 570$  and  $622$  nm.<sup>[19]</sup>



A fit of the data to the Henderson-Hasselbach equation (Chapter 7, Equation [7.7]) for a single  $pK_a$ , single proton process, yielded  $pK_a$  values of  $8.3 \pm 0.1$  for rLb (similar to previously published values ( $pK_a$  of 8.3)<sup>[6, 21, 22]</sup>) and  $8.4 \pm 0.1$  for His61Ala/Tyr30Ala.

#### 2.3.1.4 Investigation of Nicotinate Binding

Spectroscopic investigation of ligand binding equilibria of the variants of rLb provides an appropriate method to *qualitatively* assess the active site of the recombinant haem protein. Work presented in this section investigates the nicotinate binding characteristics of His61Ala/Tyr30Ala. The main objective was to understand the ability of His61Ala/Tyr30Ala to bind nicotinate and was achieved through measurement of the thermodynamic, equilibrium dissociation constant,  $K_d$ . Results were compared to those obtained previously for rLb, His61Ala and Tyr30Ala.<sup>[7]</sup> Hence, the importance of the hydrogen-bonding residues, histidine 61 and tyrosine 30, in their role to stabilise nicotinate binding, in the active site of Lb, was elucidated.

Equilibrium nicotinate binding dissociation constants for His61Ala/Tyr30Ala, Figure 2.5, were calculated from a fit of the spectrophotometric titration data to Equation [7.3], Chapter 7. Ligand binding data revealed that replacement of both distal histidine 61 and tyrosine 30 (and in effect removal of the hydrogen bonds to nicotinate) resulted in a decrease in affinity of the variant protein for nicotinate. An average value for the dissociation constant,  $K_d$ , of  $32 \pm 1 \mu\text{M}$  was obtained for His61Ala/Tyr30Ala. This value compares to the  $K_d$  values of  $1.4 \mu\text{M}$ ,  $19 \mu\text{M}$  and  $11 \mu\text{M}$  for rLb, His61Ala and Tyr30Ala, respectively,<sup>[7]</sup> and indicates that the effect of the double mutation was effectively additive when compared to the single mutations.

#### 2.3.2 pH-Dependent Nicotinate Binding

As mentioned earlier, the binding of the physiological ligand, nicotinate to Lb is a pH-dependent process. It has been previously shown that the active site residue, histidine 61 of Lb was the residue responsible for regulating nicotinate binding in the neutral to alkaline

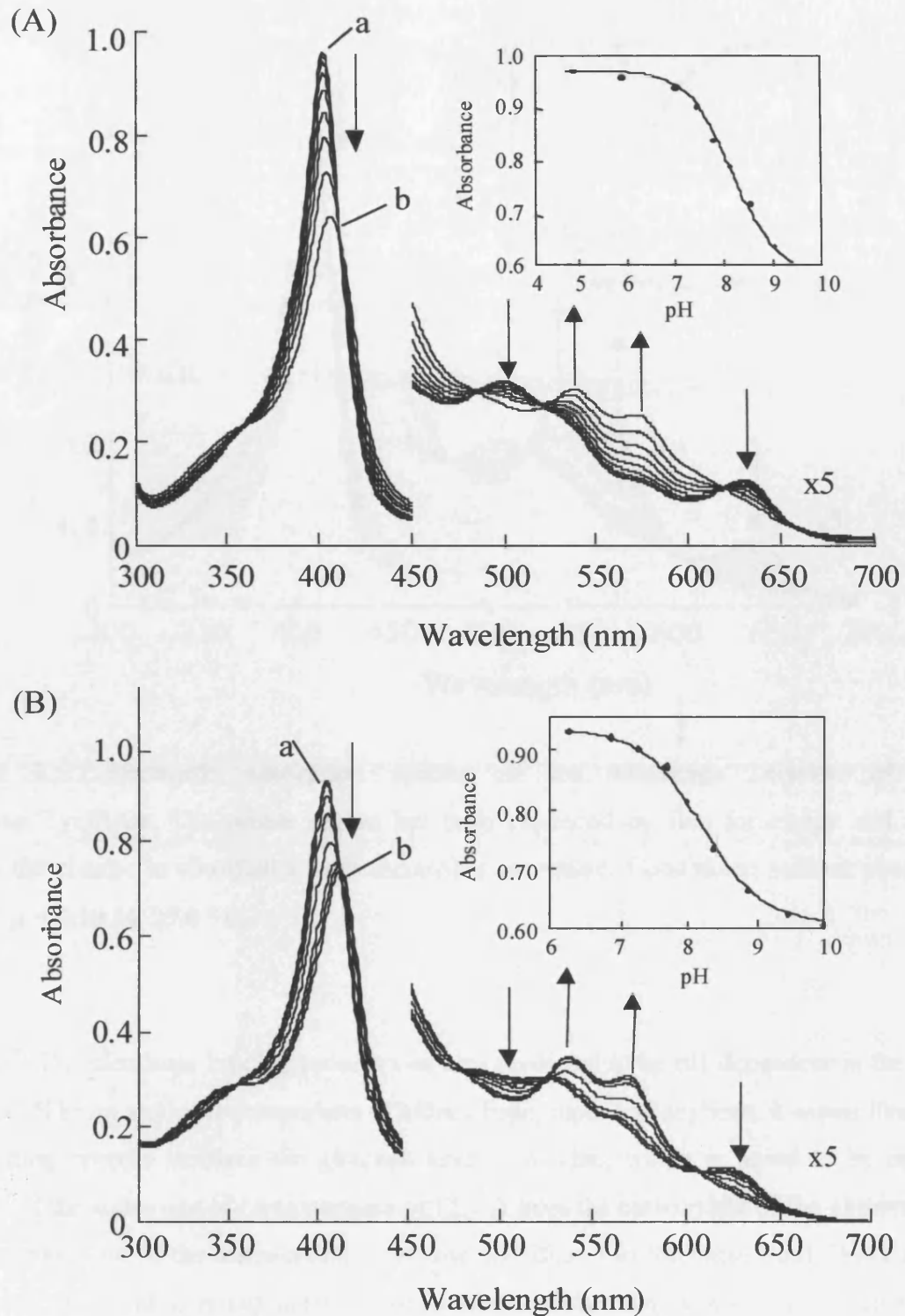


**Figure 2.4.** Spectrophotometric pH titration of (A) ferric His61Ala/Tyr30Ala: (a) 5.1, (b) 9.0 and intermediate pHs 6.0, 7.0, 7.3, 7.8, 8.1 and 8.8 and (B) ferric rLb: (a) pH 6.2, (b) pH 9.9 and intermediate pHs 6.8, 7.2, 7.6, 8.3, 8.8 and 9.4. Arrows indicate the direction of change in absorbance with pH. Inset: plot of variation in absorbance, at 403 nm for rLb and 402.5 nm for His61Ala/Tyr30Ala, with pH. The solid line represents a non-linear squares fit to Equation [7.7]. Conditions: mixed sulphonic acid buffer, 25.0 °C.

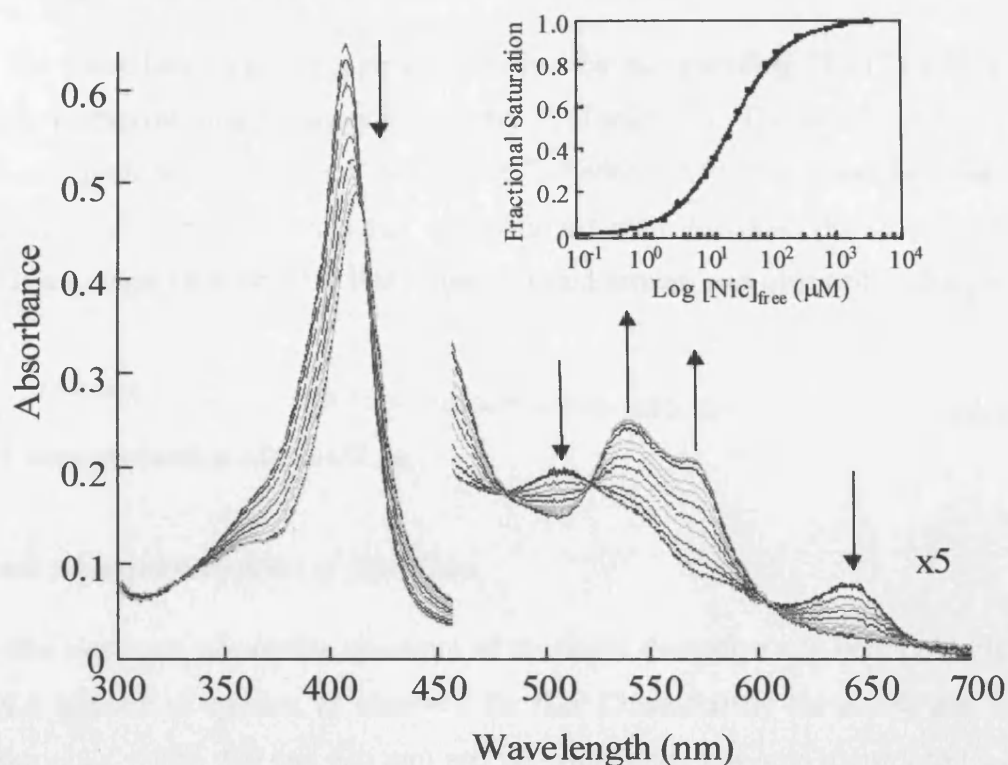


**Figure 2.5.** Electronic absorption spectra of the nicotinate titration of ferric His61Ala/Tyr30Ala. The visible region has been expanded by five for clarity and arrows denote the change in absorbance with increasing nicotinate. Conditions: sodium phosphate, pH 5.5  $\mu = 0.10$  M, 25.0 °C.

region.<sup>[7]</sup> The nicotinate binding process was also predicted to be pH-dependent in the acidic region.<sup>[1, 8]</sup> From sequence comparison of kidney bean, lupin and soybean, it seems likely that the binding process involves the glutamic acid 63 residue, which is found to be near the vicinity of the active site of Lb (a distance of 12.7 Å from the carboxylate of the glutamic acid to the carboxylate of the haem-bound nicotinate and 16.3 Å to the haem iron). Work carried out in this section aims to provide a detailed analysis of the nicotinate binding process in the acidic region, with clarification of the role of glutamic acid 63. A new variant, Glu63Leu has been generated and characterised. With the aid of equilibrium binding and nuclear magnetic resonance (NMR) spectroscopy, the nicotinate binding process in the acidic, as well as the neutral to alkaline region, has been investigated and compared to binding data for rLb.

### 2.3.2.1 Mutagenesis, Isolation and Purification of Glu63Leu

The Glu63Leu variant was generated using the rLb encoding PET11a vector and the Glu63Leu mutagenic oligonucleotide (Chapter 7, Table 7.1). The variant was expressed, isolated and purified as described in Chapter 7, Section 7.7. The Glu63Leu variant was isolated as holoprotein as for rLb and was obtained with  $A_{403}/A_{280}$  ( $R_z$  value) of  $> 4$  and migrated as a single band on SDS PAGE gel. Purified protein was obtained with a yield of  $\sim 8$  mg/l.

### 2.3.2.2 Characterisation of Glu63Leu

#### *Electronic Absorption Spectra of Glu63Leu*

The electronic absorption spectrum of the ferric derivative of Glu63Leu, Figure 2.6, revealed a mixture of species, as observed for rLb. Characteristic six-coordinate, high-spin transitions ( $\lambda_{\max} = 403, 499$  and  $626$  nm) and six-coordinate, low-spin transitions ( $\lambda_{\max} = 534$  and  $573$  nm) were apparent and were analogous to those observed for rLb ( $\lambda_{\max} = 403, 495, 530, 560$  and  $626$  nm).<sup>[6]</sup> As for rLb,<sup>[6, 18, 19]</sup> the high- and low-spin species for Glu63Leu were assigned as arising from six-coordinate, water-bound haem and histidine-bound haem, respectively.

The molar absorption coefficient for Glu63Leu was determined from the haem content of the variant protein, using the pyridine haemochromagen method<sup>[20]</sup> (Chapter 7, Section 7.2.2). A value of  $\epsilon_{403} = 153 \text{ mM}^{-1}\text{cm}^{-1}$  was determined for Glu63Leu, consistent with a six-coordinate haem species and was used to calculate the haem-based protein concentrations reported throughout this thesis.

#### *Anionic Ligand Binding*

Spectra for the ferric anionic ligand-bound derivatives of Glu63Leu, Figure 2.7, revealed that the variant behaved in a similar manner to rLb. Formation of a low-spin haem species, on binding cyanide, and formation of a high-spin haem species, on binding fluoride, was apparent and consistent with expected ligand-binding behaviour. Absorption maxima and the corresponding absorption coefficients for the various ferric and ferrous derivatives are shown in Table 2.2, illustrating that Glu63Leu readily binds exogenous ligands at the haem iron in both the ferric and ferrous oxidation states.

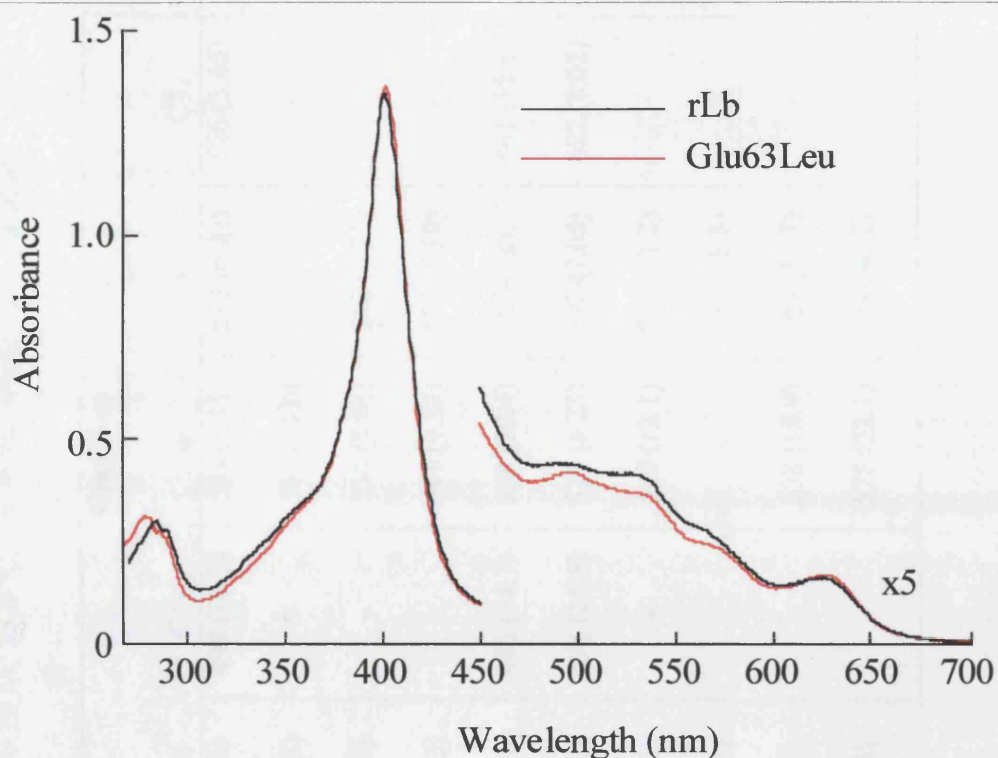


**Figure 2.6.** Electronic absorption spectra of ferric rLb and ferric Glu63Leu. Absorbance values in the visible region (450 – 700 nm) have been multiplied by a factor of five. Conditions: sodium phosphate, pH 7.0,  $\mu = 0.10$  M, 25.0 °C.

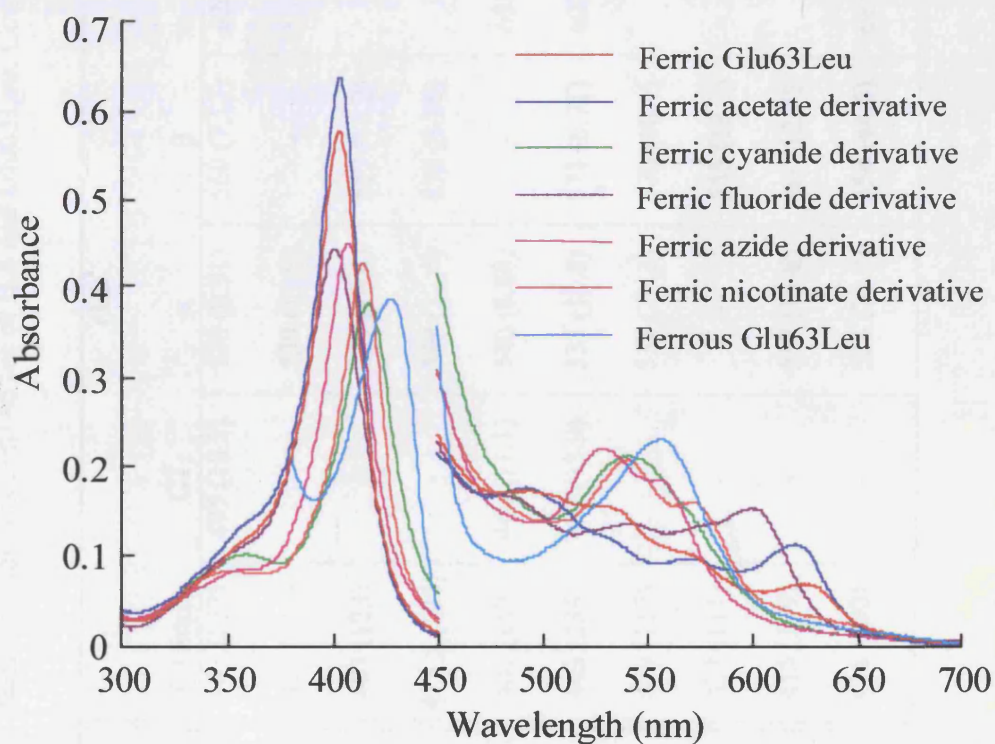


**Figure 2.7.** Electronic absorption spectrum of ferric, ferrous and the ferric anionic derivatives of Glu63Leu. Conditions: sodium phosphate, pH 7.0,  $\mu = 0.10$  M, 25.0 °C.

**Table 2.2**  
Wavelength maxima (nm) and, in parentheses, absorption coefficients ( $\text{mM}^{-1}\text{cm}^{-1}$ ) for the  
ferric and ferrous derivatives of rLb and Glu63Leu. Conditions: pH 7.0,  $\mu = 0.10 \text{ M}$ ,  $25.0 \text{ }^\circ\text{C}$ . Nic = nicotinate, sh = shoulder.

Derivative	rLb					Glu63Leu				
	( $\gamma$ ) Soret	CT <sub>2</sub>	$\alpha$	$\beta$	CT <sub>1</sub>	( $\gamma$ ) Soret	CT <sub>2</sub>	$\alpha$	$\beta$	CT <sub>1</sub>
Fe(III)	403 (157)	495 (10.7)	530 (9.91)	560 (7.13)	626 (4.92)	403 (153)	499 (10.1)	534 (8.21)	573 (6.02)	626 (3.65)
Fe(III)-CN <sup>-</sup>	415 (117)	-	539 (11.9)	-	-	416 (58.3)	-	541 (13.0)	-	-
Fe(III)-Nic	407 (123)	-	529 (13.4)	557 (11.2)	-	407 (143)	-	530 (8.01)	562 (6.22)	-
Fe(III)-N <sub>3</sub> <sup>-</sup>	413.5 (126)	-	549 (12.4)	572 (9.36)	-	415 (83.3)	-	541 (9.17)	579 (7.30)	-
Fe(III)-F <sup>-</sup>	401 (149)	484 (11.1)	540 (8.88)	-	601 (10.0)	401 (179)	486 (24.1)	538 (20.4)	574 (sh)	601 (18.6)
Fe(III)-OAc <sup>-</sup>	403 (236)	497 (13.9)	533 (10.8)	571 (8.71)	622 (9.02)	403 (169)	494 (11.5)	535 (8.28)	572 (7.05)	622 (8.02)
Fe(III)-OH <sup>-</sup>	409 (117)	-	539 (11.3)	570 (10.1)	-	412 (135)	-	540 (12.1)	573 (11.2)	-
Fe(II)	427 (111)	-	-	555 (13.3)	-	428 (113)	-	-	558 (15.5)	-
Fe(II)-CO	415 (199)	-	537 (13.6)	61 (12.7)	-	415 (177)	-	538 (15.9)	563 (14.7)	-
Fe(II)-Nic	418 (230)	-	524 (24.7)	554 (44.6)	685 (2.56)	418 (213)	-	525 (22.7)	554 (40.2)	-

**pH Titration**

Spectrophotometric titrations were carried out on Glu63Leu using the same procedure as for rLb. Titration of the 'acidic' protein to the 'alkaline' form was conducted by careful addition of 0.1M NaOH. The spectrophotometric shifts observed, Figure 2.8, were consistent with the formation of an iron-hydroxide species ( $\lambda_{\max} = 412, 540, 573 \text{ nm}$ ) at alkaline pH, essentially the same as for rLb. A fit of these data, in the pH range 6.9 – 9.8, to Equation [7.7] yielded a  $pK_a$  of  $8.3 \pm 0.2$ , similar to that observed for rLb ( $pK_a = 8.3$ ).<sup>[6]</sup> Isobestic points at  $\lambda = 410, 470, 539$  and  $607 \text{ nm}$ , for Glu63Leu, confirmed titration of a single species, which dominated the pH-dependent equilibrium. These data were consistent with the deprotonation of the haem-bound water molecule to form a six-coordinate, hydroxide-bound species as the pH was increased.

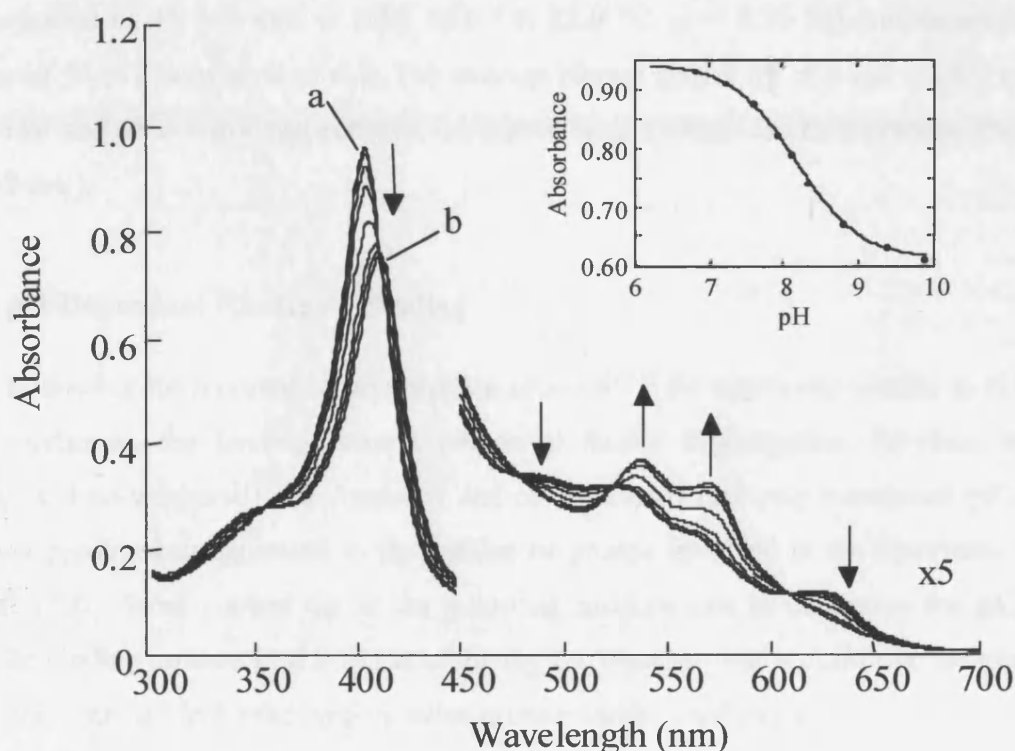


**Figure 2.8.** Spectrophotometric pH titration of ferric Glu63Leu at (a) pH 6.9, (b) pH 9.8 and intermediate pHs 7.2, 7.7, 7.0, 8.1, 8.4, 8.9, 9.5. Arrows denote the direction of change in absorbance with pH. Inset: plot of the variation in absorbance at 403 nm with pH. The solid line represents a non-linear least squares fit to Equation [7.7]. Conditions: sodium phosphate, pH 6.99,  $\mu = 0.10 \text{ M}$ ,  $25.0 \text{ }^\circ\text{C}$ .

### ***Spectroelectrochemistry***

The mid-point potentials of both rLb and Glu63Leu were measured using procedures described in Chapter 7, Section 7.2.7. Application of a potential of  $-500$  mV vs SCE across the cell reduced the ferric protein to ferrous. The reduction process was monitored by changes in absorption at the Soret wavelength. Re-oxidation of the reduced protein was effected by incremental increase in potential (typically 50 mV increments). Complete oxidation of the protein was achieved by application of a potential of  $+200$  mV vs SCE to the protein solution.

Spectroelectrochemical titration spectra for rLb and Glu63Leu as a function of applied potential are shown in Figures 2.9(A) and 2.9(B), respectively, together with their corresponding Nernst plots (inset). Determination of the ferric-ferrous mid-point potential of the two proteins was conducted by fitting data to the Nernst equation (Equation [7.9], Chapter 7). A mid-point potential of  $21 \pm 2$  mV vs SHE (pH 7.0, 25.0 °C,  $\mu = 0.10$  M) for rLb was determined and was in agreement with published values for Lb.<sup>[23]</sup> For Glu63Leu, a mid-point potential of  $45 \pm 2$  mV vs SHE (pH 7.0, 25.0 °C,  $\mu = 0.10$  M) was determined, an increase of 24 mV compared to rLb. The average Nernst slopes for rLb and Glu63Leu, were  $70 \pm 1$  mV and  $65 \pm 1$  mV respectively, consistent with a single electron process (theoretical value 59 mV).

#### **2.3.2.3 pH-Dependent Nicotinate Binding**

Following the reported second titration process<sup>[1, 8]</sup> for nicotinate binding to rLb under acidic conditions, the binding process warranted further investigation. Previous work by Appleby and co-workers<sup>[1]</sup> and Atanosov and co-workers<sup>[8]</sup> had only mentioned  $pK_a$  values, with only predicted assignments to the residue or groups involved in the nicotinate binding process in Lb. Work carried out in the following sections aim to determine the  $pK_a$  of the nicotinate binding process in rLb in the acidic region, together with a definitive assignment of the residue responsible for the binding process under acidic conditions.

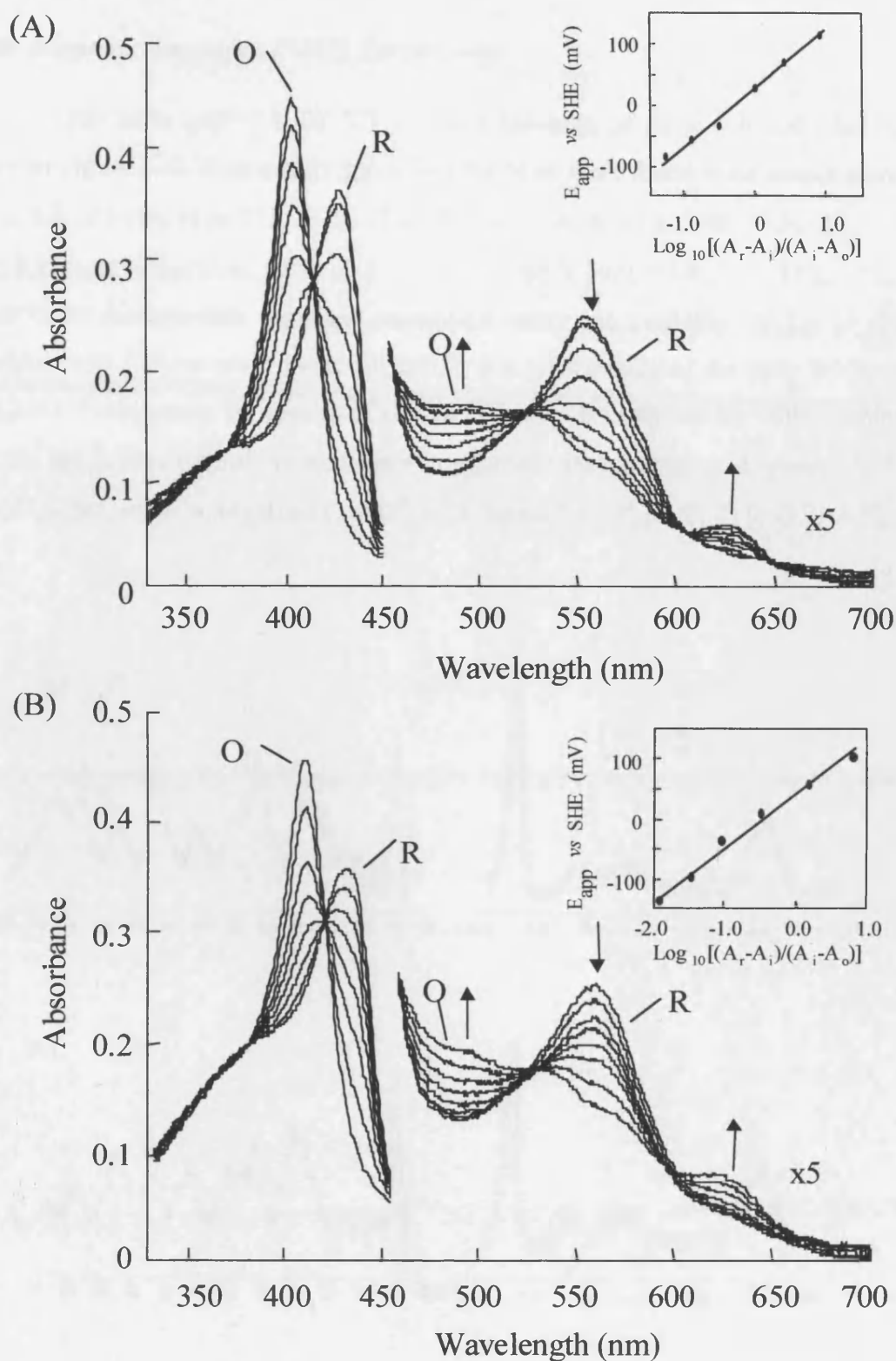


**Figure 2.9.** Thin-layer spectroelectrochemical spectra for (A) rLb and (B) Glu63Leu at various applied potentials,  $E_{app}$  (mV). Fully oxidised (O) and fully reduced (R) spectra for each derivative are indicated. The inset shows a fit of the absorbance data at 403 nm to the Nernst equation. Absorbance values in the visible region (450-700 nm) have been multiplied by a factor of five. Conditions: sodium phosphate, pH 7.0,  $\mu = 0.10$  M, 25.0 °C.

**Nuclear Magnetic Resonance (NMR) Spectroscopy**

The 300 MHz (pH\* 7.0, 25 °C)  $^1\text{H}$ -NMR spectrum of ferric rLb and Glu63Leu are depicted in Figure 2.10. Proton resonances for Glu63Leu were found to be almost identical to those of rLb ( $\delta$  (ppm) rLb: 67.2, 63.0, 57.5, 51.7, 45.1, 40.0, 35.9, 29.2, 14.3, -2.1, -3.3, -4.2 and -6.7;  $\delta$  (ppm) Glu63Leu: 68.1, 63.2, 57.1, 51.9, 46.0, 39.9, 35.8, 29.5, 15.1, -2.2, -3.3, -4.2 and -6.7). Assignments for these resonances were not available for Lb or rLb, and comparison with Lb was made more difficult by the poor quality of the early NMR data for ferric Lb.<sup>[13, 24]</sup> However, the spectra of rLb and Lb were broadly similar with chemical shift values for the proton resonances that were in approximate agreement ( $\delta$  (ppm) Lb<sup>[13, 24]</sup>:  $\approx 68^a$ ,  $\approx 63^a$ ,  $\approx 56^a$ ,  $\approx 51^a$ ,  $\approx 44$  (broad)<sup>a</sup>,  $\approx 35^a$ ,  $\approx 26$  (broad)<sup>a</sup>,  $\approx 15^a$ ,  $\approx -2^a$ , -3.0, -3.7, -6.7).

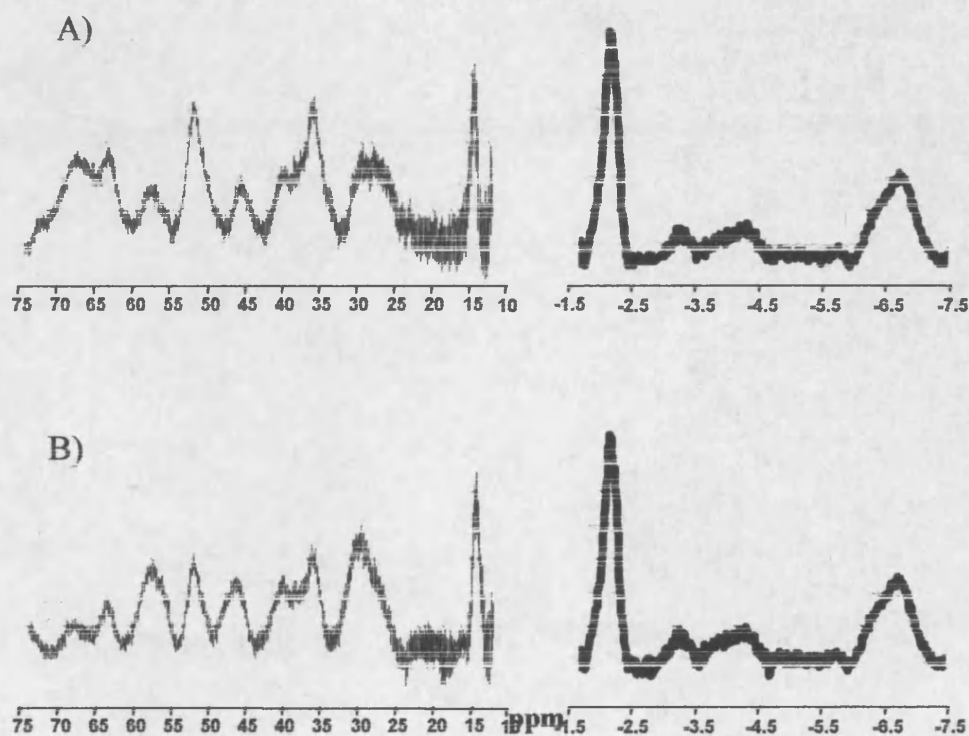


**Figure 2.10.** 300 MHz  $^1\text{H}$ -NMR spectra of (A) rLb; (B) Glu63Leu. Conditions: pH\* 7.0, 25.0 °C,  $\text{D}_2\text{O}$ , with assignments from references.<sup>[13, 24]</sup>

<sup>a</sup> Chemical shift values (ppm) estimated from published spectra.

The 300 MHz  $^1\text{H-NMR}$  spectra of the nicotinate complex of rLb are shown in Figures 2.11(A-C), illustrating changes in resonance chemical shifts at  $\text{pH}^*$  4, 7 and 9. The  $^1\text{H-NMR}$  spectrum of the nicotinate complex of rLb at  $\text{pH}^*$  7.0, Figure 2.11(B), shows chemical shifts (ppm) at 27.5, 22.3, 20.0, 15.8, 13.4, 13.1, 10.8, 10.6, -8.8 and -10.8, which were in agreement with those previously published for Lb.<sup>[5, 25]</sup> The proton resonances for Lb have been previously assigned<sup>[5, 25]</sup> and are indicated for rLb in Figures 2.11(A)-(C).

The changes in hyperfine chemical shifts for the haem resonances of rLb-nicotinate, as a function of pH, are shown in Figure 2.12(A). No apparent trends were observed as the  $\text{pH}^*$  was increased (from 3.8 to 10) for the 5-methyl, 2-vinyl  $\alpha\text{-CH}_2$ , 1-methyl, 2-vinyl  $\beta\text{-CH}_{\text{cis}}$ , 2-vinyl  $\beta\text{-CH}_{\text{trans}}$  and H-5 nicotinate resonances. However, the two  $\alpha\text{-CH}_2$  proton resonances of the 6-propionate group of Lb (designated  $6\text{-H}_\alpha$  and  $6\text{-H}_{\alpha'}$ ) have been shown to be a sensitive function of solution  $\text{pH}^*$ ,<sup>[5, 13]</sup> with chemical shifts that report on the protonation state of a nearby titratable residue. Figure 2.12(C) shows the changes in chemical shift for the  $6\text{-H}_\alpha$  and  $6\text{-H}_{\alpha'}$  proton resonances of rLb as a function of increasing  $\text{pH}^*$ . The hyperfine shifts show, in agreement with previously published work,<sup>[5, 13]</sup> that these proton resonances were sensitive to  $\text{pH}^*$  changes. A fit of these data for both resonances to Equation [7.7], Chapter 7, yielded an average  $\text{pK}_a$  of  $5.0 \pm 0.2$  (5.2 and 4.9). In view of the inherent difficulty in obtaining  $\text{pK}_a$  values in the low pH region (as a consequence of protein denaturation), an average  $\text{pK}_a$  determined from the  $6\text{-H}_\alpha$  and  $6\text{-H}_{\alpha'}$  data was used: this value was in sensible agreement with previous determinations on Lb ( $\text{pK}_a = 4.9$ ).<sup>[5, 13]</sup>

The 300MHz  $^1\text{H-NMR}$  spectra of the nicotinate complex of Glu63Leu are shown in Figures 2.11(D)-(F), illustrating changes in resonance chemical shifts at  $\text{pH}^*$  4, 7 and 9. The  $^1\text{H-NMR}$  spectrum of the nicotinate derivative of Glu63Leu at  $\text{pH}^*$  7.0 is shown in Figure 2.14(E). The hyperfine shifts ( $\delta$  (ppm): 28.0, 22.2, 19.2, 15.6, 13.9, 13.3, 10.8, 10.6, -8.8 and -10.7) were very similar to those for rLb, and tentative assignments are indicated based on peak intensity. The change in hyperfine chemical shift for the haem resonances of Glu63Leu-nicotinate as a function of  $\text{pH}^*$  are shown in Figure 2.12(B). Like rLb-nicotinate, no apparent trends were observed, upon an increase in pH (from 3.8 – 10), for the 5-methyl, 2-vinyl  $\alpha\text{-CH}_2$ , 1-methyl, 2-vinyl  $\beta\text{-CH}_{\text{cis}}$ , 2-vinyl  $\beta\text{-CH}_{\text{trans}}$  and H-5 nicotinate resonances. However, in contrast to rLb, the  $\alpha\text{-CH}_2$  proton resonances of the 6-propionate group showed no change in chemical shift as a function of  $\text{pH}^*$ , Figure 2.12(C), thereby assigning the origin of the pH-dependent profile in rLb to titration of glutamic acid 63. These results provided initial

evidence towards the assignment, indicating and confirming that the glutamic acid 63 is the residue responsible for the nicotinate binding process in the acidic region.

### ***Nicotinate Binding in rLb in the Acidic Region***

Equilibrium nicotinate binding in rLb were conducted in the pH range 3.6 – 5.5 and equilibrium dissociation constants determined at each pH. Fit of the data, to the Henderson Hasselbach equation (Equation [7.7], Chapter 7), showed binding of nicotinate to be pH dependent, Figure 2.13(A). A  $pK_a$  of  $5.2 \pm 0.1$  was determined, which compared with  $pK_a$  values of 4.9<sup>[8, 13]</sup> and 4.8<sup>[1]</sup> previously reported for Lb. The  $pK_a$  was initially assigned to the glutamic acid 63 residue of Lb. Determination of the correct assignment needed further experimental analysis. Equilibrium dissociation constants,  $K_d$ , for the binding of nicotinate to Glu63Leu were determined over a range of pH (3.6 – 9), Figure 2.13(B). For Glu63Leu in the alkaline region (pH 5.5 – 9), a  $pK_a$  of  $7.0 \pm 0.1$  was determined, Figure 2.10(B), close to the value obtained for rLb ( $pK_a$  of  $6.9 \pm 0.1$ ).<sup>[7]</sup> By contrast, a pH-independent profile was observed for Glu63Leu in the acidic region (pH 3.6 – 5.5), Figure 2.13(A). These results, with emphasis based on the pH-independent profile for the Glu63Leu data, provided evidence to the assignment that the glutamic acid 63 is the residue responsible for the nicotinate binding process in the acidic region.

To eliminate the possibility that the haem propionates are responsible for the pH-dependent behaviour, nicotinate binding titrations were carried out on rLb, His61Ala and Glu63Leu reconstituted with protoporphyrin IX dimethyl ester, in which the titratable haem carboxylates of the propionates were removed. Similar pH profiles were observed to that for the nicotinate binding process to rLb, His61Ala and Glu63Leu containing protoporphyrin IX. A pH-dependent relationship was seen for rLb and His61Ala with  $pK_a$ s of  $5.2 \pm 0.2$ , Figure 2.14(A), and  $5.3 \pm 0.2$ , Figure 2.14(B), respectively: an indication that the haem propionate groups were not involved in the nicotinate binding process in Lb. A pH-independent profile was observed for Glu63Leu, Figure 2.14(C), providing further evidence for the initial assignment made that the glutamic 63 residue regulates nicotinate binding in rLb under acidic conditions and eliminates the possibility that the glutamic 63 mutation could have any indirect effects on the titration of the propionates in the nicotinate binding process, Figure 2.15.

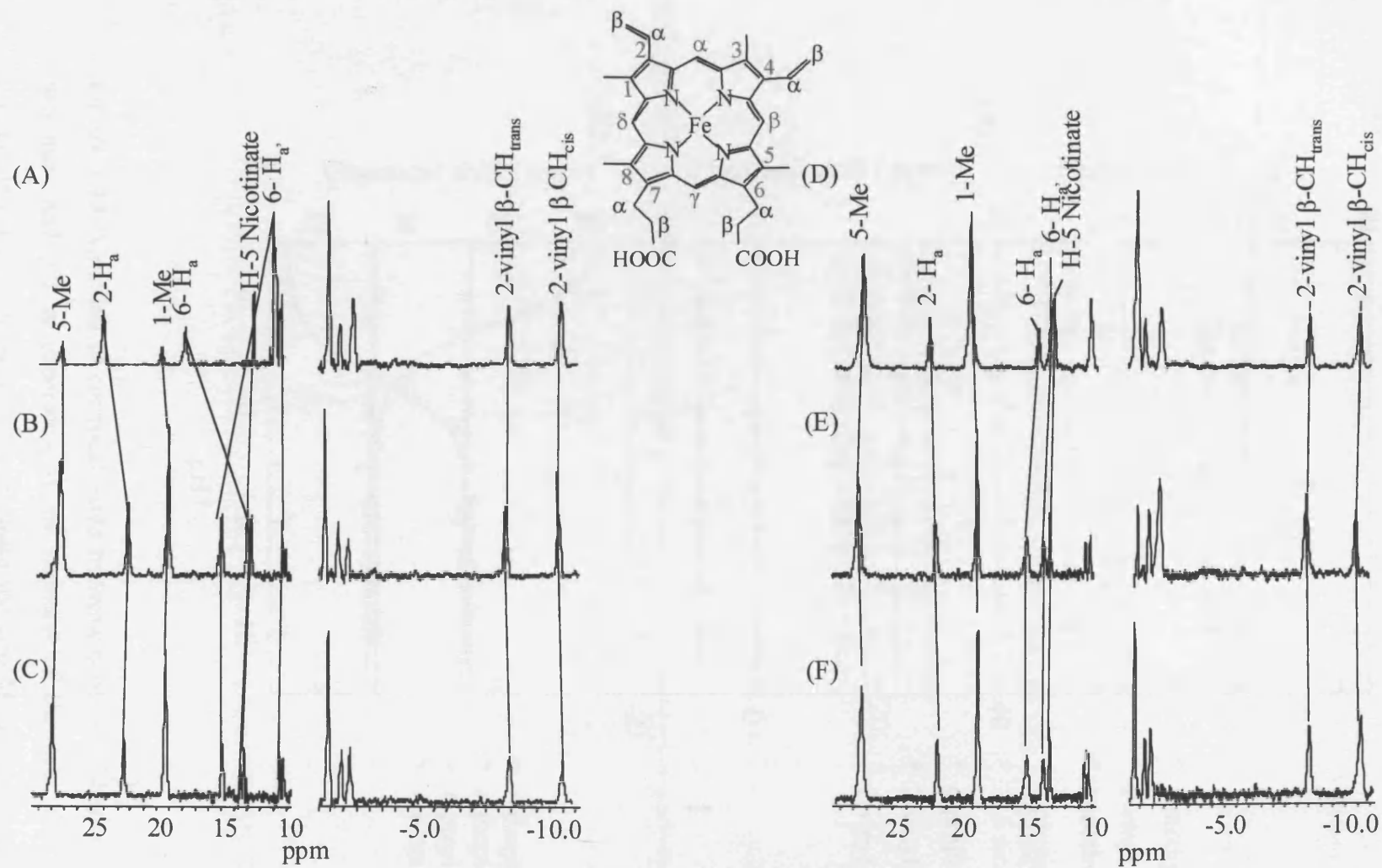


**Figure 2.11.** 300MHz <sup>1</sup>H-NMR spectra of rLb-nicotinate (left) at pH\* 4 (A), 7 (B), 9 (C) and Glu63Leu-nicotinate (right) at pH\* 4 (D), 7 (E), and 9(F). Variations of chemical shift (ppm) are indicated for the haem resonances. Iron Protoporphyrin IX (centre) indicating positions of haem resonance assignments. Conditions: 25.0 °C, D<sub>2</sub>O.

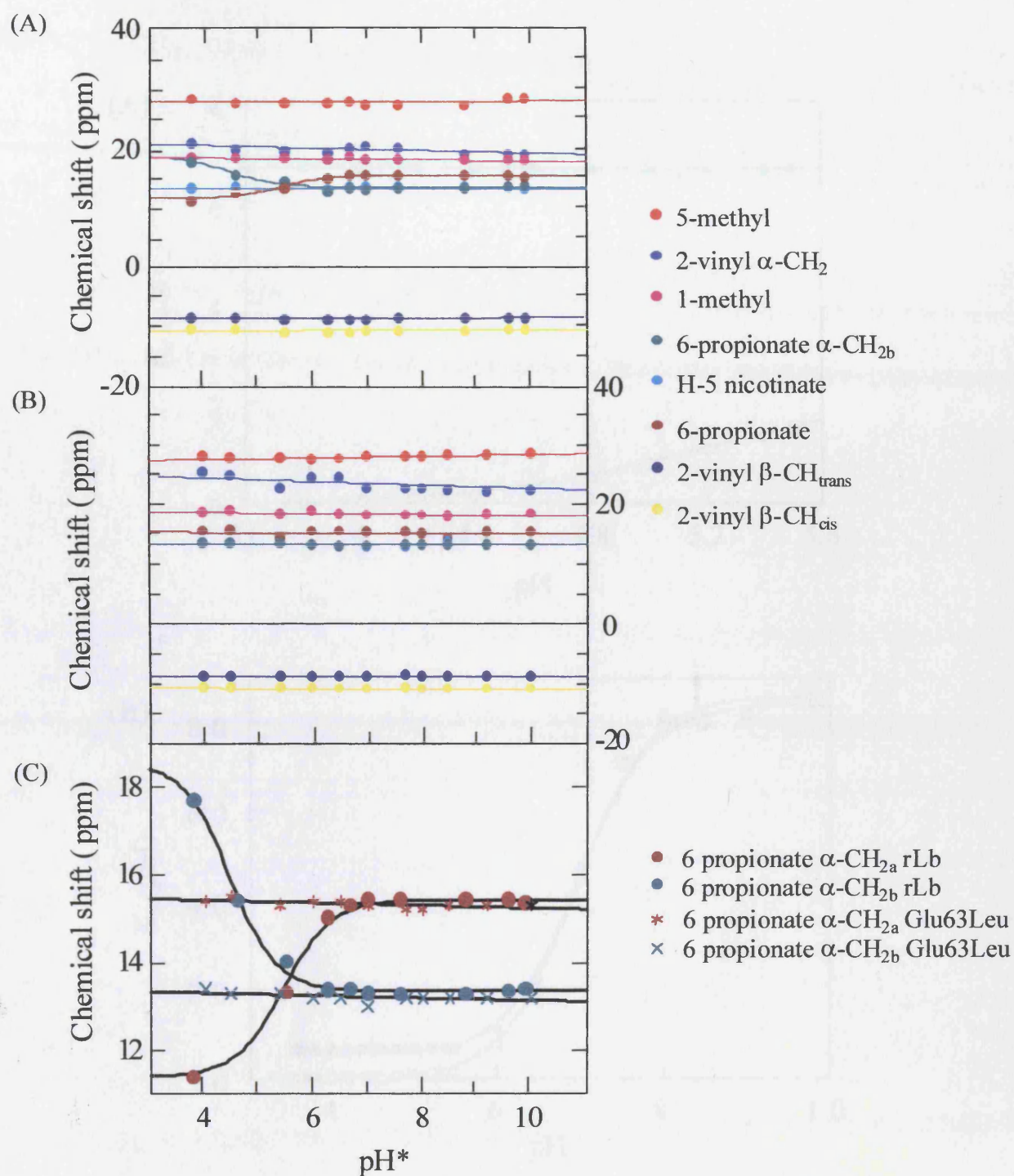


**Figure 2.12.** Variation of chemical shifts resonances of (A) rLb-nicotinate, (B) Glu63Leu-nicotinate and (C) an expansion of the variation of chemical shift positions for the 6-propionate  $\alpha$ -CH<sub>2</sub> with pH of rLb-nicotinate and Glu63Leu-nicotinate. Conditions: 25.0 °C, D<sub>2</sub>O.

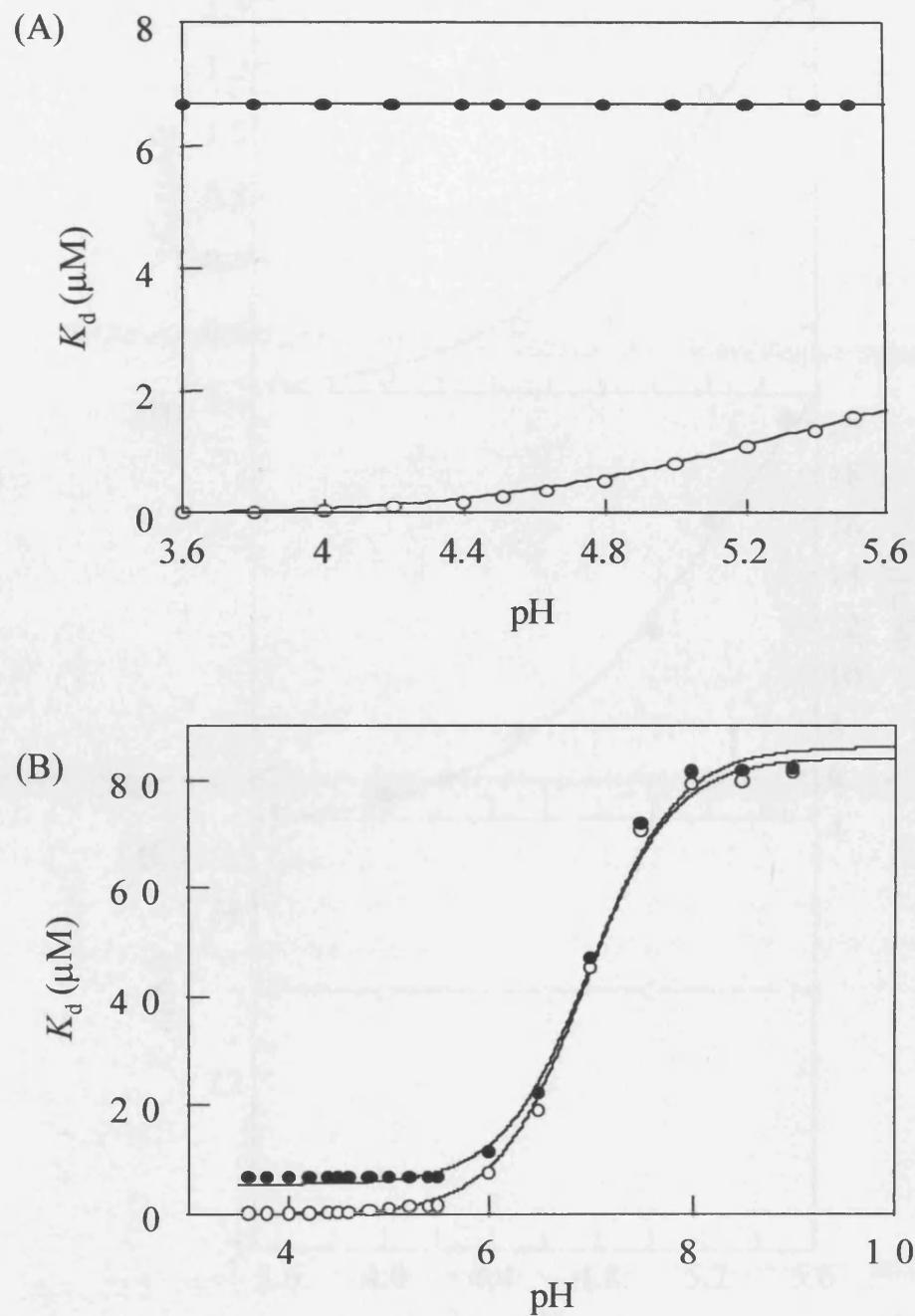


**Figure 2.13.** Variation of  $K_d$  with pH for binding of nicotinate to rLb (O) and Glu63Leu (●). Fits of the data to Equation [7.7] for rLb and Glu63Leu are shown. (A) fits for the acidic to neutral region and (B) fits for the whole pH region. Conditions:  $\mu = 0.10 \text{ M}$ ,  $25.0 \text{ }^\circ\text{C}$

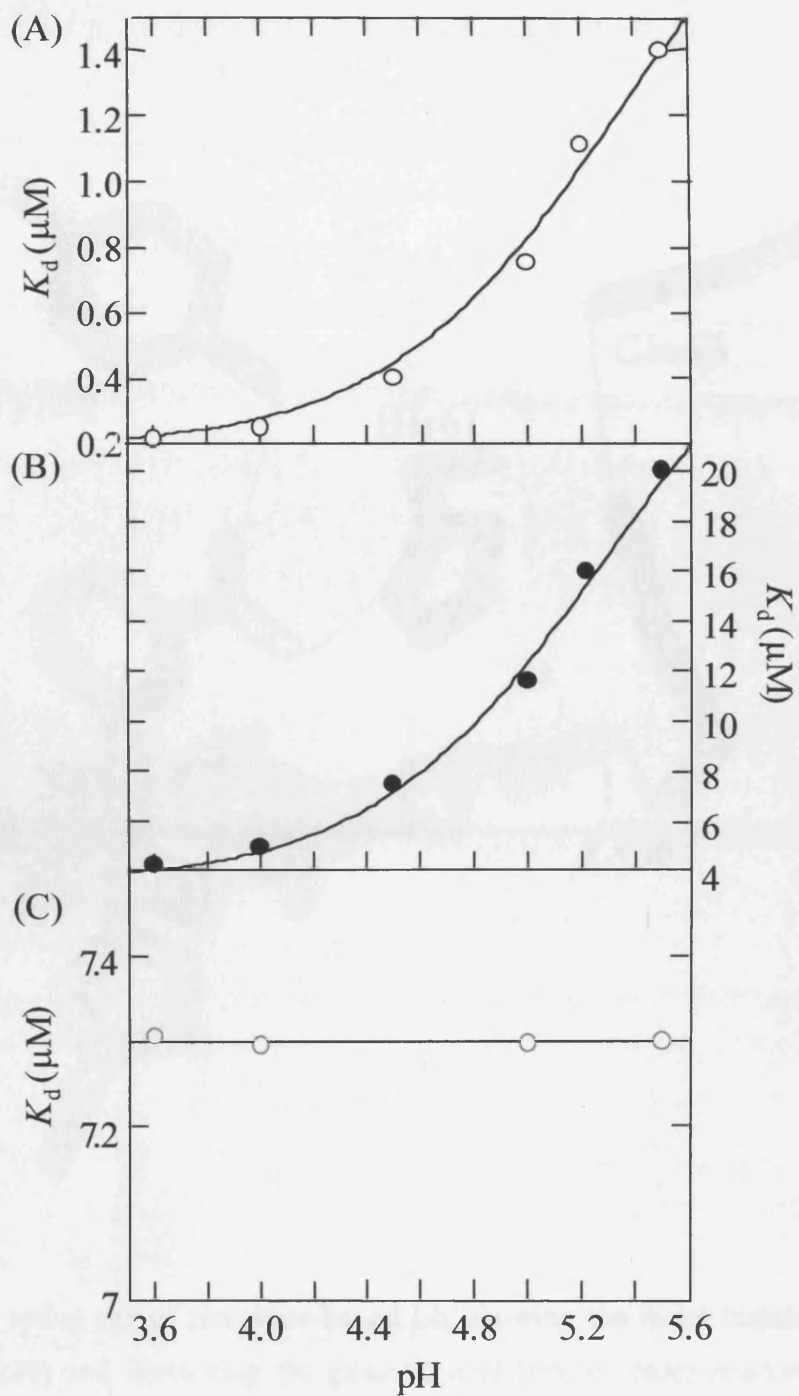


**Figure 2.14.** Variation of  $K_d$  with pH for the binding of nicotinate to (A) rLb (O), (B) His61Ala (●) and (C) Glu63Leu (O) proteins reconstituted with protoporphyrin IX dimethyl ester. Fits of the data to Equation [7.7] for rLb and variants are shown. Conditions:  $\mu = 0.10 \text{ M}$ ,  $25.0 \text{ }^\circ\text{C}$ .

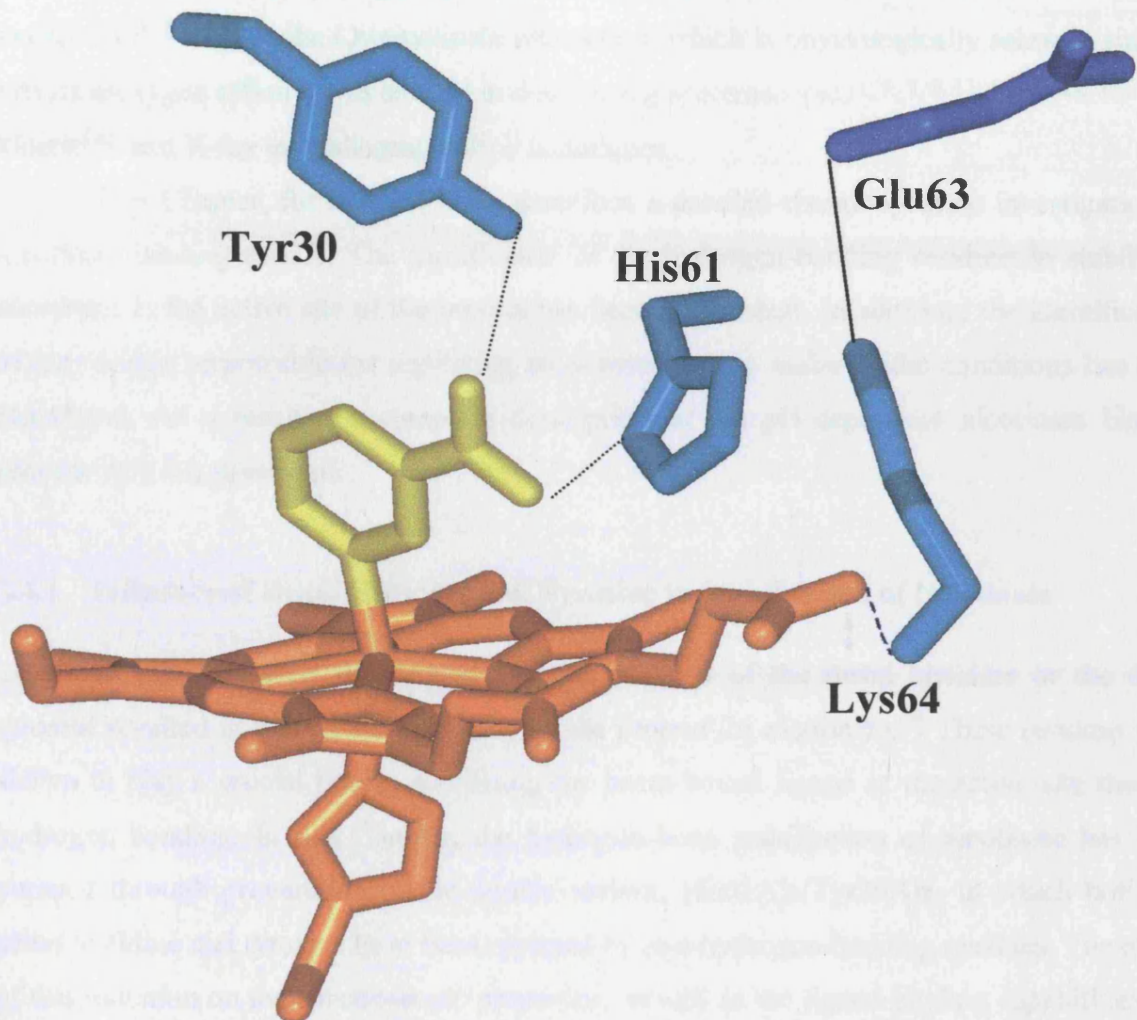


**Figure 2.15.** The active site of nicotinate-bound Lb, showing the distal histidine (His61), distal tyrosine (Tyr30) and illustrating the glutamic acid (Glu63, blue) residue bonded to lysine 64 (solid line).<sup>[2]</sup> Nicotinate is shown in yellow. Hydrogen bonds (black) and the salt bridge (blue) formed between Lys64 and the 6-propionate haem group are indicated as dotted lines.

## 2.4 Discussion

The Lb-nicotinate interaction has been the subject of intense experimental investigation since the 1960s. It was first identified when early preparations of Lb were found to be spectroscopically heterogeneous as a result of nicotinate being bound to the haem during isolation.<sup>[10, 26]</sup> Later, the Lb-nicotinate interaction, which is physiologically relevant since it affects dioxygen affinity, was studied in detail using spectroscopic,<sup>[1, 5, 7, 8, 11, 13, 19, 22, 25, 27-29]</sup> kinetic<sup>[30]</sup> and X-ray crystallographic<sup>[2, 3]</sup> techniques.

This Chapter, for the first time, describes a detailed thermodynamic investigation of nicotinate binding to rLb. The significance of the hydrogen-bonding residues in stabilising nicotinate in the active site of the protein has been established. In addition, the identification of the residue responsible for regulating nicotinate binding under acidic conditions has been elucidated. As a result, the complete description of the pH-dependent nicotinate binding process in rLb is presented.

### 2.4.1 Influence of Distal Histidine and Tyrosine in Stabilisation of Nicotinate

It was previously determined that the removal of the distal histidine or the distal tyrosine resulted in a decrease in affinity of the protein for nicotinate.<sup>[7]</sup> These residues were shown to play a crucial role in stabilising the haem-bound ligand in the active site through hydrogen bonding. In this Chapter, the hydrogen-bond stabilisation of nicotinate has been pursued through preparation of the double variant, His61Ala/Tyr30Ala, in which both the distal histidine and tyrosine have been replaced by non-hydrogen-bonding residues. The effect of this mutation on the spectroscopic properties, as well as the ligand binding capabilities has been investigated. Comparisons to rLb have been made to establish the difference in properties as a result of the mutation.

#### 2.4.1.1 Haem Electronic Structure

The electronic absorption spectrum of His61Ala/Tyr30Ala differed from that of rLb, with dominating high-spin transitions apparent for the variant. This spectrum was found to be similar to that of His61Ala (Chapter 3). As a result of the similarities observed for His61Ala and His61Ala/Tyr30Ala, it was concluded that the histidine 61 residue gives rise to the low-spin transitions (Chapter 3). The high-spin features for His61Ala/Tyr30Ala ( $\lambda_{\max}$  (nm) = 499

and 631) were attributed to water-bound haem, as for rLb ( $\lambda_{\max}$  (nm) = 495 and 626). However, the minority low-spin features observed for the double variant ( $\lambda_{\max}$  (nm) = 536 and 574) were assigned to hydroxide-bound haem (as for His61Ala (Chapter 3)), since no contribution of the low-spin transitions could arise from the distal histidine in this case ( $\lambda_{\max}$  (nm) = 530 and 560). The molar absorption coefficient determined for His61Ala/Tyr30Ala was found to be  $20 \text{ mM}^{-1}\text{cm}^{-1}$  lower than that for the rLb. This difference indicated the change in haem spin-state of the protein as a result of the mutation and is in agreement with formation of a six-coordinate, high-spin species.

Anionic ligand binding spectra for His61Ala/Tyr30Ala showed similarities to rLb. Observed changes in the haem spin-state for both proteins were consistent with previously reported ligand binding characteristics: formation of a low-spin complex on binding the strong field ligand cyanide and characteristic high-spin transitions on binding the weak field ligand fluoride. These results suggested that the mutagenic substitution did not lead to a substantial perturbation of the protein active site and that neither of these distal residues plays a significant role in the binding or stabilisation of these small ligands.

The similarity of the  $pK_a$  values observed for His61Ala/Tyr30Ala (8.4) and rLb (8.3) suggested titration of the same moiety, the distal water molecule, occurs in both proteins as the pH was increased. These data were surprising, since one might have predicted that removal of the hydrogen-bonding interactions in the haem pocket (particularly the hydrogen bond from histidine 61 to the haem-bound water<sup>[2]</sup>) would lead to a change in the  $\text{H}_2\text{O}/\text{HO}^-$  distribution. Although the structures of the water- and hydroxide-bound Lb derivatives are not known, the distal histidine itself is known to be mobile.<sup>[2, 3, 31, 32]</sup> As such the similarity in  $pK_a$ s for rLb and His61Ala/Tyr30Ala may suggest that hydrogen-bonding interactions do not have significant influence on the water/hydroxide equilibrium in Lb.

#### 2.4.1.2 Nicotinate Binding to His61Ala/Tyr30Ala

A significant decrease in binding affinity for nicotinate was observed for the His61Ala/Tyr30Ala variant. An equilibrium dissociation constant value of  $32 \pm 1 \mu\text{M}$  was determined for His61Ala/Tyr30Ala, a  $\sim 20$  fold decrease in affinity compared to rLb ( $K_d = 1.4 \pm 0.3 \mu\text{M}$ ). When compared to His61Ala ( $19 \pm 1 \mu\text{M}$ ) and Tyr30Ala ( $11 \pm 1 \mu\text{M}$ ), an additive effect was observed for His61Ala/Tyr30Ala. These results confirm the importance of the two distal residues in stabilising the haem-coordinated nicotinic acid anion in the active site of Lb. These results are however surprising, since a dissociation constant similar to that for the

binding of pyridine to rLb ( $260 \pm 50 \mu\text{M}$ )<sup>[7]</sup> was expected, for which there is no possible hydrogen bonding of the active site residues to the haem-bound ligand (no carboxylate functionality on the ligand for tyrosine 30 and histidine 61 to hydrogen bond to). However, results obtained for His61Ala/Tyr30Ala may be explained in terms of steric effects. Easier access of nicotinate into the active site (to the haem) is afforded on removal of the two bulky residues, histidine 61 and tyrosine 30, and hence an increase in ligand affinity (a lower  $K_d$  value) is observed compared to that for binding of pyridine to rLb.

## 2.4.2 pH-Dependent Nicotinate Binding (Glu63Leu)

It was recognised at an early stage that the binding interaction of nicotinate was pH-dependent<sup>[1]</sup> and recently the distal histidine 61 residue has been identified<sup>[7]</sup> as being responsible for this pH-dependence in the neutral to alkaline region. In this Chapter, the analysis of the pH-dependent nicotinate binding process has been extended. Analysis of nicotinate binding to rLb and Glu63Leu has been investigated. The data presented in this work leads to the assignment of glutamic acid 63 and provides an answer to the question, first posed more than twenty years ago,<sup>[1, 13]</sup> as to whether glutamic acid 63 acts as an ‘electrostatic gate’ in regulating nicotinate binding in Lb under acidic conditions.

### 2.4.2.1 Haem Electronic Structure

The electronic absorption spectrum of Glu63Leu showed wavelength maxima that were very similar to that of rLb, Table 2.1, indicating that the active site structure had not been seriously perturbed as a result of the mutation: NMR spectra for the ferric derivative of Glu63Leu were also consistent with those for both rLb and Lb, indicating that large-scale perturbations had not occurred. Wavelength maxima for ferric Glu63Leu showed features arising from six-coordinate, high-spin and six-coordinate, low-spin haem. For Lb, the high-spin feature has been assigned<sup>[27]</sup> as arising from coordination of a distal water molecule; the low-spin derivative has been proposed<sup>[19, 27]</sup> to arise from coordination of the distal histidine 61 residue to the haem – an assignment that has been confirmed by mutagenesis (Chapter 3). In Glu63Leu, the site of the mutation is located at a considerable distance (a distance of 16.3 Å to the carboxylate of glutamate 63) from the haem and would, therefore, be unlikely to substantially perturb the electronic transitions associated with the porphyrin. Hence, by analogy with Lb, the high- and low-spin haem signatures for Glu63Leu were assigned as

arising from water- and histidine 61-coordinated haem, respectively. At alkaline pH, the electronic spectrum of Glu63Leu showed changes that were consistent with titration of the distal water molecule. The  $pK_a$  for this transition was identical to rLb and wavelength maxima were similar in both cases, indicating that the removal of the negatively charged Glu63 group had no influence on the water/hydroxide equilibrium in the distal pocket.

The ligand binding capabilities of Glu63Leu were effectively similar to rLb. Formation of a low-spin species was seen on binding cyanide and a high-spin species on binding fluoride. These findings were in agreement with NMR data as mentioned above and indicated that the active site structure and the ligand binding capability of the protein had not been seriously perturbed.

#### 2.4.2.2 Determination of the Mid-Point Potential

The 24 mV increase in mid-point potential observed on replacement of the charged glutamic acid 63 residue with the neutral leucine is consistent with simple electrostatic arguments that predict stabilisation of the reduced derivative on removal of the negative charge. Opposite effects have recently been observed in the Leu88Asp variant of rLb, where the introduction of a negatively charged Asp residue led to a destabilisation of the reduced form.<sup>[33]</sup> Although the effects of charge substitution on redox properties of haem proteins in general are not fully understood in a quantitative manner<sup>[34]</sup>- and there are only a limited number of examples in which this has been examined for the globins<sup>[35]</sup> - these changes for Lb can be satisfactorily rationalised in a *qualitative* context.

#### 2.4.2.3 pH-Dependent Nicotinate Binding

NMR titrations provided evidence in support of the assignment of glutamic acid 63 as the titrating residue. The NMR spectrum of the nicotinate derivative of rLb showed proton resonances at almost identical chemical shifts to those previously reported<sup>[5, 13]</sup> for Lb, and proton resonances for Glu63Leu are in agreement with those for rLb, Figure 2.10(B). Values for the  $pK_a$  of the titrating residue determined by NMR ( $pK_a = 5.0 \pm 0.2$ ) were in good agreement with the  $pK_a$  determined for this residue from the equilibrium binding studies ( $pK_a = 5.2 \pm 0.1$ ), and in approximate agreement with values for the  $pK_a$  ( $pK_a = 4.1$ <sup>[36]</sup>) of glutamic acid (protein  $pK_a$ s are known to be a sensitive function of structural environment). Most importantly, replacement of glutamic acid 63 with a non-titratable residue eliminated the pH-

dependent alteration in chemical shift first identified in 1979,<sup>[13]</sup> providing further confirmation to a question that was first posed in 1973 - that glutamic acid 63 is the electrostatic gate that controls nicotinate binding in the acidic region.

In the neutral to alkaline region, binding of nicotinate to the haem was unaffected by mutation of the Glu63 residue: absolute values for  $K_d$  for rLb and Glu63Leu were very similar (consistent with the haem water-hydroxide titration properties, above) and the  $pK_a$ s derived from a fit of the data in this region for both proteins yielded very similar values ( $pK_a$ s of 6.9 and 7.0, respectively).

It has been reported previously<sup>[11, 13]</sup> that the equilibrium dissociation constant for binding of nicotinate to Lb is also pH-dependent in the acidic region, with  $pK_a$  values of 4.9<sup>[13]</sup> and 4.8<sup>[11]</sup>. With data for rLb in the pH range 3.6 – 5.5 from this work, binding of nicotinate was indeed observed to be pH-dependent with binding becoming slightly more favourable as the pH was decreased. (The direction of this change in  $K_d$  for rLb was, *qualitatively*, consistent with the titration properties of the glutamic acid 63 residue: as glutamic acid 63 protonates at low pH, charge neutralisation occurs and binding of the (anionic) nicotinate residue become slightly more favourable). Although the magnitude of these changes in  $K_d$  ( $\gg 10$ -fold) as a function of pH were broadly consistent with published data<sup>[11, 13]</sup>, and although a  $pK_a$  ( $5.2 \pm 0.1$ ) that agrees with the published data <sup>[11, 13]</sup> were obtained from a non-linear least squares fit of these data to a single proton process, the changes in  $K_d$  were much less substantial than in the alkaline region<sup>[12]</sup> and it was not possible to satisfactorily separate the two titration processes (although this has been attempted previously<sup>[13]</sup>). For this reason the NMR data was regarded as a more reliable means of establishing the origin of the pH-dependent profiles. Significantly, however, equilibrium dissociation constants for Glu63Leu were absolutely independent in the pH range 3.6 – 5.5, consistent with a role for Glu63.

Although the  $pK_a$  of nicotinate ( $pK_a = 4.8$ ) is also similar to the  $pK_a$  values obtained for nicotinate binding to rLb, His61Ala and His61Ala/Tyr30Ala in the acidic region, the nicotinate cannot be attributed to giving rise to the titration process. The pH-independent profile observed for the Glu63Leu-nicotinate binding process rules out the possibility that the titration of the nicotinate molecule was involved.

The possibility that the haem propionate groups, as predicted previously by various groups, <sup>[5, 12, 13]</sup> could be directly involved in the pH-dependent binding of nicotinate in the acidic region was also investigated. Removal of the carboxylate functionality of the haem propionate groups in rLb and His61Ala had no effect on the pH-dependent binding process,

clearly indicating that the propionate groups are not responsible for the behaviour. Further evidence was provided by the pH-independent nicotinate binding profile observed for Glu63Leu variant reconstituted with protoporphyrin IX dimethyl ester. These data also eliminate the possibility that the haem propionates are involved in the pH-regulation process and that secondary effects on the  $pK_a$  of glutamic acid 63 have been introduced as a consequence of the mutation (since, in this case, a pH-independent profile for the dimethyl ester-reconstituted rLb and His61Ala would have been observed). These results provide additional evidence to the assignment made in this work that the residue regulating nicotinate binding in the acidic region is Glu63.

Together with previous analysis,<sup>[7]</sup> in which histidine 61 was identified as a key determinant in the neutral to alkaline region, these data now provide a complete description of the pH-dependent interaction between Lb and nicotinate.

## 2.5 Summary

This Chapter has described a detailed thermodynamic investigation of nicotinate binding to rLb. The significance of the hydrogen-bonding residues in stabilising nicotinate in the active site of the protein has been established. Removal of both distal histidine 61 and tyrosine 30 residues (His61Ala/Tyr30Ala) resulted in a decrease in affinity of the variant for nicotinate. An additive effect ( $K_d = 31\mu\text{M}$ ) for His61Ala/Tyr30Ala was observed for binding of nicotinate when compared to data for the single variants His61Ala ( $K_d = 11\mu\text{M}$ ) and Tyr30Ala ( $K_d = 19\mu\text{M}$ ).<sup>[7]</sup>

The pH-dependent nicotinate binding process was also investigated. Identification of glutamic acid 63 as the residue responsible for regulating nicotinate binding under acidic conditions has been elucidated. Together with the assignment of the histidine 61 as the residue governing nicotinate binding in the neutral to alkaline condition, a complete description of the pH-dependent binding of nicotinate in rLb has now been achieved.

## 2.6 References

1. C. A. Appleby, B. A. Wittenberg and J. B. Wittenberg, *Proc. Natl. Acad. Sci. USA* (1973) 70, 564.
2. P. J. Ellis, C. A. Appleby, J. M. Guss, W. N. Hunter, D. L. Ollis and H. C. Freeman, *Acta Crystallographica Section D* (1997) 53, 302.
3. D. L. Ollis, C. A. Appleby, P. M. Colman, A. E. Cutten, J. M. Guss, M. P. Venkatappa and H. C. Freeman, *Aust. J. Chem.* (1983) 36, 451.
4. E. H. Harutyunyan, T. N. Safonova, I. P. Kuranova, A. N. Popov, A. V. Teplyakov, G. V. Obmolova, A. A. Rusakov, B. K. Vainshtein, G. G. Dodson, J. C. Wilson and M. F. Perutz, *J. Mol. Biol.* (1995) 251, 104.
5. J. Trewella and P. E. Wright, *Biochim. Biophys. Acta* (1980) 625, 202.
6. D. K. Jones, R. Badii, F. I. Rosell and E. Lloyd, *Biochem. J.* (1998) 330, 983.
7. N. Patel, D. K. Jones and E. L. Raven, *Eur. J. Biochem.* (2000) 267, 2581.
8. B. P. Atanasov, E. A. Dimitrova, N. N. Kudryavtseva, G. Y. Zhiznevskaya and C. A. Appleby, *Biochim. Biophys. Acta* (1989) 998, 80.
9. C. A. Appleby, J. H. Bradbury, M. R. J., B. A. Wittenberg, J. B. Wittenberg and P. E. Wright, *J. Biol. Chem.* (1983) 258, 2254.
10. W. H. Fuchsman and C. A. Appleby, *Biochemistry* (1979) 18, 1309.
11. R. N. Johnson, J. H. Bradbury and C. A. Appleby, *J. Biol. Chem.* (1978) 253, 2148.
12. J. Trewella, C. A. Appleby and P. E. Wright, *Aust. J. Chem.* (1986) 39, 317.
13. J. Trewella, P. E. Wright and C. A. Appleby, *Nature* (1979) 280, 87.
14. N. N. Krasnobaeva and B. P. Atanasov, *Mol. Biol.* (1978) 12, 952.
15. P. Lehtovaara and N. Ellfolk, *Eur. J. Biochem.* (1975) 54, 577.
16. C. A. Appleby, J. Trewella and P. E. Wright, *Biochim. Biophys. Acta* (1982) 700, 171.
17. P. Lehtovaara, A. Lappalainen and N. Ellfolk, *Biochim. Biophys. Acta* (1980) 623, 98.
18. C. A. Appleby, N. A. Nicola, J. G. R. Hurrell and S. J. Leach, *Biochemistry* (1975) 14, 4444.
19. C. A. Appleby, W. E. Blumberg, J. Peisach, B. A. Wittenberg and J. B. Wittenberg, *J. Biol. Chem.* (1976) 251, 6090.
20. E. Antonini and M. Brunori, in *Hemoglobin and Myoglobin in Their Reactions with Ligands*, (North Holland, Amsterdam) 1971, pp. 10.
21. N. Ellfolk, *Acta. Chem. Scand.* (1961) 15, 975.

22. U. Perttola, *Acta Chem. Scand.* (1981) 35, 435.
23. N. Bauer, *Nature* (1960) 188, 471.
24. P. E. Wright and C. A. Appleby, *FEBS Lett.* (1977) 78, 61.
25. G. N. La Mar, S. B. Kong, K. M. Smith and K. C. Langrey, *Biochem. Biophys. Res. Comm.* (1981) 102, 142.
26. C. A. Appleby, *Biochim. Biophys. Acta* (1969) 189, 267.
27. G. Sievers, P. M. A. Gadsby, J. Peterson and A. J. Thomson, *Biochim. Biophys. Acta* (1983) 742, 637.
28. P. Lehtovaara, *Finnish Chemical Letters* (1977) , 82.
29. C. S. Maskall, J. F. Gibson and P. J. Dart, *Biochem. J.* (1977) 167, 435.
30. D. Job, B. Zeba, A. Puppo and J. Rigaud, *Eur. J. Biochem.* (1980) 107, 491.
31. C. A. Appleby, W. E. Blumberg, J. H. Bradbury, W. H. Fushman, J. Peisach, B. A. Wittenberg, J. B. Wittenberg and P. E. Wright, in *Hemoglobin and Oxygen Binding*, C. Ho, Ed. (Elsevier, North Holland, Amsterdam) 1982, pp. 435.
32. D. L. Ollis, P. E. Wright, J. M. Pope and C. A. Appleby, *Biochemistry* (1981) 20, 587.
33. D. K. Jones, N. Patel and E. L. Raven, *Arch. Biochem. Biophys.* (2002) 400, 111.
34. A. G. Mauk and G. R. Moore, *J. Biol. Inorg. Chem.* (1997) 2, 119.
35. E. L. Raven and A. G. Mauk, *Adv. Inorg. Chem.* (2001) 51, 1.
36. L. Stryer, in *Biochemistry*, (Freeman, New York) 1988, pp. 148.

**Chapter 3**  
**Determination of the Haem**  
**Axial Ligation in**  
**Leghaemoglobin:**  
**Does the Origin of the Low-**  
**Spin Haem Arise from**  
**Ligation of His61?**

### **3 Determination of the Haem Axial Ligation in Leghaemoglobin: Does the Origin of the Low-Spin Haem Arise from Ligation of His61?**

#### **3.1 Introduction**

As highlighted in Chapter 1 the distal histidine in Lb is believed to be mobile and the mobility thought to be responsible for the ability of the protein to bind bulky ligands.<sup>[1, 2]</sup> This distal histidine residue was also proposed to act as a ligand to the haem at low temperatures.<sup>[2, 3]</sup> The aim of this Chapter was to elucidate the origin of the temperature-dependent change that is observed in Lb and results in conversion of a mixed high- and low-spin species at room temperature to a fully low-spin derivative at low temperature. This change in spin-state has been previously interpreted as arising from the ligation of an endogenous ligand, the mobile distal histidine, to the haem in the flexible active site pocket of Lb.<sup>[2-4]</sup>

The availability of an adequate recombinant expression system for soybean leghaemoglobin<sup>[5]</sup> has allowed the contribution of this distal histidine 61 to the formation of the low-spin species in rLb to be assessed directly. In this work, a His61Ala variant of rLb (Figure 3.1) has been generated, in an attempt to eliminate the low-spin species. A preliminary characterisation of His61Ala has been conducted to assess the effect of the mutation on the ligand binding and electrochemical properties of the protein in comparison to rLb. The main investigative study, which was based on elucidating the nature of the low-spin species found in rLb at both room and cryogenic temperature, has been conducted using the combined application of various spectroscopic techniques - electronic absorption spectroscopy, resonance Raman, magnetic circular dichroism (MCD) and electron paramagnetic resonance (EPR) spectroscopy.



## 3.2 Mutagenesis, Protein Expression and Isolation

Site-directed mutagenesis was performed, according to the QuikChange protocol (Stratagene), using the rLb encoding pET11a vector and the His61Ala mutagenic oligonucleotide (Chapter 7, Table 7.1) containing an alanine (GCT) codon at position 61 (Perkin Elmer). Sequencing across the whole rLb coding gene confirmed the required mutation and confirmed that spurious mutations had not been introduced. Bacterial expression of His61Ala was according to procedures described in Chapter 7 and protein samples were prepared as previously described<sup>[5]</sup> (Chapter 7). Isolation of His61Ala resulted in the formation of an apo-protein. Reconstitution of His61Ala was required to ensure formation of the holoprotein and was achieved by the slow addition of freshly prepared hemin chloride (10 mg, Sigma) dissolved in 0.1 M NaOH. Excess hemin was removed using a G50 Sephadex (Pharmacia) column equilibrated with 20 mM Tris/HCl buffer, pH 8.0. The His61Ala variant was prepared with high purity ( $R_z > 4$ ) and migrated as a single band on a SDS PAGE gel (Chapter 7, Figure 7.2). Yields of ~ 10 mg of pure protein per litre were obtained as for ferric rLb.

## 3.3 Results

### 3.3.1 Preliminary Characterisation of His61Ala

Preliminary characterisation of His61Ala was carried out to assess the effect of the mutation on the spectroscopic properties of the protein in comparison to rLb. This section summarises the spectroscopic data obtained for His61Ala.

#### 3.3.1.1 Electronic Absorption Spectroscopy

Analysis of the electronic absorption spectrum of the ferric derivative of His61Ala, Figure 3.2, revealed a predominant six-coordinate, high-spin species with minor contribution from a low-spin haem species. Characteristic high-spin transitions ( $\lambda_{\max} (\epsilon/\text{mM}^{-1}\text{cm}^{-1}) = 402.5$  (148), 500 and 630 nm) and minor low-spin transitions ( $\lambda_{\max} \sim 535$  and  $\sim 563$  nm) were analogous to those found for the high-spin ( $\lambda_{\max} (\epsilon/\text{mM}^{-1}\text{cm}^{-1})^{\text{[5]}} = 403$  (157), 495 and 626 nm) and low-spin ( $\lambda_{\max} = 530$  and 560 nm) transitions of rLb. The high-spin transitions were

assigned as arising from water-bound haem, as for rLb. The minority low-spin transitions were assigned to hydroxide-bound haem.

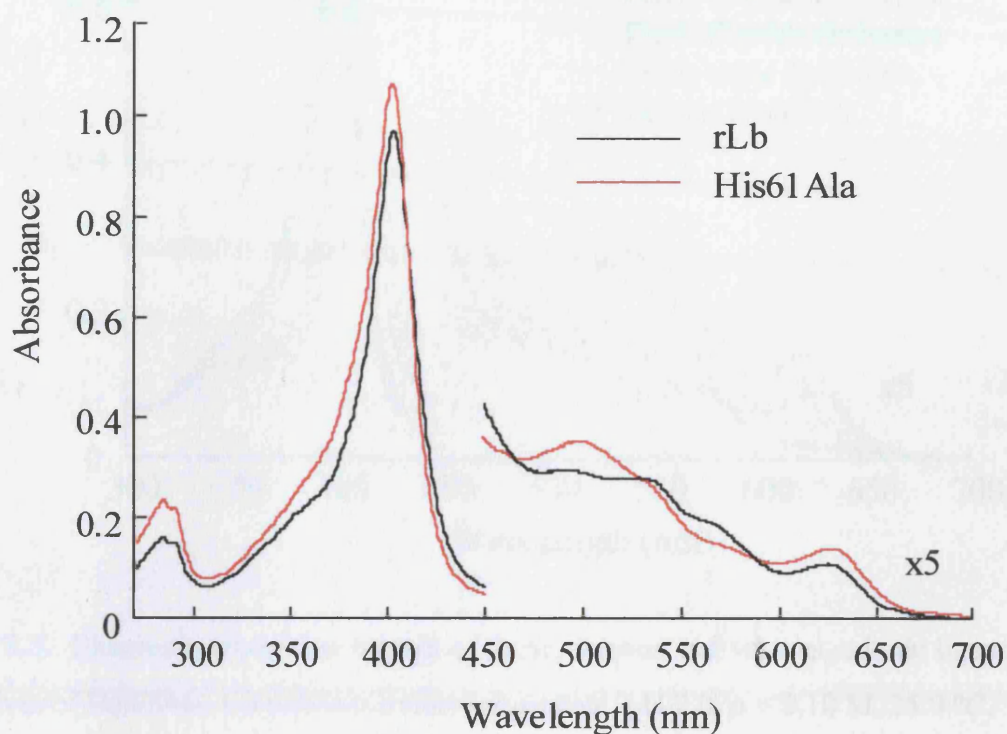


**Figure 3.2.** Electronic absorption spectra of ferric rLb and ferric His61Ala. The absorbance in the visible region has been multiplied by a factor of five. Conditions: sodium phosphate, pH 7.0,  $\mu = 0.10$  M, 25.0 °C.

### 3.3.1.2 Ligand binding

The His61Ala variant readily bound exogenous ligands at the haem iron in both the ferric and ferrous oxidation states, thus behaving in a similar manner to rLb. Formation of a low-spin haem species was observed when strong field ligands such as cyanide and nicotinate were bound to the haem, and characteristic high-spin features were observed on binding weaker field ligands such as fluoride. Anionic ligand-bound derivatives of His61Ala are depicted in Figure 3.3. Absorption maxima and corresponding absorption coefficients for the various ferric and ferrous derivatives His61Ala, Table 3.1, are similar to those of the ferric and ferrous derivatives of rLb.

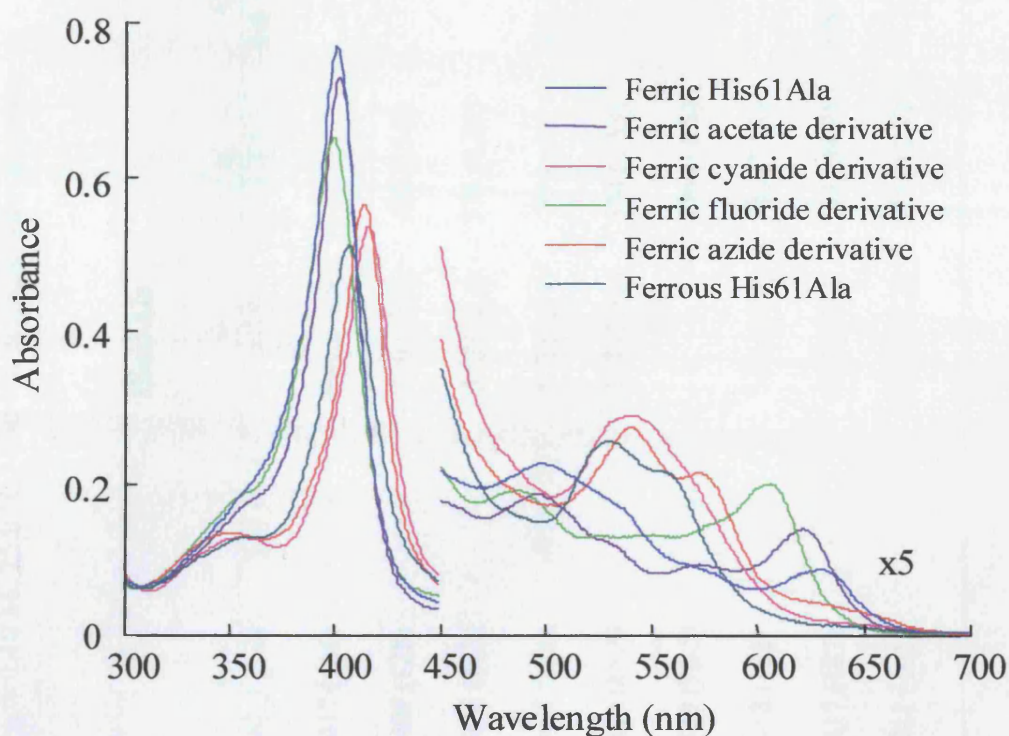


**Figure 3.3.** Electronic absorption spectra of ferric, ferrous and various anionic ligand-bound derivatives of His61Ala. Conditions: sodium phosphate, pH 7.0,  $\mu = 0.10$  M, 25.0 °C.

The ability of His61Ala to bind exogenous ligands, Equation [3.1] where L = ligand, was determined by equilibrium binding measurements. Data were fitted to Equation [7.3], Chapter 7, to determine values for  $K_d$ , the equilibrium dissociation constant.



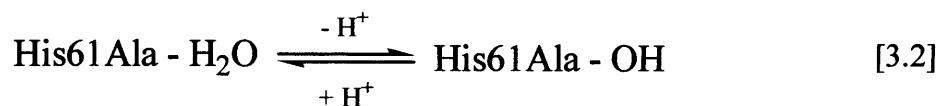
An equilibrium dissociation constant,  $K_d$ , of  $0.5 \pm 0.1$   $\mu\text{M}$  was determined for the binding of cyanide to His61Ala and was similar to that for rLb ( $K_d = 1.2 \pm 0.3$   $\mu\text{M}$ ).<sup>[5]</sup> Binding of azide to His61Ala yielded an equilibrium dissociation constant of  $12.3 \pm 0.2$   $\mu\text{M}$ , a value slightly different to that observed for the rLb-azide titration ( $K_d = 4.8 \pm 0.2$   $\mu\text{M}$ ).<sup>[5]</sup> On binding the physiological ligand, nicotinate, to His61Ala a difference in the equilibrium dissociation constant was observed: in this case, a  $K_d$  value of  $19 \pm 1.0$   $\mu\text{M}$  was determined compared to a  $K_d$  of  $75 \pm 5.0$   $\mu\text{M}$  for rLb (pH 7.0,  $\mu = 0.10$  M, 25.0 °C).<sup>[7]</sup>

**Table 3.1.**  
Wavelength maxima (nm) and, in parentheses, absorption coefficients ( $\text{mM}^{-1}\text{cm}^{-1}$ ) for the  
ferric and ferrous derivatives of rLb and His61Ala. Conditions: pH 7.0,  $\mu = 0.10\text{ M}$ ,  $25.0\text{ }^\circ\text{C}$ . Nic = nicotinate. sh = shoulder.

Derivative	rLb					His61Ala				
	( $\gamma$ ) Soret	CT <sub>2</sub>	$\beta$	$\alpha$	CT <sub>1</sub>	( $\gamma$ ) Soret	CT <sub>2</sub>	$\beta$	$\alpha$	CT <sub>1</sub>
Fe(III)	403 (157)	495 (10.7)	530 (9.91)	560 (7.13)	626 (4.92)	402.5 (148)	500 (8.74)	~535	~563	630 (3.65)
Fe(III)-CN <sup>-</sup>	415 (117)	-	539 (11.9)	-	-	417 (106)	-	541 (11.0)	-	-
Fe(III)-Nic	407 (123)	-	529 (13.4)	557 (11.2)	-	407 (128)	-	530 (13.0)	557 (11.0)	-
Fe(III)-N <sub>3</sub> <sup>-</sup>	414 (126)	-	549 (12.4)	572 (9.36)	-	415 (113)	-	542 (10.6)	574 (8.30)	-
Fe(III)-F <sup>-</sup>	401 (149)	484 (11.1)	540 (8.88)	-	601 (10.0)	400 (124)	487 (7.82)	542 (5.54)	574 (sh)	605 (8.13)
Fe(III)-OH <sup>-</sup>	409 (117)	-	539 (11.3)	570 (10.1)	-	406 (81.7)	-	537 (5.51)	574 (4.53)	-
Fe(II)	427 (111)	-	-	555 (13.3)	-	428 (96.5)	-	-	556 (11.5)	-
Fe(II)-CO	415 (199)	-	537 (13.6)	561 (12.7)	-	418 (182)	-	538 (14.7)	566 (5.33)	-
Fe(II)-Nic	418 (230)	-	524 (24.7)	554 (44.6)	685 (2.56)	417 (187)	-	525(19.4)	554 (39.2)	690 (2.4)
Fe(II)-O <sub>2</sub>	412 (108)	-	541 (10.8)	574 (10.5)	-	411 (101)	-	540 (11.2)	575 (10.9)	-

### 3.3.1.3 Spectrometric pH Titrations

The pH-dependent titration behaviour of His61Ala was similar to that previously observed for rLb, Figure 3.4. As the pH was increased, spectra indicated formation of a low-spin derivative, with maxima ( $\lambda_{\max}$  ( $\epsilon/\text{mM}^{-1}\text{cm}^{-1}$ ) = 406 (81.7), 537 (5.51) and 574 (4.53) nm) similar to those reported for the six-coordinate, hydroxide-bound derivative of rLb ( $\lambda_{\max}$  ( $\epsilon/\text{mM}^{-1}\text{cm}^{-1}$ ) = 409 (117), 539 (11.3) and 570 (10.1). These data suggested that the low-spin species in His61Ala arise from the deprotonation of the distal water molecule, as is observed for rLb, Equation [3.2]. A fit of the absorbance changes at 402.5 nm between pH 4.7 – 9.8 to the Henderson Hasselbach equation (Equation [7.7], Chapter 7) yielded a  $\text{p}K_{\text{a}}$  value of  $8.4 \pm 0.1$  ( $\mu = 0.10$  M,  $25.0$  °C), very similar to the  $\text{p}K_{\text{a}}$  obtained for rLb ( $8.3 \pm 0.03$ ).<sup>[5]</sup>



### 3.3.1.4 Spectroelectrochemistry

The ferric-ferrous mid-point potential of His61Ala was determined from thin-layer spectra obtained across an applied potential of  $-500$  mV to  $+200$  mV vs SCE. Data from two determinations were fitted to the Nernst equation (Equation [7.9], Chapter 7).

A representative family of spectra obtained for His61Ala at various applied potentials is shown in Figure 3.5 along with the corresponding Nernst plot (inset). The mid-point potential of His61Ala determined from this measurement was  $-6 \pm 2$  mV vs SHE ( $25.0$  °C, pH 7.0,  $\mu = 0.10$  M), which compared with the value of  $+21 \pm 3$  mV obtained for rLb ( $25.0$  °C, pH 7.0,  $\mu = 0.10$  M, see Chapter 2). The average Nernst slope for the mid-point potential determination was  $69 \pm 1$  mV, consistent with a single electron process (theoretical = 59 mV).

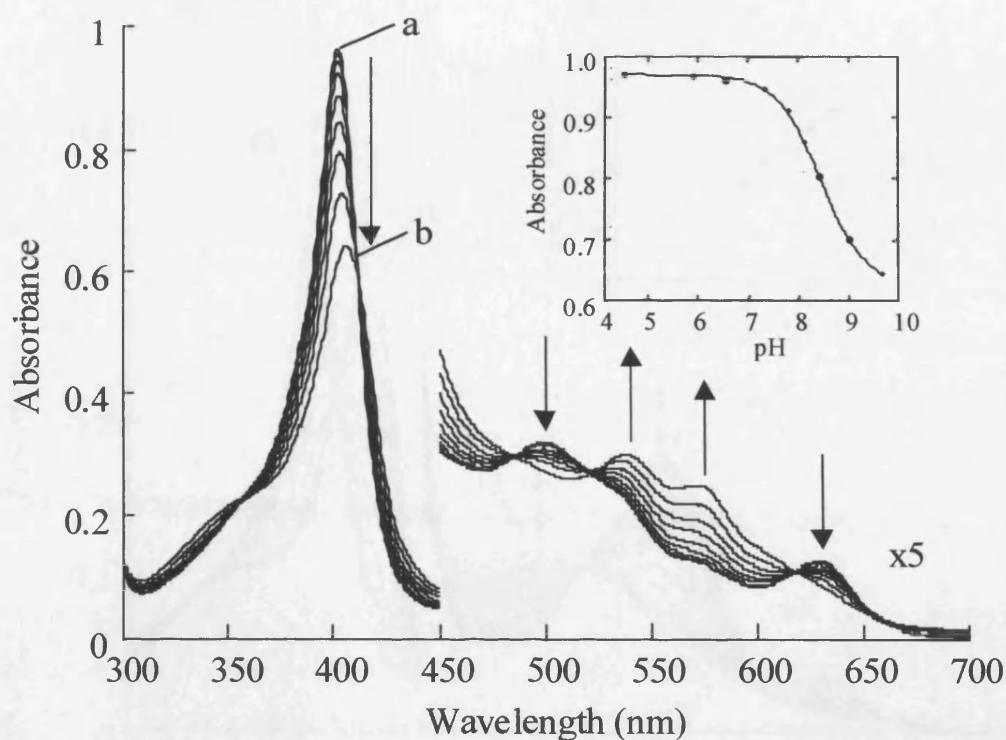


**Figure 3.4.** Spectrophotometric pH titration of ferric His61Ala. (a) spectrum of His61Ala at pH 4.7, (b) at 9.8 and at intermediate pHs 6.0, 6.5, 7.2, 7.9, 8.0, 8.2 and 9.0. Arrows indicate the direction of change in absorbance with increasing pH. Inset: plot of the variation in absorbance at 402.5 nm with pH (additionally including pH 9.8). The solid line represents a non-linear least squares fit to Equation [7.7]. Conditions: 25.0 °C.

### 3.3.2 Spectroscopic Analysis of His61Ala

#### 3.3.2.1 Electronic Absorption spectroscopy

As mentioned previously (Section 3.2.1), the electronic absorption spectrum of His61Ala revealed a predominantly high-spin protein. The initial conclusion that can be drawn from this was that the low-spin species in rLb arises from the coordination of the distal histidine. Although electronic absorption spectroscopy can indicate changes in spin-state, the technique is not diagnostic for the identity of the ligand giving rise to the various haem species. A more detailed rationalisation of the haem environment necessitated the use of techniques with greater diagnostic capabilities. Accordingly, characterisation of the low-spin form(s) using a variety of spectroscopic techniques was carried out with the aim of extending the investigation and possibly identifying the nature of the low-spin derivative of rLb at low temperature.

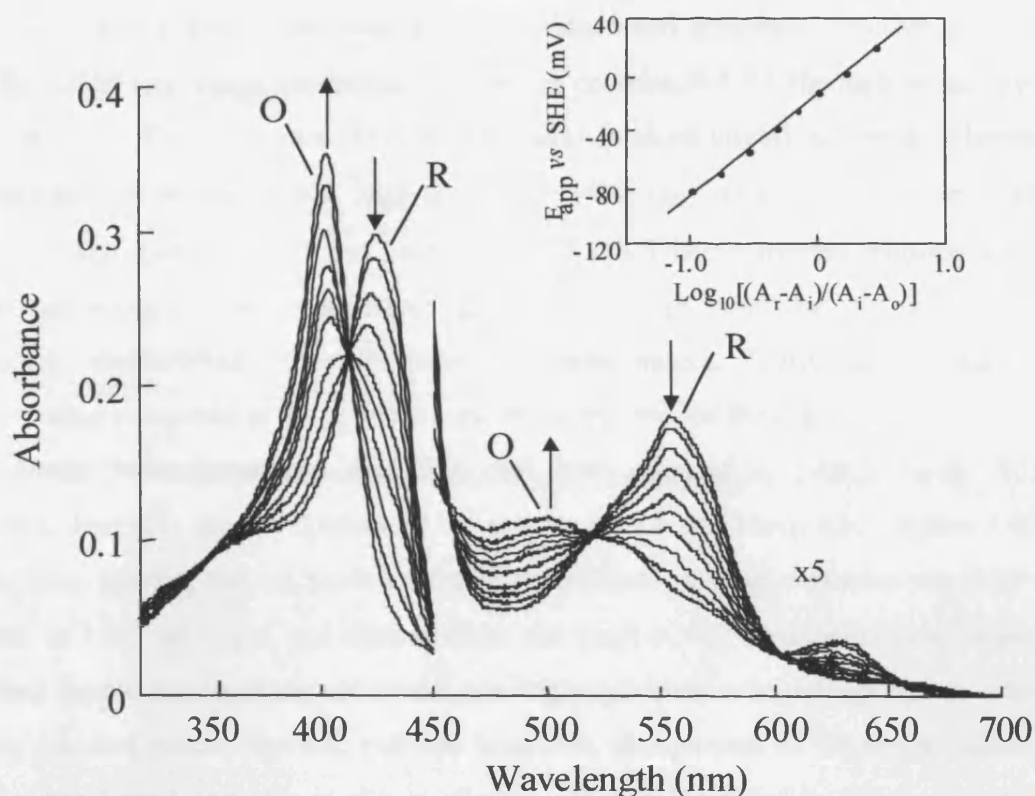


**Figure 3.5.** Thin layer spectroelectrochemical spectra of His61Ala at various applied potentials. O and R represent the oxidised and reduced forms respectively and arrows denote the change in absorbance with increasing  $E_{app}$ . The corresponding Nernst plot obtained from a fit of this data to Equation [7.9] is shown as an inset. Conditions: sodium phosphate, pH 7.0,  $\mu = 0.10$  M, 25.0 °C.

### 3.3.2.2 Resonance Raman Spectroscopy

The high frequency region of the resonance Raman spectra of haem proteins is composed of porphyrin in-plane vibrational modes that are markers of the oxidation, coordination and spin-state of the haem.<sup>[8-10]</sup> To determine the haem coordination and spin-state, resonance Raman spectra in the high frequency region (1300-1700  $\text{cm}^{-1}$ ), using 413 nm excitation, were obtained for rLb and His61Ala, Figure 3.6, under differing conditions. Characteristic and/or spin-state marker bands for both proteins under various conditions are compiled in Table 3.2.

At room temperature and neutral pH the frequency of the oxidation state marker line  $\nu_4$ , was located at 1373 and 1372  $\text{cm}^{-1}$  for the rLb and His61Ala, respectively, Figures 3.6 (A) and (B). These values fall in the typical range observed for ferric haem proteins

(1370 – 1373  $\text{cm}^{-1}$ ). The  $\nu_3$  line, which is coordination and spin-state sensitive, is detected in the 1470 – 1505  $\text{cm}^{-1}$  range for various ferric haem proteins,<sup>[8, 9, 11]</sup> The high frequency region of the resonance Raman spectra for rLb and His61Ala show vibrational modes characteristic of a mixture of six-coordinate, high-spin ( $\nu_3 \sim 1480 \text{ cm}^{-1}$  and  $\nu_2 \sim 1565 \text{ cm}^{-1}$ ) and six-coordinate, low-spin ( $\nu_3 \sim 1505 \text{ cm}^{-1}$  and  $\nu_2 \sim 1585 \text{ cm}^{-1}$ ) haem species, Figures 3.6(A) and 3.6(B). An important and distinctive feature of the spectrum for the variant was the dominating characteristic six-coordinate, high-spin modes. These modes were clearly apparent when compared to the spectroscopic high-spin modes for rLb.

Under basic conditions (pH 9.0) and low temperature (90K), bands from six-coordinate, low-spin species dominated the spectra in rLb and His61Ala, Figures 3.6(C) and (D). In these spectra, the  $\nu_{10}$  mode of the six-coordinate, low-spin species was now clearly observed at 1639  $\text{cm}^{-1}$ , and was distinct from the vinyl (C=C) stretches. These observations suggested deprotonation of the six-coordinate, high-spin (water-bound) species to a low-spin, hydroxide-bound species for both rLb and His61Ala. Assignment of the six-coordinate, low-spin hydroxy-bound complex in rLb at alkaline pH was identified by the  $\nu_{(\text{Fe-OH})}$  stretching frequency observed at 571  $\text{cm}^{-1}$ . In hydroxy-metmyoglobin (Mb),<sup>[12]</sup> the equivalent stretching mode is observed at 550  $\text{cm}^{-1}$ .

At neutral pH and 90K, the resonance Raman spectrum of ferric-rLb was largely dominated by contribution from six-coordinate, low-spin species, Figure 3.6(E). However, unlike rLb at cryogenic temperatures, the spectrum of His61Ala retained a mixture of high- and low-spin transitions, in which the low-spin transitions were less pronounced, Figure 3.6(F). Under these conditions, incubation of either protein in  $^{18}\text{O}$ -labelled water did not reveal a  $\nu_{(\text{Fe-OH})}$  stretching frequency.

**Table 3.2.**Characteristic spin-state marker bands ( $\text{cm}^{-1}$ ) for ferric derivatives of His61Ala and rLb.

	rLb			His61Ala		
	pH 7 298 K	pH 7 90 K	pH 10 298 K	pH 7 300 K	pH 7 90 K	pH 9 298 K
$\nu_{10}$	-	1636	1639	-	1647	1639
$\nu_4$	1373	1374	1378	1372	1374	1375
$\nu_3$	1482	1505	1505	1484	1485	1505
$\nu_2$	1505			1512	1512	
	1566	1565	1586	1566	1566	1565
	1582	1583		1582	1584	1590

### 3.3.2.4 Magnetic Circular Dichroism (MCD) Spectroscopy

#### *Room Temperature MCD*

Features that are resolved in the MCD spectra facilitate analysis of the spin-state composition of the species from which they are derived. Bands observed at wavelengths below 600nm are porphyrin-based  $\pi$ - $\pi^*$  transitions that shift together with an increase in intensity as the haem iron spin-state changes from high- to low-spin.<sup>[13]</sup> Figure 3.7(B) shows the room temperature UV-visible magnetic circular dichroism spectrum of His61Ala at neutral pH. A typical ferric high-spin spectrum was observed for the variant similar to that observed for ferric metmyoglobin.<sup>[13, 14]</sup> The MCD spectra correlated with the electronic absorption peaks observed in the same wavelength region, Figures 3.7 (A) and (B). The MCD spectrum showed a decrease in low-spin contribution (397, 415 and 571 nm) for His61Ala compared to rLb.<sup>[5]</sup> The Soret troughs at 397 and 415, which arise largely from the more intense low-spin contribution, Figure 3.7, had effectively halved in intensity for His61Ala ( $\lambda/\text{nm}$  ( $\Delta\epsilon/H$  ( $\text{M}^{-1}\text{cm}^{-1}\text{T}^{-1}$ )) for His61Ala: 397 (+17) and 415 (-17); for rLb 397 (+40) and 415 (-37)).<sup>[5]</sup> A prominent increase in trough intensity of the high-spin contribution at 545.5 nm and 637.5 nm was also observed for His61Ala. This increase was relative to the decrease in intensity of the low-spin feature at 571 nm: ( $\lambda/\text{nm}$  ( $\Delta\epsilon/H$  ( $\text{M}^{-1}\text{cm}^{-1}\text{T}^{-1}$ )) for His61Ala: 571 (-15); rLb 571 (-26)).<sup>[5]</sup> A high-spin feature was also apparent at 440 nm that was not apparent for rLb.<sup>[5]</sup>

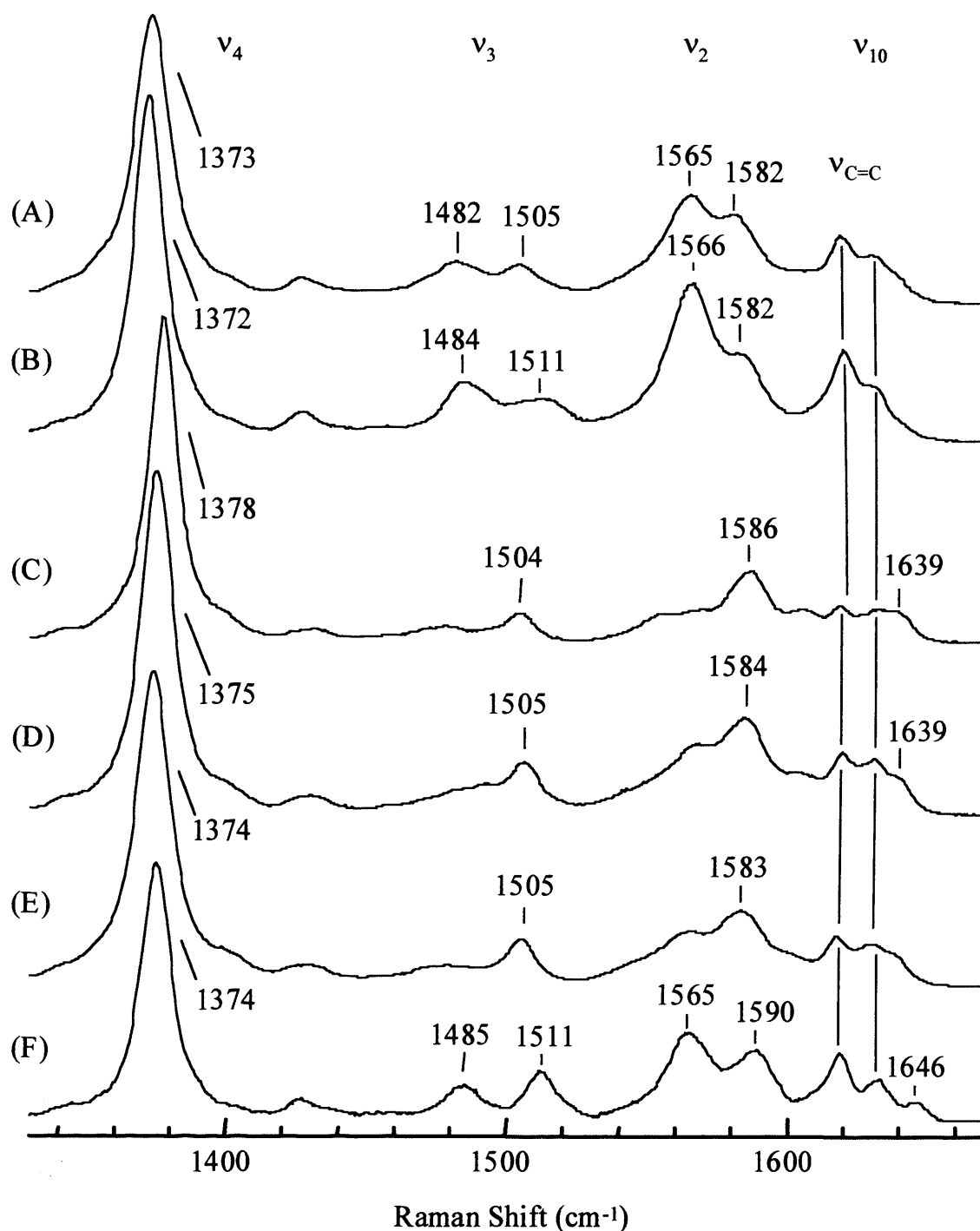


**Figure 3.6.** High frequency region of the resonance Raman spectra of rLb and His61Ala. (A) rLb at pH 7 (100 mM phosphate) and room temperature; (B) His61Ala at pH 7 and room temperature; (C) rLb at pH 10 and room temperature; (D) His61Ala at pH 10 and room temperature; (E) rLb at pH 7 and 90K; (F) His61Ala at pH 7 and 90K.

The decrease in low-spin contribution for His61Ala was similarly reflected in the near-IR region of MCD at room temperature (Figure 3.8 (B)).

At wavelengths longer than 600 nm, the energies of porphyrin( $\pi$ )  $\rightarrow$  Fe(III) charge-transfer (CT) bands give additional information of the nature of the haem axial ligands: high-spin haem give two CT bands and low-spin haem give one band.<sup>[15, 16]</sup> The higher energy high-spin band gives rise to a derivative-shaped feature, the low energy trough of which can be used as a marker for specific ligand set.<sup>[17, 18]</sup> At neutral pH, the MCD spectrum of His61Ala identified two six-coordinate, high-spin species; hence, two high-spin CT bands were observed. A broad charge-transfer band at 740 to 1260 nm, Figure 3.8(A), which corresponds to a derivative feature in the MCD spectrum, Figure 3.8(B), was characteristic of high-spin, water-bound haem.<sup>[15, 16, 19]</sup> For His61Ala this band was almost at the same position (centred at 1105 nm, Figure 3.8(B)) as is found for metMb.<sup>[20]</sup> The second high-spin CT band, also observed for rLb and metMb, was apparent at 809 nm, Figure 3.8(B) and arises from a minority population of high-spin, hydroxide-bound haem. A comparison of the intensities of these transitions with those of Mb provided an estimate that the high-spin water- and hydroxy-bound forms were present at levels of  $\approx 20\%$  and  $\approx 45\%$ , respectively, for His61Ala. The identification of the two high-spin species for His61Ala were consistent with the titration behaviour ( $pK_a = 8.4 \pm 0.1$ ) and with the spectroscopic information obtained from resonance Raman. Clarification of the low-spin species observed in the MCD spectrum for His61Ala was also sought. Thermal equilibrium of the high-spin, hydroxy-bound haem with a low-spin form characterised with a positive CT band at  $\approx 1020$  nm is usually observed. Although it is very likely that a low-spin, hydroxide-bound derivative exists for His61Ala as observed from the UV-visible spectra, unfortunately in this case the CT band in the MCD was obscured by the broad 1105 nm band, Figure 3.8(B), and was not observed.

At wavelengths longer than  $\sim 1360$  nm at room temperature, the absorption spectrum was obscured by vibrational transitions, Figure 3.8(A) dotted, and any underlying electronic transitions were not resolved. However, these vibrational transitions had no appreciable MCD intensity<sup>[21]</sup> and the MCD spectrum, Figure 3.8(B), revealed a broad positive electronic transition at 1370 – 1940 nm characteristic of a second low-spin species. Although the precise origin of this minority species was not clear, it did not derive from hydroxide-coordination since the CT transition of histidine/hydroxide ferric haem occurs in the region 1000 – 1170 nm.<sup>[20, 22-24]</sup> Bands near 1700 nm are normally associated with a second nitrogenous ligand.<sup>[13]</sup> For rLb, a broad envelope was also observed<sup>[3]</sup> at similar wavelengths but with three times the intensity and discernible peak (at  $\sim 1620$  nm), which was attributed to *bis-*

histidine ligation in ~30 % of rLb, an assignment which clearly cannot be made in the case of His61Ala. This unidentified low-spin form in His61Ala (which is present in lower concentrations than is for rLb), together with the low-spin component of the hydroxy-bound haem, presumably accounted for the remaining ~35 % of the sample and for the low-spin haem signatures in the room temperature resonance Raman and electronic absorption spectra.

### ***Low Temperature- MCD***

Consideration of the low temperature (4.2 K) spectra, showed that at wavelengths shorter than 600 nm the UV-visible MCD spectrum of His61Ala, Fig. 3.7(C), was dominated by low-spin transitions, which were at least an order of magnitude more intense than their high-spin counterparts. However, at longer wavelengths where low-spin transitions were absent, there was a detectable high-spin transition at 630 nm (a diagnostic band of this spin-state) - corresponding to the 637.5 nm trough in the room temperature spectrum, Fig. 3.7(B), which was not observed for rLb. The intensity of this transition varies substantially between haemoproteins and, although apparently small, could easily account for the levels of high-spin haem observed at room temperature, particularly since both the resonance Raman and EPR data (*vide infra*) indicated substantial contributions from high-spin haem at low temperature.

Similarly, in the Soret region, Lb<sup>[3]</sup> was previously found to have a peak-to-trough intensity of ~ 32 mM<sup>-1</sup>cm<sup>-1</sup>, indicating ~100 % conversion to low-spin at 4.2 K; for His61Ala, the Soret band, Fig. 3.7(C), had only ~ 1/3 of this intensity and was not consistent with a complete spin-state transition. Hence, the MCD data supported the existence of considerable amounts of high-spin haem even at low temperature and, as such, were consistent with the resonance Raman data. This was further supported by the low temperature spectrum in the near-IR region, Fig. 3.8(C), which contained broad low-spin, CT intensity between 1000 and 2000 nm, peaking near ~ 1540 nm, but of insufficient intensity to account for 100 % low-spin haem. A similar transition was also observed for Lb,<sup>[3]</sup> but with a very well-resolved peak at 1600 nm, indicative of *bis*-histidine ligation, and an intensity ~ 3.6 times that observed for His61Ala. A shoulder in the Lb spectrum at 900 – 1100 nm was attributed to low-spin, hydroxy-bound haem,<sup>[3]</sup> which may correspond to the ~ 1070 nm feature for His61Ala, Fig. 3.8(C), (although this was likely to be heavily overlapped with the 1105 nm high-spin CT transition).

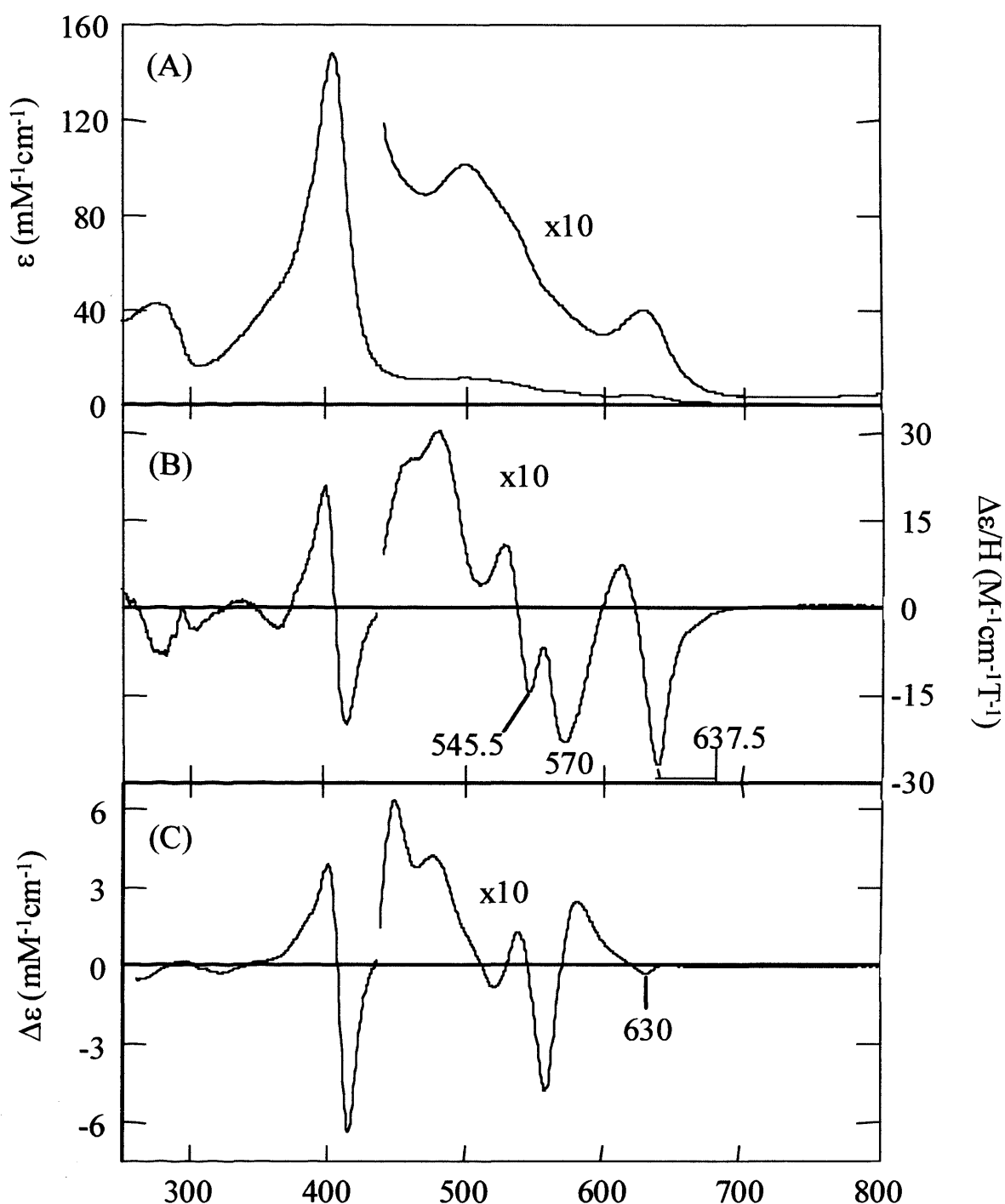


**Figure 3.7.** (A) Electronic absorption spectrum of His61Ala at room temperature, pH 7.0. (B) UV-visible MCD spectra of His61Ala (pH 7.0) recorded at room temperature using a magnetic field of 6 T and sample concentrations of 67 (in the Soret region) and 734  $\mu\text{M}$  (in the visible region) and (C) recorded at 4.2 K using a magnetic field of 5 T and sample concentrations of 34 and 340  $\mu\text{M}$ .

### 3.3.2.5 Electron Paramagnetic Resonance (EPR) Spectroscopy

Low temperature electron paramagnetic resonance spectra of His61Ala were recorded at neutral pH. EPR spectroscopy in the absence, Fig. 3.9(A), and presence, Fig. 3.9(B), of glycerol glassing agent provided a clearer indication of the relative concentrations of the low-spin species at cryogenic temperatures. As expected, the spectra were dominated by high-spin signals ( $g_x$  and  $g_y$  near 6, and  $g_z$  at  $\sim 2$ ). However, expansion of either spectrum in the  $g \approx 2$  region revealed the presence of two, distinct low-spin haem species, in agreement with the conclusions derived from the MCD spectra. In the absence of glycerol, Fig. 3.9(A), a rhombic trio with  $g_{zyx}$ -values of 2.78, 2.30 and 1.66, respectively, was observed and was assigned to a low-spin species. On addition of glycerol, Fig. 3.9(B), the freezing-induced changes were significantly reduced and led to a shift of  $g_z$  to 2.83 with concomitant emergence of a new species ( $g_z = 3.15$ ), which may correlate with an unresolved broad feature observed prior to the addition of glassing agent. Integration of these EPR intensities using published methods,<sup>[25]</sup> indicated that the  $g_z = 3.15$  and  $g_z = 2.83$  account for 10 ( $\pm 2$ ) % and 14 ( $\pm 3$ ) % of the sample concentration, respectively. This was in reasonable agreement with the estimations from the MCD spectra: that there were two low-spin species that account for approximately one quarter of the His61Ala population.

For rLb, EPR<sup>[5]</sup> has shown minority high-spin species ( $g = 6.01$  and  $2.00$ ), in comparison to that observed for the high-spin spectra for His61Ala and hence, consistent with UV-visible data at 77K for rLb. Low-spin features dominate the spectra, notably at  $g = 2.74$  and  $2.27$ . This species has been detected previously ( $g = 2.72$  and  $2.26$ <sup>[26]</sup>;  $g = 2.76$  and  $2.31$ <sup>[3]</sup>;  $g = 2.69$  and  $2.24$ <sup>[4]</sup>) and has been assigned to the formation of a *bis*-imidazole species. A weak feature at  $g = 3.1$  was also apparent, which has been detected previously<sup>[4, 26]</sup> and probably derives from a second low-spin form which is also apparent in His61Ala.

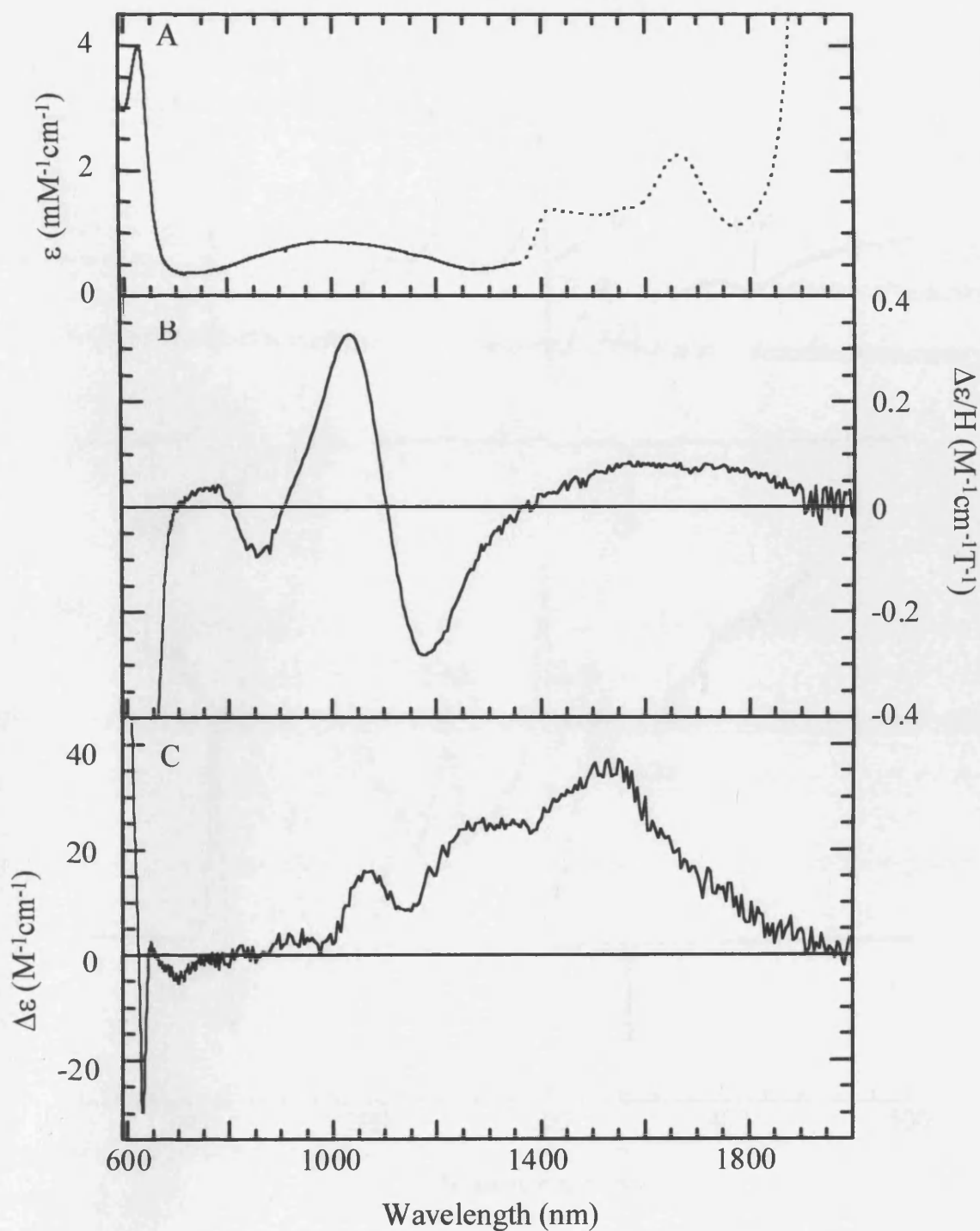


**Figure 3.8.** Near-infrared MCD spectra of His61Ala (pH 7.0). (A) room temperature UV-visible spectrum. (B) MCD spectrum recorded at room temperature using a magnetic field of 6 T and a sample concentration of 734  $\mu\text{M}$ . (C) MCD spectrum recorded at 4.2 K using a magnetic field of 5 T and a sample concentration of 340  $\mu\text{M}$ .

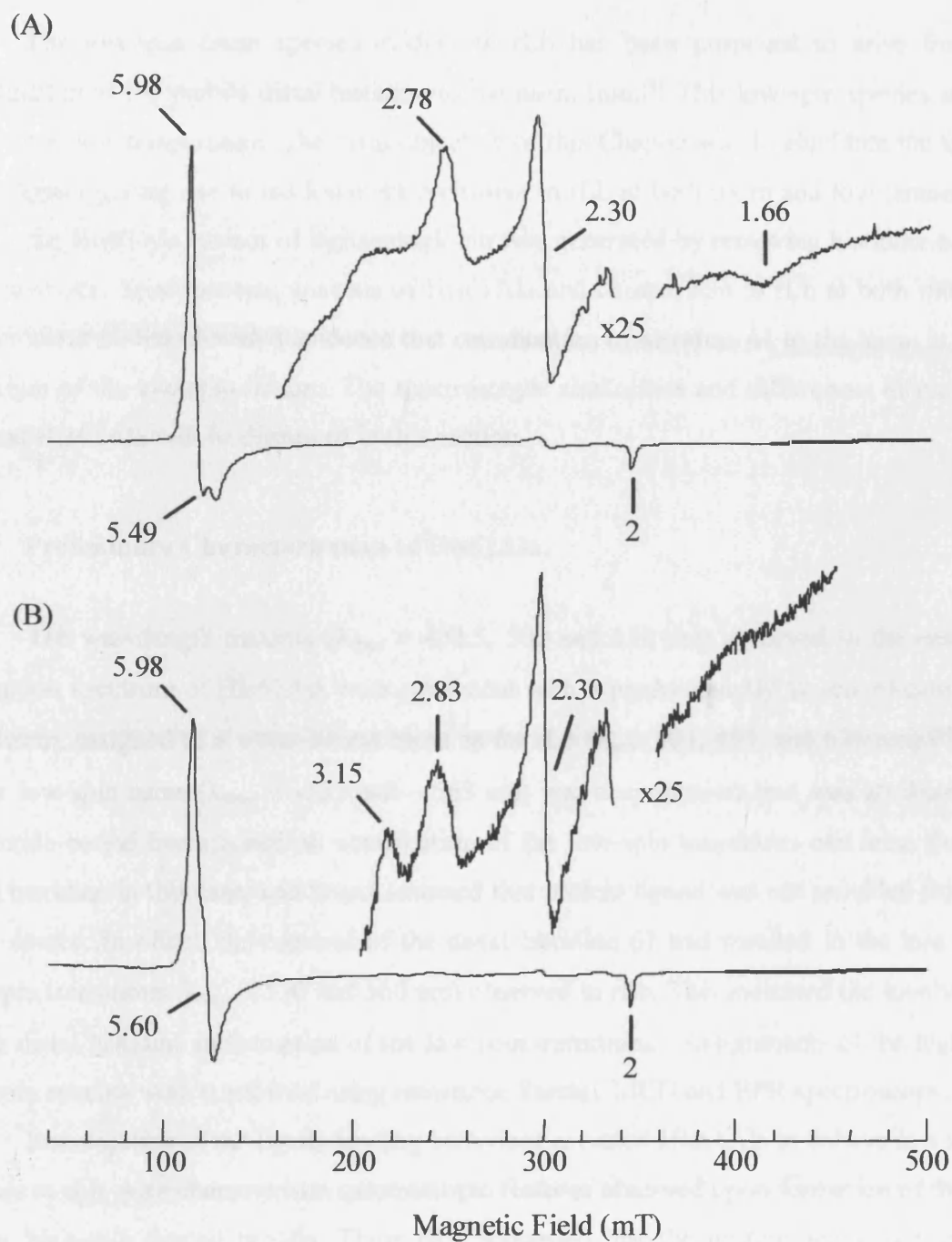


**Figure 3.9.** X-band EPR spectra of His61Ala (pH 7.0) before (A) and after (B) the addition of ~ 50 % v/v glycerol. Spectra were recorded at 10 K using 1 mT modulation amplitude and 2.01 mW microwave power. The g-values are indicated.

### 3.4 Discussion

The low-spin haem species evident in rLb has been proposed to arise from the coordination of the mobile distal histidine to the haem iron.<sup>[3]</sup> This low-spin species is more apparent at low temperature. The main objective of this Chapter was to elucidate the identity of the ligand giving rise to the low-spin derivative in rLb at both room and low temperature. Hence, the His61Ala variant of leghaemoglobin was generated by removing histidine 61 from the active site. Spectroscopic analysis of His61Ala and comparison to rLb at both room and low temperature has provided evidence that coordination of histidine 61 to the haem is indeed the origin of the low-spin feature. The spectroscopic similarities and differences displayed by rLb and His61Ala will be discussed in this section.

#### 3.4.1 Preliminary Characterisation of His61Ala.

The wavelength maxima ( $\lambda_{\max} = 402.5, 500$  and  $630$  nm) observed in the electronic absorption spectrum of His61Ala were consistent with a predominantly six-coordinate, high-spin haem, assigned to a water-bound haem as for rLb ( $\lambda_{\max} 403, 495,$  and  $626$  nm).<sup>[5]</sup> Some minor low-spin haem ( $\lambda_{\max} = \sim 535$  and  $\sim 563$  nm) was also apparent and was attributed to a hydroxide-bound haem, since no contribution of the low-spin transitions can arise from the distal histidine in this case, and it was assumed that protein ligand was not provided from any other source. In effect, the removal of the distal histidine 61 had resulted in the loss of the low-spin transitions ( $\lambda_{\max} = 530$  and  $560$  nm) observed in rLb. This indicated the involvement of the distal histidine in formation of the low-spin transitions. Assignments of the high- and low-spin species were confirmed using resonance Raman, MCD and EPR spectroscopy.

Investigation of the ligand binding behaviour revealed His61Ala to behave in a similar manner to rLb, with characteristic spectroscopic features observed upon formation of the low- and/or high-spin ligated protein. These data suggested that the protein active site and the ability of His61Ala to bind exogenous ligands had not been seriously perturbed as a result of the mutation. Equilibrium dissociation constants derived for the binding of cyanide and azide to His61Ala were found to be essentially the same as rLb, suggesting that the distal histidine does not play a significant role in binding or stabilisation of binding of these ligands in the active site. These results also support previous work,<sup>[2]</sup> which suggests that the distal histidine ligand ‘swings’ in and out of the active site haem pocket of the protein to accommodate

exogenous ligands. However, in comparison to data for rLb,<sup>[7]</sup> a decrease in the equilibrium dissociation constant was observed for His61Ala on binding the bulkier ligand, nicotinate at neutral pH. This observation can be explained in terms of steric effects: the removal of the bulky histidine residue allows easier access of nicotinate into the active site to bind to the haem.

Determination of the  $pK_a$  of His61Ala to identify the titrating residue in the variant was very similar to that of rLb and indicated titration of the distal water molecule. Formation of a low-spin species was observed for His61Ala as the pH was increased similar to rLb.<sup>[5]</sup> Wavelength maxima ( $\lambda_{\max} = 406, 537$  and  $574$ ) indicated formation of six-coordinate, hydroxide-bound haem, which derives from the deprotonation of the coordinated distal water molecule. This similarity of  $pK_a$ s was surprising, since one might have expected a change in the  $H_2O/OH^-$  distribution through removal of hydrogen-bonding interaction to the coordinated water in the haem pocket. Although the structures of the water- and hydroxide-bound Lb derivatives are not known, the distal histidine 61 residue is known to be mobile. As such, the similar  $pK_a$ s for His61Ala and rLb may suggest that the hydrogen-bonding interaction does not have a significant influence on the  $H_2O/OH^-$  equilibrium in Lb. The results are also consistent with the equilibrium binding data for cyanide and azide binding to His61Ala (see above).

#### 3.4.1.1 Spectroelectrochemistry

Determination of the mid-point potential for His61Ala ( $-6$  mV) revealed a decrease of  $27$  mV compared to rLb ( $21$  mV), indicating a slight net destabilisation of the reduced form of the haem. An explanation for these findings can be based on comparison of the active site and haem axial ligation of rLb and His61Ala. The rLb protein exists as a mixture of high- and low-spin species whereas His61Ala exists as a predominantly high-spin species. The nature of the high-spin form for both proteins has been attributed to water-bound haem. The only difference between the two proteins is the low-spin species, which arises from the coordination of hydroxide and distal histidine in rLb and from coordination of hydroxide in His61Ala. Since the two proteins have similar  $pK_a$  values, it can be assumed that at pH 7 there will be the same amount of water- and hydroxide-bound species present. Therefore the only difference between the two proteins is the lack of the distal histidine residue. Coordination of the  $\pi$ -acceptor histidine to the haem of rLb may stabilise the ferrous oxidation state due to the electron donating ability of the histidine nitrogen, which will favour the ferrous oxidation state of the protein. Absence of this residue in the His61Ala variant results in a decrease in

the mid-point potential (the ferrous oxidation state is less favourable). As a consequence the difference in the mid-point potentials observed for rLb and His61Ala must arise from the presence of the histidine-bound species (effect of the distal histidine).

### 3.4.2 Spectroscopic Correlations

Mutagenic replacement of the distal histidine with alanine resulted in a predominantly six-coordinate, high-spin ferric species with little low-spin contribution evident in the electronic absorption spectrum. Loss of the low-spin features that were apparent in the electronic absorption spectrum of rLb indicated the involvement of the histidine residue in rLb and gave initial evidence that this residue does indeed coordinate to the haem in rLb.

The nature of the high- and low-spin forms required further investigation. Resonance Raman spectroscopy gave further insight into the differences and similarities in haem coordination and spin-state distribution in both proteins. Resonance Raman spectroscopy facilitated quantitative analysis of the low-spin forms of rLb and His61Ala with changes in pH or temperature. At room temperature and neutral pH, resonance Raman spectra of rLb and His61Ala consisted of six-coordinated, high- and low-spin species, with the high-spin modes dominant for the variant in agreement with electronic absorption data. Spectra obtained at basic pH showed dominant low-spin species for both proteins, again in agreement with high pH electronic absorption spectra. The low-spin modes observed at basic pH were assigned to an iron-hydroxide derivative. Assignment of the six-coordinate, low-spin hydroxy-bound complex in rLb at alkaline pH was identified by the  $\nu_{(\text{Fe-OH})}$  stretching frequency observed at  $571\text{ cm}^{-1}$  that down shifts by  $26\text{ cm}^{-1}$  in  $^{18}\text{O}$ -labelled water. In hydroxy-metmyoglobin<sup>[12]</sup> the equivalent stretching mode was observed at  $550\text{ cm}^{-1}$ . Parallel experiments with His61Ala failed to detect any  $^{18}\text{O}$ -isotope sensitive frequency, although MCD and electronic absorption data provided evidence for hydroxide-bound haem in His61Ala. However, poor resonance enhancement of the  $\nu_{(\text{Fe-OH})}$  band in the variant may account for this apparent discrepancy.

At cryogenic temperatures and neutral pH, the variant was observed as a mixture of high- and low-spin species, in contrast to the wholly low-spin form observed for the rLb under the same conditions. The low-spin form was not attributed to a Fe-hydroxide species, as incubation of either protein in  $^{18}\text{O}$ -labelled water did not reveal a  $\nu_{(\text{Fe-OH})}$  stretching frequency. This suggested a different form for the low-spin species in both proteins.

Semi-quantitative assessment of the nature of the new/different low-spin species was sought using the diagnostic pairing of MCD and EPR. Identification of haem protein axial

ligand using the combined applications of magnetic circular dichroism and electron paramagnetic spectroscopy was facilitated by the fingerprint library that has been based upon analysis of many haem proteins of known ligation properties.<sup>[17, 18]</sup> Throughout the 450 – 600 nm region, both high- and low-spin species contributed to the MCD spectrum, with bands derived from the low-spin form being less intense than high-spin bands for His61Ala, in contrast to that observed for rLb. Spectra obtained at neutral and mildly acidic pH differed solely in the relative proportions of the six-coordinate, high- and low-spin components, with slightly increased proportion of the latter at high pH assigned to the hydroxide form of both proteins. Similar observations were observed at low temperature. The His61Ala variant displayed low-spin MCD spectroscopic features at low temperature that were similar to rLb. Accordingly, *bis*-imidazole ligation involving the distal histidine was precluded as the origin of the low temperature form in rLb, which is not possible in His61Ala. However, the low-spin band observed in the near-IR MCD spectrum at 1540 nm, a minority feature observed for the variant and which was probably hidden by the 1600 nm band for rLb, suggested that the temperature-dependent spectral changes, whilst not deriving from ligation from the distal histidine, were likely to be due to the coordination of another nitrogenous protein residue. These data suggested that two low-spin species were present for His61Ala. In conjunction with MCD data, the EPR analysis also confirmed two low-spin species for His61Ala evident at low temperature. Assignment of these two low-spin species was not straightforward. The  $g_z = 2.83$  signal was in a similar region to the alkaline forms of Mb ( $g_z \sim 2.6$ ) and horseradish peroxidase ( $g_z \sim 2.9$ ),<sup>[27, 28]</sup> and was likely to correspond to low-spin, hydroxide-bound haem, particularly since MCD and UV-visible data provided evidence for the presence of this species in the high- and low-spin forms, respectively. The second, minority low-spin species ( $g_z = 3.15$ ) – which was also detected in the MCD spectra – was more difficult to assign, but a similar species ( $g \approx 3.1$ ) has been previously observed in the EPR spectra of Lb,<sup>[4, 26]</sup> rLb,<sup>[5]</sup> His61Arg (Chapter 5) and His61Lys (Chapter 5). Clearly, this cannot arise from coordination of the distal histidine residue. At present, the second low-spin species cannot yet be specifically assigned, although from the intense signals observed in the EPR spectrum of His61Lys, it is more than likely to arise from the possible ligation of one of two lysine residues close to the active site. Examination of the distal pocket of rLb indicates lysine 64 or lysine 57 are the most likely residues able to coordinate to the haem under these conditions. Clearly, unambiguous confirmation of the structural changes and haem coordination alterations associated with formation of the low-spin species at cryogenic temperature requires crystallographic information, which is not available and quite difficult to obtain.

Attempts to probe these changes by an alternative route, by site-specific replacement of the lysine 64 and lysine 57, are currently underway.

### 3.5 Summary

To summarise, the work carried out in this Chapter has shown that the low-spin species observed in the low temperature spectrum of rLb originates from the ligation of the distal histidine 61 residue. This has been confirmed by spectroscopic analysis of the His61Ala variant of leghaemoglobin, in which the distal histidine has been replaced by a non-coordinating alanine residue. The resulting His61Ala variant was observed to be predominantly high-spin with a loss of the low-spin features that were observed in rLb. Room temperature and low temperature resonance Raman, MCD and EPR spectroscopy of His61Ala exhibited loss of the low-spin features that were assigned to *bis*-histidine ligation in rLb. In addition, minority low-spin components observed in His61Ala at room temperature were assigned as arising from hydroxide bound haem and at cryogenic temperature arising from possible ligation of a different nitrogenous ligand (also apparent in rLb), possibly a lysine residue.

### 3.6 References

1. A. Ehrenberg and N. Ellfolk, *Acta Chem. Scand.* (1963) **17**, S343.
2. C. A. Appleby, W. E. Blumberg, J. H. Bradbury, W. H. Fushman, J. Peisach, B. A. Wittenberg, J. B. Wittenberg and P. E. Wright, in *Hemoglobin and Oxygen Binding*, C. Ho, Ed. (Elsevier, North Holland, Amsterdam) 1982, pp. 435.
3. G. Sievers, P. M. A. Gadsby, J. Peterson and A. J. Thomson, *Biochim. Biophys. Acta* (1983) **742**, 637.
4. C. A. Appleby, W. E. Blumberg, J. Peisach, B. A. Wittenberg and J. B. Wittenberg, *J. Biol. Chem.* (1976) **251**, 6090.
5. D. K. Jones, R. Badii, F. I. Rosell and E. Lloyd, *Biochem. J.* (1998) **330**, 983.
6. P. J. Ellis, C. A. Appleby, J. M. Guss, W. N. Hunter, D. L. Ollis and H. C. Freeman, *Acta Crystallographica Section D* (1997) **53**, 302.
7. N. Patel, D. K. Jones and E. L. Raven, *Eur. J. Biochem.* (2000) **267**, 2581.
8. S. Hu, K. S. Smith and T. G. Spiro, *J. Am. Chem. Soc.* (1996) **118**, 12638.
9. T. G. Spiro and X. Y. Li, in *Biological Applications of Raman Spectroscopy*, T. G. Spiro, Ed. (John Wiley & Sons, New York) 1988, vol. 3.
10. L. L. Wang, *Curr. Opin. Chem. Biol.* (1988) **2**, 263.
11. T. K. Das, H. C. Lee, S. M. G. Duff, R. D. Hill, J. Peisach, D. L. Rousseau, B. A. Wittenberg and J. B. Wittenberg, *J. Biol. Chem.* (1999) **274**, 4207.
12. A. Feis, M. P. Marzocchi, M. Paoli and G. Smulevich, *Biochemistry* (1994) **33**, 4577.
13. M. R. Cheesman, C. Greenwood and A. J. Thomson, *Adv. Inorg. Chem.* (1991) **36**, 201.
14. A. J. Thomson, M. R. Cheesman and S. J. George, *Meth. Enzymol.* (1993) **226**, 199.
15. J. C. Cheng, G. A. Osborne, P. J. Stephens and W. A. Eaton, *Nature* (1973) **241**, 193.
16. P. S. Braterman, R. C. Davies and R. J. P. Williams, *Acta. Chem. Phys.* (1964) **7**, 359.
17. M. R. Cheesman, S. J. Ferguson, J. W. Moir, D. J. Richardson, W. G. Zumft and A. J. Thomson, *Biochemistry* (1997) **36**, 16267.
18. P. M. A. Gadsby and A. J. Thomson, *J. Am. Chem. Soc.* (1990) **112**, 5003.
19. A. S. Brill and R. J. P. Williams, *Biochem. J.* (1961) **78**, 246.
20. P. J. Stephens, J. C. Sutherland, J. C. Cheng and W. A. Eaton, in *Excited States of Biological Molecular Processes*, J. B. Birks, Ed. (Wiley, Chichester) 1976, pp. 434.
21. L. A. Nafie, T. A. Keiderling and P. J. Stephens, *J. Am. Chem. Soc.* (1976) **98**, 2715.
22. H. E. T. Seward, PhD Thesis, University of East Anglia (1999).

23. N. Foote, P. M. A. Gadsby, M. J. Berry, C. Greenwood and A. J. Thomson, *Biochem. J.* (1987) **246**, 659.
24. D. G. Eglinton, P. M. A. Gadsby, G. Sievers, J. Peterson and A. J. Thomson, *Biochim. Biophys. Acta* (1983) **742**, 648.
25. R. Aasa and T. Vänngård, *J. Magn. Res.* (1975) **19**, 308.
26. C. S. Maskall, J. F. Gibson and P. J. Dart, *Biochem. J.* (1977) **167**, 435.
27. F. R. N. Gurd, K. Falk, B. G. Malstrom and T. Vänngård, *J. Biol. Chem.* (1967) **242**, 5724.
28. M. Tamura and H. Hori, *Biochim. Biophys. Acta* (1972) **284**, 20.

**Chapter 4**  
**Incorporation of New Haem**  
**Axial Ligation into**  
**Leghaemoglobin:**  
**Spectroscopic,**  
**Electrochemical and Ligand**  
**Binding Analysis of the**  
**His61Tyr Variant**

## 4 Incorporation of New Haem Axial Ligation into Leghaemoglobin: Spectroscopic, Electrochemical and Ligand Binding Analysis of the His61Tyr Variant

### 4.1 Introduction

One of most challenging questions in bio-inorganic chemistry has been to identify and understand the relationships that exist between different classes of haem proteins: that is, to rationalise the mechanisms by which the protein *structure* controls the specific chemical *reactivity* of the haem group.<sup>[1, 2]</sup> Included amongst a range of structural variables that are likely to affect the functional properties of the haem, perhaps the most influential are the axial ligands. For this reason, the ways in which changes in axial ligation affect haem chemistry have been extensively examined for various haem proteins<sup>[1-19]</sup> in an attempt to rationalise the very diverse functional properties exhibited by different haem proteins and enzymes. Although clearly useful, this experimental approach is sometimes limited by the tolerance of the protein to mutagenic substitutions at the axial amino acid positions and can often be invalidated altogether if the variant protein is not able to bind haem under normal conditions.

Whilst it is recognised that the exact function of the haem group amongst *different* haem proteins can be regulated by the different axial ligation in each, it is also becoming increasingly clear that certain haem proteins are capable of *self-regulation*: that is, they are able to vary their own haem coordination geometry - and, by implication, the haem chemistry - through an *intramolecular* ligand switching mechanism in which conformational rearrangements lead to the replacement of one of the axial ligands by another protein-based residue. Examples of ligand switching mechanisms of this kind include: (a) the pH-dependent alkaline transition of ferricytochrome *c* in which the methionine axial ligand present at neutral pH is replaced by two lysine residues at alkaline pH;<sup>[20, 21]</sup> (b) reduction of the *c*-haem in cytochrome *cd*<sub>1</sub> in which the axial ligation changes on reduction from His/His to His/Met;<sup>[22, 23]</sup> (c) the pH-dependent conversion of ferric *Chlamydomonas* haemoglobin from His/H<sub>2</sub>O ligation at acidic pH to His/Tyr ligation at alkaline pH;<sup>[24]</sup> (d) the oxidation-state dependent replacement of a cysteine ligand by a histidine ligand in the haem *b*-containing transcriptional activator CooA.<sup>[25-28]</sup> Whilst the functional role - if, indeed, there is one - of these conformational rearrangements is not clear in all cases, these systems do provide a convenient and experimentally advantageous framework for the investigation of haem structure/function relationships.

In this context, a new approach to investigate the haem structure/function relationships that bypasses the inherent difficulties associated with direct ligand replacement has been used in this Chapter using rLb. Crystallographic<sup>[29, 30]</sup> studies of soybean leghaemoglobin have revealed a larger, more accessible and more flexible distal haem pocket than is encountered in the mammalian globins. This conformational flexibility gives rise to a mobile switching histidine ligand (His61) which, from spectroscopic studies<sup>[31-34]</sup> has been implicated in binding to the ferric haem species at low temperature to generate a low-spin, *bis*-histidine derivative. The unique mobility of the leghaemoglobin molecule in the study of haem structure/function relationships has been exploited by using it as an experimental framework for the examination of the effect of axial ligand substitutions.<sup>[35]</sup> Work carried out in Chapter 3 examined a variant of rLb in which the switching ligand had been replaced (His61Ala variant) and it was established that the incorporation of a non-ligating amino acid essentially eliminated the low-spin haem species (Chapter 3),<sup>[35]</sup> thereby, confirming the origin of the low-spin species. In an extension to this, work conducted in this Chapter and the following Chapter show that it is possible to incorporate new ligands into this flexible haem architecture, by replacement of the switching histidine 61 ligand. In this work, a tyrosine residue has been incorporated generating the His61Tyr variant. In effect, the mobile switching ligand has been used as a platform for the incorporation of new axial ligation in the haem protein.

## 4.2 Mutagenesis, Protein Expression and Isolation

Site-directed mutagenesis, to generate the His61Tyr variant of rLb, was carried out according to the Quikchange protocol (Stratagene), using the rLb DNA and the His61Tyr mutagenic oligonucleotide (Chapter 7, Table 7.1). Successful mutation was confirmed by sequencing of the entire rLb gene. The His61Tyr variant was expressed, isolated and purified according to published procedures<sup>[36]</sup> (Chapter 7). Isolation of His61Tyr resulted in the formation of apo-protein and required reconstitution by addition of appropriate volumes of exogenous haem. Excess haem was removed using a G50 Sephadex (Pharmacia) column, equilibrated with 20mM Tris/HCl buffer, pH 8.0. Purified protein (~ 8 mg/l) was obtained with  $A_{\text{Soret}}/A_{280}$  ( $R_z$ ) > 4 (pH 7.0, 25.0 °C,  $\mu = 0.10$  M) and migrated as a single band on a SDS PAGE gel, Figure 7.2 (Chapter 7).

### 4.3 Characterisation of His61Tyr

#### 4.3.1 Electronic Absorption Spectroscopy

The most noticeable feature of the His61Tyr variant, observed during handling and purification, was its green colour, Figure 4.1; samples of rLb are red/brown in colour.



**Figure 4.1.** His61Tyr (left) and rLb (right)

The electronic absorption spectrum of the ferric derivative of His61Tyr, Figure 4.2, revealed a six-coordinate, high-spin species ( $\lambda_{\max} (\epsilon/\text{mM}^{-1}\text{cm}^{-1}) = 404.5 (181), 488, 534, 602$  nm). The prominent band at  $\sim 600$  nm is a fingerprint band for iron-tyrosinate ligation and gives rise to the unique green colour. This high-spin species was spectroscopically distinct from the mixture of high- and low-spin species observed for rLb ( $\lambda_{\max} = 403, 495, 530, 560$  and  $626$  nm).<sup>[36]</sup> The maxima observed for His61Tyr were similar to those for the phenol derivative of rLb ( $\lambda_{\max} = 404.5, 489, 534, 568^{\text{sh}}, 603$  nm), Figure 4.3, prepared in this work and are consistent both with previously reported values for the phenol derivative of Lb ( $\lambda_{\max} = 402, 604$  nm)<sup>[34]</sup> and with the coordination of the tyrosine ligand to the haem iron. In the reduced form, Figure 4.2, wavelength maxima for His61Tyr ( $\lambda_{\max} (\epsilon/\text{mM}^{-1}\text{cm}^{-1}) = 429.5 (195)$  and  $557$  nm) were similar to those of rLb (Chapter 2, Table 2.1)<sup>[36]</sup> indicating loss of the tyrosine ligand and formation of a five-coordinate haem structure.

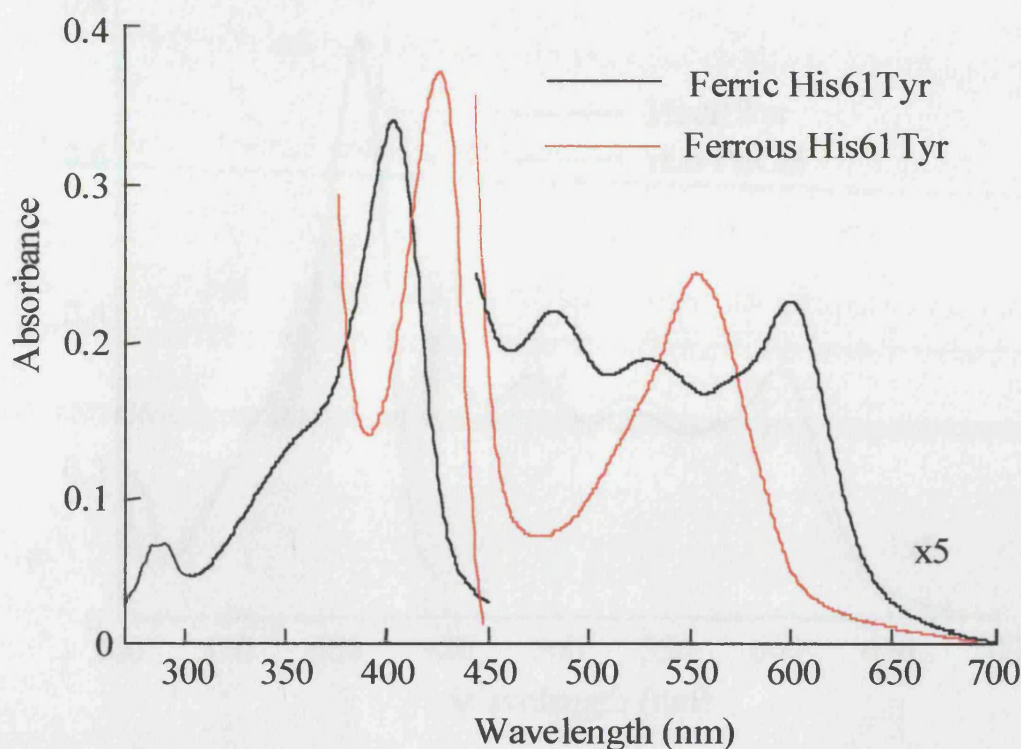


**Figure 4.2.** Electronic absorption spectra of ferric and ferrous His61Tyr. The absorbance in the visible region (450-700 nm) has been multiplied by a factor of five. Conditions: sodium phosphate, pH 7.0,  $\mu = 0.10$  M, 25.0 °C.

### 4.3.2 Ligand Binding

Addition of excess cyanide to His61Tyr, Figure 4.4, resulted in a spectrum ( $\lambda_{\text{max}}$  ( $\epsilon/\text{mM}^{-1}\text{cm}^{-1}$ ) = 420 (159) and 546 nm) that was similar to the cyanide-bound form of rLb and which was consistent with replacement of the axial tyrosine ligand with cyanide. The His61Tyr variant was observed to readily bind other strong field exogenous ligands at the haem, in the ferric and ferrous oxidation states: absorption maxima and corresponding absorption coefficients are shown in Table 4.1. In contrast, the addition of weak field ligands (*e.g.* fluoride, acetate) to His61Tyr did not perturb the electronic spectrum substantially, Figure 4.4, indicating that these ligands did not displace the haem-bound tyrosinate group. Attempts to form the oxy-derivative of His61Tyr were made difficult due to the rapid auto-oxidation of the oxy-His61Tyr, hence no Fe(II)-O<sub>2</sub> was observed for the variant.

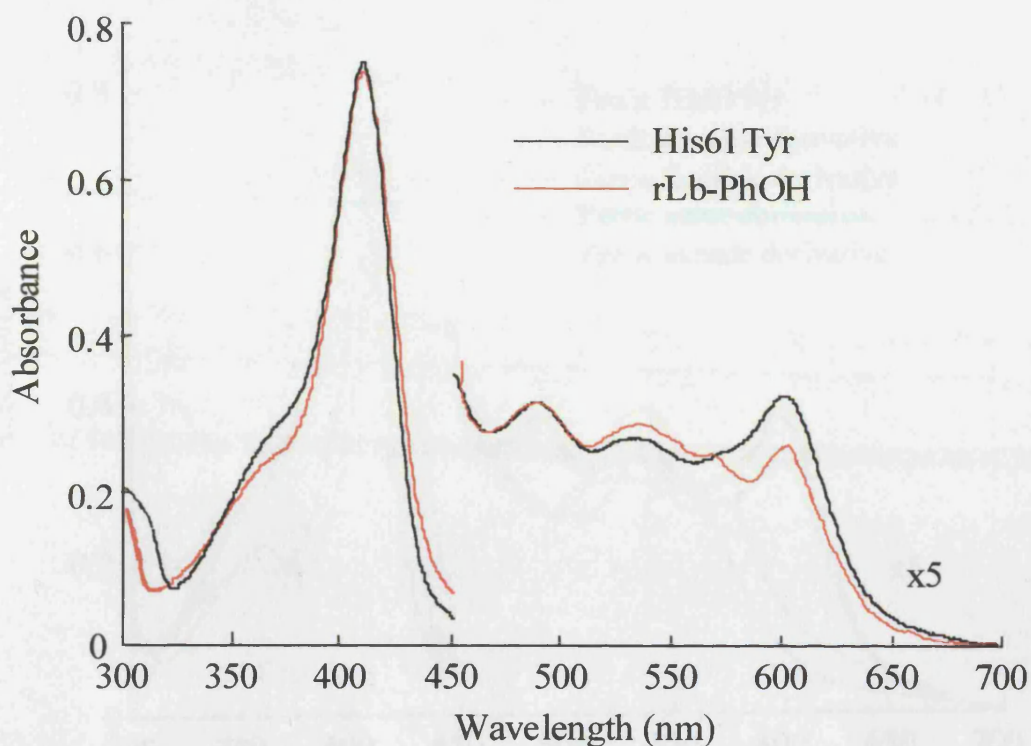


**Figure 4.3.** Electronic absorption spectra of His61Tyr and phenol derivative of rLb. The visible region (450-700 nm) has been multiplied by a factor of five. Conditions: sodium phosphate, pH 7.0,  $\mu = 0.10$  M, 25.0 °C.

Examination of the binding behaviour of the His61Tyr variant with exogenous ligands provided additional evidence in support of tyrosinate ligation. Hence, equilibrium binding constants,  $K_d$ , for binding of cyanide to His61Tyr ( $K_{d,\text{cyanide}} = 3300 \pm 100 \mu\text{M}$ ) at neutral pH, Figure 4.5(A), indicated that the affinity of the cyanide ligand for the haem was over 1000-fold lower than for rLb ( $K_{d,\text{cyanide}} = 1.1 \pm 0.1 \mu\text{M}$ ).<sup>[37]</sup> Correspondingly, binding of azide to His61Tyr ( $K_{d,\text{azide}} = 19000 \pm 1000 \mu\text{M}$ ), Figure 4.5(B), at neutral pH was also significantly lower than for rLb ( $K_{d,\text{azide}} = 4.8 \pm 0.2 \mu\text{M}$ ).<sup>[37]</sup> These data indicated that binding of the tyrosine ligand at the haem iron affects the affinity of the variant for exogenous ligands. At acidic pH (pH 4.0), binding of exogenous ligand to His61Tyr was ~10-fold more favourable ( $K_{d,\text{cyanide}} = 200 \pm 40 \mu\text{M}$ ,  $K_{d,\text{azide}} = 700 \pm 70 \mu\text{M}$ ) than at basic pH. Furthermore, although the binding affinities of His61Tyr for both ligands was still weaker than rLb, the relative affinities were more similar (~ 20-60-fold difference) than at neutral pH (~ 1000-fold difference) (rLb (pH 4.0)  $K_{d,\text{cyanide}} = 9 \pm 0.2 \mu\text{M}$ ,  $K_{d,\text{azide}} = 12 \pm 0.3 \mu\text{M}$ ).

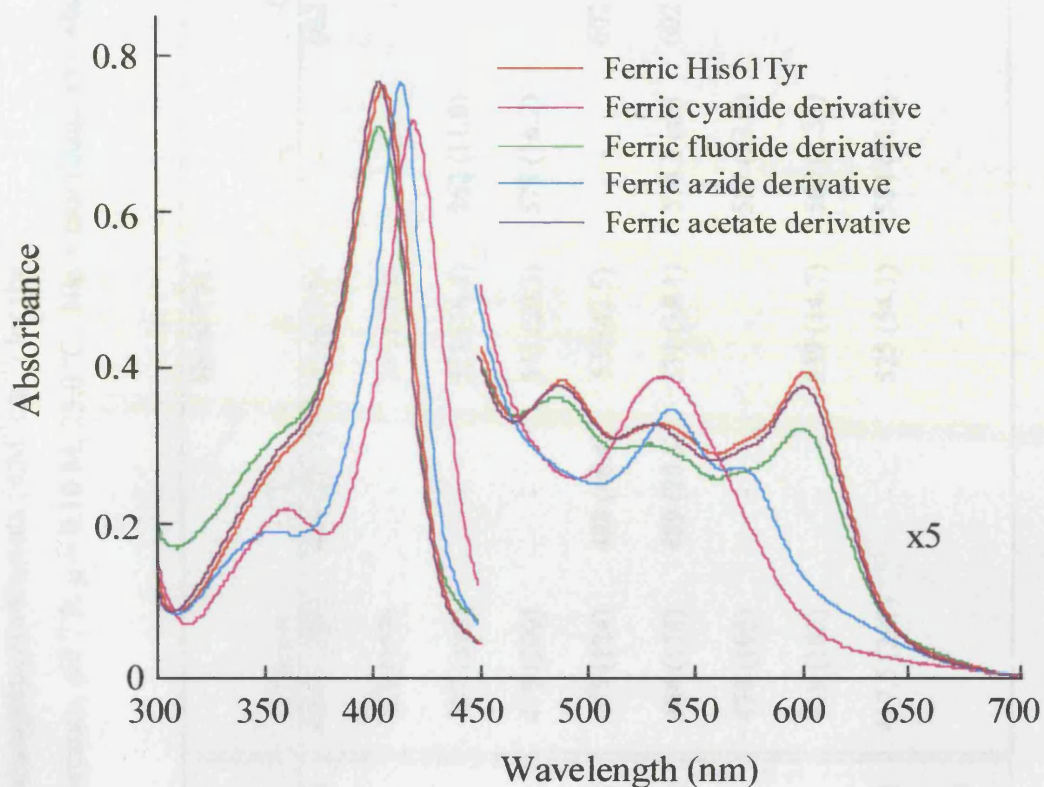


**Figure 4.4.** Electronic absorption spectra of the anionic ligand bound derivatives of ferric His61Tyr. Conditions: sodium phosphate, pH 7.0,  $\mu = 0.10$  M, 25.0 °C.

### 4.3.3 Determination of the haem $pK_a$ of His61Tyr

The change in the electronic spectrum of His61Tyr as a function of pH (pH 3.8 – 8.5) is indicated in Figure 4.6. The variant was observed to change from green, at neutral pH, to red/brown, at acidic pH. At pH values less than 4, there was a decrease in intensity of the Soret band at 404.5 nm and a shift of this band to 401 nm; a new band at 373 nm was also observed at acidic pH (pH 3.7). Below pH 3.5, denaturation and precipitation of the protein occurred. In the visible region, the intensity of the 602 nm band decreased with decreasing pH and shifted to a longer wavelength ( $\lambda_{\max} = 645$  nm). There were no changes in the electronic absorption spectrum at alkaline pH for His61Tyr, corresponding to titration of a distal water molecule (as observed for rLb, *vide infra*), consistent with the absence of the distal water molecule. A fit of the absorbance values, with change in pH, to the Henderson Hasselbach equation, for a single proton process, Figure 4.6 (inset), yielded a  $pK_a$  of  $4.6 \pm 0.2$ .

**Table 4.1.**

Wavelength maxima (nm) and, in parentheses, absorption coefficients ( $\text{mM}^{-1}\text{cm}^{-1}$ ) for the ferric and ferrous derivatives of rLb and His61Tyr. Conditions: sodium phosphate, pH 7.0,  $\mu = 0.10 \text{ M}$ ,  $25.0^\circ\text{C}$ . Nic = nicotinate. sh = shoulder.

Derivative	rLb					His61Tyr				
	( $\gamma$ ) Soret	CT <sub>2</sub>	$\beta$	$\alpha$	CT <sub>1</sub>	( $\gamma$ ) Soret	CT <sub>2</sub>	$\beta$	$\alpha$	CT <sub>1</sub>
Fe(III)	403 (157)	495 (10.7)	530 (9.91)	560 (7.13)	626 (4.92)	404.5 (181)	489 (22.1)	534(20.3)	-	602 (23.1)
Fe(III)-CN <sup>-</sup>	415 (117)	-	539 (11.9)	-	-	420 (159)	-	546 (20.0)	-	-
Fe(III)-Nic	407 (123)	-	529 (13.4)	557 (11.2)	-	407 (195)	-	529 (16.4)	562 (11.0)	-
Fe(III)-N <sub>3</sub> <sup>-</sup>	413.5 (126)	-	549 (12.4)	572 (9.36)	-	415 (200)	-	542 (20.3)	578 (16.2)	-
Fe(III)-F <sup>-</sup>	401 (149)	484 (11.1)	540 (8.88)	-	601 (10.0)	405 (124)	488 (46.4)	535(42.5)	-	602 (44.6)
Fe(III)-OAc <sup>-</sup>	403 (236)	497 (13.9)	533 (10.8)	571 (8.71)	622 (9.02)	404 (174)	489 (20.5)	531 (18.1)	574.3 (sh)	602 (20.5)
Fe(II)	427 (111)	-	-	555 (13.3)	-	430 (195)	-	-	557 (23.4)	-
Fe(II)-CO	415 (199)	-	537 (13.6)	561 (12.7)	-	419 (182)	-	539 (14.7)	566 (5.33)	-
Fe(II)-Nic	418 (230)	-	524 (24.7)	554 (44.6)	685 (2.56)	417.5 (297)	-	525 (54.1)	554 (81.2)	-
Fe(II)-O <sub>2</sub>	412(108)	-	-	541(10.8)	574 (10.5)	-	-	-	-	-

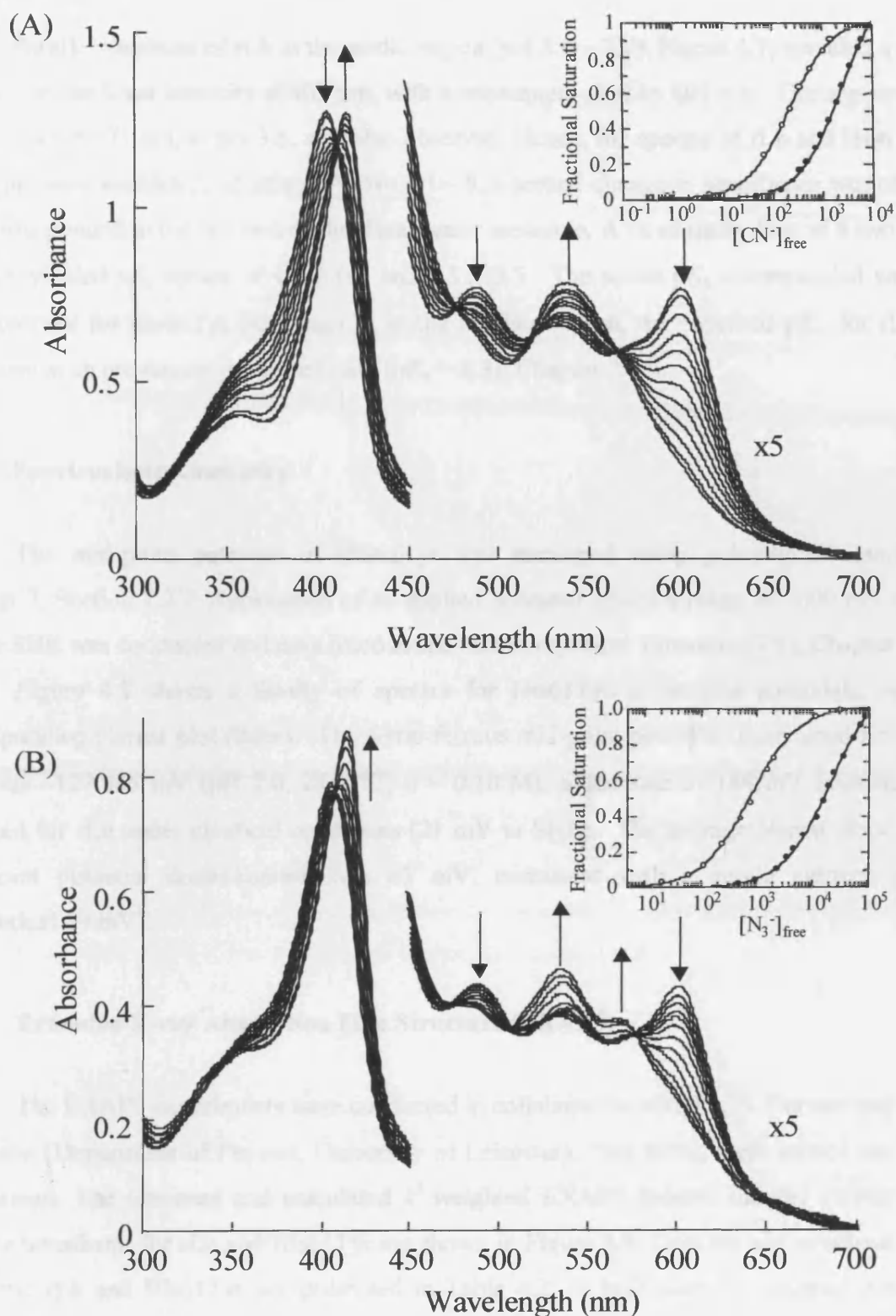


**Figure 4.5.** Spectrophotometric titration of His61Tyr with (A) cyanide and (B) azide. The visible region has been multiplied by a factor of five for clarity and arrows indicate the direction of change in absorbance upon successive addition of ligand. Inset show fit of data to Equation [7.3] for strong ligand binding and Equation [7.6] for weak binding at pH 4 (O) and pH 7 (●), respectively. Conditions: sodium phosphate, pH 7.0,  $\mu = 0.10$  M, 25.0 °C.

Parallel titrations of rLb in the acidic region (pH 3.6 – 7.0), Figure 4.7, revealed a similar decrease in the Soret intensity at 403 nm, with a subsequent shift to 401 nm. The appearance of a new band at 371 nm, at pH 3.6, was also observed. Hence, the spectra of rLb and His61Tyr at acidic pH were essentially identical. Above pH ~ 8, a second change in absorbance was observed that corresponded to the titration of the distal water molecule. A fit of these data, to a two-proton process, yielded  $pK_a$  values of  $4.4 \pm 0.1$  and  $8.3 \pm 0.5$ . The acidic  $pK_a$  corresponded well with that observed for His61Tyr (*vide supra*); in the alkaline region, the observed  $pK_a$ , for rLb, was consistent with previously published data ( $pK_a = 8.3$ ), Chapter 2.<sup>[36]</sup>

#### 4.3.4 Spectroelectrochemistry

The mid-point potential of His61Tyr was measured using procedures described in Chapter 7, Section 7.2.7. Application of an applied potential across a range of –600 mV to +100 mV vs SHE was conducted and data fitted to the Nernst equation, Equation [7.9], Chapter 7.

Figure 4.8 shows a family of spectra for His61Tyr at various potentials, with the corresponding Nernst plot (inset). The ferric-ferrous mid-point potential determined from these data was  $-127 \pm 5$  mV (pH 7.0, 25.0 °C,  $\mu = 0.10$  M), a decrease of 148 mV from the value obtained for rLb under identical conditions (21 mV vs SHE). The average Nernst slope for the mid-point potential determination was 65 mV, consistent with a single electron process (theoretical 59 mV).

#### 4.3.5 Extended X-ray Absorption Fine Structure (EXAFS)

The EXAFS experiments were conducted in collaboration with Dr. S. Gurman and Dr. A. Svensson (Department of Physics, University of Leicester). Data fitting were carried out by Dr. S. Gurman. The observed and calculated  $k^3$  weighted EXAFS spectra and the corresponding Fourier transforms for rLb and His61Tyr are shown in Figure 4.9. Data fits and structural results for ferric rLb and His61Tyr are presented in Table 4.2. In both cases, a distorted octahedral coordination of the haem iron gave a significantly better fit than a symmetric octahedral arrangement. In addition, the six bonding neighbours were clearly all best fit by light atoms (*i.e.* C, N or O) and were distinguishable from heavy atoms (*i.e.* S). Inclusion of the three distant carbon shells, which arises from the porphyrin ring structure, required the use of multiple

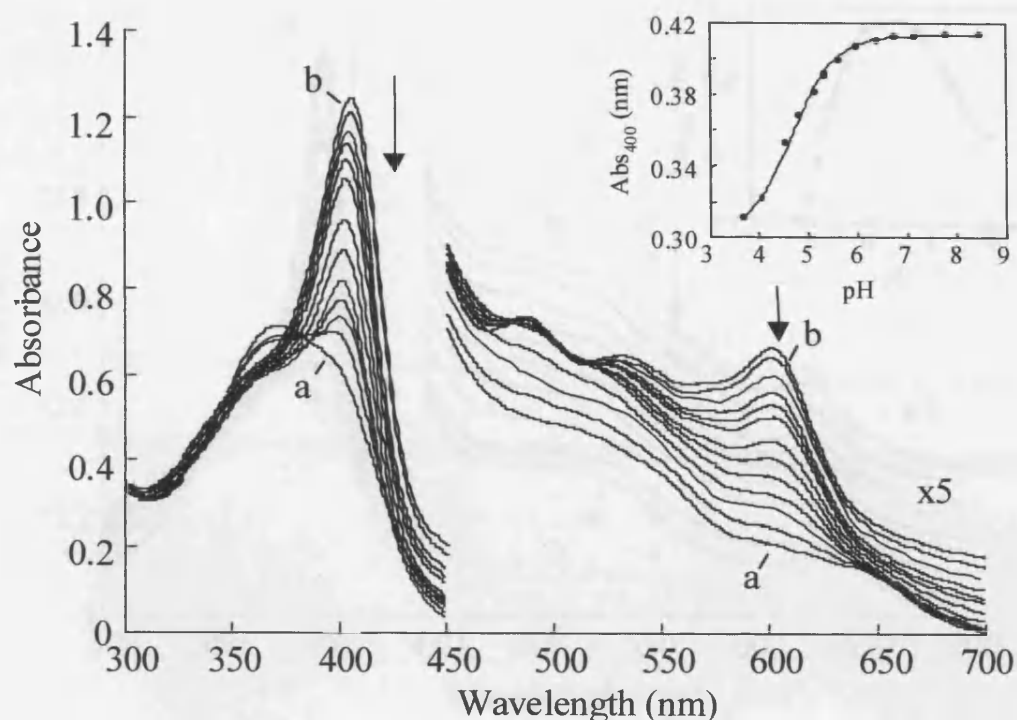


**Figure 4.6.** Spectrophotometric pH titration of His61Tyr in the acidic and alkaline regions. Spectrum of His61Tyr at (a) pH 3.8, (b) 8.5 and intermediate pHs 4.1, 4.6, 4.9, 5.1, 5.3, 5.7, 5.9, 6.2, 6.5, 6.9, and 7.7. Arrows denote the direction of change in absorbance with decreasing pH in each case. Inset: plot of variation in absorbance 400 nm with pH. The solid line represents non-linear least squares fit to Henderson Hasselbach equation for a single proton process. For His61Tyr, no further change in absorbance is observed above pH 8.5

scattering contributions: in this case, it was necessary to split the five N atoms at  $\sim 200$  pm into two shells, four in the ring plane and one out of plane ( $4 + 1 + 1$ ). These two contributions were always found to lie at similar distances. Comparison spectra for rLb, at 298 K and 77 K, are depicted in Figure 4.9(A). All significant structure had been fitted for the protein. The results for myoglobin, Table 4.2, which were collected to establish the reliability of the rLb and His61Tyr data, were in good agreement with published data.<sup>[38]</sup> The Brookhaven nomenclature for haem atoms, Scheme 1, has been used throughout. The data for rLb were very similar to those for Mb and were in agreement with the close similarity in Fe environments between ferric Mb and ferric Lb found by Rich *et al.*<sup>[38]</sup> For rLb at 300K, the short bond ( $190 \pm 5$  pm) was assigned as a Fe- $\text{O}_{\text{H}_2\text{O}}$  bond arising from coordination of a water molecule by comparison with spectroscopic data

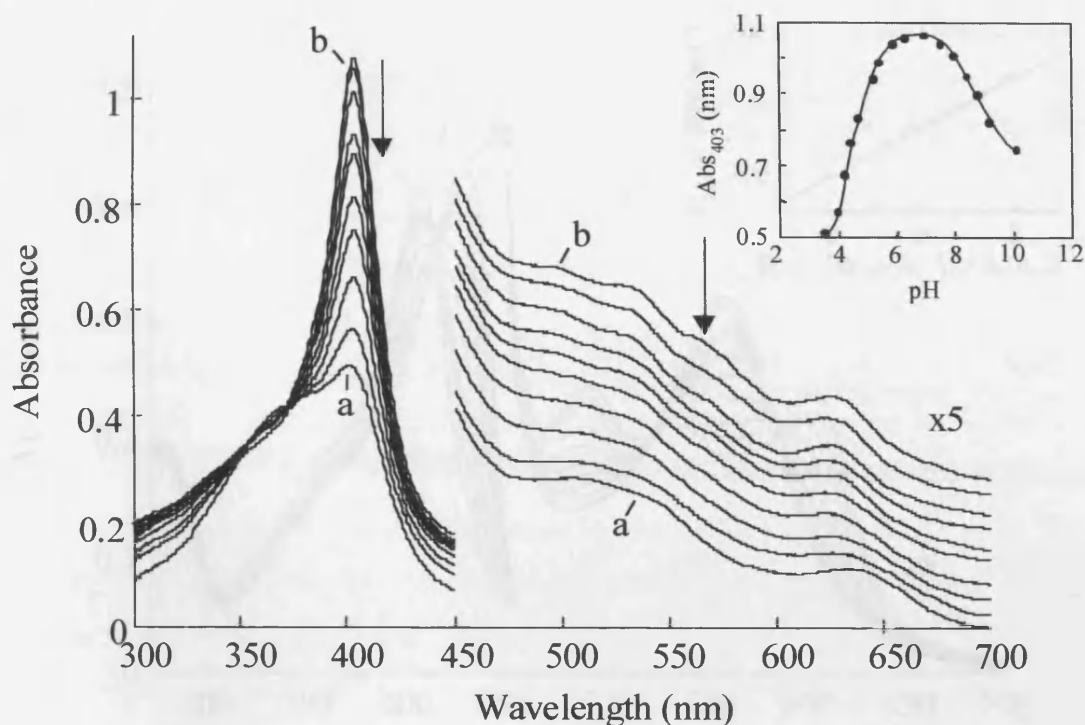


**Figure 4.7.** Spectrophotometric pH titration of rLb in the acidic region. Spectrum of rLb at (a) pH 3.7, (b) pH 7.0 and intermediate pHs 4.0, 4.2, 4.6, 4.9, 5.4, 5.7, 6 and 6.1. Arrows denote the direction of change in absorbance with decreasing pH in each case. Inset: plot of variation in absorbance 403 nm with pH in the acidic and alkaline regions (pHs 3.7, 4.0, 4.2, 4.6, 4.9, 5.4, 5.7, 6, 6.1, 7.0, 7.6, 8.0, 8.4, 8.8, 9.2, and 10.1); the solid line represents non-linear least squares fit to Henderson Hasselbach equation for a two proton (two  $pK_a$ ) process.

that have independently confirmed this assignment.<sup>[34, 35]</sup> At low temperature, the Fe-O bond distance did not significantly alter in length. The inability of EXAFS to distinguish between O and N has made assignment of this bond difficult. However, significant changes in the Debye-Waller factor were observed. An increase by a factor of 3 suggested a structural change was associated with this bond (Fe-O) with change in temperature. A heavier unit than the water molecule was likely to be ligated to the haem, likely histidine, in agreement with other spectroscopic data. In addition the EXAFS spectra for rLb at both room and cryogenic temperature were different at  $k = 7 \text{ \AA}^{-1}$  and  $9 \text{ \AA}^{-1}$ , suggesting a significant change in structure, Figure 4.9(A). At low temperature, rLb is known to exist as a *bis*-histidine coordinated species,<sup>[31, 34, 37]</sup> the bond length of 190 pm at 77 K was assigned as a Fe-N<sub>His</sub> distance.

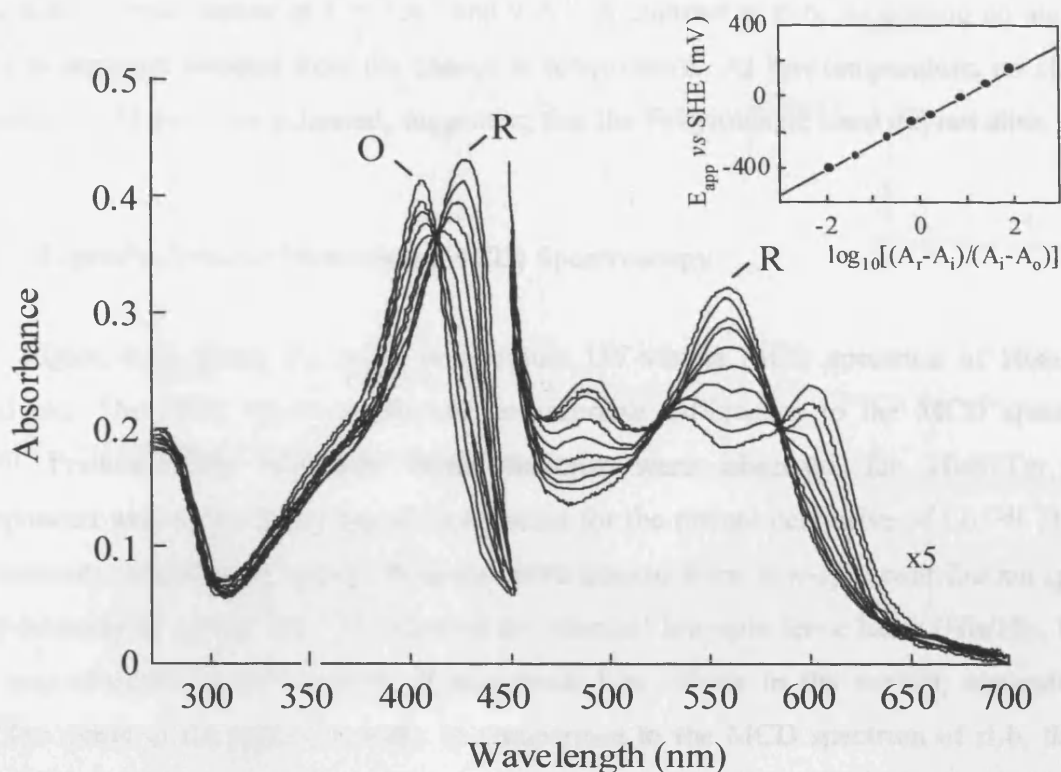


**Figure 4.8.** Thin-layer spectroelectrochemical spectra for His61Tyr at various applied potentials,  $E_{app}$  (mV). Fully oxidized (O) and fully reduced (R) spectra for each derivative are indicated. The inset shows a fit of the absorbance data at 405 nm. to the Nernst equation. Absorbance values in the visible region (450-700 nm) have been multiplied by a factor of five. Conditions: sodium phosphate, pH 7.0, 25.0 °C,  $\mu = 0.10$  M.

Comparison EXAFS spectra for His61Tyr, at 298 K and 77 K, are depicted in Figure 4.9(C). The EXAFS data for His61Tyr, Table 4.2, were very similar to those for rLb and were presumably due to the dominating (invariant) four-fold symmetric porphyrin ring structure. In both cases the distances of the iron atom to the main porphyrin ring atoms ( $N_p$ ) indicated that the iron lies in, or very close to, the plane of the porphyrin ring. The most significant difference between rLb and His61Tyr, at 300K, was observed in the parameters of the short bond: this was found to be 5pm shorter for His61Tyr but with a significantly lower Debye-Waller factor, Table 2. The lower Debye-Waller factor suggested that this atom was part of a heavier unit than a water molecule – although the vibration frequency was only  $250\text{ cm}^{-1}$  – and was consistent with tyrosinate ligation. The EXAFS spectra for His61Tyr at both room and cryogenic temperature,

Figure 4.8(C), were similar at  $k = 7 \text{ \AA}^{-1}$  and  $9 \text{ \AA}^{-1}$ , in contrast to rLb, suggesting no significant change in structure resulted from the change in temperature. At low temperature, no change in bond length (185 pm) was indicated, suggesting that the Fe-tyrosinate bond did not alter.

#### 4.3.6 Magnetic Circular Dichroism (MCD) Spectroscopy

Figure 4.10 shows the room temperature UV-visible MCD spectrum of His61Tyr at neutral pH. The MCD spectrum showed considerable differences to the MCD spectrum of rLb.<sup>[36]</sup> Predominantly high-spin ferric features were observed for His61Tyr, which corresponded well to the MCD spectrum reported for the phenol derivative of Lb.<sup>[34]</sup> The Soret band intensity, which arise largely from the more intense ferric low-spin contribution (peak-to-trough intensity of  $150 \text{ M}^{-1}\text{cm}^{-1}\text{T}^{-1}$  expected for 'normal' low-spin ferric haem (His/His, His/Met *etc*)), was observed to be an order of magnitude less intense in the variant, suggesting that His61Tyr exists in the high-spin state. In comparison to the MCD spectrum of rLb, the Soret band of His61Tyr had almost halved in intensity: ( $\lambda(\text{nm}) (\Delta\epsilon/H (\text{M}^{-1}\text{cm}^{-1}\text{T}^{-1}))$ ) for His61Tyr 397 (+21) and 420 (-20); for rLb 397 (+40) and 415 (-37).<sup>[36]</sup> In the region 580-980 nm, two charge-transfer bands were observed at 621 and 830 nm, which were characteristic of high-spin ferric haem. A  $\text{CT}_2$  band (usually observed  $\sim 600\text{-}660 \text{ nm}$ ) was detected with a cross over at 606 nm and a trough at 621 nm. A second charge-transfer transition ( $\text{CT}_1$  (750-1400 nm)) was observed with a cross over at 797 nm and a trough centring at 830 nm. The charge-transfer transition, at  $\sim 830 \text{ nm}$ , is indicative of histidine-tyrosinate-bound, high-spin haem and is analogous to that reported for the phenol derivative of Lb<sup>[34]</sup> indicating tyrosinate-haem ligation in the His61Tyr variant.

#### 4.3.7 Electron Paramagnetic Resonance (EPR) Spectroscopy

Figure 4.11, shows the EPR spectrum of His61Tyr recorded at neutral pH. The His61Tyr variant exhibited rhombic high-spin signals ( $g_x$  6.43, 5.83, 4.99 and  $g_z$  2.0), which were similar to those reported for the His64Tyr variants of sperm whale and horse heart myoglobin (sperm whale: 6.63, 5.31 and 1.98;<sup>[17]</sup> horse heart: 6.64, 5.34 and 1.98)<sup>[39]</sup> and Hb M Saskatoon (6.65, 5.35 and 2.0)<sup>[39, 40]</sup> in which histidine-tyrosine haem ligation has been established. However, low-spin signals were also apparent for His61Tyr ( $g_y$  2.67, 2.17 and 1.79), which closely

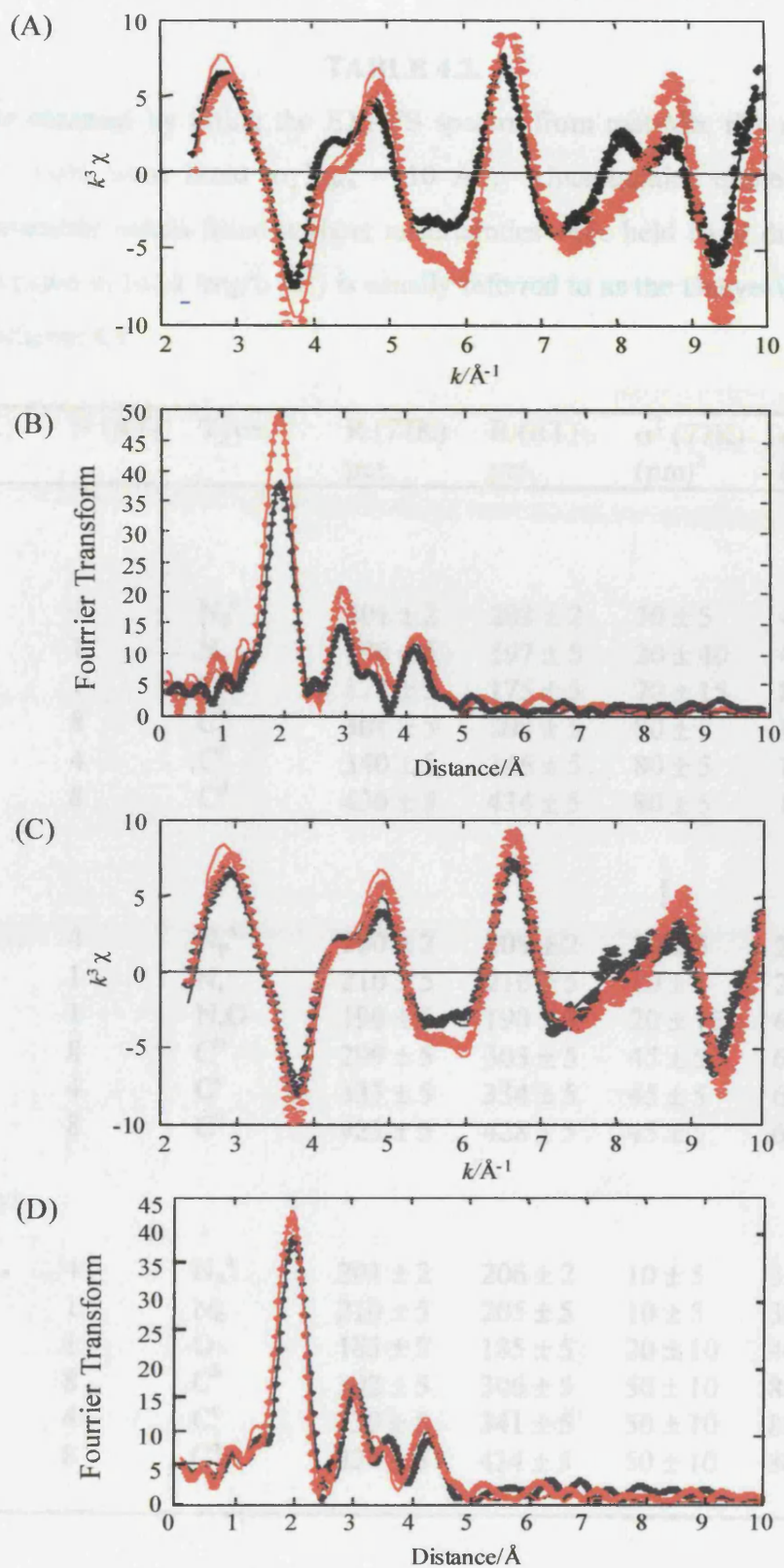


**Figure 4.9.** The EXAFS spectra (A) and Fourier transform amplitude of EXAFS (B) of rLb, the EXAFS spectra (C) and Fourier transform amplitude of EXAFS (D) of His61Tyr: observed ( $\diamond$ ) at 298K and ( $\circ$ ) at 77K. The solid lines represent the calculated data from refined models at 298K ( $\text{—}$ ) and at 77K ( $\text{—}$ ).

TABLE 4.2.

Structural results obtained by fitting the EXAFS spectra from met-Mb, rLb and the His61Tyr variant of rLb. Data were fitted to  $k_{\max} = 10 \text{ \AA}^{-1}$ . Uncertainties quoted are  $\pm 2\sigma$  (95% confidence). Parameter values listed without uncertainties were held fixed during the fit. The mean square deviation in bond length ( $\sigma^2$ ) is usually referred to as the Debye-Waller factor. For nomenclature, Scheme 4.1.

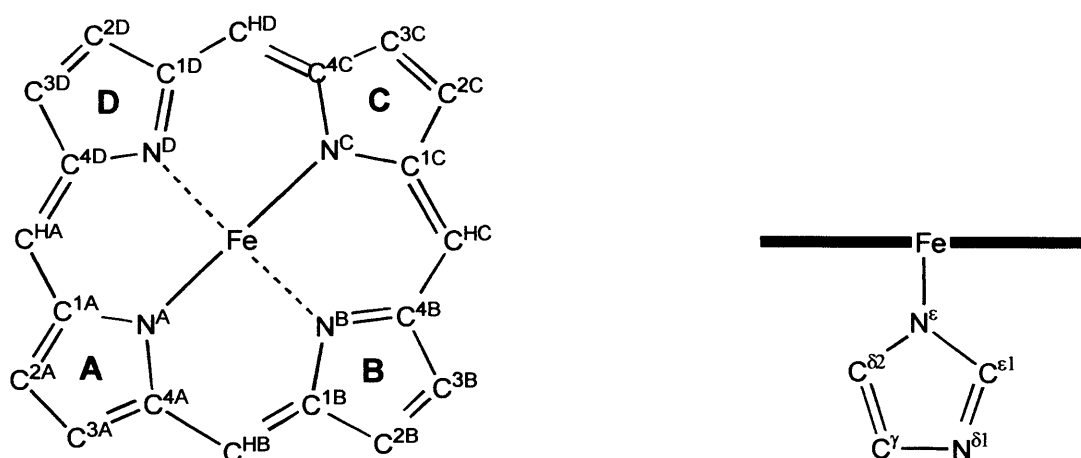
N (77K)	N (RT)	Type	R (77K) pm	R (RT) pm	$\sigma^2$ (77K) (pm) <sup>2</sup>	$\sigma^2$ (RT) (pm) <sup>2</sup>
<b>Mb</b>						
4	4	N <sub>p</sub> <sup>a</sup>	201 ± 2	203 ± 2	30 ± 5	45 ± 10
1	1	N <sub>e</sub>	196 ± 5	197 ± 5	20 ± 40	45 ± 20
1	1	O	172 ± 5	175 ± 5	70 ± 15	80 ± 20
8	8	C <sup>b</sup>	301 ± 5	308 ± 5	80 ± 5	110 ± 10
4	4	C <sup>c</sup>	340 ± 5	346 ± 5	80 ± 5	110 ± 10
8	8	C <sup>d</sup>	436 ± 5	434 ± 5	80 ± 5	110 ± 10
<b>rLb</b>						
4	4	N <sub>p</sub> <sup>a</sup>	200 ± 2	205 ± 2	10 ± 5	20 ± 10
1	1	N <sub>e</sub>	210 ± 5	210 ± 5	10 ± 5	20 ± 10
1	1	N,O	190 ± 5	190 ± 5	20 ± 15	60 ± 20
8	8	C <sup>b</sup>	299 ± 5	303 ± 5	45 ± 5	60 ± 10
4	4	C <sup>c</sup>	337 ± 5	334 ± 5	45 ± 5	60 ± 10
8	8	C <sup>d</sup>	423 ± 5	428 ± 5	45 ± 5	60 ± 10
<b>His61Tyr</b>						
4	4	N <sub>p</sub> <sup>a</sup>	201 ± 2	206 ± 2	10 ± 5	35 ± 5
1	1	N <sub>e</sub>	210 ± 5	205 ± 5	10 ± 5	35 ± 5
1	1	O	185 ± 5	185 ± 5	20 ± 10	40 ± 20
8	8	C <sup>b</sup>	302 ± 5	306 ± 5	50 ± 10	80 ± 10
4	4	C <sup>c</sup>	339 ± 5	341 ± 5	50 ± 10	80 ± 10
8	8	C <sup>d</sup>	426 ± 5	434 ± 5	50 ± 10	80 ± 10

<sup>a</sup> N<sub>p</sub> = N<sup>A</sup>, N<sup>B</sup>, N<sup>C</sup>, N<sup>D</sup>

<sup>b</sup> C<sup>1A</sup>, C<sup>1B</sup>, C<sup>1C</sup>, C<sup>1D</sup>, C<sup>4A</sup>, C<sup>4B</sup>, C<sup>4C</sup>, C<sup>4D</sup>

<sup>c</sup> C<sup>HA</sup>, C<sup>HB</sup>, C<sup>HC</sup>, C<sup>HD</sup>

<sup>d</sup> C<sup>2A</sup>, C<sup>3A</sup>, C<sup>2B</sup>, C<sup>3B</sup>, C<sup>2C</sup>, C<sup>3C</sup>, C<sup>2D</sup>, C<sup>3D</sup>



**Scheme 4.1.** The Brookhaven haem nomenclature used in this work.

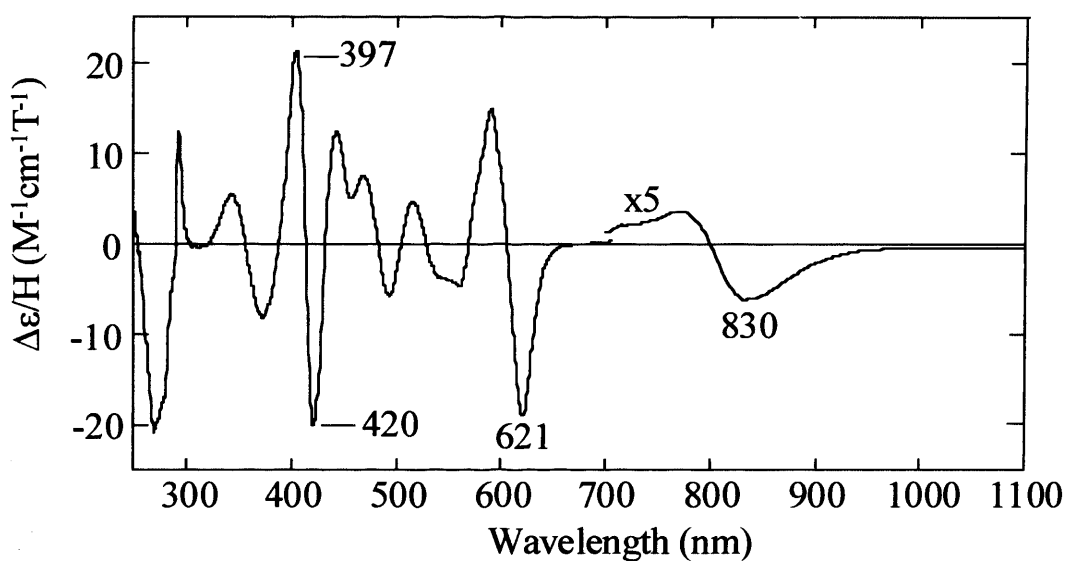


**Figure 4.10.** UV-visible MCD spectrum of His61Tyr (pH 7.0) recorded at room temperature using a magnetic field of 6 T and sample concentration of 67 (in the Soret region) and 734  $\mu\text{M}$  (in the visible region)

resembled the g-values of the phenol derivative of Lb.<sup>[34]</sup> The phenol derivative has been previously established to be high-spin at room temperature and predominantly low-spin at low-temperature, with tyrosinate-haem ligation in both states. This suggests that tyrosine is also ligated to the haem in the His61Tyr variant, in a predominantly low-spin population.

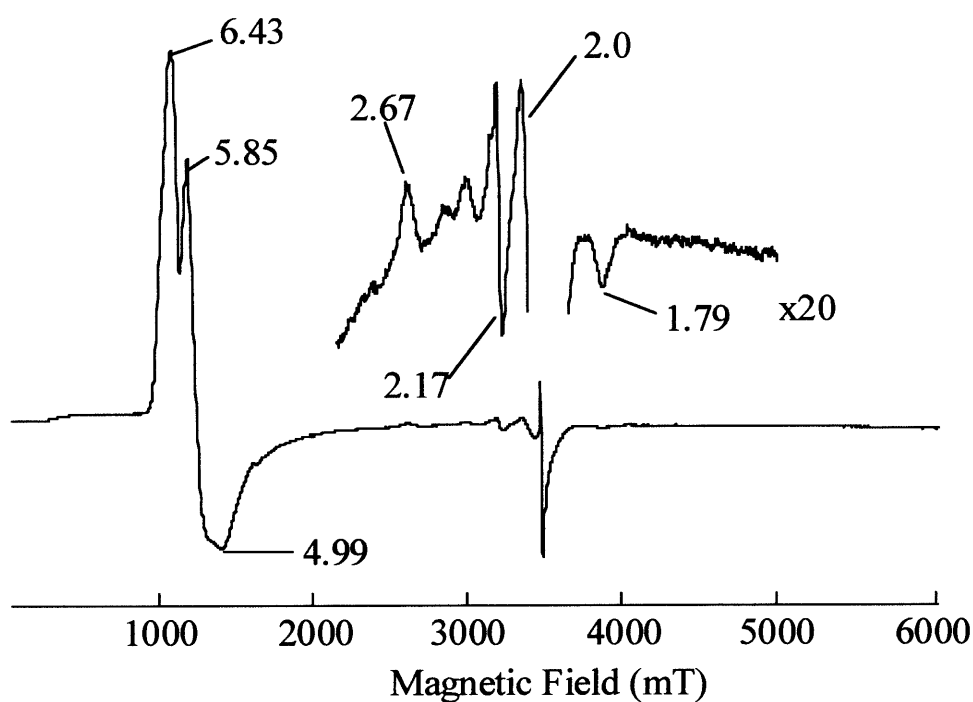


**Figure 4.11.** X-band EPR spectrum of His61Tyr (pH 7.0) recorded at 10 K using 1 mT modulation amplitude and 2.0 mW microwave power. The g-values are indicated.

## 4.4 Discussion

It has been known, for more than 30 years,<sup>[32]</sup> that the haem structure of leghaemoglobin is conformationally mobile and that at low temperature, the ferric haem rearranges to a low-spin derivative. The recent mutagenesis experiments, carried out in Chapter 3, have confirmed that this low-spin derivative is a *bis*-histidine species generated by ligation of histidine 61 to the haem at low temperature. In this work, it has been demonstrated that this conformational mobility of rLb is also able to support axial ligation by other amino acids, within the haem architecture. A His61Tyr variant was generated in which the mobile distal histidine 61 residue was replaced to incorporate tyrosine. Spectroscopic characterisation of His61Tyr was carried out to establish the effect of the mutation on the spectroscopic and ligand binding properties of the protein.

The electronic absorption spectrum of ferric His61Tyr displayed fingerprint bands for iron-tyrosinate proteins (intense band at 602 nm), which gives rise to the unique green colour of His61Tyr. The charge-transfer bands seen at ~480 and ~600 nm for the variant, which are characteristic for high-spin ferric haem, are also seen for bovine liver catalase,<sup>[1, 6]</sup> Hb M Saskatoon<sup>[41, 42]</sup> and the distal His64Tyr variant of sperm whale myoglobin ( $\lambda_{\max} = 410, 486, 542$  and 600 nm), in which coordination of Tyr64 to the haem has been established.<sup>[9, 17, 39, 43]</sup> Similar absorption bands, in the range of 470 and 490 nm, have been observed in non haem iron-phenolate proteins and model compounds<sup>[44]</sup> and have been previously assigned to phenolate-Fe(III)  $p_{\pi}-d_{\pi^*}$  charge-transfer bands.<sup>[45]</sup> Accordingly, the assignment of phenolate (tyrosinate) ligation to the haem iron, in the His61Tyr variant was made. Comparison of the His61Tyr spectrum with the ferric-phenol derivative of rLb revealed very similar features ( $\lambda_{\max} = 404.5, 489, 534, 568^{\text{sh}}, 603$  nm), providing further evidence in support of tyrosinate ligation. The appearance of charge-transfer bands of the phenol-derivative at 489 and 603nm, characteristic of six-coordinate, high-spin ferric haem, was similarly observed as for His61Tyr. Absorption maxima for these variants and other tyrosine coordinated haem proteins are shown in Tables 4.3 and 4.4. In the reduced form, wavelength maxima for His61Tyr ( $\lambda_{\max} (\epsilon/\text{mM}^{-1}\text{cm}^{-1}) = 429.5$  (195) and 557 nm) were similar to those of rLb (Chapter 2, Table 2.1),<sup>[36]</sup> indicating loss of the tyrosine ligand and formation of a five-coordinate haem structure.

EXAFS analysis of rLb and His61Tyr allowed further insight into the structural changes associated with the His61Tyr mutation. Determination of the Fe-H<sub>2</sub>O bond length for rLb, at

neutral pH, revealed a bond length value of 190 pm. This value is believed to be the first reported Fe-H<sub>2</sub>O distance for rLb (previous crystals structure determinations have only revealed Fe-nicotinate (209 pm), Fe-porphyrin ( $N_A = 198$  pm,  $N_B = 209$  pm,  $N_C = 215$  pm,  $N_D = 185$  pm) and Fe-histidine 92 (226 pm) bond for Lb).<sup>[46]</sup> The Fe-H<sub>2</sub>O distance for rLb compares to the analogous bond length in met-Mb (1.75 Å), determined in this work, Table 4.2. In general, longer bond lengths were observed for rLb than Mb. At cryogenic temperatures, the distance of the short bond length (Fe-sixth ligand) was the same as observed at neutral pH. However, differences observed in the Debye-Waller factor at the two temperatures, indicated that a heavier unit than water was bound to the haem iron. Previous spectroscopic studies (Chapter 3)<sup>[35]</sup> have clearly established that the sixth ligand in rLb, at low temperature, is nitrogen from histidine 61. Together with EXAFS data determined in this work, a full confirmation of the nature of ligation and the temperature dependent ligand conversion, from Fe-H<sub>2</sub>O to Fe-N<sub>His</sub>, has been established for rLb. In addition, a value for the Fe-N<sub>His</sub> bond length (at cryogenic temperature) has been reported for the first time.

The Fe(III)-O bond length observed for the distal tyrosyl residue, in the His61Tyr variant, was 1.85 Å. This bond length was shorter than observed in rLb and suggested a stronger and different ligation to the haem than H<sub>2</sub>O. This was similarly reflected by the Debye-Waller factor, which indicated a heavier unit bound to the haem iron. The variant did not display a temperature-dependent ligand switch, as observed for rLb, the O(tyrosine) remained ligated to the haem at both 77K and 298K. Interestingly, the Fe-O(tyrosine) distance, determined in this work, compares with a value of 1.89 Å, determined by x-ray crystallography, for the bond length formed between the proximal tyrosine ligand and the haem iron in bovine liver catalase,<sup>[47]</sup> Table 4.4, and is also similar to that observed for the Fe(III)-O(tyrosine) bond length of the His64Tyr variant of myoglobin,<sup>[48]</sup> Table 4.3. Notably this behaviour, is in contrast to the situation of the corresponding haemoglobin  $\alpha$ -chain variant, HbM Boston. In this case, replacement of the HisE7 with tyrosine produces a five-coordinate haem iron centre in which the distal tyrosine binds to the iron and coordination by the proximal histidine residue is disrupted,<sup>[49]</sup> Table 4.4.

The strength of the Fe-O(tyrosine) bond, as indicated by EXAFS, was reflected in the ability of the variant to bind exogenous ligands. The haem-bound phenolate was readily displaced by strong field ligands, such as cyanide and azide, however, weak field ligands, such as fluoride and acetate, were incapable of displacing the bound phenolate (little change in electronic absorption spectrum was observed, Figure 4.4).

**Table 4.3.**

Summary of spectroscopic data for haem proteins and variants in which the distal ligand to the haem is provided by a tyrosine.

Source	Variant	Axial Ligation	Spectroscopic information	Electronic absorption spectra $\lambda_{\max}$ (nm)	Midpoint potential (mV)	Fe-O <sub>Tyr</sub> bond length (Å)	Reference
<b>MetMb</b> Horse heart	His64Tyr	Tyr64	X-Ray			2.18	[9]
			EPR				
			EXAFS				[48]
			Electronic Electrochem.	412, 430, 530, 600	20		[48]
<b>MetMb</b> Sperm Whale	His64Tyr	Tyr64	XANES			1.88	[17]
			Electronic	350, 410, 486, 542, 600			[17, 39, 50]
			ESR				[17]
			EPR				[17, 39, 50]
			RR				[39, 43, 51]
<b>Hb M Saskatoon</b>	His(β63)Tyr	Tyr(β63)	Electronic	485, 600			[17, 39, 41, 42]
			RR				[41, 42]
			EPR				[39]
<b>Hb M Boston</b>	His(α58)Tyr	Tyr(α 58)	RR	490, 600			[41, 42]
			Electronic				[42]
			EPR				[39]
<b>Chloroplast Hemoglobin</b> Chlamydomonas		Tyr63 at high pH		410, 535, 572 (sh)			[24]
<b>Cytochrome <i>cd<sub>1</sub></i></b> <i>d<sub>1</sub></i> haem		Tyr25(C-terminus)					[23]
			NIR MCD				[52]
<b>Cytochrome P450<sub>LM2</sub></b>							[53, 54]
			Difference spectroscopy				[55]
<b>Cytochrome <i>f</i></b> Chlamydomonas reinhardtii.		Tyr32 (N-terminus)	Electronic				[56]
							[57]
<b>human hemalbumin.</b>		Tyr148	Electronic				[58]

**Table 4.4.**

Summary of spectroscopic data for haem proteins and variants in which the proximal ligand to the haem is provided by a tyrosine.

Source	Variant	Axial ligation	Spectroscopic information	Electronic absorption spectra $\lambda_{\max}$ (nm)	Midpoint potential (mV)	Fe-O <sub>Tyr</sub> bond length (Å)	Reference
MetMb Horse heart	His93Tyr	Tyr93	NMR EPR Electronic Electrochem. X-Ray	403, 487, 524, 599	-208 pH 8.0		[6]
MetMb Human	His93Tyr	Tyr93	Electronic Electrochem. X-Ray	402, 480, 598	-190	1.92 Å	[59-61]
MetMb Sperm Whale	His93Tyr	Tyr93	Electronic	350, 402, 480, 524, 598			[17, 39]
Hb M Iwate	His( $\alpha$ 87)Tyr	Tyr( $\alpha$ 87)	RR Electronic EPR	480, 590 nm			[41, 42, 62] [39, 42, 62] [39]
Hb M Hyde Park	His( $\beta$ 92)Tyr	Tyr( $\beta$ 92)	RR Electronic EPR	490, 580 nm			[42] [39, 42] [39]
Catalase Bovine liver		Tyr357	Electrochem. MCD CD RR X-Ray EXAFS		< -500		[63-66] [63, 66-68] [63] [69, 70] [71]
Ascomycete fungus: <i>Aspergillus niger</i>			MCD			1.84 Å	[72]
Penicillin vitale			RR			1.88 Å	[67]
Bacterium: <i>Micrococcus luteus</i>		Tyr345	RR X-Ray MCD RR				[69] [73] [63] [69]

Formation of the hexa-coordinate tyrosine-haem species also had a significant impact on the affinity of the variant for exogenous ligands. Specifically, at neutral pH, His61Tyr bound azide ( $K_{d,azide} = 19000 \pm 1000 \mu\text{M}$ ) with  $\sim 4000$ -fold lower affinity than rLb ( $K_{d,azide} = 4.8 \pm 0.2 \mu\text{M}$ ),<sup>[37]</sup> while cyanide binding affinity ( $K_{d,cyanide} = 3300 \pm 100 \mu\text{M}$ ) was decreased by  $\sim 3000$ -fold in the variant (rLb:  $K_{d,cyanide} = 1.1 \pm 0.1 \mu\text{M}$ ).<sup>[37]</sup> These results were consistent with coordination of tyrosine to the haem. At acidic pH (pH 4), binding of exogenous ligands to His61Tyr was seen to be more favourable. The variant exhibited azide ( $K_{d,azide} = 700 \pm 70 \mu\text{M}$ ) and cyanide ( $K_{d,cyanide} = 200 \pm 40 \mu\text{M}$ ) binding affinities that were  $\sim 50$ -fold weaker than that of rLb ( $K_{d,azide} = 12 \pm 0.3 \mu\text{M}$  and  $K_{d,cyanide} = 9 \pm 0.2 \mu\text{M}$ ) and were  $\sim 20$ - $30$ -fold stronger than His61Tyr at neutral pH. Under these conditions the His61Tyr variant is believed to exist in a form in which the distal tyrosine 61 ligation is either lost or in a form in which it is weakly ligated to the haem iron. In the former case, the increase in relative binding affinity observed at pH 4 (compared to binding data at pH 7) could be rationalised in terms of the steric bulk of the distal tyrosine residue, which still inhibits the binding of anions to the haem iron, even when it was not bound to the haem iron. In the latter case, where tyrosine may be weakly bound to the haem, the increase in relative binding affinity could be explained in terms of ease with which the exogenous anionic ligands can displace the weakly bound tyrosine relative in comparison to that at neutral pH. However, the ligation in the haem in the acid form of the variant could not be assigned with certainty (see below).

The change in the electronic absorption spectrum of oxidised His61Tyr, observed on decreasing pH, suggested a change in haem coordination with change in pH ( $pK_a = 4.6$ ). Analysis of the pH titration spectrum of His61Tyr suggested that the haem iron coordination change was according to a single proton process. The  $pK_a$  determined via this process could arise from one of two possibilities, Scheme 4.2. The first possibility is that the  $pK_a$  could correspond to the protonation of the tyrosine 61 residue, which would involve release of the tyrosine from the haem iron and protonation of the phenolic oxygen atom. This assignment could be supported by the loss of the CT<sub>1</sub> transition at  $\sim 600$  nm, which is characteristic of histidine-tyrosine-haem ligation, on decreasing pH. However, the phenol group of the free tyrosine has a  $pK_a$  value of 10.5.<sup>[74]</sup> Hence, the assertion that the sixth haem ligand of the His61Tyr is a tyrosinate ion requires the haem pocket to have drastically altered the intrinsic tyrosine phenol group  $pK_a$  of 10.5. Often basic residues are required to cause such shifts in the  $pK_a$ .<sup>[74]</sup> Since the tyrosine side chain is not significantly larger than a histidine side chain and is bound to the haem, it is assumed that the tyrosine ring is in close proximity to the original position of the histidine 61

ring in rLb. There are two main basic residues near residue 61, they are lysine 57 and lysine 64. Typically, in the environment such polar residues, shifts are not by more than 3 pH units away from their values. The polarity of the haem pocket may make the tyrosine residue deprotonate more easily and hence lower its  $pK_a$ . In support of this rationalisation, similar decrease in  $pK_a$  have been observed for the His61Lys and His61Arg variants of rLb (Chapter 5) for which the  $pK_a$  have been assigned to the titration of the lysine and arginine residues, respectively. The drastic drop in  $pK_a$  of these residues were rationalised in terms of the hydrophobic nature of the active site pocket of rLb and the presence of basic residues (lysine 57 and lysine 64), factors which have been known to cause decreases in  $pK_a$ s of amino acid residues.<sup>[74]</sup>

The second possibility is that the  $pK_a$  determined for the pH titration of His61Tyr corresponds to the titration of the proximal histidine 92 residue, which results in the residue no longer binding to the haem iron under these conditions. This assignment was indicated and supported by the appearance of a band at 370 nm, at pH 4 and below, a form usually corresponding to a molecule, in which the proximal iron-histidine bond has been cleaved or severely weakened.<sup>[75-77]</sup> The appearance of the band at  $\sim 370$  nm was similarly observed in the pH titration of rLb with a similar  $pK_a$  (4.4) to that of His61Tyr, further supporting the assignment, and was again close to the transition for the dissociation of the haem iron-proximal histidine bond.<sup>[75-77]</sup> These similarities suggested that at least one of the axial bonds of the haem in rLb was cleaved or severely weakened, at low pH, and the observations indicate that the axial ligand coordination to the haem, in His61Tyr and rLb, was essentially the same. In both cases, the fifth coordination appeared to be occupied by a weak axial ligand, likely water for rLb and either water or tyrosine for His61Tyr. This could explain the similarities in the electronic absorption spectra observed for the two proteins at acidic pH (the five-coordinate, tyrosine-bound haem (weak ligation of tyrosine), in this case, could possibly give rise to a similar spectrum to that of five-coordinate, water-bound haem). This observation would also explain the disappearance of the transition at  $\sim 600$  nm observed for acidic His61Tyr, the loss of the proximal histidine ligation could affect the characteristic histidine-tyrosine transition. However, to confirm either possibility of haem ligation, in 'acidic' His61Tyr, additional spectroscopic characterisation under acidic conditions would have to be carried out, which were beyond the scope of this work.

After the transition evident from the optical titration spectra at pH 4.6, no additional transitions were seen up to pH 9.2, there were no obvious transitions associated with the deprotonation of the phenol oxygen when it is bound to the haem iron. These observations

indicate no alteration of haem axial ligation (tyrosinate ligation) in the variant only at pH 4.6 and above.

A two  $pK_a$  process was determined for rLb. The first  $pK_a$  (4.4) was assigned to the titration of the proximal histidine residue as described above. The second titration process for rLb occurs with a  $pK_a$  of 8.3 and corresponds to the titration of the distal water molecule to form the hydroxide-bound haem consistent with previously published data, Chapter 2.<sup>[36]</sup>

The change in ligation observed for His61Tyr with pH are in agreement with the ligand binding data for the variant and rationalise the lower affinities for anions at high pH in comparison to the higher affinities for anions observed at low pH. If the haem-ligation of the distal tyrosine 61 residue is lost at acidic pH, then the increase in relative binding affinity observed at pH 4 (compared to binding data at pH 7) could arise from the steric constraints of the bulky tyrosine residue in the active site, which still inhibits the binding of anions to the haem iron, even when it was not bound. If the tyrosine is weakly bound to the haem iron at acidic pH, then the increase in relative binding affinity can be explained in terms of ease of displacement of the weakly bound tyrosine with exogenous anionic ligands at acidic pH. This compares to the displacement of the strongly bound tyrosine at neutral pH.

Further evidence for tyrosinate-haem ligation at neutral pH in the His61Tyr variant was indicated by the large destabilisation (148 mV destabilisation) of the reduced form in comparison to rLb. Such low mid-point potentials have also been observed for other haem enzymes with anionic axial ligands such as P450<sub>cam</sub> (high-spin -170 mV, low-spin -270 mV), horse radish peroxidase (-250 mV) and catalase (< -500 mV) and have been previously interpreted as arising from a more electron rich metal centre, due to the push effect of the anionic axial ligand.<sup>[78, 79]</sup> Hence, the decrease in mid-point potential observed for His61Tyr strongly suggested anionic tyrosinate ligation to the haem in His61Tyr. In accordance with this, the rapid auto-oxidation of oxy-His61Tyr observed can now be understood in terms of greater stabilisation of the Fe(III) oxidation state relative to Fe(II) (the Fe(II) is essential for O<sub>2</sub> binding) resulting from the substitution of histidine 61 with tyrosine.

The diagnostic pairing of MCD and EPR provided complementary evidence supporting the identity of the haem axial ligation of the His61Tyr variant. The order of magnitude drop in the Soret intensity in the MCD spectrum of the variant indicated high-spin ferric haem, consistent with electronic absorption data. The most important information however, was provided by analysis of the region 580-980nm. Two derivative high-spin ferric haem signals were observed: a CT<sub>2</sub> with a cross over at 606 nm and trough at 621 nm; a CT<sub>1</sub> with a cross over

at 797 nm and trough centring at 830 nm. In comparison to rLb which has histidine-water-haem ligation (water as the sixth ligand) and charge-transfer bands at 635 and 1100 nm,<sup>[36]</sup> a blue-shift of the charge-transfer transitions was observed in the MCD spectrum of His61Tyr. Such blue-shifts are usually diagnostic of the haem systems containing one histidine ligand and usually a second ligand that is anionic in nature – hydroxide or tyrosinate. To distinguish between the two, the hydroxy-derivative of Mb was considered, for which a thermal equilibrium of high- and low-spin exists.<sup>[80]</sup> In reference to Table 4.5, the charge-transfer wavelengths for hydroxy-myoglobin fall within the ranges for several histidine-tyrosine haem proteins. Therefore, the difference between the hydroxide and tyrosine for the His61Tyr variant cannot be distinguished on this basis alone. However, the shape of the spectra of His61Tyr and hydroxy-Mb are different.<sup>[80]</sup> The two charge-transfer MCD bands for hydroxy-Mb have asymmetric intensity between the positive and negative lobes. For the tyrosinate haem proteins, these bands are considerably symmetric. The close resemblance of the MCD spectrum of His61Tyr and the symmetric nature of the charge-transfer bands, to those for tyrosinate-haem bound proteins supported the ligation of tyrosine to the haem in the His61Tyr variant.

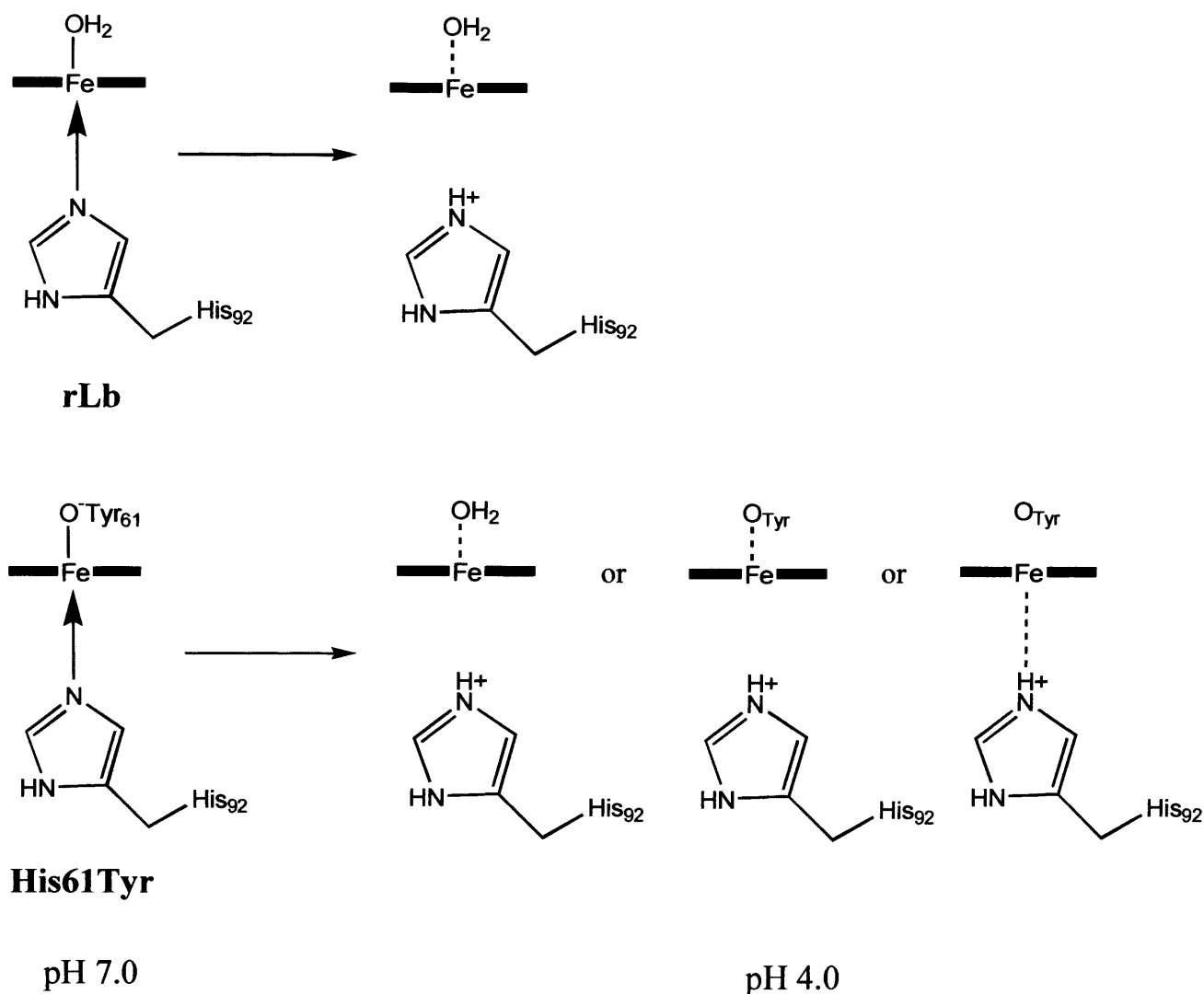
Additional confirmation of tyrosine-haem ligation was established by EPR. The rhombic nature of the high-spin signals in the EPR exhibited closely resembled the rhombicity in the EPR of His64Tyr Mb<sup>[9, 17, 39, 50]</sup> and Hb Saskatoon,<sup>[39]</sup> for which tyrosine-haem ligation has been well established. The low-spin signals also apparent in the EPR of His61Tyr ( $g = 2.67, 2.17, 1.79$ ) closely matched the  $g$ -values of the phenolate derivative of Lb,<sup>[34]</sup> for which phenolate ligation gives rise to low-spin signals at low-temperature. In accordance, the low-spin signals observed in the EPR spectrum of His61Tyr were also assigned to histidine-tyrosine-haem ligation.

**Table 4.5.**

The charge-transfer transitions (from the MCD) and low-spin g-values (from the EPR) of haem hydroxy-, water- and phenolate- and tyrosinate-ligated proteins.

	High-spin MCD at RT		Low-spin		
	CT <sub>2</sub> trough ( <i>cross-over</i> ) λ (nm)	CT <sub>1</sub> cross- over λ (nm)	CT peak λ (nm)	Low-spin component EPR g-values	References
<b>rLb H61Y</b>	<b>621 (606)</b>	<b>797</b>	<b>?</b>	<b>2.67, 2.17, 1.79</b>	<b>This work</b>
Lb + phenol(ate)	618	815	1160	2.65, 2.24, 1.86	[34]
rLb-OH <sup>-</sup>	~ 630 (615)		1015	2.52, 2.18, 1.85	[36]
Mb- OH <sup>-</sup>	619	804	1035	2.57, 2.16, 1.85	[80]
SW Mb H64Y	618 (603)	797	-	-	[81]
HH Mb F43Y	627	~ 855	1070	3.06, 2.02, 1.50	[81]
Misc. his/H <sub>2</sub> O	625-646	1066-1107	-	-	[34, 80, 82-86]

HH = horse heart and SW = sperm whale



**Scheme 4.2.** Predicted ligation of rLb (top) and His61Tyr (bottom) at neutral and acidic pH as observed through electronic absorption spectroscopy. At pH 7, rLb and His61Tyr exist as six-coordinate proteins with the sixth ligand as water for rLb and tyrosine for His61Tyr. At acidic pH, the two proteins are believed to be essentially five-coordinate with the fifth (distal) ligand as water for rLb and water or tyrosine for His61Tyr and the proximal ligand, either lost or severely weakened. However, the possibility that His61Tyr under acidic conditions could also be five-coordinate where tyrosine ligation (distal ligand) is lost and the proximal ligation is weakened was also considered.

## 4.5 Summary

In summary, exploitation of the mobile distal histidine 61 residue in rLb has allowed incorporation of tyrosine-haem ligation and has resulted in altered axial ligation of the rLb protein analogous to that of Hb M Saskatoon and His64Tyr variant of Mb. Tyrosine coordination to the ferric haem iron (evident from the green colour of the protein) was confirmed by various spectroscopic methods. A switch in axial ligation to the haem was observed with a change in pH. At low pH, the variant existed in a 'five-coordinate' state, with the distal ligand predicted to be weakly bound water or tyrosine and loss or severely weakening of the proximal ligand. The possibility that the variant exist in a form where the tyrosine ligation is lost and proximal ligation is weakened at acidic pH was also considered. At pH 4.6 and above the variant was six-coordinate, high-spin, with tyrosine as the distal ligand and histidine as the proximal ligand. Ligand binding affinities were significantly decreased due to the strength of the Fe-O<sub>Tyr</sub> bond and the mid-point potential of the ferric/ferrous couple for the His61Tyr variant was substantially lowered in comparison to rLb due to the ligation of the anionic ligand to the haem as a result of the His-Tyr mutation. In addition, EXAFS analysis carried out in this Chapter, reports the first determination of the Fe-O<sub>water</sub> and Fe-N<sub>His</sub> bond lengths for rLb and the Fe-O<sub>Tyr</sub> bond length for His61Tyr.

## 4.6 References

1. J. H. Dawson, *Science* (1988) **240**, 433.
2. P. R. Ortiz de Montellano, *Acc. Chem. Res.* (1987) **20**, 289.
3. Y. Liu, P. Moënne-Loccoz, D. P. Hildebrand, A. Wilks, T. M. Loehr, A. G. Mauk and P. R. Ortiz de Montellano, *Biochemistry* (1991) **38**, 3733.
4. K. L. Bren and H. B. Gray, *J. Am. Chem. Soc.* (1993) **115**, 10382.
5. J. A. Sigman, A. E. Pond, J. H. Dawson and Y. Lu, *Biochemistry* (1999) **38**, 11122.
6. D. P. Hildebrand, D. L. Burk, R. Maurus, J. C. Ferrer, G. D. Brayer and A. G. Mauk, *Biochemistry* (1995) **34**, 1997.
7. D. P. Hildebrand, J. C. Ferrer, H.-L. Tang, M. Smith and A. G. Mauk, *Biochemistry* (1995) **34**, 11598.
8. E. Lloyd, D. P. Hildebrand, K. M. Tu and A. G. Mauk, *J. Am. Chem. Soc.* (1995) **117**, 6434.
9. R. Maurus, R. Bogumil, Y. Luo, H.-L. Tang, M. Smith, A. G. Mauk and G. D. Brayer, *J. Biol. Chem.* (1994) **269**, 12606.
10. A. L. Raphael and H. B. Gray, *J. Am. Chem. Soc.* (1991) **113**, 1038.
11. K. Choudhury, M. Sundaramoorthy, J. M. Mauro and T. L. Poulos, *J. Biol. Chem.* (1992) **267**, 25656.
12. G. D. DePhillis, S. M. Decateur, D. Barrick and S. G. Boxer, *J. Am. Chem. Soc.* (1994) **116**, 6981.
13. D. Barrick, *Biochemistry* (1994) **33**, 6546.
14. T. K. Das, S. Franzen, A. Pond, J. H. Dawson and D. L. Rousseau, *Inorg. Chem.* (1999) **38**, 1952.
15. S. M. Decatur, K. L. Belcher, P. K. Rickert, S. Franzen and S. G. Boxer, *Biochemistry* (1999) **38**, 11086.
16. A. E. Pond, M. P. Roach, M. Sono, A. H. Rux, S. Franzen, R. Hu, M. R. Thomas, A. Wilks, Y. Dou, M. Ikeda-Saito, P. R. Ortiz de Montellano, W. H. Woodruff, S. G. Boxer and J. H. Dawson, *Biochemistry* (1999) **38**, 7601.
17. S. Pin, B. Alpert, R. Cortes, I. Ascone, M. L. Chiu and S. G. Sligar, *Biochemistry* (1994) **33**, 11618.
18. J. Hirst, S. K. Wilcox, J. Y. Ai, P. Moenne-Loccoz, T. M. Loehr and D. B. Goodin, *Biochemistry* (2001) **40**, 1274.
19. Y. Lu, S. M. Berry and T. D. Pfister, *Chem. Rev.* (2001) **101**, 3047.

20. S. Döpner, P. Hildebrand, F. I. Rosell and A. G. Mauk, *J. Am. Chem. Soc.* (1998) **120**, 11246.
21. F. I. Rosell, J. C. Ferrer and A. G. Mauk, *J. Am. Chem. Soc.* (1998) **120**, 11234.
22. E. Steensma, E. Gordon, L. M. Oster, S. J. Ferguson and J. Hajdu, *J. Biol. Chem.* (2001) **276**, 5846.
23. P. A. Williams, V. Fulop, E. F. Garman, N. F. Saunders, S. J. Ferguson and J. Hajdu, *Nature* (1997) **389**, 406.
24. K. T. Das, M. Couture, H. C. Lee, J. Peisach, D. L. Rousseau, B. A. Wittenberg, J. B. Wittenberg and H. Guertin, *Biochemistry* (1999) **38**, 15360.
25. W. N. Lanzilotta, D. J. Schuller, M. V. Thorsteinsson, R. L. Kerby, G. P. Roberts and T. L. Poulos, *Nat. Struct. Biol.* (2000) **7**, 876.
26. S. Aono, K. Ohkubo, T. Matsuo and H. Nakajima, *J. Biol. Chem.* (1998) **273**, 25757.
27. I. K. Dhawan, D. Shelver, M. V. Thorsteinsson, G. P. Roberts and M. K. Johnson, *Biochemistry* (1999) **38**, 12805.
28. D. Shelver, M. V. Thorsteinsson, R. L. Kerby, S.-Y. Chung and G. P. Roberts, *Biochemistry* (1999) **38**, 2669.
29. P. J. Ellis, C. A. Appleby, J. M. Guss, W. N. Hunter, D. L. Ollis and H. C. Freeman, *Acta Crystallographica Section D* (1997) **53**, 302.
30. D. L. Ollis, C. A. Appleby, P. M. Colman, A. E. Cutten, J. M. Guss, M. P. Venkatappa and H. C. Freeman, *Aust. J. Chem.* (1983) **36**, 451.
31. C. A. Appleby, W. E. Blumberg, J. H. Bradbury, W. H. Fushman, J. Peisach, B. A. Wittenberg, J. B. Wittenberg and P. E. Wright, in *Hemoglobin and Oxygen Binding*, C. Ho, Ed. (Elsevier, North Holland, Amsterdam) 1982, pp. 435.
32. A. Ehrenberg and N. Ellfolk, *Acta Chem. Scand.* (1963) **17**, S343.
33. C. A. Appleby, W. E. Blumberg, J. Peisach, B. A. Wittenberg and J. B. Wittenberg, *J. Biol. Chem.* (1976) **251**, 6090.
34. G. Sievers, P. M. A. Gadsby, J. Peterson and A. J. Thomson, *Biochim. Biophys. Acta* (1983) **742**, 637.
35. D. K. Jones, N. Patel, M. R. Cheesman, A. J. Thomson and E. L. Raven, *Inorg. Chim. Acta* (2002) **331**, 303.
36. D. K. Jones, R. Badii, F. I. Rosell and E. Lloyd, *Biochem. J.* (1998) **330**, 983.
37. N. Patel, D. K. Jones and E. L. Raven, *Eur. J. Biochem.* (2000) **267**, 2581.
38. A. M. Rich, R. S. Armstrong, P. J. Ellis, H. C. Freeman and P. A. Lay, *Inorg. Chem.* (1998) **37**, 5743.

39. K. D. Egeberg, B. A. Springer, S. A. Martinis, S. G. Sligar, D. Morikis and P. M. Champion, *Biochemistry* (1990) **29**, 9783.
40. A. Hayashi, T. Suzuki, K. Imai, H. Morimoto and H. Watanabe, *Biochim. Biophys. Acta* (1969) **194**, 6.
41. M. Nagai, T. Kagimoto, A. Hayashi, F. Taketa and T. Kitagawa, *Biochemistry* (1983) **22**, 1305.
42. M. Nagai, Y. Yoneyama and T. Kitagawa, *Biochemistry* (1989) **28**, 2418.
43. D. Morikis, P. M. Champion, B. A. Springer, K. D. Egeberg and S. G. Sligar, *J. Biol. Chem.* (1990) **265**, 12143.
44. J. L. Que, in *Biological Applications of Raman Spectroscopy*, T. G. Spiro, Ed. (Wiley, New York) 1988, vol. 3, pp. 491.
45. B. P. Gaber, V. Miskowski and T. G. Spiro, *J. Am. Chem. Soc.* (1974) **96**, 6868.
46. W. N. Hunter, C. A. Appleby, J. M. Guss, D. L. Ollis and H. C. Freeman, *Acta Crystallographica* (1984) **40**, C35.
47. I. T. J. Reid, M. R. N. Murthy, A. Sicignano, N. Tanaka, W. D. L. Musick and M. G. Rossman, *Proc. Natl. Acad. Sci. USA* (1981) **78**, 4767.
48. H. L. Tang, B. Chance, A. G. Mauk, L. S. Powers, K. S. Reddy and M. Smith, *Biochim. Biophys. Acta* (1994) **1206**, 90.
49. P. D. Pulsinelli, M. F. Perutz and R. L. Nagel, *Proc. Natl. Acad. Sci. USA* (1973) **70**, 3870.
50. M. S. Hargrove, E. W. Singleton, M. L. Quillin, L. A. Ortiz, G. N. Phillips, J. S. Olson and A. J. Mathews, *J. Biol. Chem* (1994) **269**, 4207.
51. J. R. Christian, M. Unno, J. T. Sage, P. M. Champion, E. Chien and S. G. Sligar, *Biochemistry* (1997) **36**, 11198.
52. M. R. Cheeseman, S. J. Ferguson, J. W. Moir, D. J. Richardson, W. G. Zumft and A. J. Thomson, *Biochemistry* (1997) **36**, 16267.
53. G. R. Jaenig, G. Smattan, J. Friedrich, R. Bernhardt, O. Ristau and K. Ruckpaul, *Biochemistry* (1982) **23**, 513.
54. G. R. Jaenig, A. Makower, H. Rabe, R. Bernhardt and K. Ruckpaul, *Biochim. Biophys. Acta* (1984) **787**, 8.
55. K. Ruckpaul, H. Rein, D. P. Ballou and M. J. Coon, *Biochim. Biophys. Acta* (1980) **626**, 41.
56. F. Baymann, F. Zito, R. Kuras, L. Minai, W. Nitschke and F.-A. Wollman, *J. Biol. Chem* (1999) **274**, 22957.

57. S. N. Datta, B. G. S. Prabhakar and V. Nehra, *J. Phys. Chem B* (1999) **103**, 2291.
58. M. Fasano, S. Baroni, A. Vannini, P. Ascenzi and S. Aime, *J. Biol. Inorg. Chem.* (2001) **276**, 650.
59. T. Matsui, S. Nagano, K. Ishimori, Y. Watanabe and I. Morishima, *Biochemistry* (1996) **35**, 13118.
60. S. Adachi, S. Nagano, Y. Watanabe and I. Morishima, *Biochem. Biophys. Res. Commun.* (1991) **180**, 138.
61. S. Adachi, S. Nagano, K. Ishimori, Y. Watanabe, I. Morishima, T. Egawa, T. Kitagawa and R. Makino, *Biochemistry* (1993) **32**, 241.
62. M. Nagai, M. Aki, R. Li, Y. Jin, S. Sakai, S. Nagatomo and T. Kitagawa, *Biochemistry* (2000) **39**, 13093.
63. W. R. Browett and M. J. Stillman, *Biochim. Biophys. Acta* (1974) **577**, 291.
64. J. H. Dawson and M. Sono, *Chem. Rev.* (1987) **87**, 1255.
65. D. Dolphin, in *The Porphyrins*, (Academic Press, New York) 1978.
66. R. Maranon, M. Jose, M. Dennis, V. Huystee, B. Robert and S. J. Martin, *Biochem. J.* (1994) **301**, 335.
67. L. A. Andersson, A. K. Johnson, M. D. Simms and T. R. Willingham, *FEBS Letter* (1995) **370**, 97.
68. D. G. Eglinton, P. M. A. Gadsby, G. Sievers, J. Peterson and A. J. Thomson, *Biochim. Biophys. Acta* (1983) **742**, 648.
69. K. S. Sharma, A. Andersson, T. M. Loehr, J. Turner and H. M. Goff, *J. Biol. Chem* (1989) **22**, 12772.
70. W.-J. Chuang, S. Johnson and H. E. V. Wart, *Biochemistry* (1988) **34**, 201.
71. I. Fita and M. G. Rossmann, *J. Mol. Biol.* (1985) **185**, 465.
72. M. R. N. Murthy, T. J. Reid, A. III Sicignano, N. Tanaka and M. G. Rossmann, *J. Mol. Biol.* (1981) **152**, 465.
73. B. K. Vainshtein, W. R. Melik-Adamyanyan, V. V. Barynin, A. A. Vagin, A. I. Grebenko, V. V. Borisov, K. S. Bartels, I. Fita and M. G. Rossmann, *J. Mol. Biol.* (1986) **188**, 49.
74. L. Stryer, in *Biochemistry*, (Freeman, New York) 1988, pp. 148.
75. T. G. Traylor, L. A. Deardurff, M. Coletta, P. Ascenzi, E. Antonini and M. Brunori, *J. Biol. Chem.* (1983) **258**, 12147.
76. J. T. Sage, D. Morikis and P. M. Champion, *Biochemistry* (1991) **30**, 1227.
77. G. M. Giacometti, T. G. Traylor, P. A. Ascenzi, M. Brunori and E. Antonini, *J. Biol. Chem.* (1977) **252**, 7447.

78. R. J. P. Williams, in *Iron in Biochemistry and Medicine*, E. A. Jacobs and M. Worwood, Ed. (Academic Press, New York) 1974, pp.183.
79. I. C. Gunsalus, J. R. Meek, J. D. Lipscomb, P. Debrunner and E. Munk, in *Molecular Mechanisms of Oxygen Activation*, (Academic Press, New York) 1974, pp. 559.
80. P. M. A. Gadsby and A. J. Thomson, *J. Am. Chem. Soc.* (1990) **112**, 5003.
81. H. E. T. Seward, PhD Thesis, University of East Anglia (1999).
82. Y. A. Sharanov, *Sov. Sci. Rev. D. Physiochem. Biol.* (1991) **10**, 1.
83. S. Yoshida, T. Iizuka, T. Nozawa and M. Hatano, *Biochim. Biophys. Acta* (1975) **405**, 122.
84. J. Springall, M. J. Stillman and A. J. Thomson, *Biochim. Biophys. Acta* (1976) **453**, 494.
85. M. J. F. Rots and P. J. Zandstra, *Mol. Phys.* (1982) **46**, 1283.
86. N. J. Watmough, M. R. Cheesman, C. Greenwood and A. J. Thomson, *Biochem. J* (1994) **300**, 469.

**Chapter 5**  
**Alteration of the Haem Axial**  
**Ligation in Leghaemoglobin:**  
**Spectroscopic,**  
**Electrochemical and Ligand**  
**Binding Analysis of the**  
**His61Lys and His61Arg**  
**Variants**

## **5 Alteration of the Haem Axial Ligation in Leghaemoglobin: Spectroscopic, Electrochemical and Ligand Binding Analysis of the His61Lys and His61Arg Variants**

### **5.1 Introduction**

The role of haem iron axial ligation in modulating the spectroscopic and functional properties of the protein has been of considerable interest for some time.<sup>[1-19]</sup> A number of studies have been reported in which alteration of axial ligands to the haem using site-directed mutagenesis has been conducted within a variety of six-coordinate haem proteins in an attempt to mimic properties of other haem proteins.<sup>[1-19]</sup> In the previous Chapter, the mobile distal histidine of rLb was replaced with tyrosine to successfully generate a tyrosine-ligated haem protein that mimicked spectroscopic properties of other tyrosine-ligated haem proteins. The success of this experimental strategy provided a means to incorporate other amino acids to the haem in an attempt to mimic axial ligation and spectroscopic properties of other haem proteins. In Nature there are various biologically important haem proteins that contain tetrahedral nitrogen as axial ligands to the haem iron. These include the lysine-coordinated haem proteins, 'alkaline' cytochrome *c*<sup>[20, 21]</sup> and nitrite reductase.<sup>[22]</sup> Other examples include cytochrome *f* where the polypeptide N-terminus binds the iron<sup>[23]</sup> and CooA, a transcription factor of the CAP family in which the iron is coordinated by the main chain nitrogen of a proline.<sup>[24]</sup>

In this study, the mobility of histidine 61 has been further exploited to incorporate nitrogenous axial ligands, lysine and arginine to generate two new variants, His61Lys and His61Arg, respectively. Spectroscopic, electrochemical and ligand binding analyses have been undertaken with the aim of establishing the haem ligation of the new variants and assess the effect of the mutations on the properties of proteins. The data are compared with rLb and spectroscopic similarities to naturally occurring nitrogenous-ligated haem proteins have been highlighted.

## 5.2 Mutagenesis, Expression, Isolation and Purification

Preparation of the His61Lys and His61Arg variants of rLb using site-directed mutagenesis was conducted according to the Quikchange protocol (Stratagene), using the rLb encoded gene and the His61Lys and His61Arg mutagenic oligonucleotides, respectively (Chapter 7, Table 7.1). Sequencing of the whole rLb gene confirmed desired mutation. The His61Lys and His61Arg variants were expressed, isolated and purified according to published procedures<sup>[25]</sup> (Chapter 7, Section 7.1). Both variants were isolated as apo-protein and required reconstitution by addition of appropriate volumes of hemin. Excess hemin was removed as described in Chapter 7, Section 7.1.8. Purified proteins (~ 8 mg/l) were obtained with  $R_z > 4$  (pH 7.0, 25.0 °C,  $\mu = 0.10$  M) and migrated as a single band on a SDS PAGE gel (Figure 7.2, Chapter 7).

## 5.3 Results

### 5.3.1 Electronic Absorption Spectra

The electronic absorption spectra of His61Lys and His61Arg are depicted in Figures 5.1(A) and (B), respectively. For the ferric His61Lys variant, an entirely low-spin species ( $\lambda_{\max}$  ( $\epsilon/\text{mM}^{-1}\text{cm}^{-1}$ ) = 408 (158), 532 and 563 nm) was observed that is distinct from the mixture of high- and low-spin species observed for rLb ( $\lambda_{\max} = 403, 495, 530, 560$  and 626 nm).<sup>[25]</sup> The red-shift in the Soret absorption and the relative intensities of the  $\alpha$  and  $\beta$  regions ( $\beta > \alpha$ ) were characteristic of a nitrogenous-ligand-bound form of ferric rLb, Table 5.1. Maxima for His61Lys were similar to those observed for the methylamine derivative of rLb ( $\lambda_{\max} = 410, 537$  and 570 nm), Figure 5.2, prepared in this work and strongly suggested lysine as the sixth ligand in the variant. The reduced form of His61Lys, ( $\lambda_{\max} = 427, 527$  and 557 nm), Figure 5.1(A), was also spectroscopically similar to the methylamine derivative of ferrous rLb ( $\lambda_{\max} = 419, 527$  and 555 nm), Figure 5.2, suggesting that lysine 61 remained coordinated to the haem in the reduced form of His61Lys. These data were in contrast to those for ferrous rLb ( $\lambda_{\max} = 427$  and 555 nm) where formation of a five-coordinate haem species is observed.

Similarly, the electronic absorption spectrum of ferric His61Arg revealed a

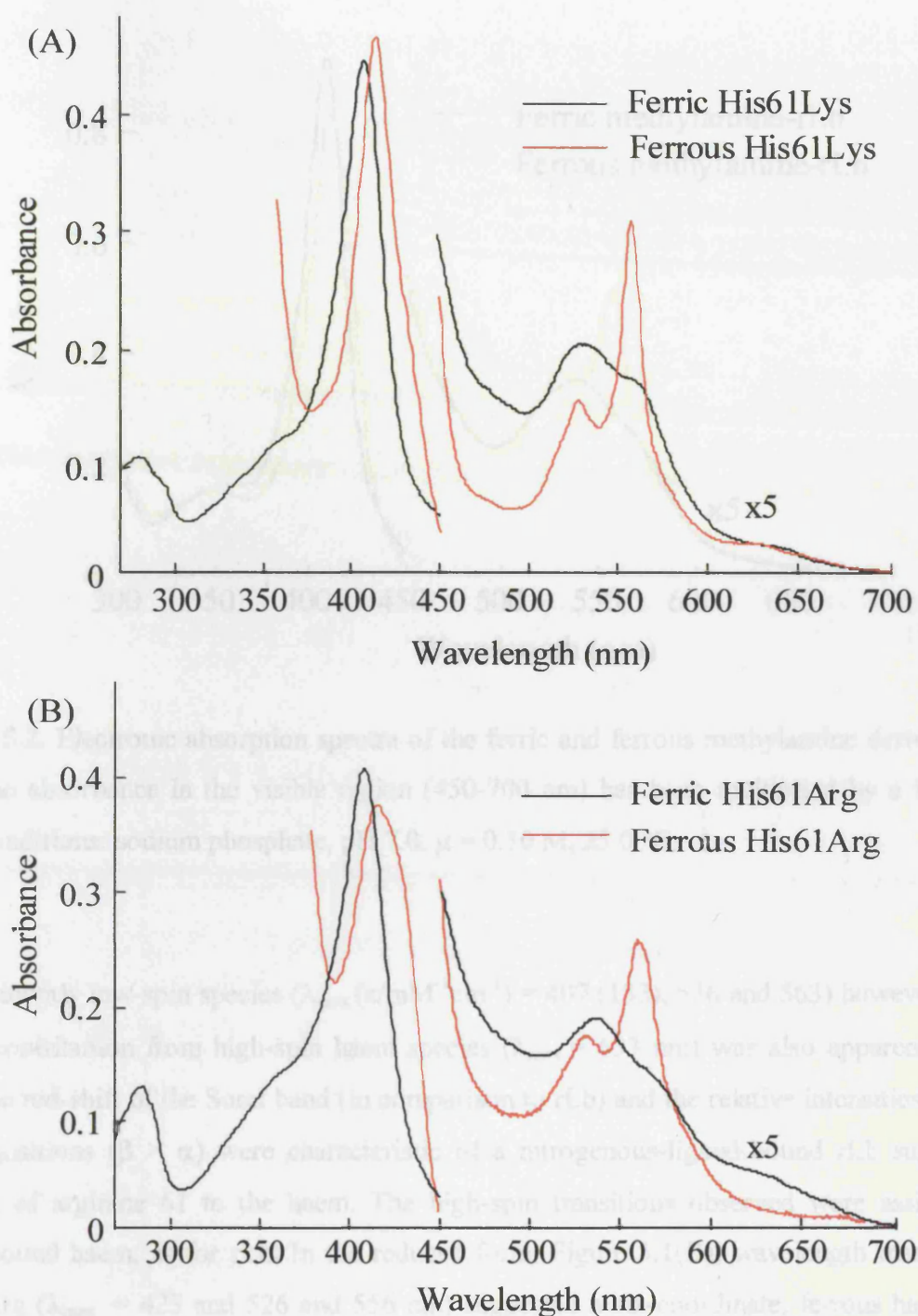


**Figure 5.1.** Electronic absorption spectra of ferric and ferrous His61Lys (A) and His61Arg (B). The absorbance in the visible region (450-700 nm) has been multiplied by a factor of five. Conditions: sodium phosphate, pH 7.0,  $\mu = 0.10$  M, 25.0 °C.

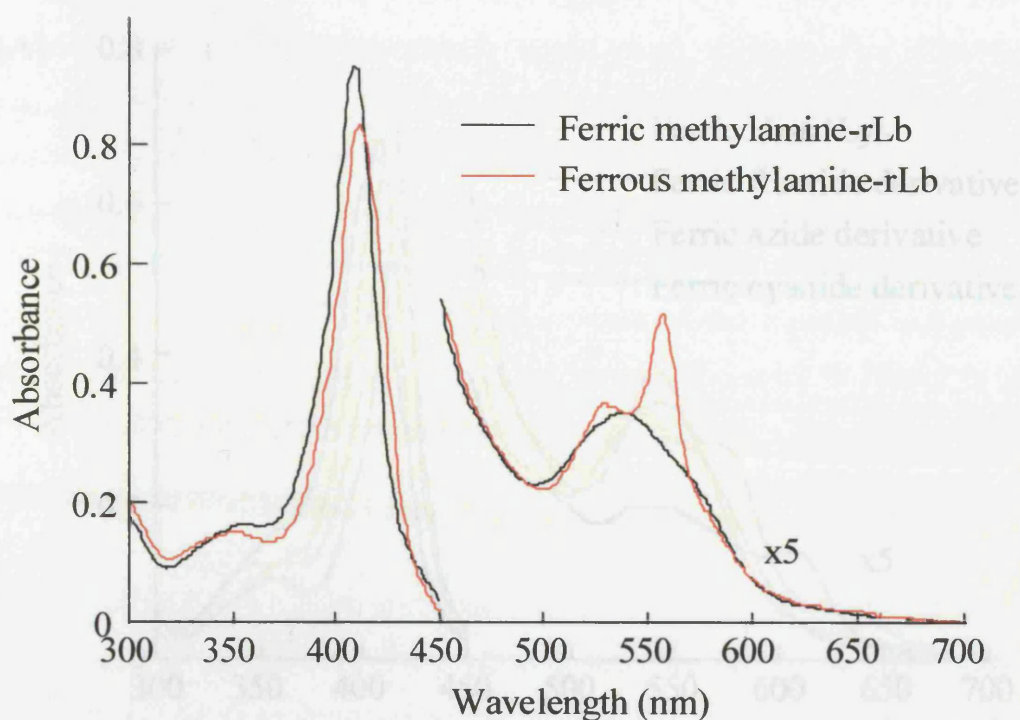


**Figure 5.2.** Electronic absorption spectra of the ferric and ferrous methylamine derivative of rLb. The absorbance in the visible region (450-700 nm) has been multiplied by a factor of five. Conditions: sodium phosphate, pH 7.0,  $\mu = 0.10$  M, 25.0 °C.

predominantly low-spin species ( $\lambda_{\max} (\epsilon/\text{mM}^{-1}\text{cm}^{-1}) = 407$  (133), 536 and 563) however, some minor contribution from high-spin haem species ( $\lambda_{\max} = 633$  nm) was also apparent, as for rLb. The red-shift of the Soret band (in comparison to rLb) and the relative intensities of low-spin transitions ( $\beta > \alpha$ ) were characteristic of a nitrogenous-ligand-bound rLb suggesting ligation of arginine 61 to the haem. The high-spin transitions observed were assigned to water-bound haem, as for rLb. In the reduced form, Figure 5.1(B), wavelength maxima for His61Arg ( $\lambda_{\max} = 423$  and 526 and 556 nm) suggested a six-coordinate, ferrous haem with possible ligation of arginine as the sixth ligand, again distinct to that for ferrous rLb.<sup>[25]</sup>

### 5.3.2 Ligand Binding

The ligand binding behaviour of both His61Lys and His61Arg were similar to that of rLb. Addition of excess anionic ligand to the variants resulted in characteristic formation of a

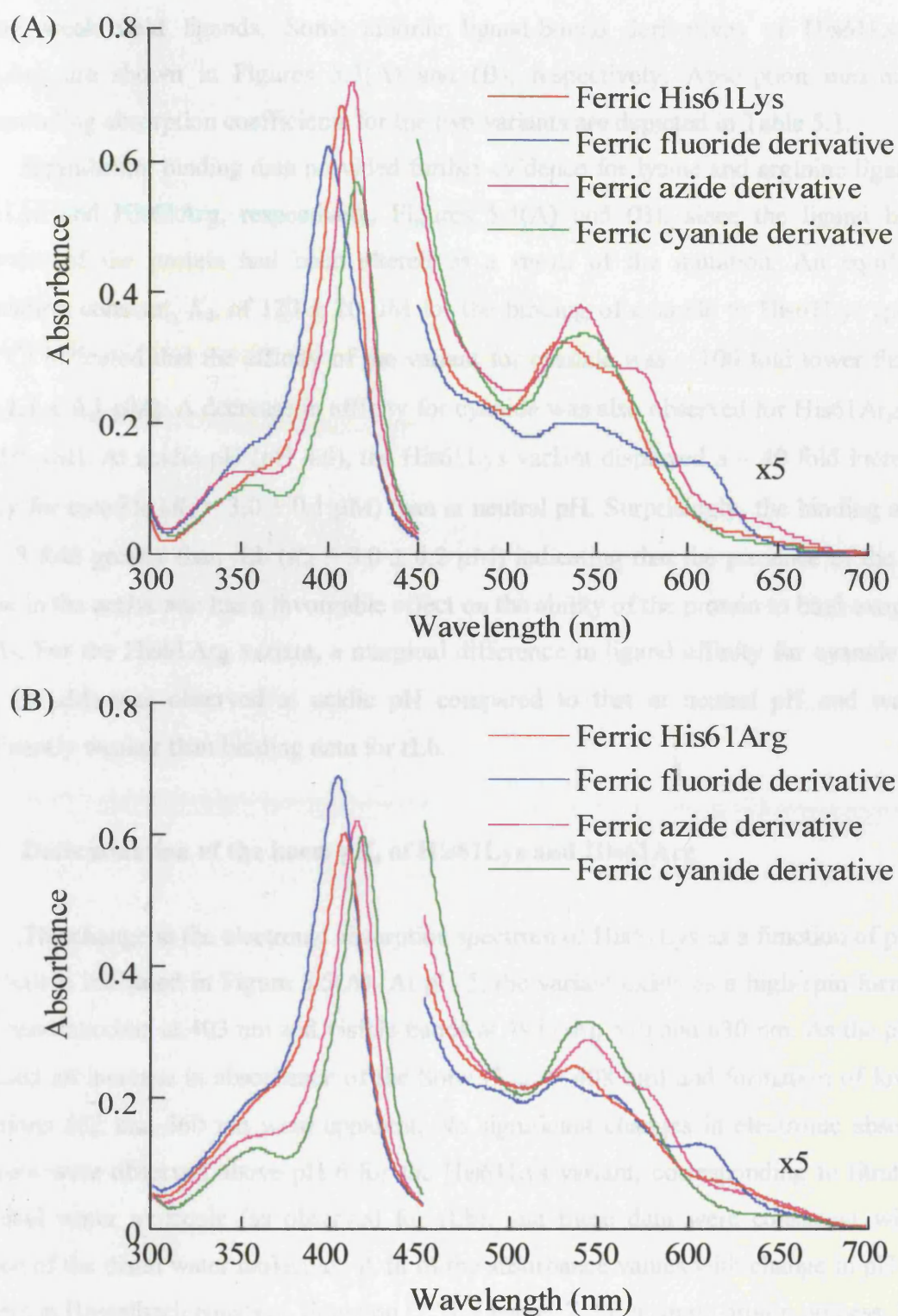


**Figure 5.3.** Electronic absorption spectra of the anionic ligand-bound derivatives of ferric His61Lys (A) and His61Arg (B). Conditions: sodium phosphate, pH 7.0,  $\mu = 0.10$  M, 25.0 °C.

low-spin haem species, on binding strong field ligands, and a high-spin haem species on binding weak field ligands. Some anionic ligand-bound derivatives of His61Lys and His61Arg are shown in Figures 5.3(A) and (B), respectively. Absorption maxima and corresponding absorption coefficients for the two variants are depicted in Table 5.1.

Equilibrium binding data provided further evidence for lysine and arginine ligation in His61Lys and His61Arg, respectively, Figures 5.4(A) and (B), since the ligand binding properties of the protein had been altered as a result of the mutation. An equilibrium dissociation constant,  $K_d$ , of  $120 \pm 20 \mu\text{M}$  for the binding of cyanide to His61Lys (pH 7.0, 25.0 °C) indicated that the affinity of the variant for cyanide was  $\sim 100$  fold lower than rLb ( $K_d = 1.1 \pm 0.1 \mu\text{M}$ ). A decrease in affinity for cyanide was also observed for His61Arg ( $K_d = 83 \pm 10 \mu\text{M}$ ). At acidic pH (pH 4.0), the His61Lys variant displayed a  $\sim 40$  fold increase in affinity for cyanide ( $K_d = 3.0 \pm 0.1 \mu\text{M}$ ) than at neutral pH. Surprisingly, the binding affinity was  $\sim 3$  fold greater than rLb ( $K_d = 9.0 \pm 0.2 \mu\text{M}$ ) indicating that the presence of the lysine residue in the active site has a favourable effect on the ability of the protein to bind exogenous ligands. For the His61Arg variant, a marginal difference in ligand affinity for cyanide ( $K_d = 75 \pm 10 \mu\text{M}$ ) was observed at acidic pH compared to that at neutral pH and was still significantly weaker than binding data for rLb.

### 5.3.3 Determination of the haem $pK_a$ of His61Lys and His61Arg

The change in the electronic absorption spectrum of His61Lys as a function of pH (pH 5.1 – 9.0) is indicated in Figure 5.5(A). At pH 5, the variant exists as a high-spin form with Soret band maxima at 403 nm and visible bands at 497 (sh), 510 and 630 nm. As the pH was increased an increase in absorbance of the Soret ( $\lambda_{\text{max}} = 408 \text{ nm}$ ) and formation of low-spin transitions 532 and 560 nm were apparent. No significant changes in electronic absorption spectrum were observed above pH 6 for the His61Lys variant, corresponding to titration of the distal water molecule (as observed for rLb), and these data were consistent with the absence of the distal water molecule. A fit of the absorbance values with change in pH to the Henderson Hasselbach equation, Equation [7.7], Chapter 7, for a single proton process, Figure 5.5(A) (inset), yielded a  $pK_a$  of  $5.7 \pm 0.2$ .

**Table 5.1.**

Wavelength maxima (nm) and, in parentheses, absorption coefficients ( $\text{mM}^{-1}\text{cm}^{-1}$ ) for the ferric and ferrous derivatives of His61Lys and His61Arg. Conditions: pH 7.0,  $\mu = 0.10 \text{ M}$ ,  $25.0 \text{ }^\circ\text{C}$ . Nic = nicotinate. sh = shoulder.

Derivative	His61Lys					His61Arg				
	( $\gamma$ ) Soret	CT <sub>2</sub>	$\beta$	$\alpha$	CT <sub>1</sub>	( $\gamma$ ) Soret	CT <sub>2</sub>	$\beta$	$\alpha$	CT <sub>1</sub>
Fe(III)	408 (158)	-	532 (14.9)	561 (12.3)	-	407 (133)	-	536 (13.1)	563 (8.99)	633 (4.12)
Fe(III)-CN <sup>-</sup>	417 (146)	-	543 (16.2)	-	-	417 (128)	-	542 (15.3)	-	-
Fe(III)-F <sup>-</sup>	401 (219)	488 (28.0)	529 (26.1)	562 (25.3)	610 (24.8)	403.5 (136)	487 (11.4)	529(10.8)	560 (10.2)	610 (6.68)
Fe(III)-N <sub>3</sub> <sup>-</sup>	415 (158)	-	541 (15.8)	579 (10.2)	-	414 (128)	-	543 (14.2)	582 (9.3)	644 (sh)
Fe(III)-Nic	408 (153)	-	529 (11.8)	561 (9.1)	-	408 (143)	-	528 (19.3)	561 (15.7)	-
Fe(III)-OAc <sup>-</sup>	402 (170)	494 (9.49)	533 (sh)	570 (4.63)	622 (5.91)	402.5 (162)	495 (8.56)	534 (sh)	571 (4.5)	622 (5.61)
Fe(II)	427 (122)	-	527 (10.4)	557 (20.3)	-	423 (133)	-	526 (sh)	556 (20.7)	-
Fe(II)-CO	419 (289)	-	538 (21.2)	566 (20.7)	-	418 (201)	-	537.5 (17.1)	565 (16.3)	-
Fe(II)-Nic	419.5 (234)	-	525 (23.6)	555 (45.3)	-	419 (225)	-	525 (22.7)	555 (37.6)	-
Fe(II)-O <sub>2</sub>	411 (109)	-	541 (13.7)	575 (12.6)	-	411 (89.2)	-	541 (11.2)	575 (10.3)	-

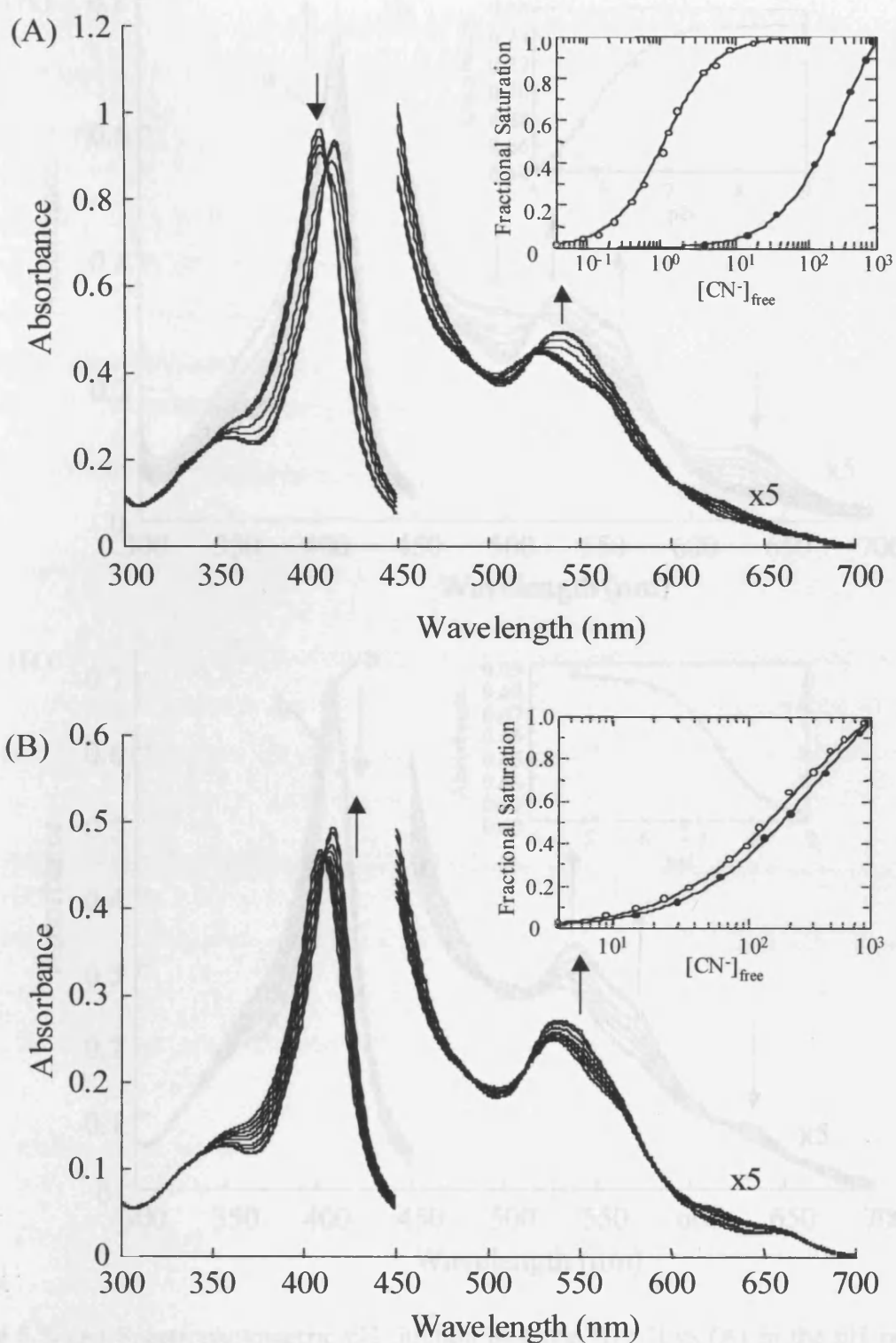


**Figure 5.4.** Spectrophotometric titration of His61Lys (A) and His61Arg (B) with cyanide. The visible region has been multiplied by a factor of five and arrows indicate the direction of change in absorbance upon successive addition of cyanide. Inset show fit of data to Equation [7.7] at pH 4 (O) and pH 7 (●). Conditions: sodium phosphate, pH 7.0,  $\mu = 0.10$  M, 25.0 °C.

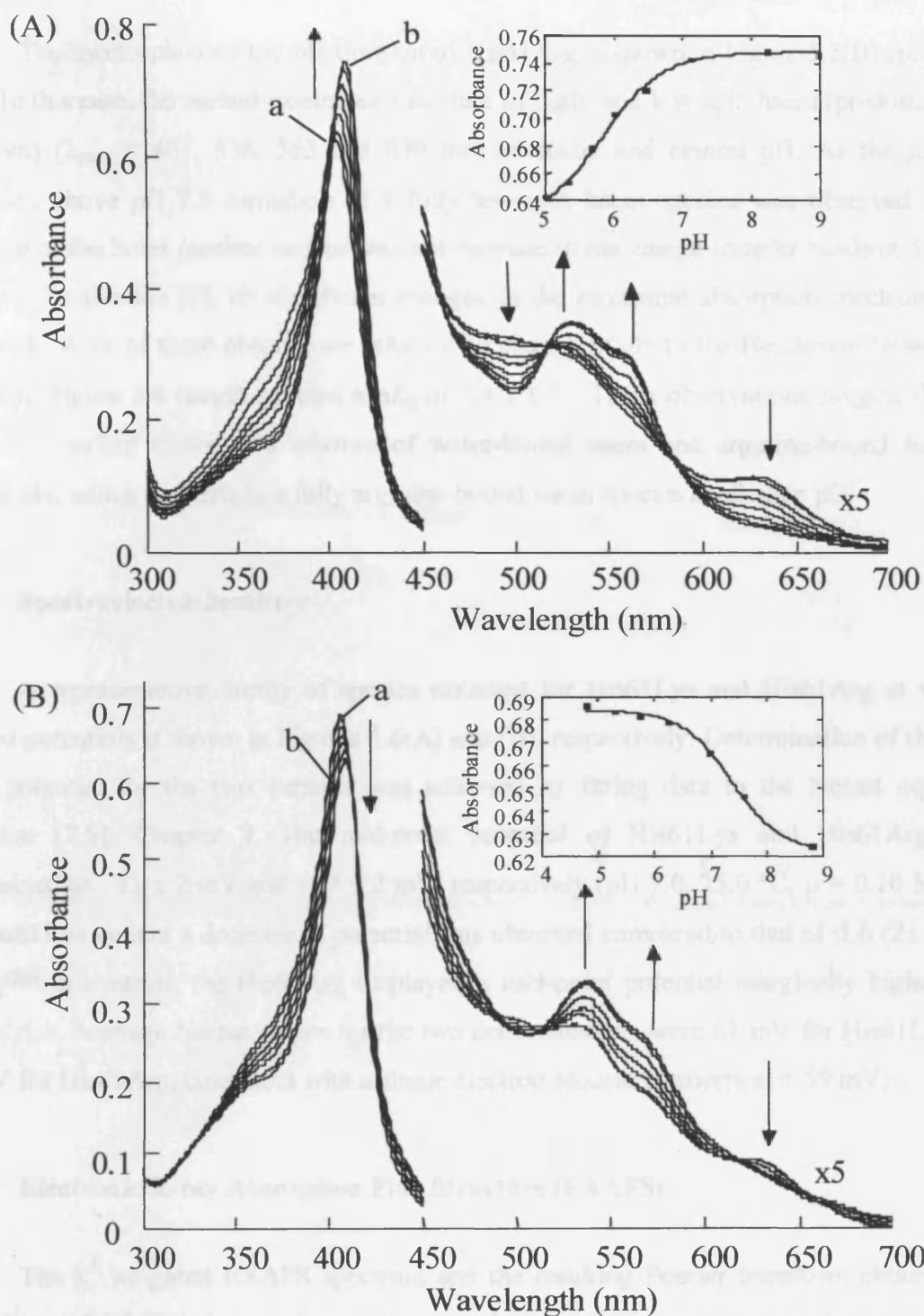


**Figure 5.5.** (A) Spectrophotometric pH titration of ferric His61Lys (A) in the pH range (a) pH 5.1, (b) 9.0 and intermediate pHs 5.4, 5.7, 6.0, 6.5, 7.1 and 8.2. (B) Spectrophotometric pH titration of ferric His61Arg showing spectra at (a) pH 4.8, (b) 8.8 and intermediate pHs 5.3, 5.8, 6.3, 7.0 and 7.6. Arrows denote the direction of change in absorbance with increase of pH. Inset: plot of variation in absorbance 408 nm for His61Lys and 407 nm for His61Arg with pH. The solid line represents non-linear least squares fit to Henderson Hasselbach equation for a single proton process.

The spectrophotometric pH titration of His61Arg is shown in Figure 5.5(B) (pH 4.8 – 8.8). In this case, the variant existed as a mixture of high- and low-spin haem (predominantly low-spin) ( $\lambda_{\text{max}} = 407, 536, 563$  and  $630$  nm) at acidic and neutral pH. As the pH was increased above pH 7.5 formation of a fully low-spin haem species was observed with a decrease of the Soret maxima and subsequent increase of the charge-transfer bands at 536 and 563 nm. At alkaline pH, no significant changes in the electronic absorption spectrum were observed. A fit of these absorbance values with change in pH to the Henderson Hasselbach equation, Figure 5.6 (inset), yielded a  $pK_a$  of  $7.4 \pm 0.1$ . These observations suggest that the His61Arg variant exists as a mixture of water-bound haem and arginine-bound haem at neutral pH, which converts to a fully arginine-bound haem species at alkaline pH.

### 5.3.4 Spectroelectrochemistry

A representative family of spectra obtained for His61Lys and His61Arg at various applied potentials is shown in Figures 5.6(A) and (B), respectively. Determination of the mid-point potential for the two variants was achieved by fitting data to the Nernst equation, Equation [7.9], Chapter 7. The mid-point potential of His61Lys and His61Arg were determined as  $-31 \pm 2$  mV and  $+29 \pm 2$  mV, respectively (pH 7.0, 25.0 °C,  $\mu = 0.10$  M). For the His61Lys variant a decrease in potential was observed compared to that of rLb (21 mV vs SHE),<sup>[26]</sup> in contrast, the His61Arg displayed a mid-point potential marginally higher than that of rLb. Average Nernst slopes for the two determinations were 61 mV for His61Lys and 57 mV for His61Arg, consistent with a single electron process (theoretical = 59 mV).

### 5.3.5 Electronic X-ray Absorption Fine Structure (EXAFS)

The  $k^3$  weighted EXAFS spectrum and the resulting Fourier transform obtained for His61Lys and His61Arg at room temperature and cryogenic temperature are shown in Figure 5.7. Fit of data for the two variants from the EXAFS spectra were the same as those described for rLb (Chapter 4) and are presented in Table 5.2. The Brookhaven nomenclature for haem atoms, Scheme 5.1, has been used throughout.

The structural results for the His61Lys and His61Arg variants were similar to those of rLb at both temperatures. The strong similarities were likely due to the dominating (invariant) four-fold symmetric porphyrin ring structure. The Fe-N<sub>p</sub> distances for both

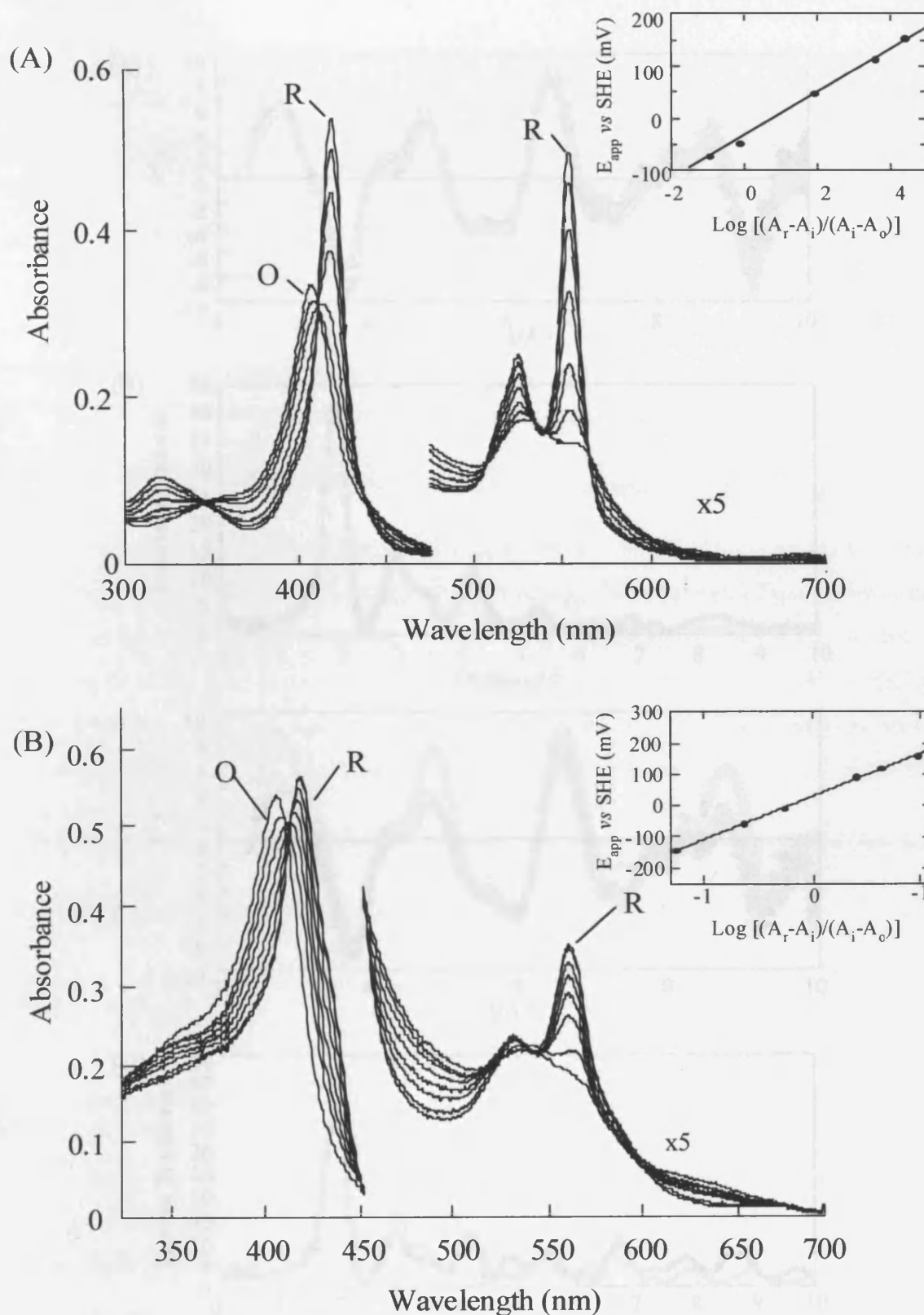


**Figure 5.6.** Thin-layer spectroelectrochemical spectra of His61Lys (A) and His61Arg (B) at various applied potentials,  $E_{app}$  (mV). Fully oxidized (O) and fully reduced (R) spectra for each derivative are indicated. The inset shows a fit of the absorbance data at 408 nm for His61Lys and 407 nm for His61Arg to the Nernst equation. Conditions: sodium phosphate, pH 7.0, 25.0 °C,  $\mu = 0.10$  M.

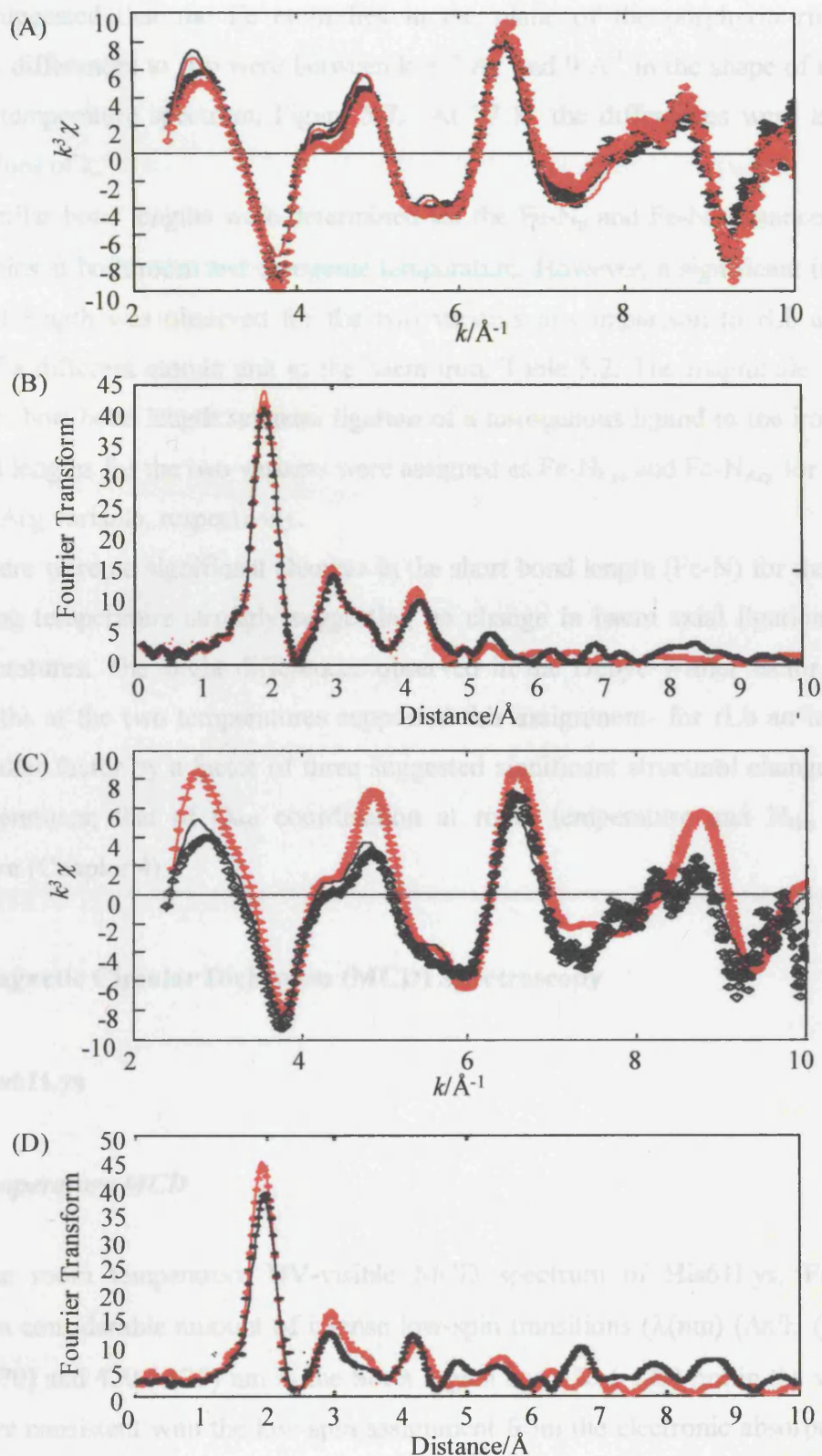


**Figure 5.7.** The EXAFS spectra (A) and Fourier transform amplitude of EXAFS (B) of His61Lys; the EXAFS spectra (C) and Fourier transform amplitude of EXAFS (D) of His61Arg observed ( $\diamond$ ) at 298K and ( $\blacklozenge$ ) at 77K. The solid lines represent the calculated data from refined models at 298K (—) and at 77K (—).

variants suggested that the Fe atom lies in the plane of the porphyrin ring. The only significant differences to rLb were between  $k = 7 \text{ \AA}^{-1}$  and  $9 \text{ \AA}^{-1}$  in the shape of the doublet in the room temperature spectrum, Figure 5.7. At 77 K, the differences were less with very similar values of  $k$ .

Similar bond lengths were determined for the Fe-N<sub>p</sub> and Fe-N<sub>e</sub> distances between all three proteins at both room and cryogenic temperature. However, a significant increase in the short bond length was observed for the two variants in comparison to rLb and suggested ligation of a different atomic unit to the haem iron, Table 5.2. The magnitude increase (~10 pm) of the short bond length suggests ligation of a nitrogenous ligand to the iron. Hence, the short bond lengths for the two variants were assigned as Fe-N<sub>Lys</sub> and Fe-N<sub>Arg</sub> for the His61Lys and His61Arg variants, respectively.

There were no significant changes in the short bond length (Fe-N) for the two variants on lowering temperature strongly suggesting no change in haem axial ligation between the two temperatures. The slight differences observed in the Debye-Waller factor for the Fe-N bond lengths at the two temperatures supported this assignment- for rLb an increase in the Debye-Waller factor by a factor of three suggested significant structural change between the two temperatures; that of O<sub>H<sub>2</sub>O</sub> coordination at room temperature and N<sub>His</sub> at cryogenic temperature (Chapter 4).

### 5.3.6 Magnetic Circular Dichroism (MCD) Spectroscopy

#### 5.3.6.1 His61Lys

##### *Room Temperature MCD*

The room temperature UV-visible MCD spectrum of His61Lys, Figure 5.8(A), exhibited a considerable amount of intense low-spin transitions ( $\lambda(\text{nm})$  ( $\Delta\epsilon/H$  ( $\text{mM}^{-1}\text{cm}^{-1}\text{T}^{-1}$ )) at 397 (+70) and 420 (-125) nm in the Soret region and 550 (-125) nm in the visible region, which were consistent with the low-spin assignment from the electronic absorption data. The only detectable high-spin transition was a small CT<sub>2</sub> trough at 638 nm (-5  $\text{mM}^{-1}\text{cm}^{-1}\text{T}^{-1}$ ), suggestive of minor amounts (~ 5%) of histidine-water haem species. The dominant low-spin nature of His61Lys was further supported in the near-IR region, Figure 5.9. One low-spin CT band at 1600 nm was observed (the band at ~ 1300 nm is a vibrational band and not a second

**Table 5.2.**

Structural results obtained by fitting the EXAFS spectra from rLb and the His61Arg and His61Lys variants of rLb. Data were fitted to  $k_{\text{max}} = 10 \text{ \AA}^{-1}$ . Uncertainties quoted are  $\pm 2\sigma$  (95% confidence) Parameter values listed without uncertainties were held fixed during the fit.  $\sigma^2$  is the mean square deviation in bond length, usually referred to as the Debye-Waller factor.

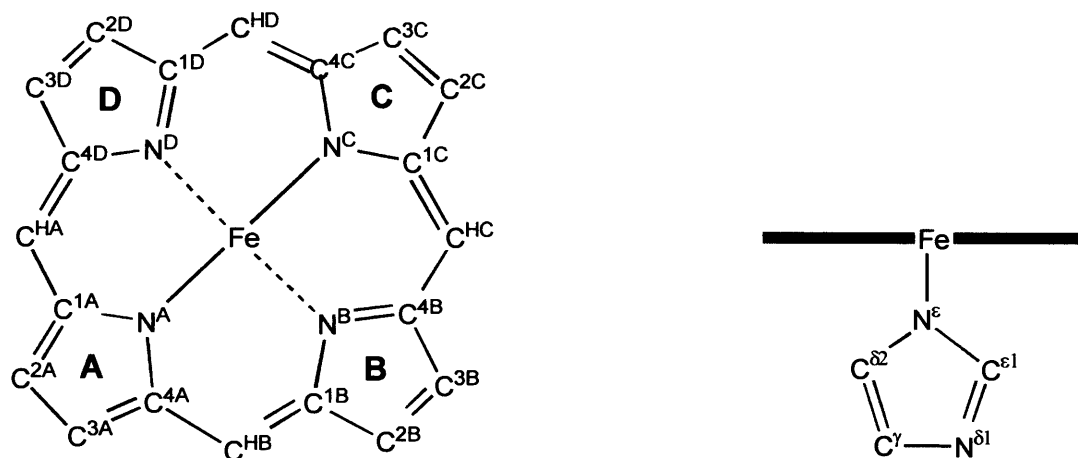
N (77K)	N (RT)	Type	R (77K) pm	R (RT) pm	$\sigma^2$ (77K) (pm) <sup>2</sup>	$\sigma^2$ (RT) (pm) <sup>2</sup>
<b>rLb</b>						
4	4	$N_p^a$	200 ± 2	205 ± 2	10 ± 5	20 ± 10
1	1	$N_e$	210 ± 5	210 ± 5	10 ± 5	20 ± 10
1	1	N,O	190 ± 5	190 ± 5	20 ± 15	60 ± 20
8	8	$C^b$	299 ± 5	303 ± 5	45 ± 5	60 ± 10
4	4	$C^c$	337 ± 5	334 ± 5	45 ± 5	60 ± 10
8	8	C	423 ± 5	428 ± 5	45 ± 5	60 ± 10
<b>His61Arg</b>						
4	4	$N_p^a$	202 ± 2	202 ± 2	30 ± 5	50 ± 10
1	1	$N_e$	210 ± 10	205 ± 5	40 ± 10	50 ± 10
1	1	N	200 ± 10	202 ± 10	40 ± 10	50 ± 20
8	8	$C^b$	300 ± 5	299 ± 5	60 ± 10	90 ± 10
4	4	$C^c$	343 ± 5	347 ± 5	60 ± 10	90 ± 10
8	8	$C^d$	428 ± 5	430 ± 5	60 ± 10	90 ± 10
<b>His61Lys</b>						
4	4	$N_p^a$	201 ± 2	204 ± 2	25 ± 5	25 ± 10
1	1	$N_e$	205 ± 10	205 ± 10	30 ± 10	40 ± 10
1	1	N	202 ± 10	203 ± 10	30 ± 10	40 ± 10
8	8	$C^b$	301 ± 5	302 ± 5	65 ± 10	80 ± 10
4	4	$C^c$	341 ± 5	342 ± 5	65 ± 10	80 ± 10
8	8	$C^d$	428 ± 5	429 ± 5	65 ± 10	80 ± 10

<sup>a</sup>  $N_p = N^A, N^B, N^C, N^D$

<sup>b</sup>  $C^b = C^{1A}, C^{1B}, C^{1C}, C^{1D}, C^{4A}, C^{4B}, C^{4C}, C^{4D}$

<sup>c</sup>  $C^c = C^{HA}, C^{HB}, C^{HC}, C^{HD}$

<sup>d</sup>  $C^d = C^{2A}, C^{3A}, C^{2B}, C^{3B}, C^{2C}, C^{3C}, C^{2D}, C^{3D}$



**Scheme 5.1.** The Brookhaven haem nomenclature used in this work.

real band) and has been similarly observed for alkaline cytochrome *c*.<sup>[27]</sup> The wavelength of the CT band was characteristic of ligation of two nitrogenous ligands to the haem, likely histidine and lysine.

### ***Low Temperature MCD***

The low temperature UV-visible MCD spectrum of His61Lys, Figure 5.8(B), also exhibited considerable amount of intense low-spin transitions ( $\lambda$  (nm) ( $\Delta\epsilon/H$  ( $\text{mM}^{-1}\text{cm}^{-1}\text{T}^{-1}$ )) at 397 (+21) and 425 (-42) nm in the Soret region and 520 (-5) and  $\sim$  550 (-15) nm in the visible region). However, in this case no high-spin transitions were seen in the region  $\sim$  630 – 650 nm indicating the fully low-spin nature of the His61Lys variant. The intense derivative-shaped MCD spectrum of His61Lys in the Soret region was very similar to the MCD spectra observed previously for other low-spin haem proteins.<sup>[28, 29]</sup> The Soret region of His61Lys (maximum at 397, a zero crossing at 412 nm and a minimum at  $\sim$  425 nm) resembled that of cytochrome *f* (maximum at 403nm, zero crossing at 410 nm and minimum at 417 nm<sup>[30]</sup>) and alkaline cytochrome *c* (maximum at 397 nm, zero crossing at 405 nm and minimum at 415 nm<sup>[27]</sup>). The MCD spectrum of His61Lys in the visible region also showed marked resemblance to the MCD of cytochrome *f* and alkaline cytochrome *c*, for which lysine–haem ligation has been well established.<sup>[27, 30]</sup> In particular, troughs evident at  $\sim$  425

nm and  $\sim 325$  nm in the Soret region of the MCD spectra of His61Lys, resembled that of alkaline cytochrome *c* (430 nm)<sup>[27]</sup> and the butylamine derivative of Lb (330 nm),<sup>[27]</sup> respectively, further suggesting lysine (amine) ligation to the haem in the His61Lys variant and hence confirming the histidine-lysine haem ligation assignment.

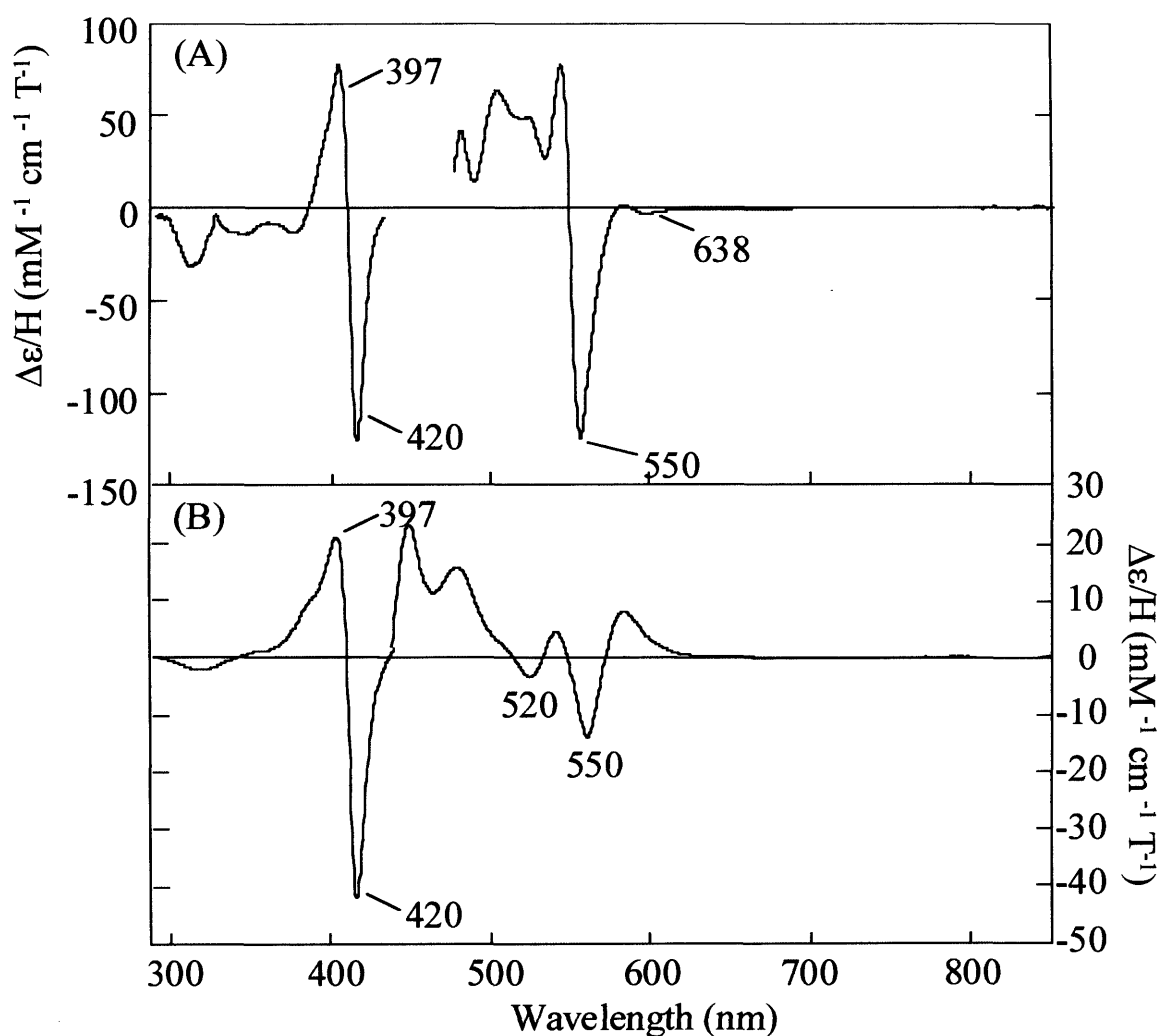


**Figure 5.8.** UV-visible MCD spectrum of His61Lys (pH 7.0) recorded at (A) room temperature using a magnetic field of 6 T and (B) 4.2 K using a magnetic field of 5 T.

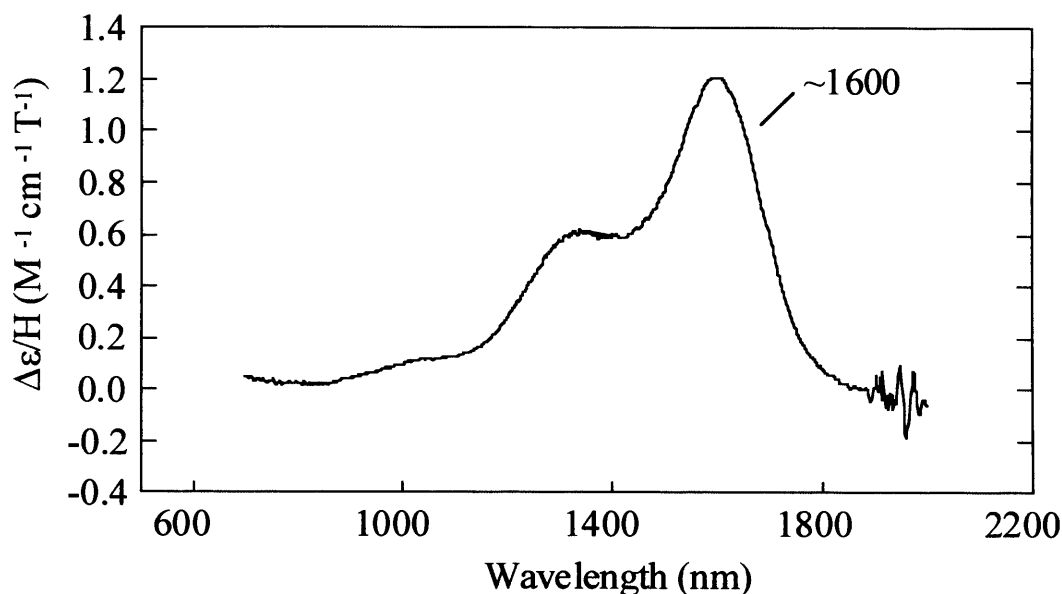


**Figure 5.9.** Near-IR MCD spectrum of His61Lys (pH 7.0) recorded at room temperature using a magnetic field of 6 T.

### 5.3.6.2 His61Arg

#### *MCD at Acidic pH (pH 4.4)*

The room temperature spectrum UV-visible MCD spectrum of His61Arg recorded at acidic pH is depicted in Figure 5.10. The low intensity peak (397 nm (+16  $\text{mM}^{-1}\text{cm}^{-1}\text{T}^{-1}$ )) and trough (420 nm (-28  $\text{mM}^{-1}\text{cm}^{-1}\text{T}^{-1}$ )) were observed in the Soret region and suggested that His61Arg existed in a predominantly high-spin state at acidic pH. However, in the visible region of the MCD spectrum, a mixture of high- and low-spin transitions were evident. Low intensity, low-spin transitions ( $\lambda$  (nm) ( $\Delta\epsilon/H$  ( $\text{mM}^{-1}\text{cm}^{-1}\text{T}^{-1}$ ))) at  $\sim 530$  (+8) and  $\sim 550$  (+2) and a more intense low-spin transition at  $\sim 570$  (-58) were observed and corresponded well to the low-spin transitions in the electronic absorption spectrum of His61Arg at pH 4.8, Figure 5.5(B). High-spin transitions ( $\lambda$  (nm) ( $\Delta\epsilon/H$  ( $\text{mM}^{-1}\text{cm}^{-1}\text{T}^{-1}$ ))) at 480 (+10) and  $\sim 630$  (-18) were also apparent and were again corresponding with the electronic absorption spectrum of His61Arg at pH 4.8. The signal observed at  $\sim 630$  nm is characteristic of histidine-water-bound haem and accordingly the high-spin transitions were assigned to histidine-water haem in the variant. The low-spin transitions were similar to those detected for His61Lys, indicating *bis*-nitrogenous haem ligation (most likely histidine-arginine) in His61Arg. Accordingly the low-spin transitions were assigned to arginine-bound haem.

**MCD at Alkaline pH (pH 8.8)**

The room temperature UV-visible MCD spectrum of His61Arg recorded at alkaline pH (pH 8.8) is depicted in Figure 5.10. At alkaline pH the low-spin transitions were more pronounced. An increase in the Soret intensity was observed ( $\lambda$  (nm) ( $\Delta\epsilon/H$  ( $\text{mM}^{-1}\text{cm}^{-1}\text{T}^{-1}$ ))) at 397 (+50) and 420 (-58) indicating more low-spin haem. Analysis of the visible region also indicated a considerable amount of low-spin haem ( $\lambda$  (nm) ( $\Delta\epsilon/H$  ( $\text{mM}^{-1}\text{cm}^{-1}\text{T}^{-1}$ ))) at  $\sim 530$  (+26) and  $\sim 550$  (+26) and 575 (-58) and was in agreement with the electronic absorption spectrum of His61Arg at pH 8.8. In contrast, some high-spin haem was also apparent in the MCD spectrum ( $\lambda$  (nm) ( $\Delta\epsilon/H$  ( $\text{mM}^{-1}\text{cm}^{-1}\text{T}^{-1}$ ))) at  $\sim 480$  (+26) and 638 (-18)), which was not observed in the electronic absorption of alkaline His61Arg. The signal at 638 nm indicated water-bound haem, however, at this pH the water would be expected to be deprotonated, hence, assignment for the high-spin haem was difficult.

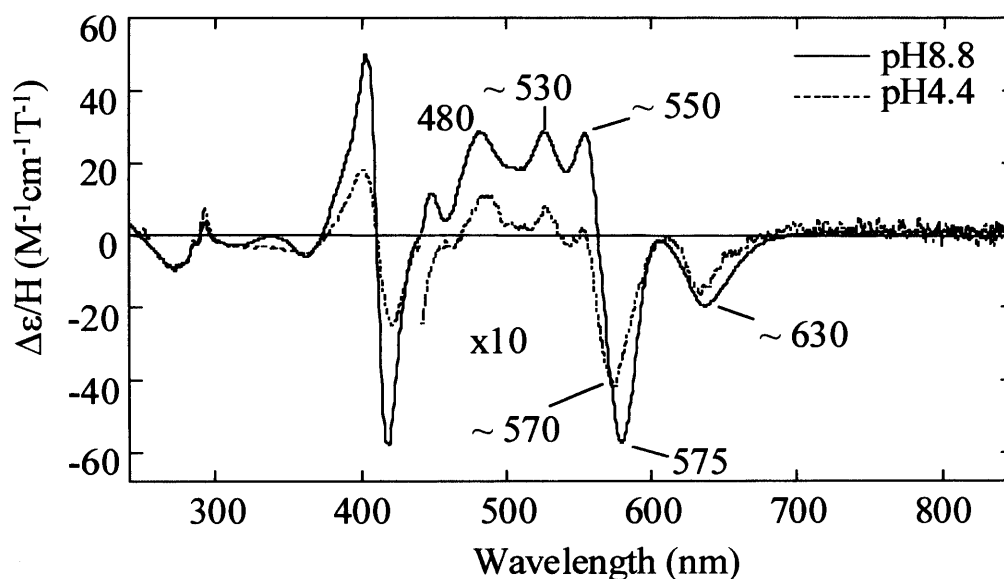


**Figure 5.10.** UV-visible MCD spectrum of His61Arg recorded at room temperature, using a magnetic field of 6 T.

### 5.3.7 Electronic Paramagnetic Resonance (EPR) Spectroscopy

#### 5.3.7.1 His61Lys

The EPR spectrum of His61Lys, Figure 5.11, exhibited the expected low-spin transitions (low-spin transitions are usually centred in the regions  $g = 2.5 - 3.7$  ( $g_z$ ),  $2.0 - 2.5$  ( $g_y$ ) and  $1.2 - 1.9$  ( $g_x$ )) with  $g_z = 3.3$ ,  $2.92$ ,  $2.76$   $g_y = 2.24$  and  $g_x = 1.66$ , similar to those observed for histidine-lysine ligated haem proteins (in which lysine acts as the sixth ligand to the haem).<sup>[27, 30-32]</sup> In particular, the value of  $g_z$  ( $3.3$ ) for His61Lys falls towards the low-end of the range of  $g$ -values expected for a histidine-lysine ligated haem protein ( $g_z$   $3.3 - 3.5$ ),<sup>[33, 34]</sup> confirming haem ligation in the His61Lys variant. The low-spin  $g$ -values at  $2.2$  and  $1.67$  have also been tentatively assigned to histidine-lysine ligation. However, the EPR of His61Lys also provided some evidence for the presence of histidine-hydroxide coordinated haem (the  $g$ -value apparent at  $2.92$ , falls in the region for hydroxide bound haem) suggesting a mixture of haem species in His61Lys at low temperature.

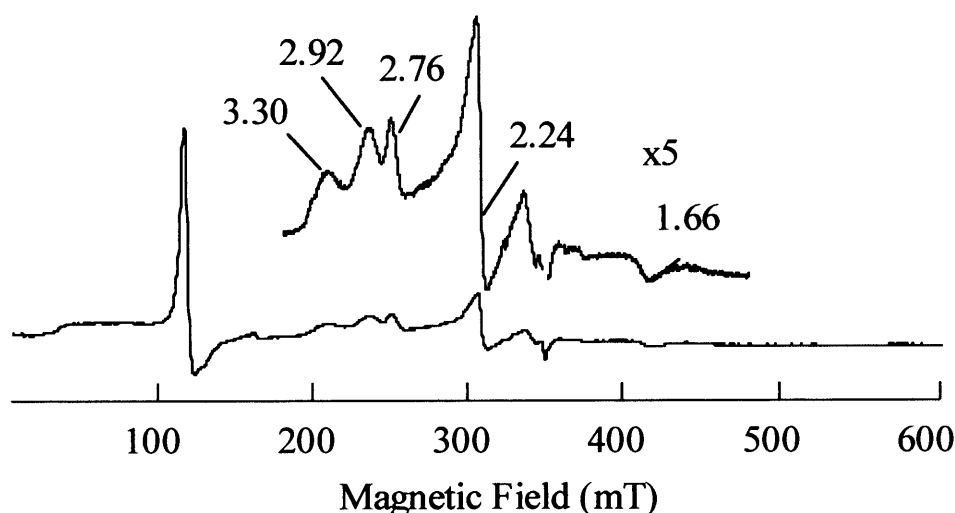


**Figure 5.11.** X-band EPR spectra of His61Lys (pH 7.0). The spectrum was recorded at 10 K using 1 mT modulation amplitude and 2.01 mW microwave power. The  $g$ -values are indicated.

### 5.3.7.2 His61Arg

The low temperature EPR spectrum (pH 7.0) of His61Arg, Figure 5.12, revealed predominantly low-spin signals ( $g_z = 3.3, 2.92, 2.78$  and  $2.68, g_y = 2.27$ ) indicative of *bis*-nitrogenous-ligated haem. High-spin signals were also apparent with  $g$ -values of  $\sim 6$  ( $g_z$ ) and  $1.92$  and  $1.87$  ( $g_x$ ) and were consistent with histidine-water-haem ligation. The EPR spectrum correlated well with the electronic absorption of His61Arg at pH 7.0, which also observed a mixture of high- and low-spin haem species.

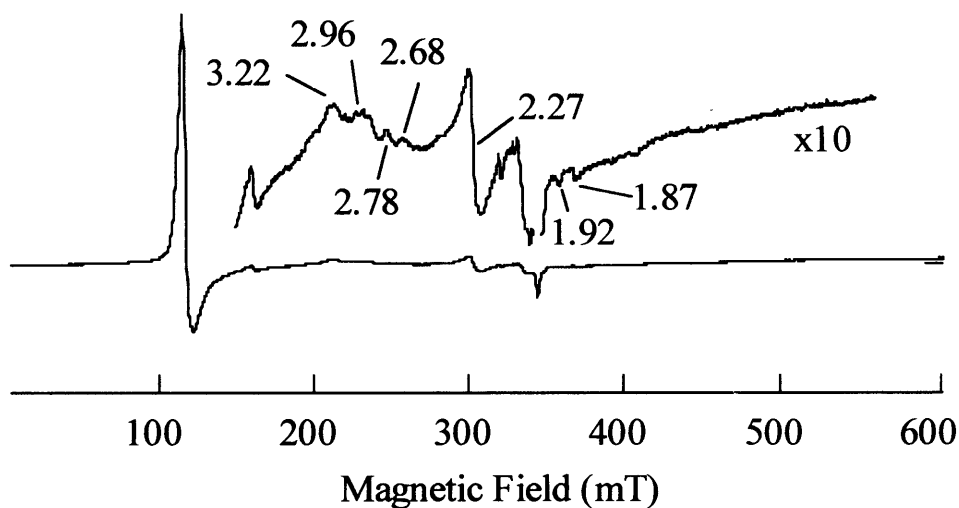


**Figure 5.12.** X-band EPR spectra of His61Arg (pH 7.0). The spectrum was recorded at 10 K using 1 mT modulation amplitude and 2.01 mW microwave power. The  $g$ -values are indicated.

## 5.4 Discussion

Axial ligand haem ligation in haem proteins has been known for some time to be vitally important in the functional and spectroscopic properties of the proteins.<sup>[1-19]</sup> A number of studies have been reported in which alteration of axial ligands using site-directed mutagenesis has been conducted within a variety of six-coordinate haem proteins<sup>[1-19]</sup> in an attempt to mimic properties of other haem proteins. In this work, a new approach to engineer haem axial ligation in haem proteins has been used. The unique conformational mobility displayed by histidine 61 in rLb has been exploited and substituted with lysine or arginine to generate two new six-coordinate, nitrogenous-ligated variants. Spectroscopic analyses of the two variants were carried out and the spectroscopic properties of the two variants, His61Lys and His61Arg, have been compared to rLb and other nitrogenous ligated haem proteins.

### 5.4.1 Spectroscopic Characterisation of His61Lys and His61Arg

Introduction of lysine or arginine in the active site of rLb substantially altered the spectroscopic characteristics of the protein in both the oxidised and reduced form. The predominant low-spin features observed for the ferric variants ( $\lambda_{\max}$  (His61Lys) = 408, 532 and 563 nm and  $\lambda_{\max}$  (His61Arg) = 407, 536 and 563 nm) and ferrous variants ( $\lambda_{\max}$  (His61Lys) = 423, 527 and 557 nm and (His61Arg) = 423, 526 and 556 nm) reflected this change and strongly suggested (six-coordinate) ligation of the nitrogenous residues to the haem iron in both oxidation states. This was in contrast to rLb which in the oxidised form exists as a mixture of high- (water-bound haem) and low-spin (histidine-bound haem).<sup>[25]</sup> In the reduced form rLb exists as a five-coordinate protein with a vacant sixth coordination site. The spectroscopic properties of His61Lys in both the oxidised and reduced form closely resembled those of the methylamine derivative of rLb ( $\lambda_{\max(\text{oxidised})}$  = 410, 537 and 570 nm and  $\lambda_{\max(\text{reduced})}$  = 419, 527 and 555 nm) providing evidence that the sixth coordination position to the haem iron of His61Lys is likely to be occupied by the  $\epsilon$ -amino group of lysine 61. Similarities between the low-spin transitions evident in His61Lys and those observed for ferric and ferrous 'alkaline' cytochrome *c* ( $\lambda_{\max(\text{oxidised})}$  = 406, 529 and 536 nm and  $\lambda_{\max(\text{reduced})}$  = 415, 520 and 550 nm) (this work), which has been established to have lysine-haem ligation, further support the haem-lysine assignment for His61Lys. Table 5.3 lists the spectroscopic data for some haem proteins in which the distal haem ligation is provided by a lysine residue.

**Table 5.3.**

Summary of spectroscopic data for haem proteins and variants in which the distal ligand to the haem is provided by a lysine.

<b>Protein</b>	<b>Source</b>	<b>Variant</b>	<b>Axial ligation</b>	<b>Spectroscopic information</b>	<b>Reference</b>
<b>Alkaline cytochrome <i>c</i></b>	Horse heart		Lys79 or Lys 72	EPR MCD	[27, 35]
<b>Alkaline Iso-1-ferricytochrome <i>c</i></b>	Yeast		Lys79 or Lys 73	Electrochem	[36]
	Yeast		Lys79 or Lys 73	NMR	[21, 37]
				EPR Electrochem RR	[37] [38]
<b>Alkaline ferricytochrome <i>c</i></b>	Mitochondrial		Lys79 or Lys 72		[39]
<b>Alkaline cytochrome <i>c</i><sub>550</sub></b>			Lys 84 or 97 or 103?	NMR	[40]
<b>Cytochrome <i>c</i><sub>550</sub></b>	Pracoccus versutus (Thiobaulus versutus)	Met100Lys	Lys100	NMR Electronic EPR Cyclic Voltammetry	[41] [42]
<b>Cytochrome <i>f</i></b>	Turnip		Lys145?	RR	[43] [44]
	Charlock		Lys145?	NMR	[32]
	Rape		Lys145?	EPR	
	Woad		Lys145?	MCD	
	Spinach		Lys145?	EPR Electronic MCD	[30]
<b>Alkaline Cytochrome <i>b</i><sub>562</sub></b>			Lys11 or 12?	Electronic	[45]
<b>P450II<sub>C2</sub></b>		Thr301Lys	Lys301	Electronic	[46]
<b>Myoglobin</b>		His64Lys	Lys64	EPR	[47]

Similar observations were observed for the His61Arg variant where the guanidium group of arginine is thought to occupy the sixth position to the haem in both oxidised and reduced states. Hence, the six-coordinate, low-spin transitions observed for His61Arg were assigned to arginine coordinated haem. Some high-spin haem apparent in His61Arg ( $\lambda_{\max} = 633$  nm) was assigned to water-bound haem as for rLb. The low-spin spectrum of His61Arg has been similarly observed for the His64Arg variant of myoglobin,<sup>[48]</sup> however, ligation of the arginine was not established with confidence. The low-spin features were assumed to arise either from the ligation of the arginine residue to the haem or formation of a hydrogen bond between arginine and a haem-bound water or hydroxide ion increasing the field strength sufficiently to produce the low-spin state.<sup>[49]</sup>

EXAFS analysis of the His61Lys and His61Arg haem coordination also suggested ligation of a nitrogenous group to the haem iron at both room and cryogenic temperature. An increase in the short bond length by  $\sim 10$  pm was assigned to the Fe-N ligation and was distinct from the Fe-O<sub>H<sub>2</sub>O</sub> bond length in rLb, strongly supporting this assignment. The variants did not display a temperature-dependent ligand switch as observed for rLb, reflected in the slight change in the Debye-Waller factor at room and cryogenic temperature. This work presents the first reported determination of the Fe-N<sub>Lys</sub> (202 pm) and 'Fe-N<sub>Arg</sub>' (200 pm) bond lengths in rLb and haem-globin family of proteins. Similar Fe-N distances have been observed for Lb (Fe-N<sub>Nicotinate</sub> = 209 pm)<sup>[50]</sup> and *Wolinella Succinogenes* nitrite reductase (proximal Fe-N<sub>Lys</sub> ligation = 210 pm)<sup>[51]</sup> strongly indicating nitrogenous ligation to the haem iron as a result of the His61Lys and His61Arg mutations in rLb.

Substitution of the distal histidine 61 with lysine resulted in a destabilisation (52 mV) of the reduced form. The negative mid-point potential observed is characteristic of the coordination of a basic residue to the haem iron and is a result of the better electron donating ability of the amine nitrogen than water therefore lowering the mid-point potential and stabilising the ferric oxidation state of the haem. In contrast, a slight increase of the mid-point potential (8 mV) was observed by introducing arginine to the haem (His61Arg). This determination was surprising and cannot be explained in terms of electron donating ability of the guanidium nitrogen, since arginine is a more basic residue than lysine or water and should serve as a better electron donor, leading to a greater decrease in mid-point potential of the protein than observed for His61Lys. The similarity in the mid-point potentials of rLb and His61Arg suggests that the haem ligation of the arginine has marginal effect on the stability of the ferrous oxidation state of the protein.

A possible rationalisation for this observation can be provided in terms of ligand field similarities between rLb and His61Arg. As previously suggested for the His18Arg variant of cytochrome *c*<sup>[52, 53]</sup> and argued by Martin,<sup>[54]</sup> arginine has an  $sp^2$  nitrogen that could coordinate to the haem iron by assuming a torsional geometry similar to that of histidine 61 in rLb, Figure 5.13. Since the mid-point potential of rLb has been partially attributed to His61 haem ligation (Chapter 3), replacing His61 with arginine may give rise to only slight conformational distortions of the active site structure and still provide ligand field similar to that of rLb.

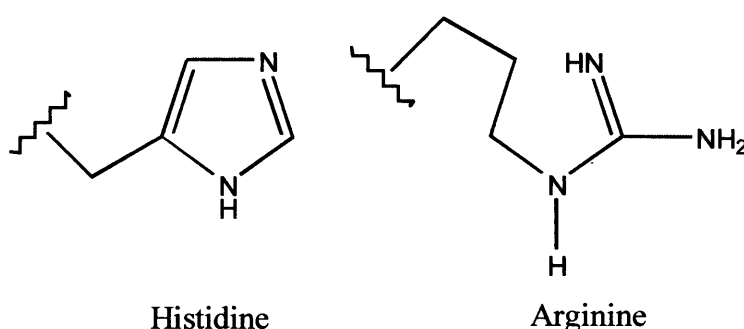


**Figure 5.13.** A comparison of torsional geometries of histidine and arginine

In addition, if the arginine ligates in the conformation as depicted in Figure 5.13, then the exposure of the haem to surrounding solvent would be marginally less than rLb and would be considerably less than His61Lys. As a consequence, an increase in mid-point potential would be observed. The greater hydrophobicity of the arginine relative to lysine could also rationalise the positive mid-point potential observed for His61Arg, as proposed by Kassner.<sup>[55]</sup> Hence, the greater the hydrophobic nature of haem environment, the greater the increase in the mid-point potential would be observed

These arguments, on their own are not able to fully rationalise the observed potential. Indeed, it is well known that there are a number other factors that effect mid-point potentials of haem proteins involving a complex combination of factors, *e.g.* the size<sup>[56]</sup> and polarity<sup>[55]</sup> of the amino acid side chains, as reflected by their volumes and hydrophobicities and the energetics of the protein structures should also be considered. At present, a fully quantitative assessment of the individual contribution of each variable is not experimentally viable using mutagenesis alone and the absence of suitably sophisticated theoretical and predictive models

makes a fully quantitative rationalisation of these experimental observations very difficult.

Occupation of the sixth coordination haem site with lysine and arginine in the His61Lys and His61Arg variants, respectively, was also observed to interfere with the proteins ability to bind exogenous ligands effectively. A decrease in binding affinity for cyanide by  $\sim 100$ -fold and  $\sim 70$ -fold was observed for His61Lys and His61Arg, respectively. However, significant differences in cyanide affinity for the two variants were observed at acidic pH. A  $\sim 40$ -fold increase in affinity for cyanide was observed for His61Lys in comparison to that at neutral pH. Under these conditions the His61Lys variant is believed to exist in a form in which the lysine no longer occupies the sixth coordination position, since loss of the low-spin transitions ( $\lambda_{\text{max}}$  532 and 562 nm), characteristic of low-spin haem, are observed and only high-spin transitions are apparent ( $\lambda_{\text{max}}$  497 (sh), 520 and 630 nm). Therefore the ease with which cyanide binds to the haem is reflected in a decrease in the equilibrium dissociation constant. In contrast to ligand affinity displayed by His61Lys, the His61Arg variant exhibited a similar affinity for cyanide at acidic pH ( $K_d = 75 \mu\text{M}$ ) as at neutral pH ( $K_d = 83 \mu\text{M}$ ). This may suggest that there is ligation of arginine at the haem iron at both pH values and therefore, under these conditions the arginine is believed to remain the sixth ligand to the haem in the His61Arg variant and interferes with exogenous ligand binding. These ligation changes were reflected in the pH dependent study.

Analysis of the electronic absorption spectra as a function of pH for His61Lys revealed a titration process with a  $\text{p}K_a$  of 5.7 which was attributed to the titration of the lysine 61. The  $\epsilon$ -amino group of free lysine has a  $\text{p}K_a$  of 10.0.<sup>[57]</sup> Hence, for the lysine to serve as a ligand to the haem iron it must be in the deprotonated state, even at pH 7. This would require a considerable shift of the  $\text{p}K_a$  of the lysine group serving as the sixth ligand. One factor, which might produce such a shift, is the haem environment effect; placement of the lysine in a hydrophobic environment would stabilise the deprotonated state. The active site of rLb accommodates this hydrophobic environment and as a consequence is a possible factor in lowering the  $\text{p}K_a$  of the lysine residue. The presence of basic residues in the active site is also known to shift the  $\text{p}K_a$  of titrating residues. There are two main residues, lysine 57 and lysine 64, which are close to residue 61 and could additionally contribute to the lowering of  $\text{p}K_a$  of the titrating residue lysine. A similar drop in  $\text{p}K_a$  was observed for the titration of tyrosine in the His61Tyr variant, Chapter 4 ( $\text{p}K_a$  of free tyrosine = 10.5, proposed  $\text{p}K_a$  of His61Tyr = 4.6).

The change in the electronic absorption spectrum with decreasing pH indicated a

change in the haem coordination of His61Lys. At acidic pH, loss of the low-spin transitions were apparent and formation of a high-spin haem species was observed ( $\lambda_{\max} = 403, 497$  (sh), 510 and 630 nm). Wavelength maxima were similar to those of six-coordinate water-bound haem and accordingly it was thought that the sixth coordination site for the acidic form of His61Lys was no longer occupied by lysine 61 but by a water molecule. This assignment was supported by the loss of the low-spin transitions apparent for lysine-bound haem, ( $\lambda_{\max} = 408, 532$  and 563 nm) suggesting release of the distal lysine coordination from the haem iron and protonation of the  $\epsilon$ -amino group with a decrease in pH. After this transition, there were no obvious transitions associated with the deprotonation of the  $\epsilon$ -amine group when it is bound to the haem iron.

Analysis of the pH titration spectra of His61Arg revealed a change in ligand coordination of the variant with an increase in pH. Formation of a fully low-spin haem species was apparent with the transition occurring with a  $pK_a$  of 7.4 and was assigned to the titration of the arginine 61 residue. Similarly, as for the distal lysine in His61Lys, a drop in the  $pK_a$  was observed for the distal arginine ( $pK_a$  of free arginine = 12)<sup>[57]</sup> and can be explained in terms of the hydrophobicity of the active site environment and the presence of the two basic lysine residues near residue 61 which influence the shift in  $pK_a$  of arginine.

At pH 7 and below the His61Arg variant existed in a form in which it was majority low-spin, arginine-coordinated haem with some minor high-spin, water-bound haem. Above pH 7.4 the variant converted to a fully low-spin form in which arginine is believed to solely occupy the sixth position of the haem ( $\lambda_{\max} = 409, 536$  and 563 nm). Above pH 7.5, no significant changes were observed in the electronic absorption spectra indicating there was no change in the haem electronic structure. The distal haem axial ligand of His61Arg is presumed to be arginine 61 since a strong ligand field is needed to explain the low-spin species observed. An alternative possibility, as proposed for the His64Arg variant of Mb, is that the arginine residue hydrogen bonds to a haem-bound water or hydroxide ion increasing the field strength sufficiently to produce the low-spin state.<sup>[49]</sup> The possibility of the titration of the distal water molecule, as observed for rLb, was ruled out due to the difference in  $pK_a$  ( $pK_a = 8.4$ ) and wavelength maxima ( $\lambda_{\max} = 408.5, 539$  and 570 nm) of the resultant hydroxide-bound haem species.

Semi-quantitative assessment of the identity of the haem ligation in His61Lys and His61Arg was determined through the diagnostic pairing of MCD and EPR. For His61Lys, throughout the 450-600 nm region, only low-spin transitions were detected and dominated the

MCD spectra. These transitions were attributed to arising from the lysine 61 ligation to the haem, since considerable similarities to other lysine ligated haem proteins were observed.<sup>[27, 30-32]</sup> Only minority amounts (5%) of high-spin species were observed in the room temperature MCD spectrum, with a trough at 638 nm, which was assigned to water-bound haem. However, in the low temperature MCD spectrum no high-spin signals were observed, indicating fully low-spin species at low-temperature. In the near-IR MCD spectrum of His61Lys the transition observed at ~1600 nm (indicative of lysine/histidine haem ligation) also confirmed the lysine-haem ligation. This band (which is more intense in His61Lys) has been similarly observed for the minority low-spin species observed in the low temperature rLb<sup>[25]</sup> and His61Ala and gives a clue to the likely identity of the haem ligation in that low-spin species (Chapter 3).

In conjunction with the MCD, the EPR analysis also confirmed the presence of low-spin haem, characteristic  $g$ -values for the His61Lys variant were detected in the regions characteristic of low-spin transitions and in particular were very similar to other histidine-lysine ligated haem proteins. The value of  $g_z$  (3.3) for His61Lys falls towards the low-end of the range of  $g$ -values expected for a histidine-lysine ligated haem proteins ( $g_z$  3.3-3.5), Table 5.4, confirming haem ligation in the His61Lys variant. The  $g$ -values at 2.2 and 1.67 have also been assigned to histidine-lysine ligation of the haem iron (similarity to EPR of the M100K (form III) variant of cytochrome  $c_{550}$ ).<sup>[42]</sup> However, the EPR spectrum of His61Lys also provided some evidence for the presence of histidine-hydroxide coordinated haem, well known examples of which are provided by the alkaline forms of myoglobin and horseradish peroxidase ( $g_z$ -values of ~ 2.6 and ~ 2.9 respectively<sup>[58, 59]</sup>). For His61Lys a  $g$ -value at 2.92 falls in the region for hydroxide bound haem, suggesting a mixture of haem species in the variant at low temperature. The  $g$ -value observed at 2.92 in His61Lys has also been observed for the M100K variant of cytochrome  $c_{550}$  ( $g_z = 2.93$ ), Table 5.4, and has been assigned and established as arising from lysine-haem ligation.<sup>[42]</sup> Hence, the peak at 2.92 in the EPR spectrum of His61Lys has also been assigned as arising from histidine-lysine haem ligation.

The high similarity between the MCD and, more particularly, the EPR data of His61Lys to that of other well-established lysine ligated haem proteins, strongly suggested that the axial ligands in the proteins are identical. The similarity of the MCD and EPR spectrum of His61Lys to that of the butylamine derivative of Lb provided further confirmation for the assignment.

**Table 5.4.**

EPR and Near-IR-MCD properties of Lys/His liganded low-spin ferric haems.

Hemoprotein	EPR $g_z$ -values	Wavelength ( $\lambda$ ) and intensity ( $\Delta\epsilon$ ) of the NIR-CT MCD band. <sup>a</sup>		Reference
		$\lambda_{\text{NIR-CT}} / \text{nm}$	$\Delta\epsilon / \text{M}^{-1} \text{cm}^{-1}$	
Cytochrome <i>c</i> ,				
yeast iso-1 pH 12.3	3.36, 2.06, -	1464	-	[31]
tuna yeast iso-2	3.38, 2.05	1480	430	[27]
horse heart pH 11.0	3.33, 2.05, [1.13] 3.5, -, 1.81			
Cytochrome <i>c</i> <sub>550</sub> M100K				
I	3.53, 1.69, 0.82	-		[42]
II	3.30, 2.00, 1.18	-		
III	2.93, 2.23, 1.67	-		
cytochrome <i>f</i>				[32]
rape	3.51, -, - 3.55, -, 1.7	1520	675	[30] [31]
spinach	3.48, 2.07, -	-	-	
spinach	3.53, -, - 3.06, -, -	1506	-	
Soybean leghemoglobin + n-butylamine	3.38, 2.05, -	1550	330	[27]

For His61Arg the identity of haem ligation using MCD and EPR was difficult since there were no histidine-arginine haem proteins to correlate to and the changes in the MCD spectra of His61Arg recorded at the different pH were more difficult to rationalise. At acidic pH, the MCD spectrum of His61Arg revealed that the variant existed in a mixture of high- and low-spin states and was in agreement with the electronic absorption spectrum of the variant at pH 4.8. The high-spin species was assigned to water-bound haem as indicative from the transition at  $\sim 630$  nm. The low-spin signals were tentatively assigned to arising from arginine-haem ligation. At alkaline pH (pH 8.8) the low-spin signals became more apparent

<sup>a</sup> Values refer to data recorded at 4.2 K using 5 T magnetic field except where brackets denote room temperature measurements for which  $\Delta\epsilon$  is expressed in units of  $\text{M}^{-1} \text{cm}^{-1} \text{T}^{-1}$ .

and dominated the MCD spectrum and were in agreement with the electronic absorption spectrum of His61Arg at pH 8.8. In contrast, high-spin signals were also apparent in the MCD spectrum (480 and 638 nm) which were not detected in the electronic absorption spectrum of the variant. The transition at 638 nm corresponded to water-bound haem, however at this pH the water would be expected to be in the hydroxide form. Hence the assignment for this transition was ambiguous. In addition, the increase in pH resulted in an increase of the Soret intensity and corresponded to a change of  $\sim 1/3$  low-spin at acidic pH to  $2/3$  low-spin at alkaline pH in the His61Arg variant. However, the rest of the spectrum did not change accordingly (a decrease of the high-spin signals would have been expected) which was quite peculiar and made rationalisation of data very difficult. A preliminary near-IR MCD spectrum of His61Arg at neutral pH (data not available) detected a band at  $\sim 1600$  nm indicative of *bis*-nitrogenous haem ligation, suggesting arginine haem ligation. However, a similar band has been previously observed for His61Lys (intense band), rLb<sup>[25]</sup> and His61Ala (Chapter 3) (minority low-spin species) and could therefore arise from the low-spin species which is believed to result from lysine-haem coordination.

The EPR spectrum of His61Arg (pH 7.0) was seen to be in a mixture of high- and low-spin states. The *g*-value at  $\sim 6$  and 1.92 and 1.87 corresponded well with high-spin, water-bound haem and was assigned accordingly. The low-spin *g*-values (*g<sub>z</sub>*) 3.22, 2.96, 2.78 and 2.68 and (*g<sub>y</sub>*) 2.27 indicated *bis*-nitrogenous haem ligation, likely histidine-arginine as indicative from other spectroscopic data. However, the *g*-values also correlated to His61Lys and the minor low-spin species in rLb<sup>[25]</sup> and His61Ala (Chapter 3), thereby making definitive assignment difficult.

## 5.5 Summary

In summary, mutagenic replacement of the mobile distal histidine 61 residue, in rLb, with lysine and arginine has resulted in altered axial ligation of the rLb protein. Spectroscopic characterisation of the His61Lys variant revealed considerable similarities to alkaline cytochrome *c* and cytochrome *f*, for which lysine haem coordination has been well established, and also to the butylamine derivative of Lb, confirming lysine-haem coordination in His61Lys. In addition, the MCD and EPR data had also confirmed histidine-lysine ligation and spectra were similar to those of other histidine-lysine ligated haem proteins. As a result of the ligation, the ligand binding affinities were decreased and a drop in the mid-point potential was observed, consistent with the ligation of a basic residue to the haem iron. EXAFS analysis carried out on the variant also indicated nitrogenous-haem ligation and reports the first determination of the Fe-N<sub>Lys</sub> bond length.

Spectroscopic characterisation of His61Arg also suggested alteration in haem ligation as a result of the mutation. A similar decrease in ligand binding affinities were observed for His61Arg, as for His61Lys. In contrast, a marginal increase in the mid-point potential was observed as a result of the mutation. EXAFS analysis carried out on the variant also suggested nitrogenous-haem ligation and accordingly the bond length determined was assigned to Fe-N<sub>Arg</sub>. All data suggested *bis*-nitrogenous haem ligation, likely histidine and arginine, in the variant. However, only a tentative assignment for arginine-haem ligation could be made in light of uncertainties in assignments from the MCD and EPR data.

## 5.6 References

1. J. H. Dawson, *Science* (1988) **240**, 433.
2. P. R. Ortiz de Montellano, *Acc. Chem. Res.* (1987) **20**, 289.
3. Y. Liu, P. Moënné-Loccoz, D. P. Hildebrand, A. Wilks, T. M. Loehr, A. G. Mauk and P. R. Ortiz de Montellano, *Biochemistry* (1991) **38**, 3733.
4. K. L. Bren and H. B. Gray, *J. Am. Chem. Soc.* (1993) **115**, 10382.
5. J. A. Sigman, A. E. Pond, J. H. Dawson and Y. Lu, *Biochemistry* (1999) **38**, 11122.
6. D. P. Hildebrand, D. L. Burk, R. Maurus, J. C. Ferrer, G. D. Brayer and A. G. Mauk, *Biochemistry* (1995) **34**, 1997.
7. D. P. Hildebrand, J. C. Ferrer, H.-L. Tang, M. Smith and A. G. Mauk, *Biochemistry* (1995) **34**, 11598.
8. E. Lloyd, D. P. Hildebrand, K. M. Tu and A. G. Mauk, *J. Am. Chem. Soc.* (1995) **117**, 6434.
9. R. Maurus, R. Bogumil, Y. Luo, H.-L. Tang, M. Smith, A. G. Mauk and G. D. Brayer, *J. Biol. Chem.* (1994) **269**, 12606.
10. A. L. Raphael and H. B. Gray, *J. Am. Chem. Soc.* (1991) **113**, 1038.
11. K. Choudhury, M. Sundaramoorthy, J. M. Mauro and T. L. Poulos, *J. Biol. Chem.* (1992) **267**, 25656.
12. G. D. DePhillis, S. M. Decateur, D. Barrick and S. G. Boxer, *J. Am. Chem. Soc.* (1994) **116**, 6981.
13. D. Barrick, *Biochemistry* (1994) **33**, 6546.
14. T. K. Das, S. Franzen, A. Pond, J. H. Dawson and D. L. Rousseau, *Inorg. Chem.* (1999) **38**, 1952.
15. S. M. Decatur, K. L. Belcher, P. K. Rickert, S. Franzen and S. G. Boxer, *Biochemistry* (1999) **38**, 11086.
16. A. E. Pond, M. P. Roach, M. Sono, A. H. Rux, S. Franzen, R. Hu, M. R. Thomas, A. Wilks, Y. Dou, M. Ikeda-Saito, P. R. Ortiz de Montellano, W. H. Woodruff, S. G. Boxer and J. H. Dawson, *Biochemistry* (1999) **38**, 7601.
17. S. Pin, B. Alpert, R. Cortes, I. Ascone, M. L. Chiu and S. G. Sligar, *Biochemistry* (1994) **33**, 11618.
18. J. Hirst, S. K. Wilcox, P. A. Williams, J. Blankenship, D. E. McRee and D. B. Goodin, *Biochemistry* (2001) **40**, 1265.

19. Y. Lu, S. M. Berry and T. D. Pfister, *Chem. Rev.* (2001) **101**, 3047.
20. F. I. Rosell, J. C. Ferrer and A. G. Mauk, *J. Am. Chem. Soc.* (1998) **120**, 11234.
21. J. C. Ferrer, J. G. Guillemette, R. Bogumil, S. C. Inglis, M. Smith and A. G. Mauk, *J. Am. Chem. Soc.* (1993) **115**, 7507.
22. O. Einsle, A. Messerschmidt, P. Stach, G. P. Bourenkov, H. D. Bartunik, R. Huber and P. M. H. Kroneck, *Nature* (1999) **400**, 476.
23. S. E. Martinez, D. Huang, A. Szezepaniak, W. A. Cramer and J. L. Smith, *Structure* (1994) **2**, 95.
24. W. Lanzilotta, D. J. Schuller, M. V. Thorsteinsson, R. L. Kerby, G. P. Roberts and T. L. Poulos, *Nature Struct. Biol.* (2000) **7**, 876.
25. D. K. Jones, R. Badii, F. I. Rosell and E. Lloyd, *Biochem. J.* (1998) **330**, 983.
26. N. Patel, D. K. Jones and E. L. Raven, *Eur. J. Biochem.* (2000) **267**, 2581.
27. P. A. Gadsby, J. Peterson, N. Foote, C. Greenwood and A. J. Thomson, *Biochem. J.* (1987) **246**, 43.
28. K. K. Ho and D. W. Krogman, *Plant. Physiol* (1978) **61s**, 76.
29. L. Vickery, T. Nozawa and K. Sauer, *J. Am. Chem. Soc.* (1976) **98**, 343.
30. J. N. Siedow, L. E. Vickory and G. Palmer, *Arch. Biochem. Biophys.* (1980) **203**, 101.
31. D. Simpkin, G. Palmer, F. J. Devlin, M. C. McKenna, G. M. Jensen and P. J. Stephens, *Biochemistry* (1989) **28**, 8033.
32. S. E. J. Rigby, G. R. Moore, J. C. Gray, P. M. A. Gadsby, S. J. George and A. J. Thomson, *Biochem. J.* (1988) **256**, 571.
33. D. L. Brautigan, B. A. Feinberg, B. M. Hoffman, E. Margoliash, J. Peisach and W. E. Blumberg, *J. Biol. Chem* (1977) **252**, 574.
34. W. E. Blumberg and J. Peisach, in *Probes of Structure and Function of Macromolecules and Membranes*, B. Chance, T. Yonetani, A. S. Mildvan, Eds. (Academic Press, New York) 1971, vol. 2, pp. 215.
35. I. Morishima, S. Ogawa, T. Yonezawa and T. Iizuka, *Biochim. Biophys. Acta* (1977) **495**, 287.
36. P. D. Barker and A. G. Mauk, *J. Am. Chem. Soc.* (1992) **114**, 3619.
37. F. I. Rosell, J. C. Ferrer and A. G. Mauk, *J. Am. Chem. Soc.* (1998) **120**, 11234.
38. S. Dopner, P. Hildebrandt, F. I. Rosell and A. G. Mauk, *J. Am. Chem. Soc.* (1998) **120**, 11246.
39. G. R. Moore and G. W. Pettigrew, in *Cytochromes c*, G. W. Ed., (Springer-Verlag, Berlin) 1990.

40. A. Lommon, A. Ratsma, N. Bylsma, G. W. Canters, J. E. van Wielink, J. Frank and J. van Beeumen, *Eur. J. Biochem.* (1990) **192**, 653.
41. R. O. Louro, E. C. de Waal, M. Ubbink and D. L. Turner, *FEBS Lett.* (2002) **510**, 185.
42. M. Ubbink, A. P. Campos, M. Teixeira, N. I. Hunt, H. A. O. Hill and G. W. Canters, *Biochemistry* (1994) **33**, 10051.
43. S. E. Martinez, D. Huang, A. Szczepaniak, W. A. Cramer and J. L. A. Smith, *Structure* (1994) **2**, 95.
44. D. L. Davies, M. K. Frame and D. A. Johnson, *Biochim. Biophys. Acta* (1988) **936**, 61.
45. Y. P. Myer and P. A. Bullock, *Biochemistry* (1978) **17**, 3723.
46. Y. Imai and M. Nakamura, *J. Biochem.* (1991) **110**, 884.
47. R. Bogumil, C. L. Hunter, R. Maurus, H.-L. Tang, H. Lee, E. Lloyd, G. D. Brayer, M. Smith and A. G. Mauk, *Biochemistry* (1994) **33**, 7600.
48. R. J. Rohlfs, A. J. Mathews, T. E. Carver, J. S. Lison, B. A. Springer, K. E. Egeberg and S. G. Sligar, *J. Biol. Chem.* (1990) **265**, 3168.
49. D. Morikis, P. M. Champion, B. A. Springer, K. D. Egeberg and S. G. Sligar, *J. Biol. Chem.* (1990) **265**, 12143.
50. P. J. Ellis, C. A. Appleby, J. M. Guss, W. N. Hunter, D. L. Ollis and H. C. Freeman, *Acta Crystallographica Section D* (1997) **53**, 302.
51. O. Einsle, P. Stach, A. Messerschmidt, J. Simon, A. Kroger, R. Huber and P. M. H. Kroneck, *J. Biol. Chem.* (2000) **275**, 39608.
52. L. L. Garcia, Z. Fredericks, T. N. Sorrell and G. J. Pielak, *New. J. Chem* (1992) **16**, 629.
53. T. N. Sorrell and P. K. Martin, *J. Am. Chem. Soc.* (1989) **111**, 766.
54. P. K. Martin, PhD Thesis, University of North Carolina (1989).
55. R. J. Kassner, *J. Am. Chem. Soc.* (1973) **95**, 2674.
56. E. Stellwagen, *Nature* (1978) **275**, 73.
57. L. Stryer, in *Biochemistry*, . (Freeman, New York) 1988, pp. 148.
58. F. R. N. Gurd, K. Falk, B. G. Malstrom and T. Vänngård, *J. Biol. Chem.* (1967) **242**, 5724.
59. M. Tamura and H. Hori, *Biochim. Biophys. Acta* (1972) **284**, 20.

**Chapter 6**  
**Introducing New Haem**  
**Functionality into**  
**Leghaemoglobin: A**  
**Functional Analysis of the**  
**Haem Oxygenase Reactivity**  
**of the His61Ala Variant.**

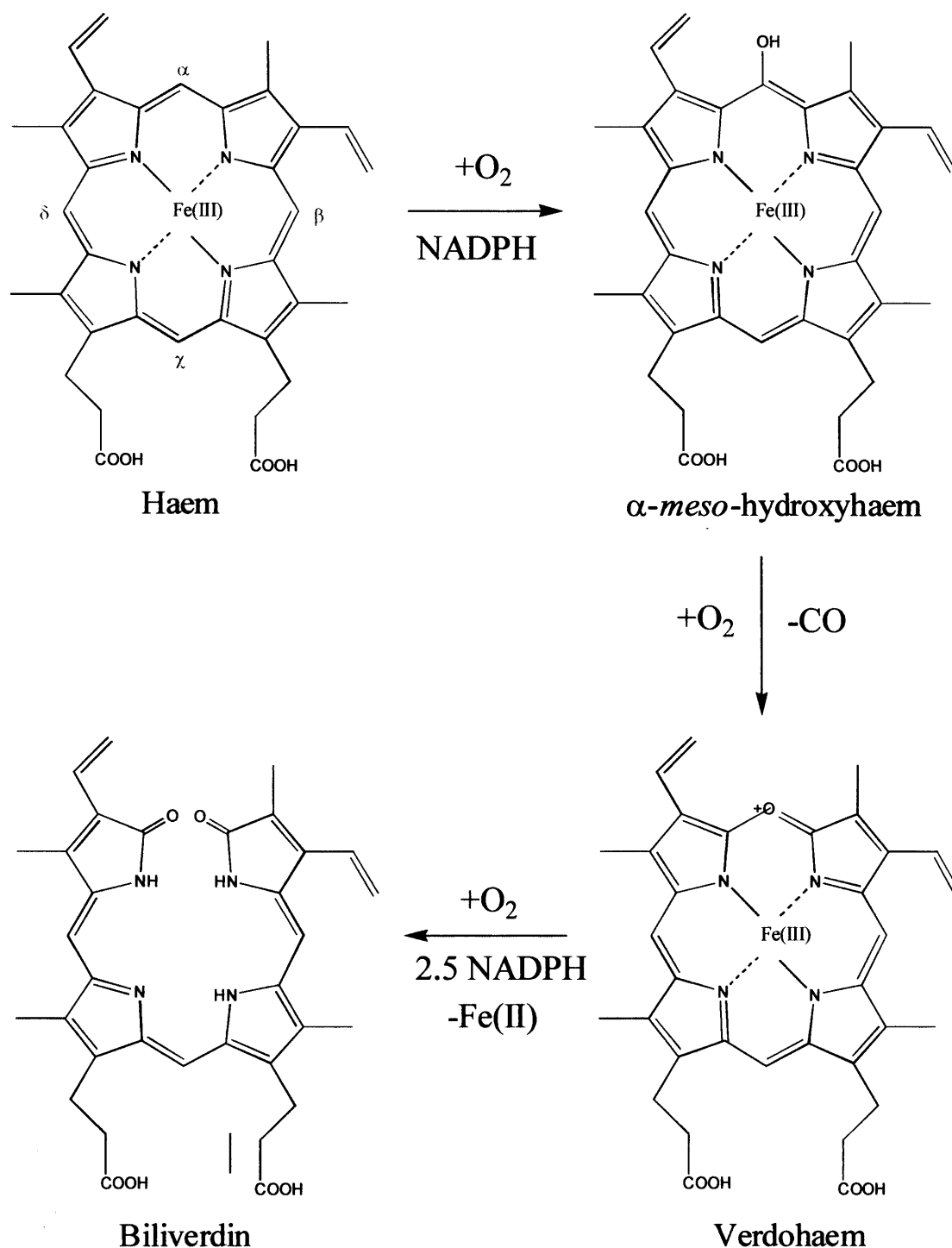
## **6 Introducing New Haem Functionality into Leghaemoglobin: A Functional Analysis of the Haem Oxygenase Reactivity of the His61Ala Variant.**

### **6.1 Introduction**

Oxidative degradation of haem is an important catabolic step in biology. The reaction is catalysed by the enzyme haem oxygenase (HO) in the presence of dioxygen and NADPH-dependent cytochrome P450 reductase<sup>[1-4]</sup> to generate biliverdin, iron and carbon monoxide, via the  $\alpha$ -meso hydroxyhaem and verdohaem intermediates Scheme 6.1.<sup>[2]</sup> The enzyme is unique in the sense that it employs haem as both the prosthetic group and substrate and is physiologically important because of the biologically active properties associated with the reaction products. The haem degradation product, biliverdin, is a precursor of the potent antioxidant bilirubin,<sup>[5]</sup> CO is thought to share some of the biological properties of NO in signal transduction and communication<sup>[6-8]</sup> and the free iron released by HO activity is known to regulate genes, including that of NO synthase.<sup>[3]</sup>

Haem oxygenase activity has been observed in several other haem proteins, including myoglobin (Mb)<sup>[9-12]</sup> and variants of cytochrome *b*<sub>5</sub><sup>[13, 14]</sup> and cytochrome *b*<sub>562</sub><sup>[15]</sup> upon their exposure to dioxygen and a reductant, such as ascorbate. This process has been termed coupled oxidation and has been used as a model for HO because it shares several features of HO reaction, including product formation and, in some cases, regioselectivity.<sup>[3, 16]</sup> However, important differences have been noted between HO and the proteins involved in the coupled oxidation process, including reaction rates, reductant requirements, haem binding affinities and regioselectivity.<sup>[16]</sup>

The work carried out in this Chapter demonstrates that on replacement of the distal histidine 61 (with alanine), new haem oxygenase activity is introduced into rLb. The resulting variant, His61Ala, is capable of performing the coupled oxidation of haem to Fe(III)-biliverdin as is observed for HO. The work carried out in this Chapter describes the coupled oxidation reaction of His61Ala, together with a kinetic and regiospecific analysis. A mechanism for the reaction is proposed, based on the intermediates and products identified during the haem degradation process. To our knowledge, this work reports the first variant of rLb that is capable of exhibiting haem oxygenase activity.



**Scheme 6.1.** The reaction sequence catalysed by haem oxygenase. The sequence is shown as occurring in three steps separated by two well-defined intermediates,  $\alpha$ -meso-hydroxyhaem and verdohaem. The final products of the reaction are CO, biliverdin and free iron.[2]

## 6.2 Results

### 6.2.1 Aerobic Coupled Oxidation of His61Ala.

The time-dependent oxidation of haem, following aerobic addition of ascorbate to the His61Ala variant, was monitored spectrophotometrically (270-800 nm), Figure 6.1. On the basis of these spectroscopic changes, the reaction appeared to be biphasic. A rapid decrease of the absorbance at the Soret maxima and a shift of this band, from 402.5 nm to 411 nm, with concomitant increase of the  $\alpha$  and  $\beta$  bands ( $\lambda_{\max} = 574$  and  $537$  nm), was observed in the initial phase, generating a transient intermediate that was spectroscopically similar to Fe(II)-O<sub>2</sub> His61Ala ( $\lambda_{\max} = 411, 540$  and  $575$  nm), Figure 6.2. In the second phase, the Fe(II)-O<sub>2</sub> intermediate was transformed into a reaction product (end product) ( $\lambda_{\max} = 414, 526, 566, \sim 640$  (broad) and  $\sim 700$  (broad) nm) that had spectroscopic features similar to those of Fe(III)-biliverdin, notable by the broad band at  $\sim 700$  nm.<sup>[12, 17, 18]</sup> This was observed through bleaching of the Soret band and a decrease of the  $\alpha$  and  $\beta$  bands, indicating the disappearance of the Fe(II)-O<sub>2</sub> species (411 nm). A broad feature at  $\sim 640$  nm was also apparent, and persisted throughout the reaction, which may be attributable to one of the intermediates, verdohaem, a well-established intermediate of the haem oxygenase and coupled oxidation reaction.<sup>[19]</sup>

On the basis of time-dependent absorbance changes at 402.5nm, the kinetics of the coupled oxidation reaction of His61Ala can be described as a double exponential process. A rate constant,  $k_1$ , of  $1.8 \pm 0.3 \times 10^{-2} \text{ min}^{-1}$  was determined for the formation of the first intermediate (Fe(III)  $\rightarrow$  Fe(II)-O<sub>2</sub>). For the second phase, a rate constant,  $k_2$ , of  $4.4 \pm 0.1 \times 10^{-3} \text{ min}^{-1}$  was determined, corresponding to the conversion of the Fe(II)-O<sub>2</sub> intermediate to the final product, Fe(III)-biliverdin (Fe(II)-O<sub>2</sub>  $\rightarrow$  Fe(III)-biliverdin), Figure 6.1 inset.

### 6.2.2 Aerobic Coupled Oxidation of rLb

The parallel coupled oxidation reaction of rLb (carried out as a control), Figure 6.3, proceeded through a single phase, with slow conversion of rLb ( $\lambda_{\max} = 403, 495, 530, 560$  and  $626$  nm) to a haem complex ( $\lambda_{\max} = 412, 541$  and  $574$  nm) with wavelength maxima identical to that of Fe(II)-O<sub>2</sub> rLb ( $\lambda_{\max} = 412, 541$  and  $574$  nm), Figure 6.2. Further incubation of the rLb with ascorbate revealed no further change in the electronic absorption spectrum and no

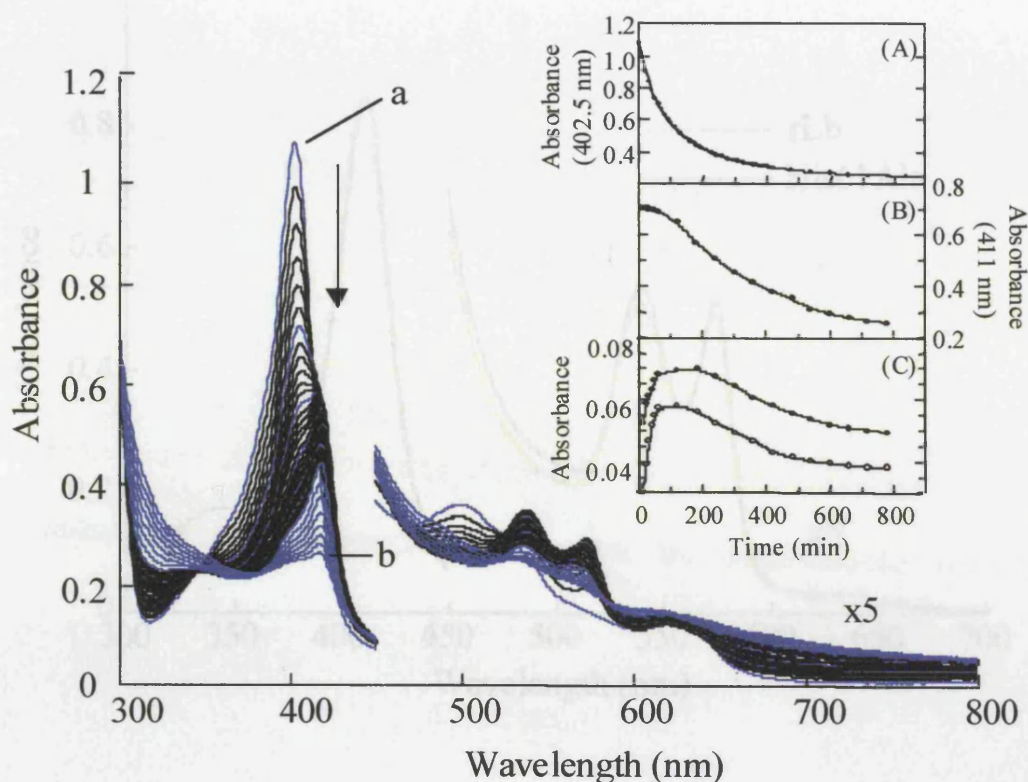


**Figure 6.1.** Changes in the electronic absorption spectrum during the coupled oxidation of His61Ala. Conditions: sodium phosphate buffer,  $\mu = 0.1$  M, pH 7.0, 32.0 °C, ascorbate (1.0 mM) and His61Ala (5  $\mu$ M). Black lines represent changes at 10 minute intervals and blue lines at 1 hour intervals. Inset: kinetic time traces for the coupled oxidation reaction of His61Ala following absorbance changes at (A) 402.5 nm, (B) 411 nm (decay of Fe(II)-O<sub>2</sub> species) and (C) 537 (●) and 574 nm (○) illustrating the formation and decay of the Fe(II)-O<sub>2</sub> species. (a) spectrum at the beginning of the reaction, (b) spectrum at the end of the reaction.

new reaction products were observed. The rate constant of conversion ( $k_1$ ), of the ferric haem to Fe(II)-O<sub>2</sub> haem was determined as  $2.3 \pm 0.1 \times 10^{-3} \text{ min}^{-1}$ , Figure 6.3 inset. Hence, formation of the Fe(II)-O<sub>2</sub> species of rLb was  $\sim 10$ -fold slower than the formation of the Fe(II)-O<sub>2</sub> species of His61Ala.

### 6.2.3 Analysis of Haem Degradation Products

The nature and identity of the final reaction product from the coupled oxidation reaction of His61Ala and rLb were examined by extraction of the product into chloroform,

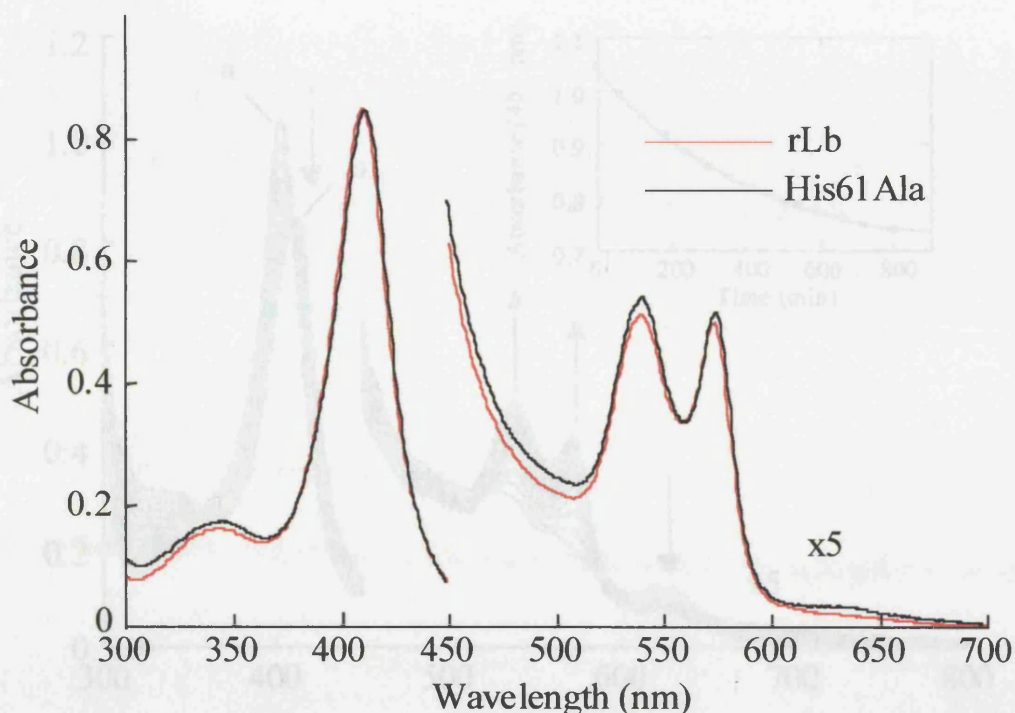


**Figure 6.2.** Electronic absorption spectra of Fe(II)-O<sub>2</sub> rLb and Fe(II)-O<sub>2</sub> His61Ala. Conditions: sodium phosphate buffer,  $\mu = 0.1$  M, pH 7.0, 25.0 °C.

after removal of the unreacted haem with ether, under acidic conditions (Chapter 7, Section 7.2.12.3). This process converts any Fe(III)-biliverdin to biliverdin. The electronic absorption spectrum of the chloroform extract of Fe(III)-biliverdin from the coupled oxidation of His61Ala, was identical to that obtained for authentic biliverdin, Figure 6.4, thereby demonstrating that His61Ala catalyses the coupled oxidation of haem to Fe(III)-biliverdin.

However, no biliverdin reaction product was observed for rLb, an indication that rLb was not able to perform the coupled oxidation reaction. High Performance Liquid Chromatography (HPLC) analysis of the chloroform extract of the His61Ala Fe(III)-biliverdin, Figure 6.5(A), exhibited a product with a retention time of 19 min, identical to that of authentic biliverdin obtained under identical conditions (19 min), Figure 6.5(B). Analysis of the rLb reaction product exhibited a retention time of 23 min, Figure 6.5(C), identical to that of unmodified haem, Figure 6.5(D), providing further evidence that rLb is unable to carry out the coupled oxidation reaction. Electrospray Ionisation Mass Spectrometry (ESI-MS) was employed to further confirm the identity of haem degradation products. Analysis of rLb and His61Ala, prior to addition of ascorbate, resulted in the observation of a peak at  $m/z = 616$ ,

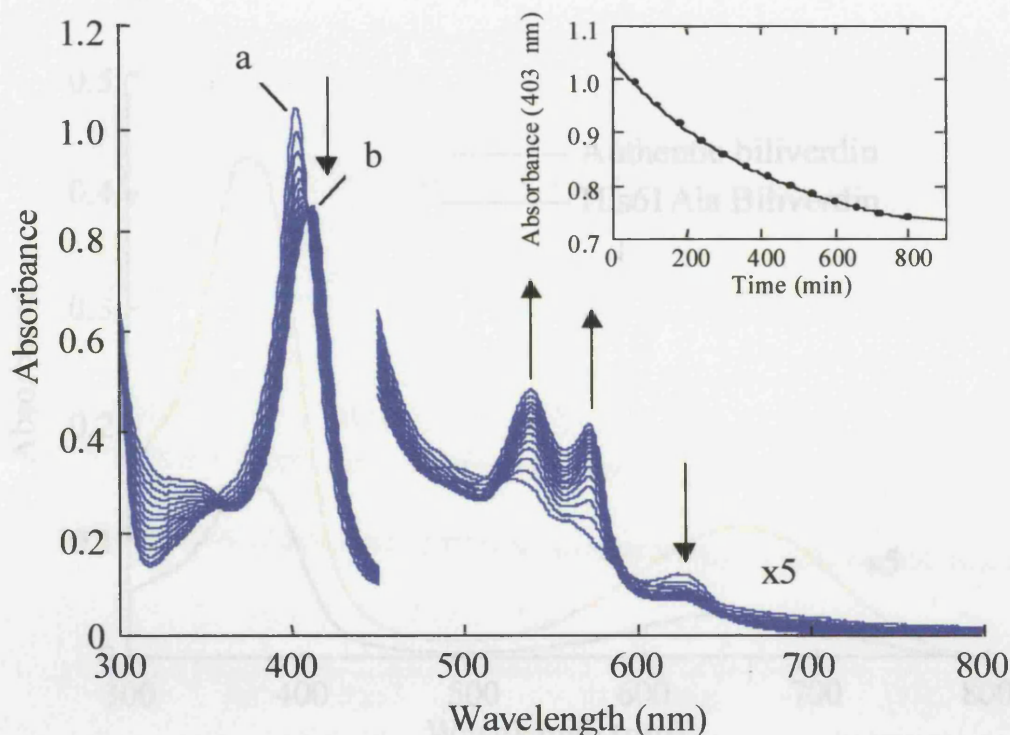


**Figure 6.3.** Changes in the electronic absorption spectrum (at 1 hour intervals) during the coupled oxidation of rLb (sodium phosphate buffer,  $\mu = 0.1$  M, pH. 7.0, 32.0 °C) containing ascorbate (1.0 mM) and rLb (5  $\mu$ M). Inset: kinetic time traces for the coupled oxidation reaction of rLb following absorbance changes at 403 nm. (a) spectrum at the beginning of the reaction, (b) spectrum at the end of the reaction.

for both proteins, corresponding to the unmodified haem, Figure 6.6(A). An identical spectrum was observed for rLb after the addition of ascorbate and allowing the coupled oxidation reaction to proceed for 14 hours, Figure 6.6(B), supporting the HPLC and electronic absorption analyses. However, the coupled oxidation reaction product of His61Ala (*i.e.* Fe(III)-biliverdin) displayed a spectrum with  $m/z = 635$ , Figure 6.6(C), corresponding to the molecular mass of Fe(III)-biliverdin, indicating that Fe(III)-biliverdin is formed, (some unmodified haem was also detected). The chloroform extract of the Fe(III)-biliverdin from the His61Ala coupled oxidation reaction (*i.e.* biliverdin) yielded a peak at  $m/z$  583, Figure 6.6(D), identical to that for authentic biliverdin and further supporting Fe(III)-biliverdin as the end product for His61Ala (since any Fe(III)-biliverdin formed is converted to biliverdin during acidification and chloroform extraction). Surprisingly, the verdohaem intermediate (broad peak at  $\sim 640$  nm) was not detected, an indication that the intermediate may have been short lived (very reactive).

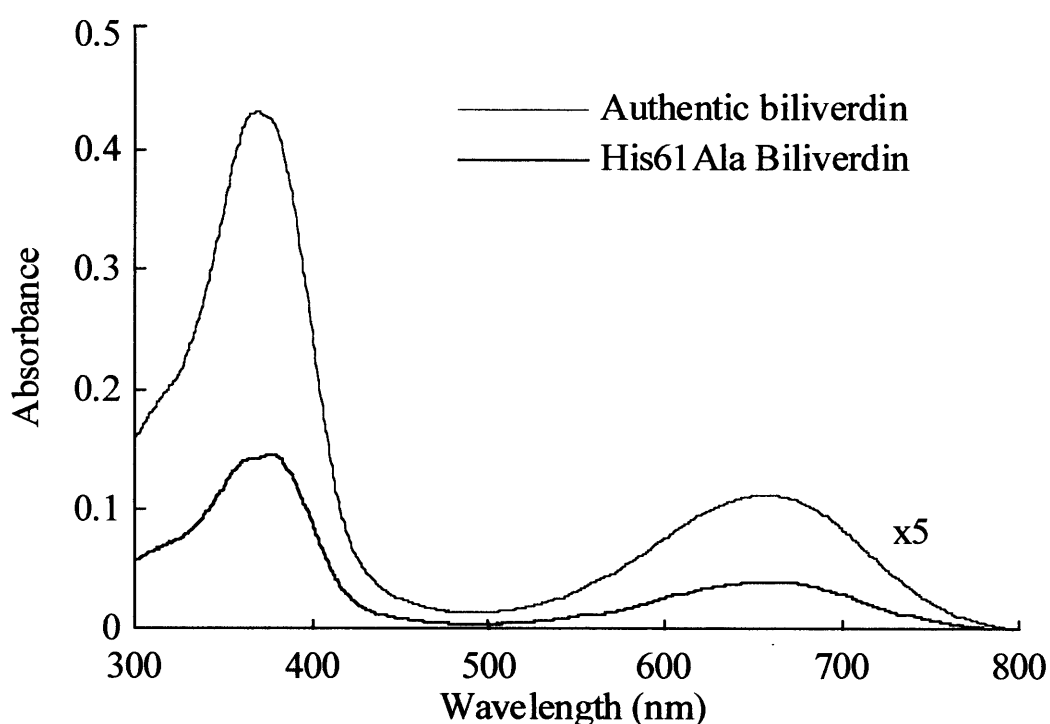


**Figure 6.4.** Electronic absorption spectrum of authentic biliverdin and the chloroform extracted biliverdin from coupled oxidation of His61Ala. Conditions: Chloroform, 25.0 °C.

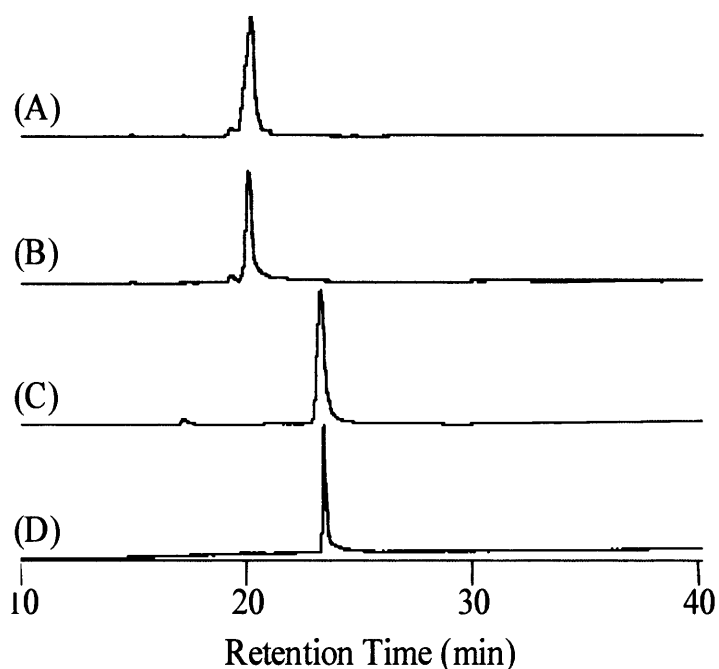


**Figure 6.5.** HPLC analysis of the product isolated from the coupled oxidation reaction of rLb and His61Ala. (A) biliverdin extracted from His61Ala; (B) authentic biliverdin; (C) reaction product from rLb and (D) unmodified haem. Conditions: ammonium phosphate/methanol buffer, 37 °C.

## 6.2.4 Dependence of Oxygen in the Coupled Oxidation Reaction

The importance of oxygen for the coupled oxidation, and hence the haem degradation process, was investigated by carrying out a series of reactions under anaerobic and limited oxygen conditions. Accordingly, the reaction was reproducible and a possible reaction mechanism or profile for the coupled oxidation of His61Ala could therefore be identified.

## 6.7.1 Anaerobic Coupled Oxidation of His61Ala

The coupled oxidation reaction of His61Ala carried out under anaerobic conditions produced a decrease and shift of the Soret band, at 402.5 nm to 414 nm, with a subsequent increase of the  $\alpha$  and  $\beta$  bands ( $\lambda_{max} = 573$  and 541 nm) (Figure 6.7B). The resulting spectrum was similar to that of the typical coupled oxidation product, which is normally observed with prolonged incubation of the reaction mixture under anaerobic conditions. The typical coupled oxidation product, however, is not observed under anaerobic conditions, an indication that oxygen is required for the coupled oxidation reaction.

The coupled oxidation reaction of His61Ala was carried out under anaerobic conditions with His61Ala and rLb were completely within 4 hours. Rate constants of  $1.4 \times 10^{-3} \text{ min}^{-1}$  and  $0.23 \times 10^{-3} \text{ min}^{-1}$  were determined for His61Ala and rLb, respectively. When the anaerobically prepared His61Ala and rLb reacted with  $\text{O}_2$  (the product) was exposed to oxygen, the Soret band shifted to 402.5 nm, indicating that the coupled oxidation changes were observed as for the aerobic reaction. For rLb, the reaction proceeded at the  $\text{Fe(II)-O}_2$  product, however, with His61Ala, the reaction proceeded with

**Figure 6.6.** ESI-MS analysis of product isolated from the coupled oxidation reaction of rLb and His61Ala. (A) unmodified haem; (B) reaction product from the coupled oxidation reaction of rLb; (C) Fe(III)-biliverdin from the coupled oxidation of His61Ala ( $m/z$  648 = MeOH adduct of haem) and (D) chloroform extracted biliverdin from the coupled oxidation of His61Ala.

The coupled oxidation reaction of His61Ala, identified Fe(II) as the product, was exposed to oxygen, the Soret band shifted to 402.5 nm, indicating that the coupled oxidation changes were observed as for the aerobic reaction. For rLb, the reaction proceeded at the  $\text{Fe(II)-O}_2$  product, however, with His61Ala, the reaction proceeded with

## 6.2.4 Dependence of Oxygen in the Coupled Oxidation Reaction

The importance of oxygen for the coupled oxidation, and hence, the haem degradation process, was investigated by carrying out a series of reactions under anaerobic and limited oxygen conditions. Accordingly, the reaction intermediates and a possible reaction mechanism or profile for the coupled oxidation of His61Ala could therefore be identified.

### 6.2.4.1 Anaerobic Coupled Oxidation of His61Ala and rLb

The coupled oxidation reaction of His61Ala carried out under anaerobic conditions showed a decrease and shift of the Soret maxima, at 402.5 nm to 414 nm, with a subsequent increase of the  $\alpha$  and  $\beta$  bands ( $\lambda_{\max} = 573$  and 541 nm), Figure, 6.7(A). The resulting spectrum closely resembled that reported of 'Lb(IV)' ( $\lambda_{\max} = 574$  and 543 nm), which is formed *in vivo*, in high ascorbate concentrations.<sup>[20, 21]</sup> No further spectroscopic changes or reactions were observed with prolonged incubation of the reaction mixture under anaerobic conditions. The typical coupled oxidation products and/or intermediates were not observed under anaerobic conditions, an indication that oxygen is essential for the coupled oxidation reaction. The analogous coupled oxidation of rLb under anaerobic conditions also showed a typical 'Lb(IV)-like' spectrum, Figure 6.7(B).

The time-dependent spectroscopic changes during the anaerobic reaction of ascorbate with His61Ala and rLb were complete within 4 hours. Rate constants of  $2.4 \pm 0.1 \times 10^{-3} \text{ min}^{-1}$  and  $2.3 \pm 0.1 \times 10^{-3} \text{ min}^{-1}$  were determined for His61Ala and rLb, respectively.

When the anaerobically generated His61Ala and rLb product ('Lb(IV)-like' product) was exposed to oxygen, the Soret peak underwent a further decrease in intensity and similar coupled oxidation changes were observed as for the aerobic reaction. For rLb, the reaction arrested at the Fe(II)-O<sub>2</sub> product, however, with His61Ala, the reaction proceeded with subsequent formation of Fe(III)-biliverdin, via the Fe(II)-O<sub>2</sub> intermediate as observed previously under aerobic conditions. Rate constants of  $k_1 = 2.1 \pm 0.3 \times 10^{-2} \text{ min}^{-1}$  and  $k_2 = 4.7 \pm 0.3 \times 10^{-3} \text{ min}^{-1}$ , were determined for the coupled oxidation reaction after exposure to oxygen and were similar to the rate constants determined for the aerobic reaction ( $k_1 = 1.8 \pm 0.3 \times 10^{-2} \text{ min}^{-1}$  and  $k_2 = 4.4 \pm 0.1 \times 10^{-3} \text{ min}^{-1}$ ). Electronic absorption, HPLC and ESI-MS analysis of the coupled oxidation product of His61Ala, identified Fe(III)-biliverdin as the end product which was converted to biliverdin after chloroform extraction, identical to that for the aerobic reaction .

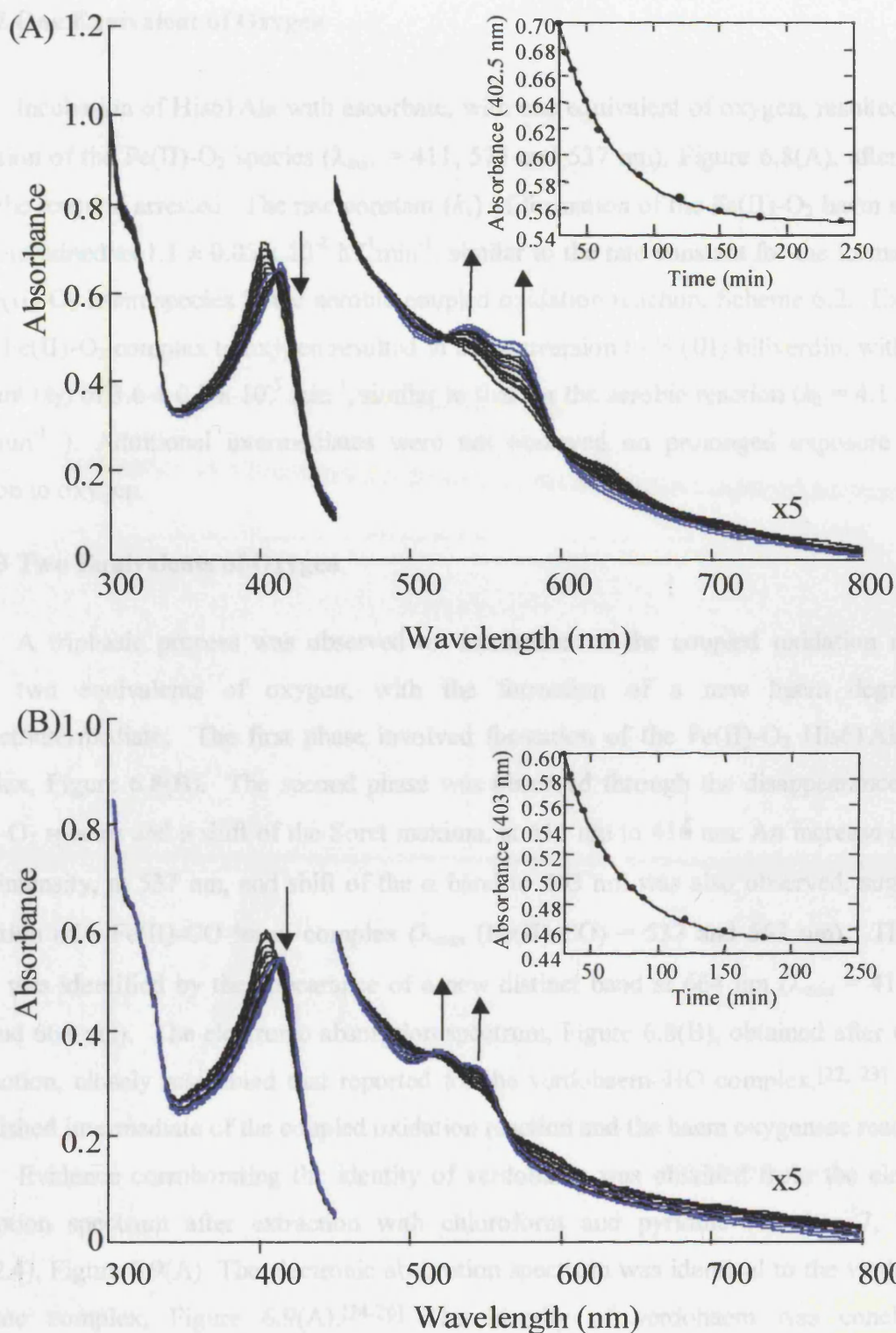


**Figure 6.7.** Changes in the electronic absorption spectrum during anaerobic coupled oxidation of (A) His61Ala and (B) rLb. Conditions: sodium phosphate buffer,  $\mu = 0.1$  M, pH. 7.0, 32.0 °C), ascorbate (1.0 mM) and protein (5 $\mu$ M). Black lines represent changes at 10 minute intervals and blue lines at 1 hour intervals. Inset: kinetic time traces for the anaerobic coupled oxidation reaction following absorbance changes at 402.5 nm for His61Ala and 403 nm for rLb.

#### 6.2.4.2 One Equivalent of Oxygen

Incubation of His61Ala with ascorbate, with one equivalent of oxygen, resulted in the formation of the Fe(II)-O<sub>2</sub> species ( $\lambda_{\max} = 411, 575$  and  $537$  nm), Figure 6.8(A), after which stage the reaction arrested. The rate constant ( $k_1$ ) of formation of the Fe(II)-O<sub>2</sub> haem species, was determined as  $1.1 \pm 0.05 \times 10^{-2} \text{ M}^{-1} \text{ min}^{-1}$ , similar to the rate constant for the formation of the Fe(II)-O<sub>2</sub> haem species in the aerobic coupled oxidation reaction, Scheme 6.2. Exposure of the Fe(II)-O<sub>2</sub> complex to oxygen resulted in the conversion to Fe(III)-biliverdin, with a rate constant ( $k_2$ ) of  $3.6 \pm 0.3 \times 10^{-3} \text{ min}^{-1}$ , similar to that for the aerobic reaction ( $k_2 = 4.1 \pm 0.1 \times 10^{-3} \text{ min}^{-1}$ ). Additional intermediates were not observed on prolonged exposure of the reaction to oxygen.

#### 6.2.4.3 Two Equivalents of Oxygen

A triphasic process was observed on incubation of the coupled oxidation reaction under two equivalents of oxygen, with the formation of a new haem degradation product/intermediate. The first phase involved formation of the Fe(II)-O<sub>2</sub> His61Ala haem complex, Figure 6.8(B). The second phase was observed through the disappearance of the Fe(II)-O<sub>2</sub> species and a shift of the Soret maxima, at 411 nm to 416 nm. An increase of the  $\beta$  band intensity, at 537 nm, and shift of the  $\alpha$  band to 563 nm was also observed, suggesting formation of a Fe(II)-CO haem complex ( $\lambda_{\max}(\text{Fe(II)-CO}) = 537$  and  $563$  nm). The third phase was identified by the appearance of a new distinct band at 664 nm ( $\lambda_{\max} = 416, 565, 537$  and  $664$  nm). The electronic absorption spectrum, Figure 6.8(B), obtained after 6 hours of reaction, closely resembled that reported for the verdohaem–HO complex,<sup>[22, 23]</sup> a well-established intermediate of the coupled oxidation reaction and the haem oxygenase reaction.

Evidence corroborating the identity of verdohaem was obtained from the electronic absorption spectrum after extraction with chloroform and pyridine (Chapter 7, Section 7.2.12.4), Figure 6.9(A). The electronic absorption spectrum was identical to the verdohaem-pyridine complex, Figure 6.9(A).<sup>[24-26]</sup> The identity of verdohaem was conclusively demonstrated by ESI-MS analysis. The verdohaem product was dialysed with NH<sub>4</sub>HCO<sub>3</sub> (40 mM) at 4 °C and mixed with ammonium acetate (10 mM) prior to mass spectral analysis, Chapter 7, Section 7.2.12.4. The mass spectrum displayed a peak at  $m/z = 619$ , Figure 6.9(B), consistent with the mass of verdohaem ( $m/z = 619$ ) (a minor signal with  $m/z = 616$  was also apparent and assigned to unmodified haem).

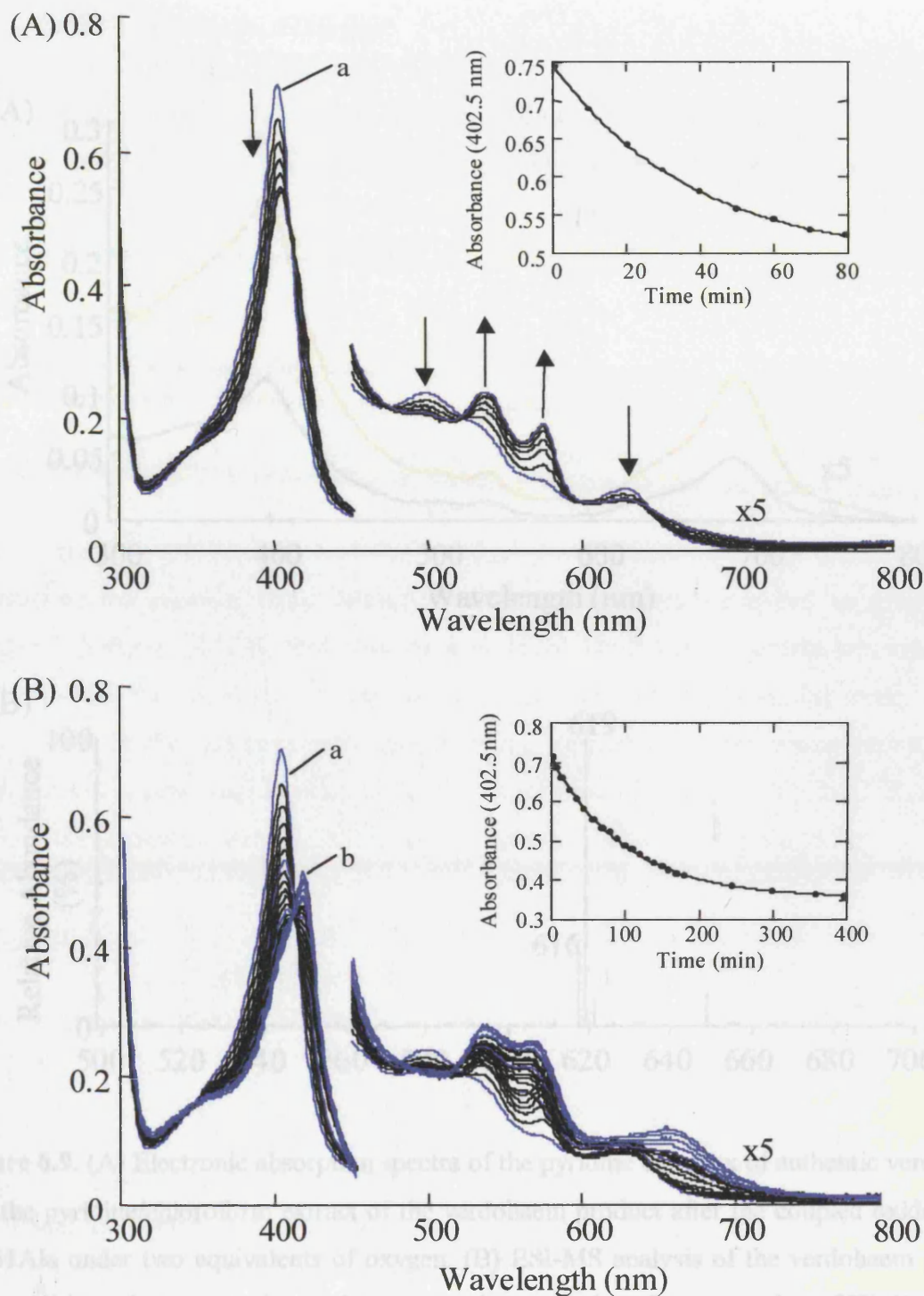


**Figure 6.8.** Changes in the electronic absorption spectrum during the coupled oxidation of His61Ala in the presence of (A) one equivalent and (B) two equivalents of oxygen. Conditions: sodium phosphate buffer,  $\mu = 0.1$  M, pH. 7.0, 32.0 °C, containing ascorbate (1.0 mM) and protein (5  $\mu$ M). Black lines represent changes at 10 minute intervals and blue lines at 1 hour intervals. Inset: kinetic time traces for the coupled oxidation reaction following absorbance changes at 402.5 nm. (a) spectrum at the beginning of the reaction, (b) spectrum at the end of the reaction.

## 6.2.4.4 Three Equivalents of Oxygen

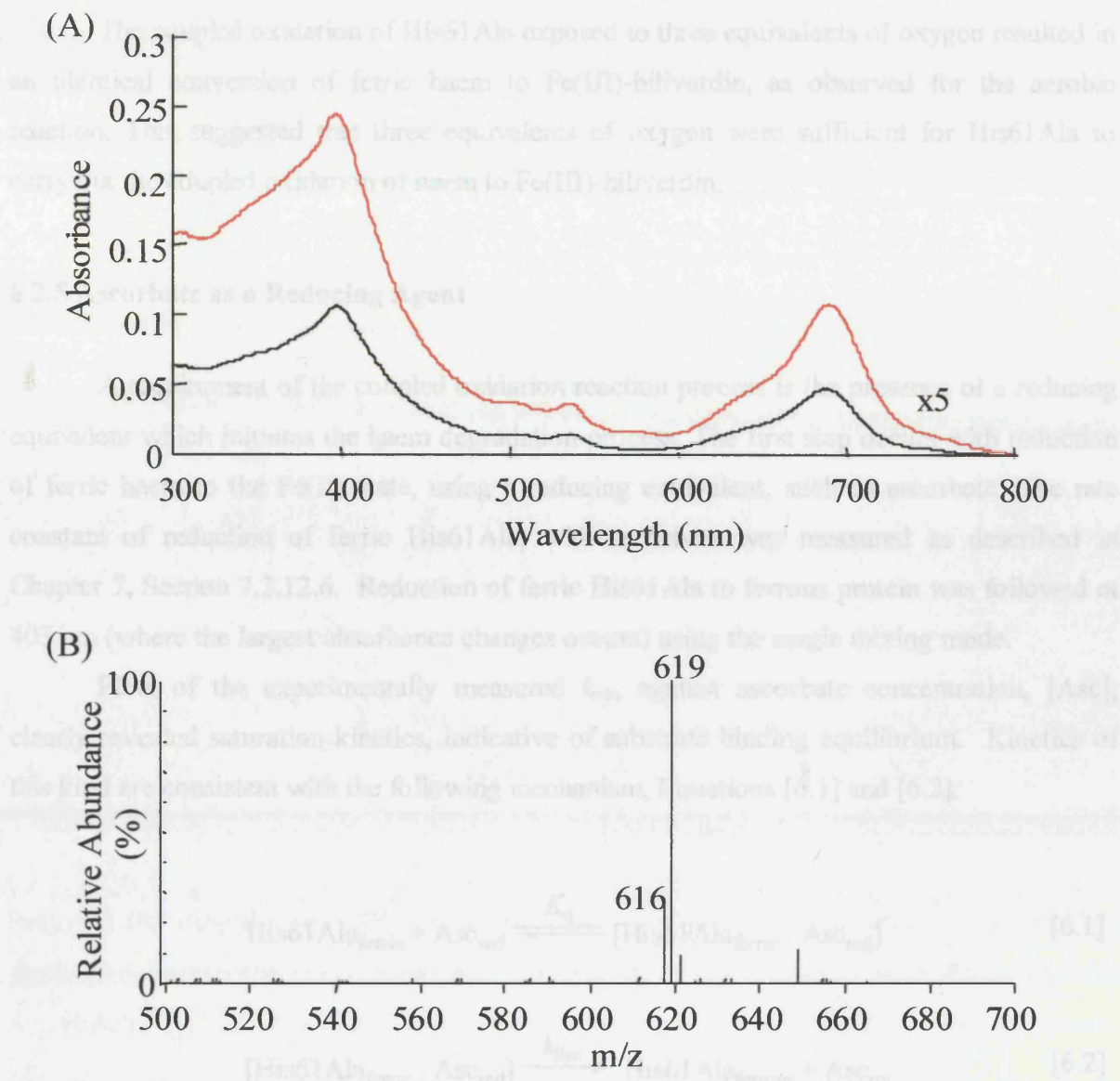


**Figure 6.9.** (A) Electronic absorption spectra of the pyridine complex of authentic verdohaem and the pyridine/chloroform extract of the verdohaem product after the coupled oxidation of His61Ala under two equivalents of oxygen. (B) ESI-MS analysis of the verdohaem product after addition of two equivalents of oxygen to the coupled oxidation reaction of His61Ala.

Exposure of the reaction mixture to oxygen resulted in a rapid conversion of the verdohaem intermediate to Fe(III)-biliverdin, identified by a peak at  $m/z$  635 in ESI-MS spectrum. The conversion of the intermediate (verdohaem complex) to Fe(III)-biliverdin suggested that the new identified intermediate is a precursor of Fe(III)-biliverdin.

#### 6.2.4.4 Three Equivalents of Oxygen

The coupled oxidation of His61Ala exposed to three equivalents of oxygen resulted in an identical conversion of ferric haem to Fe(III)-biliverdin, as observed for the aerobic reaction. This suggested that three equivalents of oxygen were sufficient for His61Ala to carry out the coupled oxidation of haem to Fe(III)-biliverdin.

#### 6.2.5 Ascorbate as a Reducing Agent

A requirement of the coupled oxidation reaction process is the presence of a reducing equivalent which initiates the haem degradation process. The first step occurs with reduction of ferric haem to the Fe(II) state, using a reducing equivalent, such as ascorbate. The rate constant of reduction of ferric His61Ala, with ascorbate was measured as described in Chapter 7, Section 7.2.12.6. Reduction of ferric His61Ala to ferrous protein was followed at 403 nm (where the largest absorbance changes occurs) using the single mixing mode.

Plots of the experimentally measured  $k_{\text{obs}}$  against ascorbate concentration, [Asc], clearly revealed saturation kinetics, indicative of substrate binding equilibrium. Kinetics of this kind are consistent with the following mechanism, Equations [6.1] and [6.2]:



from which an expression for  $k_{\text{obs}}$  can be derived, Equation [6.3],

$$k_{\text{obs}} = \frac{k_{\text{lim}}}{1 + K_d / [\text{Asc}_{\text{red}}]} \quad [6.3]$$

where  $[\text{Asc}_{\text{red}}]$  is the concentration of ascorbate and  $K_d$  is the equilibrium dissociation constant, for the substrate bound complex ( $K_d = 1/K_a$ ).

Therefore, according to Equation [6.3], a non-linear least-squares fit of the plot of  $k_{obs}$  against  $[Asc_{red}]$  allowed a  $K_d$  of  $65 \pm 5 \mu\text{M}$  to be calculated for His61Ala. The limiting rate constant,  $k_{lim}$ , for the reduction of the His61Ala-bound ascorbate was  $0.82 \pm 0.03 \text{ s}^{-1}$ , Figure 6.10. This rate was comparable to that measured for the reduction of haem by NADPH-cytochrome P450 reductase in the haem oxygenase reaction ( $0.49 \text{ s}^{-1}$ ).<sup>[27]</sup>

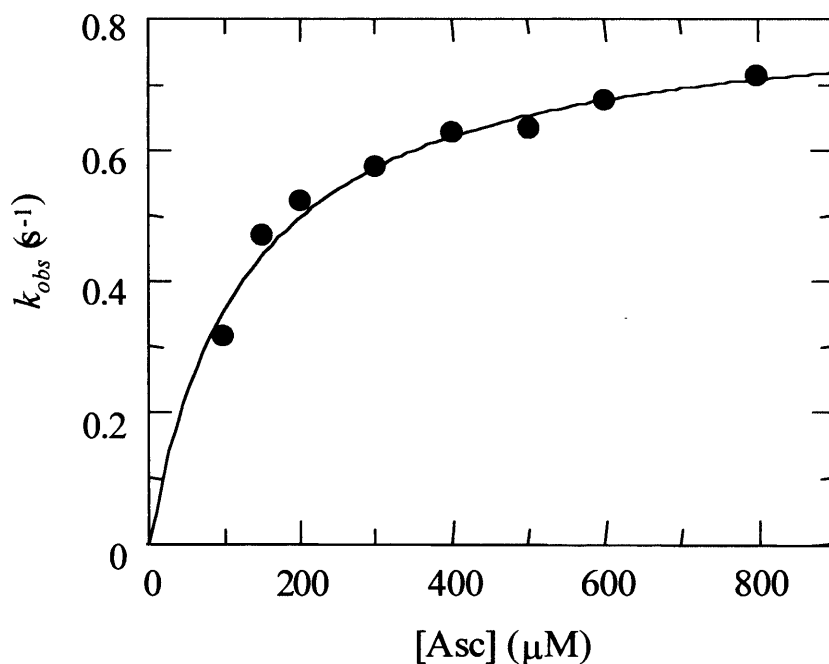


**Figure 6.10.** Reduction of His61Ala by ascorbate. The pseudo-first order rate constant,  $k_{obs}$ , plotted against ascorbate concentration,  $[Asc]$ , is shown. Measurements were obtained at 403 nm, close to the Soret maxima of His61Ala. Conditions: His61Ala ( $5 \mu\text{M}$ ), sodium phosphate, pH 7.0,  $\mu = 0.10 \text{ M}$ ,  $32.0 \text{ }^\circ\text{C}$ .

### 6.2.6 Regiospecificity of the Coupled Oxidation Reaction

The regiospecificity of the coupled oxidation of His61Ala was examined by incubation of His61Ala with ascorbate, under aerobic conditions at  $37 \text{ }^\circ\text{C}$  for 7 hours, Chapter 7, Section 7.2.12.7. The Fe(III)-biliverdin product was converted to biliverdin (Chapter 7, Section 7.2.12.3) and the biliverdin isomers isolated and methylated as described by O'Caara and Cameron.<sup>[28]</sup> The resulting dimethyl esters of the biliverdin isomers were separated using reverse-phase HPLC, Figure 6.10(A). Peaks at retention times of 6.9, 7.15, 7.25 and 7.5

minutes were observed. The isomer with a retention time of 6.9 minutes was identified as the  $\alpha$ -isomer, by comparison to authentic biliverdin IX $_{\alpha}$ , Figure 6.10(B). The other isomers were tentatively assigned according to the dimethyl ester biliverdin isomers previously observed for protoporphyrin IX.<sup>[28]</sup> The HPLC analysis of the dimethyl ester biliverdin isomers revealed that the coupled oxidation of His61Ala was non-regiospecific, producing all four isomers of biliverdin. In contrast, the coupled oxidation of haem oxygenase<sup>[19]</sup> and myoglobin<sup>[9]</sup> are regiospecific and products obtained as  $\alpha$ -isomers only.

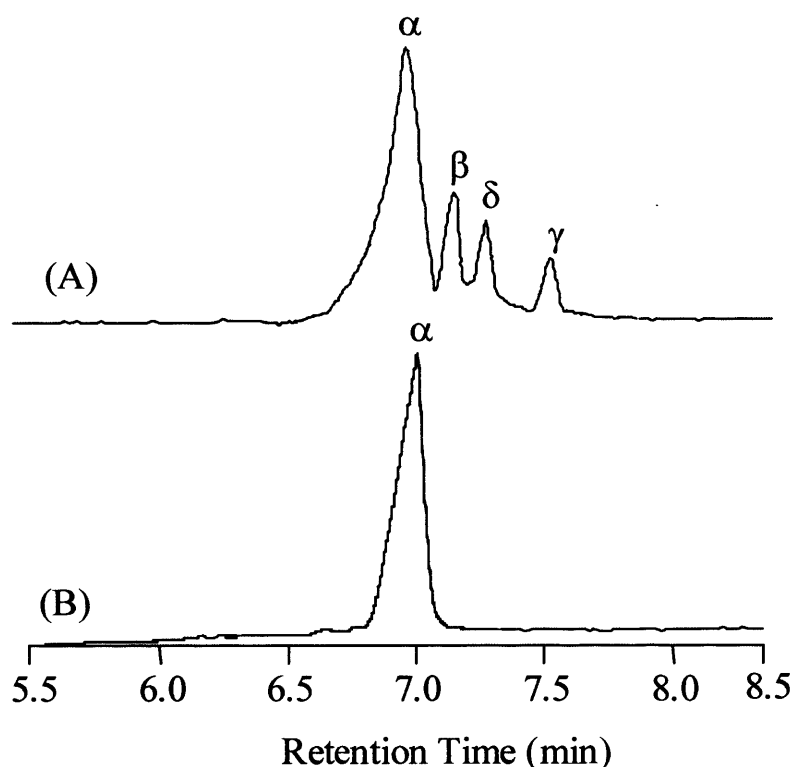


**Figure 6.11.** HPLC analysis of the dimethyl ester derivatives isolated from (A) biliverdin obtained from the coupled oxidation reaction of His61Ala showing the four isomers:  $\alpha$ ,  $\beta$ ,  $\gamma$ ,  $\delta$  dimethyl ester biliverdin and (B) the  $\alpha$  isomer obtained from authentic biliverdin IX $_{\alpha}$ .

### 6.2.7 $^{18}\text{O}_2$ -Labelled Coupled Oxidation

The origin of the oxygen found in the haem degradation products, of the haem oxygenase reaction has been shown to derive from molecular oxygen.<sup>[29, 30]</sup> To determine whether this is also true for the coupled oxidation carried out by His61Ala, the reaction was carried out using labelled molecular oxygen containing  $^{18}\text{O}^{18}\text{O}$  (Chapter 7, Section 7.2.12.9). Some of the Fe(III)-biliverdin product was analysed by ESI-MS and some Fe(III)-biliverdin

converted to biliverdin prior to mass spectrometric analysis. Figure 6.12 illustrates the mass spectra for the haem degradation products. The mass spectrum of Fe(III)-biliverdin displayed three peaks at  $m/z$  of 635, 637 and 639. Similarly, three peaks at  $m/z$  of 583, 585 and 587 were observed for the biliverdin extract. The three peaks corresponded to the incorporation of  $^{16}\text{O}^{16}\text{O}$ ,  $^{16}\text{O}^{18}\text{O}$  and  $^{18}\text{O}^{18}\text{O}$ , respectively, in the haem degradation product, suggesting that the oxygen atoms incorporated into the coupled oxidation product was derived from two separate oxygen molecules. These data supported earlier work, for both the biological and chemical reactions, reinforcing the validity of coupled oxidation as a model for biological haem cleavage.<sup>[29, 30]</sup>

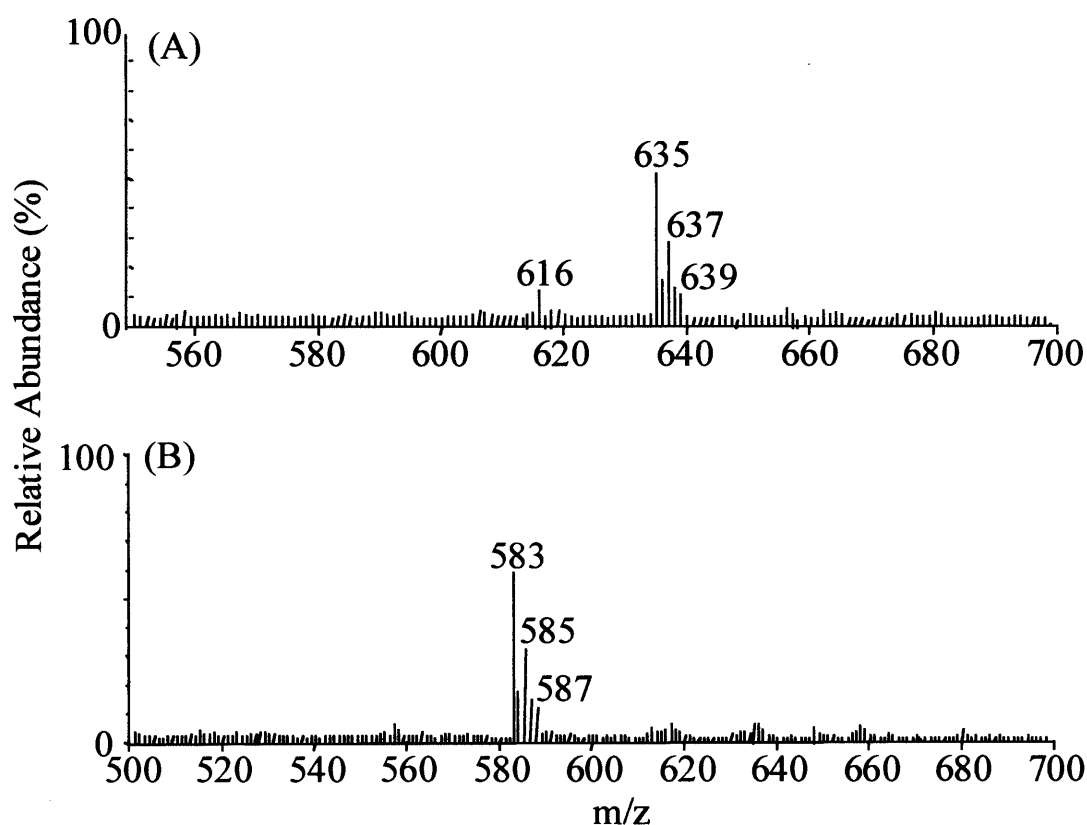


**Figure 6.12.** ESI-MS of  $^{18}\text{O}$ -labelled Fe(III)-biliverdin (A) and  $^{18}\text{O}$ -labelled biliverdin (B) obtained from the coupled oxidation of His61Ala carried out under  $^{18}\text{O}^{18}\text{O}$ . The mass spectra clearly show incorporation of labelled oxygen at  $m/z$  of 637 and 639 in the Fe(III)-biliverdin product and  $m/z$  of 585 and 587 in biliverdin.

### 6.2.8 Extended X-ray Absorption Fine Structure (EXAFS) Spectroscopy

The  $k^3$  weighted EXAFS spectrum and the resulting Fourier transform obtained for His61Ala, at room temperature and cryogenic temperature, are shown in Figure 6.13. A fit of the data for His61Ala, from the EXAFS spectrum, was analogous to those described for rLb. The distances of the iron atom to the main porphyrin ring atoms ( $N_p$ ), Table 6.1, suggest that the Fe atom lies in plane of the porphyrin structure. The structural results for His61Ala appeared to be similar to that of rLb, at both temperatures. The strong similarities were presumably due to the dominating (invariant) four-fold symmetry of porphyrin ring structure. The only significant differences between the two proteins were observed between  $k = 7 \text{ \AA}^{-1}$  and  $9 \text{ \AA}^{-1}$ , in the shape of the doublet, in the room temperature spectrum, Figure 6.13(A) and Figure 4.8, Chapter 4. At 77 K, the differences between the two proteins were less, all being very similar at all values of  $k$ . A decrease in the short bond length ( $\text{Fe-O}_{\text{water}}$ ), by 5 ppm, was observed for the variant as the temperature was lowered, with a corresponding increase in the  $N_e$  bond length, Table 6.1. However, a change in the Debye-Waller factor, by a factor of  $< 3$ , suggested no significant structural changes were associated with this ligand, with the change in temperature, in contrast to that observed for the rLb. Shortening of the Fe-O bond for the His61Ala variant, was thought to arise from a change of a water-bound haem at room temperature, to a hydroxide-bound haem at lower temperature, as indicated using the other spectroscopic methods, Chapter 3. The difficulty in distinguishing between O and N atoms by EXAFS only permitted tentative assignment of the ligating groups to the distal side of the haem, with the change in temperature.

The EXAFS data for ferric His61Ala, revealed Fe- $N_p$  distances at 2.05 Å, the proximal histidine distance (Fe- $N_e$ ) at 2.05 Å and the sixth ligand distance, Fe- $O_{\text{water}}$  at 1.95 Å. These results are similar to the analogous Fe-ligand distances of ferric myoglobin<sup>[31]</sup> and haem-haem oxygenase complex,<sup>[32]</sup> Table 6.2. The similarities in the Fe-ligand distances indicate that there may be similarities in haem structure between His61Ala and haem oxygenase, and may be one of the factors contributing to the ability of the His61Ala variant to carry out the coupled oxidation. However, these observations do not explain the inability of rLb to carry out the reaction successfully, which also has similar Fe- $N_p$  (2.05 Å), Fe- $N_e$  (2.10 Å) and Fe- $O_{\text{water}}$  (1.90 Å) distances.

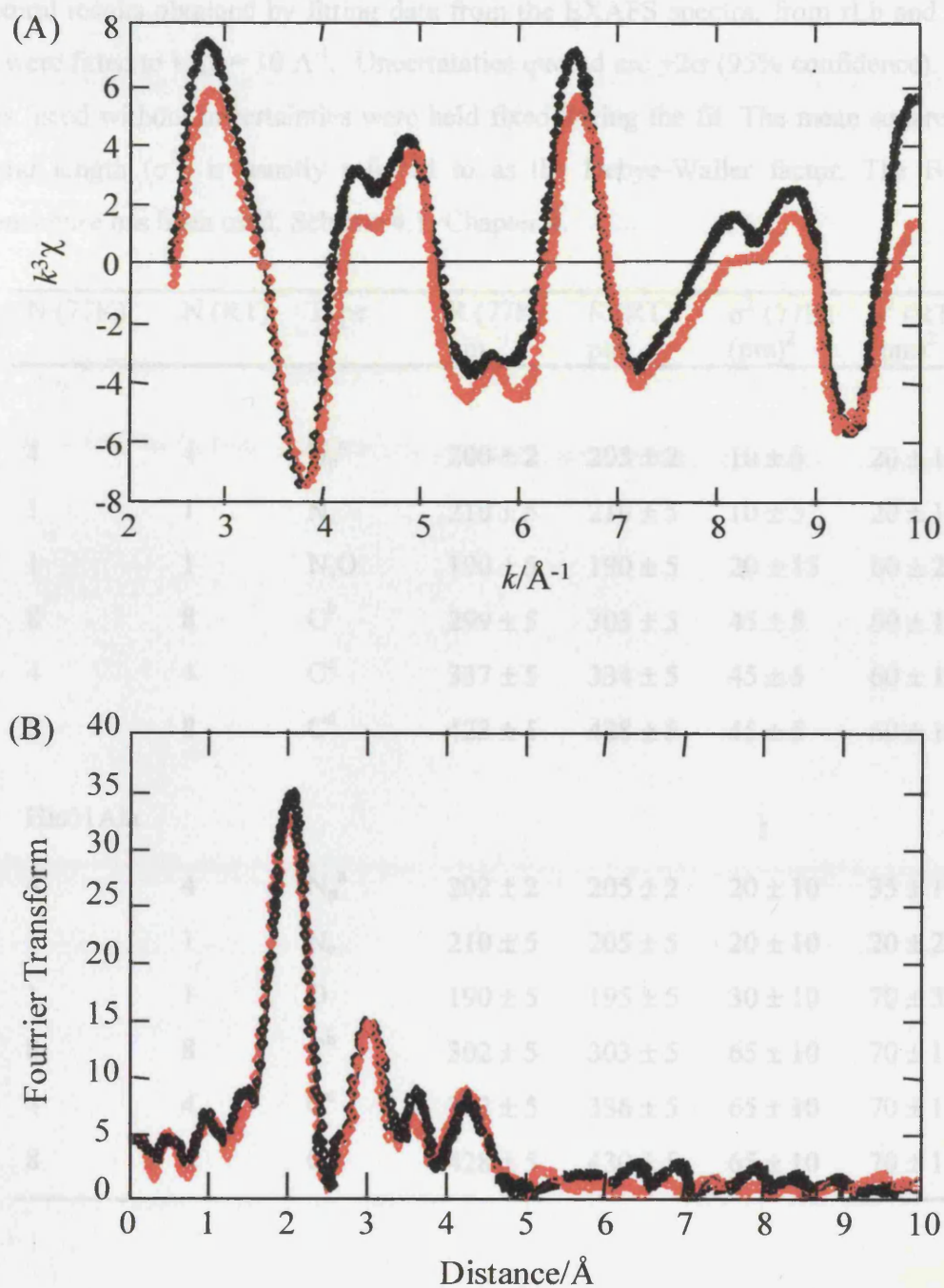


**Figure 6.13.** (A) the EXAFS spectrum and (B) Fourier transform amplitude of EXAFS, of His61Ala, observed at 298K ( $\diamond$ ) and 77K( $\diamond$ ). The solid lines indicate the calculated data from the refined model at 298K ( $\text{---}$ ) and 77K ( $\text{---}$ ).

**Table 6.1**

Structural results obtained by fitting data from the EXAFS spectra, from rLb and His61Ala. Data were fitted to  $k_{\max} = 10 \text{ \AA}^{-1}$ . Uncertainties quoted are  $\pm 2\sigma$  (95% confidence). Parameter values listed without uncertainties were held fixed during the fit. The mean square deviation in bond length ( $\sigma^2$ ) is usually referred to as the Debye-Waller factor. The Brookhaven nomenclature has been used, Scheme 4.1, Chapter 4.

N (77K)	N (RT)	Type	R (77K) pm	R (RT) pm	$\sigma^2$ (77K) (pm) <sup>2</sup>	$\sigma^2$ (RT) (pm) <sup>2</sup>
<b>rLb</b>						
4	4	N <sub>p</sub> <sup>a</sup>	200 ± 2	205 ± 2	10 ± 5	20 ± 10
1	1	N <sub>e</sub>	210 ± 5	210 ± 5	10 ± 5	20 ± 10
1	1	N,O	190 ± 5	190 ± 5	20 ± 15	60 ± 20
8	8	C <sup>b</sup>	299 ± 5	303 ± 5	45 ± 5	60 ± 10
4	4	C <sup>c</sup>	337 ± 5	334 ± 5	45 ± 5	60 ± 10
8	8	C <sup>d</sup>	423 ± 5	428 ± 5	45 ± 5	60 ± 10
<b>His61Ala</b>						
4	4	N <sub>p</sub> <sup>a</sup>	202 ± 2	205 ± 2	20 ± 10	35 ± 10
1	1	N <sub>e</sub>	210 ± 5	205 ± 5	20 ± 10	20 ± 20
1	1	O	190 ± 5	195 ± 5	30 ± 10	70 ± 30
8	8	C <sup>b</sup>	302 ± 5	303 ± 5	65 ± 10	70 ± 10
4	4	C <sup>c</sup>	342 ± 5	336 ± 5	65 ± 10	70 ± 10
8	8	C <sup>d</sup>	428 ± 5	430 ± 5	65 ± 10	70 ± 10

<sup>a</sup> N<sub>p</sub> = N<sup>A</sup>, N<sup>B</sup>, N<sup>C</sup>, N<sup>D</sup>

<sup>b</sup> C<sup>1A</sup>, C<sup>1B</sup>, C<sup>1C</sup>, C<sup>1D</sup>, C<sup>4A</sup>, C<sup>4B</sup>, C<sup>4C</sup>, C<sup>4D</sup>

<sup>c</sup> C<sup>HA</sup>, C<sup>HB</sup>, C<sup>HC</sup>, C<sup>HD</sup>

<sup>d</sup> C<sup>2A</sup>, C<sup>3A</sup>, C<sup>2B</sup>, C<sup>3B</sup>, C<sup>2C</sup>, C<sup>3C</sup>, C<sup>2D</sup>, C<sup>3D</sup>

**Table 6.2.**

Comparison of the EXAFS determined haem bond distances of His61Ala, horse heart Mb<sup>[31]</sup> and haem oxygenase.<sup>[32]</sup>

	Bond distances (Å)		
	His61Ala	Horse heart Mb	Haem oxygenase
Fe-N <sub>p</sub>	2.05 ± 0.02	2.06	1.99 ± 0.03
Fe-N <sub>ε</sub>	2.05 ± 0.05	2.18	2.08 ± 0.03
Fe-O <sub>water</sub>	1.95 ± 0.05	2.08	1.93 ± 0.03

### 6.3 Discussion

It has been known for many years that some haem proteins, such as myoglobin (Mb)[10, 12, 16, 28, 33-37] and variants of cytochrome  $b_5$ [13, 14] and cytochrome  $b_{562}$ ,[15] undergo a series of reactions in the presence of ascorbate and oxygen (coupled oxidation) that resemble the catalytic cycle of haem oxygenase. An addition to this list can now be made, on the basis of work carried out in this Chapter. In this work, it has been demonstrated that upon removal of the distal histidine 61 residue in rLb, the His61Ala variant is capable of performing coupled oxidation of haem to Fe(III)-biliverdin with non-regiospecificity.

Spectroscopic characterisation of His61Ala presented, in this work and in Chapter 3, strongly supports the conclusion that the haem coordination structure of His61Ala closely resembles that of haem oxygenase[32] (a) The haem iron of ferric His61Ala is in a hexacoordinate, high-spin state ( $\lambda_{\max} = 402.5, 500, 630$  nm) and is consistent with histidine-aqua axial coordination as is observed in mammalian and bacterial haem oxygenase ( $\lambda_{\max} = 404, 500$  and  $630$  nm).[38-41] (b) The  $pK_a$  of the two proteins are also similar (a  $pK_a$  of 8.4 for His61Ala and a  $pK_a$  of 8.5 for HO[32]) and are consistent with the titration of the distal water ligand to form a low-spin, hydroxide-bound haem at alkaline pH. (c) EXAFS data for the ferric His61Ala revealed that the average distances, Fe-N<sub>p</sub> (2.05 Å), the proximal histidine distance (Fe-N<sub>e</sub> = 2.05 Å) and the sixth ligand distance, Fe-O<sub>water</sub> (1.95 Å) were considerably similar to those for the haem-haem oxygenase complex (Fe-N<sub>p</sub> = 1.99 Å, Fe-N<sub>e</sub> = 2.08 Å and Fe-O<sub>water</sub> = 1.93 Å).[32] The only difference is observed in the Fe-N<sub>p</sub> distances, which have been previously rationalised as possibly arising from the temperature-dependent, spin-state changes in haem oxygenase at low temperature in order to prevent radiation damage.[32]

Although there are some spectroscopic similarities between His61Ala and haem oxygenase, the mechanism of haem degradation for the two proteins differs. The first difference is the nature of the reducing agent used in the reaction. Catalytic turnover of haem oxygenase requires an NADPH-dependent P450 reductase as a source of reducing equivalent, whereas the coupled oxidation requires a reductant, such as ascorbate. The ability of ascorbate to act as a reductant is demonstrated by the fast reduction of the His61Ala ferric haem ( $0.82 \pm 0.03$  s<sup>-1</sup>) to ferrous haem. The rate constant of reduction was ~ two-fold slower than that reported for the reduction of ferric haem oxygenase haem by NADPH-reductase ( $0.49$  s<sup>-1</sup>).[27] The reduction of ferric haem to ferrous haem is believed to be the first step of the coupled oxidation reaction mechanism (Scheme 6.2).

The second difference between the reaction mechanism of haem oxygenase and coupled oxidation are the intermediates observed and the final reaction product. The haem oxygenase catalysed oxidation of haem generates biliverdin as the final product with  $\alpha$ -meso-hydroxyhaem and verdohaem as intermediates (Scheme 6.1). The His61Ala variant of rLb underwent coupled oxidation through biphasic kinetics, in the presence of excess ascorbate and oxygen. This process involved the formation of an Fe(II)-O<sub>2</sub> intermediate ( $\lambda_{\text{max}} = 411, 574 \text{ and } 537 \text{ nm}$ ), with a rate constant ( $k_1$ ) of  $1.8.1 \pm 0.3 \times 10^{-2} \text{ min}^{-1}$  and its subsequent decay to Fe(III)-biliverdin ( $\lambda_{\text{max}} = 414, 526, 566, \sim 640 \text{ (broad) and } \sim 700 \text{ (broad) nm}$ ) ( $k_2 = 4.4 \pm 0.1 \times 10^{-3} \text{ min}^{-1}$ ), via a possible verdohaem intermediate (broad band at  $\sim 640 \text{ nm}$ , characteristic band for verdohaem). A similar reaction product has been reported for the coupled oxidation of haem oxygenase,<sup>[42]</sup> when ascorbate is used as a reductant. However, although the reaction products are similar, different intermediates were observed between the proteins. With haem oxygenase, the coupled oxidation proceeds via the  $\alpha$ -meso hydroxyhaem and verdohaem intermediates without the observation of the Fe(II)-O<sub>2</sub> intermediate.<sup>[19]</sup> In addition, the rate of haem degradation proceeded with greater efficiency than that carried out by His61Ala, determined in this work.<sup>[19]</sup>

The reaction products and intermediates of the His61Ala coupled oxidation reaction, were identified as follows: (a) the Fe(II)-O<sub>2</sub> intermediate was identified by comparison of the electronic absorption spectra to that of oxy-His61Ala generated by reduction of ferric protein with sodium dithionite and passage through a G25 (Sephadex) column; (b) the identity of the Fe(III)-biliverdin reaction product and the chloroform extract of the Fe(III)-biliverdin product (*i.e.* biliverdin) were confirmed by the electronic absorption spectra, HPLC and ESI-MS analyses. All the analysis techniques identified and confirmed Fe(III)-biliverdin as the final reaction product of the coupled oxidation of His61Ala. Surprisingly, the verdohaem intermediate, which was possibly formed through the aerobic reaction (broad band at  $\sim 640 \text{ nm}$ ) was not detected by ESI-MS and could be rationalised in terms of its high reactivity with oxygen (short-lived intermediate), and rapid formation of the Fe(III)-biliverdin product.

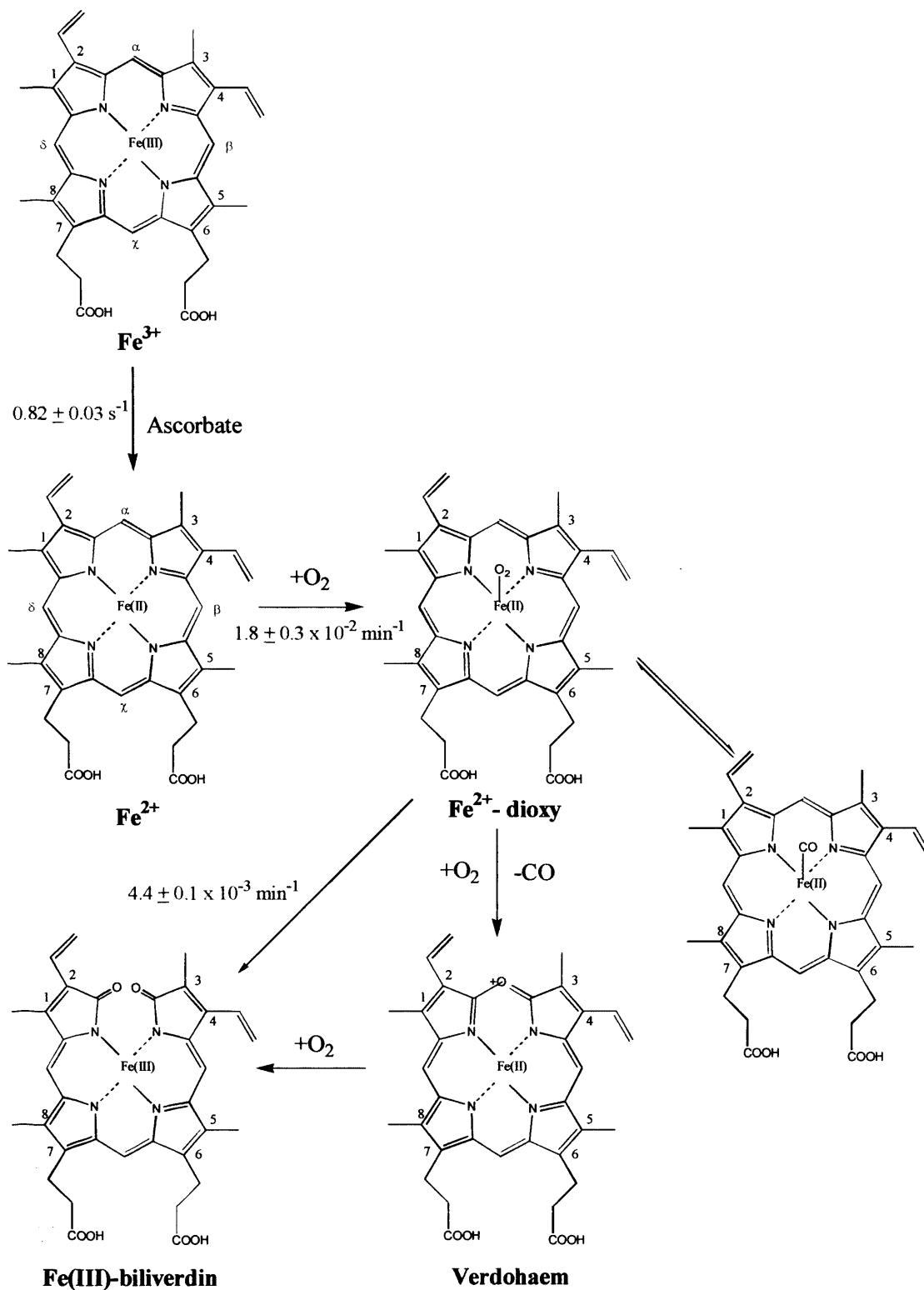
In contrast to His61Ala, the coupled oxidation reaction of rLb resulted in the formation of the Fe(II)-O<sub>2</sub> rLb ( $\lambda_{\text{max}} = 412, 541 \text{ and } 574 \text{ nm}$ ) with a rate constant ( $k_1$ ) of  $2.3 \pm 0.1 \times 10^{-3} \text{ min}^{-1}$ ), at which point the reaction ceased and no further haem degradation products were observed. It has been reported that the oxygen-bound haem is stabilised by a hydrogen bond from histidine 61, in the active site.<sup>[43]</sup> According to the haem oxygenase mechanism,<sup>[19]</sup> an 'activated oxygen' is required to react with the methine bridge, after

reduction, to form the hydroxy-haem intermediate and initiate the haem degradation process. The stability of the hydrogen bond from histidine 61 to the oxygen-bound haem could inhibit the reduction of the oxy species or could possibly reduce the activity of the oxygen and hence, be a possible explanation to why no further reaction is observed.

The dependence of the coupled oxidation reaction mechanism on oxygen was determined through anaerobic reaction of His61Ala in the presence of excess ascorbate. Under these conditions, the typical haem degradation products were not observed, indicating that the coupled oxidation mechanism not only requires a reducing agent but also oxygen. Instead, under anaerobic conditions, an electronic absorption spectra resembling that of a “Fe(IV)-like” species ( $\lambda_{\text{max}} = 414, 541 \text{ and } 573 \text{ nm}$ ) was observed. This species, has been previously reported to be formed, on exposure of ferric Lb to excess ascorbate. [20, 21] Exposure of the ‘Fe(IV)-like’ species to oxygen, resulted in the reaction proceeding to the Fe(III)-biliverdin product, via the Fe(II)-O<sub>2</sub> His61Ala intermediate. Similar reaction kinetics were observed to that for the aerobic coupled oxidation reaction, suggesting that the ‘Fe(IV)-like’ species is a very unstable intermediate. In the presence of ascorbate and oxygen, the ‘Fe(IV)-like’ species was rapidly reduced back to the ferric haem and then reduced further to ferrous haem, followed by subsequent formation of the Fe(II)-O<sub>2</sub> ‘activated’ species, initiating the coupled oxidation reaction.

Stoichiometric addition of oxygen to the coupled oxidation reaction provided further insight into the reaction mechanism of the haem degradation process carried out by His61Ala and provided a means of identifying (new) intermediates. The coupled oxidation reaction in the presence of one equivalent of oxygen resulted in the formation of the Fe(II)-O<sub>2</sub> His61Ala species, with a rate constant ( $k_1$ ) of  $1.1 \pm 0.05 \times 10^{-2} \text{ min}^{-1}$ , similar to that, for the first step, of the aerobic oxidation (Section 6.1.1). No new reaction products were evident on prolonged incubation of the reaction. These observations indicated that one equivalent of oxygen is required for the conversion of ferric haem to Fe(II)-O<sub>2</sub> species (Scheme 6.2), as expected. Conversion of the Fe(II)-O<sub>2</sub> species to Fe(III)-biliverdin was observed spectrophotometrically upon exposure of the reaction mixture to oxygen, without any new intermediates being observed during the process. Addition of two equivalents of oxygen to the His61Ala-ascorbate mixture, resulted in a triphasic reaction. Formation of the transient intermediate, the Fe(II)-O<sub>2</sub> species, was observed in the initial phase, as indicated by the typical wavelength maxima of Fe(II)-O<sub>2</sub> His61Ala and the rate constant for formation of the intermediate,  $k_1 = 1.8 \pm 0.3 \times 10^{-2} \text{ min}^{-1}$  (Section 6.2.1). The second phase involved conversion of the Fe(II)-O<sub>2</sub>

species to a new intermediate with wavelength maxima ( $\lambda_{\max}$ ) of 416, 563 and 537 nm resembling that of Fe(II)-CO complex of His61Ala. The appearance of a prominent peak at 664 nm, in the third phase, indicated formation of verdohaem. The accumulation of the CO-complex appears to be due to product inhibition, as a result of limited oxygen. Carbon monoxide (CO), which is known to be a by-product of the haem degradation (but released at a later stage in the mechanism than here), binds to the ferrous haem iron. The verdohaem product observed at the end of the reaction suggested that there was some slow release of the bound CO, followed by re-binding of any oxygen present in the system leading to further haem degradation to the verdohaem complex (Scheme 6.2). These observations also highlight the ability of the His61Ala variant to discriminate between oxygen and carbon dioxide during the haem degradation process. An oxygen association rate constant of  $290 \mu\text{M}^{-1}\text{s}^{-1}$  and a dissociation rate constant of  $3.1 \text{ s}^{-1}$  have been reported for His61Ala.<sup>[43]</sup> In comparison to the rate constants reported for rLb (oxygen association rate constant of  $130 \mu\text{M}^{-1}\text{s}^{-1}$  and dissociation rate constant  $5.6 \text{ s}^{-1}$ ),<sup>[43]</sup> it is clear that the His61Ala variant has higher affinity for oxygen than rLb (easier access of the ligand into the active site on removal of the distal histidine).<sup>[43]</sup> The carbon monoxide association constant for rLb has been reported as  $15 \mu\text{M}^{-1}\text{s}^{-1}$  and the dissociation constant as  $0.0084 \text{ s}^{-1}$ ,<sup>[43]</sup> although has not been reported for His61Ala. However on comparison to data for the rLb, it is clear that the rLb protein favours CO binding over oxygen, as a result of the remarkable slow CO dissociation rates. A similar trend would probably be expected for His61Ala, since an increase in oxygen association and decrease in dissociation is observed on removal of the distal histidine. In light of the discussion above and the haem degradation pathway with which the coupled oxidation reaction of His61Ala proceeds, as shown in this work, it is clear that during haem degradation, the His61Ala variant of rLb exhibits a remarkable discrimination for oxygen over carbon monoxide. The means by which haem oxygenase discriminates between  $\text{O}_2$  and CO is unclear at present, although it has been reported that the verdohaem-HO complex has a much lower affinity for CO than either haem-HO or the  $\alpha$ -meso hydroxyhaem-HO complex,<sup>[44]</sup> thereby preventing product inhibition by discriminating against CO after verdohaem formation. Like the reaction intermediates of HO, the coupled oxidation reaction intermediates of His61Ala may exhibit different affinities for CO which help prevent product inhibition.  $\text{O}_2$  and CO binding measurements for His61Ala and the haem degradation intermediates would have to be carried out in order to investigate this discrimination.



**Scheme 6.2.** The haem degradation pathway of His61Ala as determined from the coupled oxidation of His61Ala under aerobic and stoichiometric addition of oxygen. For simplicity only one regioisomer has been shown.

The formation of the verdohaem product (formed after addition of two equivalents of oxygen to the coupled oxidation reaction mixture) was confirmed by electronic absorption spectroscopy. Addition of 20 % pyridine to the protein solution, and extraction in chloroform, after addition of two equivalents of oxygen to the reaction, produced a typical spectrum of verdohaem-pyridine complex.<sup>[24, 45]</sup> Additional confirmation was acquired through ESI-MS, which displayed a peak at  $m/z$  619, that of authentic verdohaem, with some minor signal from unmodified haem ( $m/z$  616). These results indicate that a second equivalent of oxygen is required to transform Fe(II)-O<sub>2</sub> species to the verdohaem intermediate (Scheme 6.2). Exposure of this intermediate to oxygen resulted in the rapid conversion to Fe(III)-biliverdin, as shown through ESI-MS ( $m/z$  635).

Exposure of the reaction to three equivalents of oxygen resorted to the same reaction profile as observed for the aerobic addition of ascorbate to His61Ala, suggesting that three equivalents of oxygen are required for the coupled oxidation, of haem to Fe(III)-biliverdin. During its catalytic cycle, HO consumes 3 mol of O<sub>2</sub> for the degradation of one mol of haem by haem oxygenase to the biliverdin product.<sup>[19]</sup> Thereby indicating that although the reaction products and some intermediates may differ, the haem degradation carried out by His61Ala essentially follows a similar pathway to HO.

Under aerobic conditions, as well as under stoichiometric addition of oxygen, the formation of hydroxyhaem intermediate, Scheme 6.1, a distinct intermediate in haem oxygenase reaction mechanism, was not observed in the enzymatic reaction, and could be rationalised in terms of the high reactivity of the hydroxyhaem intermediate with oxygen.

The results from the coupled oxidation experiment carried out under labelled oxygen (<sup>18</sup>O<sub>2</sub>) indicated oxygen incorporation occurs via a two-molecule mechanism,<sup>[30]</sup> in which each of the two oxygen atoms, found in the final reaction product, derive from separate oxygen molecules, as is evident from the mixture of labelled products observed in the mass spectrum of Fe(III)-biliverdin and biliverdin (essentially <sup>16</sup>O<sup>16</sup>O, <sup>16</sup>O<sup>18</sup>O and <sup>18</sup>O<sup>18</sup>O). The mechanism of the coupled oxidation reaction carried out by His61Ala is in agreement with the haem oxygenase mechanism, with respect to the incorporation of oxygen into the haem degradation products and reinforces the efficacy of coupled oxidation as a model for biological haem cleavage.

A distinct difference between the coupled oxidation of His61Ala and HO and Mb was observed in the regiospecificity of the haem degradation reaction. Whereas the coupled oxidation reaction of HO and Mb is  $\alpha$ -regiospecific,<sup>[9]</sup> determination of the regiospecificity of

the coupled oxidation reaction of His61Ala revealed that the reaction was non-regiospecific. This was illustrated by the formation of the four dimethyl ester biliverdin isomers, observed in the HPLC chromatogram. Although rLb did not display coupled oxidation reactivity in this work, it has been previously reported that native Lb undergoes haem catabolism with formation of a biliverdin-like product obtained after acid treatment.<sup>[46]</sup> Lehtovaara and Perttola later established that the soybean Lba underwent haem degradation with  $\alpha$ -,  $\beta$ - and  $\delta$ -specificity.<sup>[47]</sup> The site specificity of haem degradation was explained with respect to the amino acids that are in the vicinity of the appropriate methine bridges and also the larger, open haem pocket architecture of Lb, and therefore less hindrance to attack at the methine bridges of the haem by the surrounding residues in Lb. The absence of the  $\gamma$ -isomer, which was never observed for Lb and for mammalian globins, <sup>[48]</sup> was explained in terms of the steric hindrance of the histidine-E7 residue, which inhibits attack at the methine bridge at the  $\gamma$ -position, of the haem. Following the observations from earlier studies,<sup>[46, 47]</sup> the four biliverdin isomers obtained for the His61Ala variant in this work, supports the early proposal that the histidine 61 residue prevents the formation of the  $\gamma$ -isomer. Hence, on removal of histidine 61, the  $\gamma$ -isomer is also observed. The differences that are observed in the regiospecificity of HO, Mb and His61Ala could be rationalised in terms of the active site pocket and the surrounding active site residues. For HO, the distal helix is believed to exercise a significant level of steric control and the polar interactions, between Fe-O-O and the surrounding environment may assist in steering the peroxide toward the  $\alpha$ -meso carbon.<sup>[3]</sup> For Mb, the  $\alpha$ -isomer is believed to be observed due to haem contact near the  $\alpha$ -methine bridge on the ligand binding side provided by the isoleucine 107 residue. The  $\delta$ -site is hindered by the valine 68 residue, the  $\beta$ -site is hindered by CD1, phenylalanine 43 residue and the  $\gamma$ -site is hindered by the E7, histidine 64 residue.<sup>[47, 48]</sup>

## 6.4 Summary

In summary, the present studies show that it is possible to introduce new reactivity into the rLb protein, by replacement of the distal histidine 61 residue (with alanine). The His61Ala variant exhibited coupled oxidation reaction, and a reaction following the pathway, Scheme 6.2, had been proposed. The initial step involved reduction of the ferric haem to ferrous haem. The second step was observed with formation of a Fe(II)-O<sub>2</sub> species. This was followed by conversion of the Fe(II)-O<sub>2</sub> species to verdohaem and then to Fe(III)-biliverdin, the reaction product. The origin of the oxygen found in the haem degradation products, has been shown, by ESI-MS analysis, to derive from molecular oxygen and the two oxygen atoms incorporated in the reaction product as arising from two separate oxygen molecules, similar to that reported for the haem oxygenase mechanism. The conversion of haem to Fe(III)-biliverdin for the coupled oxidation of His61Ala required 3 mol equivalents of oxygen, similar to that for the haem oxygenase reaction. The formation of the reaction product and intermediates, albeit formed with less efficiency, were different to those observed for the haem oxygenase reaction, but were similar to those observed for the coupled oxidation reaction of Mb. However, unlike Mb and HO, for which haem degradation occurs with  $\alpha$ -meso regioselectivity, the haem degradation of His61Ala was observed to be non-regioselective.

## 6.5 References

1. T. L. Poulos, H. Li, C. S. Raman and D. J. Schuller, *Adv. Inorg. Chem.* (2001) **51**, 243.
2. P. R. Ortiz de Montellano, *Acc. Chem. Res.* (1998) **31**, 543.
3. P. R. Ortiz de Montellano and A. Wilks, *Adv. Inorg. Chem.* (2001) **51**, 243.
4. M. Ikeda-Saito, H. Fujii, K. M. Matera, S. Takahashi, C. T. Migita, D. L. Rousseau and T. Yoshida, *Keio Univ. Symp. Life Sci. Med.* (1998) **1**, 304.
5. S. Dore, M. Takahashi, C. D. Ferris, R. Zakhary, L. D. Hester, D. Guastella and S. H. Snyder, *Proc. Natl. Acad. Sci. U.S.A.* (1999) **96**, 2445.
6. M. Zhuo, S. A. Small, E. R. Kandel and R. D. Hawkins, *Science* (1993) **260**, 1946.
7. A. Verma, D. L. Hirsch, C. E. Glatt, G. V. Ronnett and S. H. Snyder, *Science* (1993) **259**, 381.
8. C. F. Stevens and Y. Wang, *Nature* (1993) **364**, 147.
9. T. Murakami, I. Morishima, T. Matsui, S.-I. Ozaki, I. Hara, H.-J. Yang and Y. Watanabe, *J. Am. Chem. Soc.* (1999) **121**, 2007.
10. T. Murakami, I. Morishima, T. Matsui, S.-I. Ozaki and Y. Watanabe, *Chem. Commun.* (1998), 773.
11. D. P. Hildebrand, H.-L. Tang, Y. Luo, C. L. Hunter, M. Smith, G. D. Brayer and A. G. Mauk, *J. Am. Chem. Soc.* (1996) **118**, 12909.
12. S. Sano, T. Sano, I. Morishima, Y. Shiro and Y. Maeda, *Proc. Natl. Acad. Sci. U. S. A.* (1986) **83**, 531.
13. L. Avila, H.-W. Huang, J. C. Rodriguez, P. Moenne-Loccoz and M. Rivera, *J. Am. Chem. Soc.* (2000) **122**, 7618.
14. J. C. Rodriguez and M. Rivera, *Biochemistry* (1998) **37**, 13082.
15. J. K. Rice, I. M. Fearnley and P. D. Barker, *Biochemistry* (1999) **38**, 16847.
16. E. L. Raven and A. G. Mauk, *Adv. Inorg. Chem.* (2001) **51**, 1.
17. I. Morishima, H. Fujii and Y. Shiro, *Inorg. Chem.* (1995) **34**, 1528.
18. J. C. Lagarias, *Biochim. Biophys. Acta* (1982) **717**, 12.
19. P. R. Ortiz de Montellano and A. Wilks, *Adv. Inorg. Chem.* (2001) **51**, 359.
20. A. Puppo, C. Monny and M. J. Davies, *Biochem. J.* (1993) **289**, 435.
21. S. Moreau, A. Puppo and M. J. Davies, *Phytochemistry* (1995) **39**, 1281.
22. Y. Liu, P. Moenne-Loccoz, T. M. Loehr and P. R. Ortiz de Montellano, *J. Biol. Chem.* (1997) **272**, 6909.

23. S. Takahashi, K. M. Mansfield, H. Fujii, H. Zhou, K. Ishikawa, T. Yoshida, M. Ikeda-Saito and D. L. Rousseau, *Biochemistry* (1997) **36**, 1402.
24. T. Yoshida and M. Noguchi, *J. Biochem.* (1984) **96**, 563.
25. T. Yoshida and M. Noguchi, *J. Biochem.* (1980) **88**, 557.
26. A. Wilks and P. R. Ortiz de Montellano, *J. Biol. Chem.* (1993) **268**, 22357.
27. Y. Lui and P. R. Ortiz de Montellano, *J. Biol. Chem.* (2000) **275**, 5297.
28. P. O'Carra and E. Colleran, *FEBS Lett.* (1969) **5**, 295.
29. S. B. Brown and R. F. G. J. King, *Biochem. J.* (1978) **170**, 297.
30. R. F. G. J. King and S. B. Brown, *Biochem. J.* (1978) **174**, 103.
31. A. M. Rich, R. S. Armstrong, P. J. Ellis, H. C. Freeman and P. A. Lay, *Inorg. Chem.* (1998) **37**, 5743.
32. B. K. Hawkins, A. Wilks, L. S. Powers, P. R. Ortiz de Montellano and J. H. Dawson, *Biochim. Biophys. Acta* (1996) **1295**, 165.
33. R. Lemberg, *Rev. Pure. Appl. Chem.* (1956) **6**, 1.
34. P. O'Carra, in *Porphyrins Metalloporphyrins*, K. M. S. Ed., (Elsevier, Amsterdam, The Netherlands) 1975, pp.123.
35. S. B. Brown, A. A. Chabot, E. A. Enderby and A. C. North, *Nature* (1981) **289**, 93.
36. S. Saito and H. A. Itano, *Proc. Natl. Acad. Sci. U. S. A.* (1982) **79**, 1393.
37. D. P. Hildebrand, H.-L. Tang, Y. Luo, C. L. Hunter, M. Smith, G. D. Brayer and A. G. Mauk, *J. Am. Chem. Soc.* (1996) **118**, 12909.
38. S. J. Takahashi, J. Wang, D. L. Rousseau, K. Ishikawa, T. Yoshida, N. Takeuchi and M. Ikeda-Saito, *Biochemistry* (1994) **33**, 5531.
39. A. Wilks and P. Moenne-Loccoz, *J. Biol. Chem.* (2000) **275**, 11686.
40. J. Sun, A. Wilks, P. R. Ortiz de Montellano and T. M. Loehr, *Biochemistry* (1993) **32**.
41. G. C. Chu, T. Tomita, F. D. Sonnichsen, T. Yoshida and M. Ikeda-Saito, *J. Biol. Chem.* (1999) **274**, 24490.
42. T. Yoshida, K. Ishikawa and M. Sato, *Eur. J. Biochem.* (1991) **199**, 729.
43. M. S. Hargrove, J. K. Barry, E. A. Brucker, M. B. Berry, G. N. Phillips, J. S. Olson, P. R. Arredondo, J. M. Dean, R. V. Klucas and G. Sarath, *J. Mol. Biol.* (1997) **266**, 1032.
44. C. T. Mitiga, C. M. Matera and M. Ikeda-Saito, *J. Biol. Chem.* (1998) **273**, 945.
45. E. Y. Levin, *Biochemistry* (1966) **9**, 2845.
46. A. I. Virtanen and J. K. Miettinen, *Acta. Chem. Scand.* (1949) **3**, 17.
47. P. Lehtovaara and U. Perttila, *Biochem. J.* (1978) **176**, 359.
48. S. Brown, *Biochem. J.* (1976) **159**, 23.

# **Chapter 7**

# **Experimental**

## 7 Experimental

This chapter describes the experimental methods and techniques used throughout this thesis.

### 7.1 Leghaemoglobin

Recombinant wild-type leghaemoglobin DNA was obtained from Dr. D. K. Jones (University of Leicester) and was the starting point for mutagenesis and protein isolation of the leghaemoglobin variants.

#### 7.1.1 Oligonucleotides

Complementary oligonucleotides (29-35 bases in length) containing the desired mutation were synthesised and purified by the Protein and Nucleic Acid Chemistry Laboratory, University of Leicester. The complementary pairs of oligonucleotides containing the appropriate mismatch bases (indicated in red), depicted in Table 7.1, were used to prepare the variants of rLb studied in this thesis. Generation of the His61Ala/Tyr30Ala mutant DNA was achieved by mutation of His61Ala with a further complementary pair of oligonucleotides containing the Tyr30Ala mismatch bases.

#### 7.1.2 Mutagenesis

Site-directed mutagenesis, using the appropriate pair of oligonucleotides, was carried out using the Quikchange™ mutagenesis kit (Stratagene). Reactions were prepared in thin-walled PCR tubes by mixing 10 × reaction buffer (5 µl, Appendix A), the recombinant leghaemoglobin DNA template (2 µl, 50 ng/6 Kb), the forward and reverse oligonucleotide mutagenesis primers (125 ng of each) and dNTP mix (1 µl). The reaction mixture was made up to a final volume of 50 µl using filter-sterilised doubly deionised water. *Pfu* polymerase was added to the reaction mixture and the reaction cycled by PCR. PCR reactions were initiated by a denaturation step of 30 seconds at 95 °C followed by 16 cycles of denaturation (30 seconds, 95 °C), annealing (1 minute, 55 °C) and extension (12 minutes (2 mins per kb of plasmid length), 68 °C). At the end of the reaction, samples were placed on ice

**Table 7.1.**

The forward and reverse oligonucleotides used to generate the variants of rLb.

**The mismatch codons are highlighted in red.**

Variant
<p><b>His61Ala/Tyr30Ala</b></p> <p>Forward: 5' TCC GTT GTT TTC <b>GCT</b> ACC TCC ATC CTG 3'</p> <p>Reverse: 3' AGG CAA CAA AAG <b>CGA</b> TGG AGG TAG GAC 5'</p>
<p><b>Glu63Leu</b></p> <p>Forward: 5' ACC GGT CAC GCT <b>CTG</b> AAA CTG TTC GCT 3'</p> <p>Reverse: 3' TGG CCA GTG CGA <b>GAC</b> TTT GAC AAG CGA 5'</p>
<p><b>His61Ala</b></p> <p>Forward: 5' CCC GAA ACT GAC CGG <b>TGA</b> <b>CGC</b> TGA AAA ACT GTT CG 3'</p> <p>Reverse: 3' GGG CTT TGA CTG GCC <b>ACT</b> <b>GCG</b> ACT TTT TGA CAA GC 5'</p>
<p><b>His61Tyr</b></p> <p>Forward: 5' CCC GAA ACT GAC CGG <b>TTA</b> <b>CGC</b> TGA AAA ACT GTT CG 3'</p> <p>Reverse: 3' GGG CTT TGA CTG GCC <b>AAT</b> <b>GCG</b> ACT TTT TGA CAA GC 5'</p>
<p><b>His61Lys</b></p> <p>Forward: 5' CCC GAA ACT GAC CGG <b>TAA</b> <b>AGC</b> TGA AAA ACT GTT CG 3'</p> <p>Reverse: 3' GGG CTT TGA CTG GCC <b>ATT</b> <b>TCG</b> ACT TTT TGA CAA GC 5'</p>
<p><b>His61Arg</b></p> <p>Forward: 5' CCC GAA ACT GAC CGG <b>TCG</b> <b>TGC</b> TGA AAA ACT GTT CG 3'</p> <p>Reverse: 3' GGG CTT TGA CTG GCC <b>AGC</b> <b>ACG</b> ACT TTT TGA CAA GC 5'</p>

for 2 minutes to cool. Digestion of the methylated and hemimethylated parental DNA was carried out by the addition of *DpnI* (1 µl). Mixtures were then centrifuged (1 minute) and immediately incubated at 37 °C for 1 hour to digest the parental DNA. The reaction product was transformed into 50 µl of super-competent Epicurian Coli XL1-Blue cells (Stratagene) in prechilled Falcon® 2059 Propylene Tubes (15 ml), and stored on ice for 30 minutes. The cells were heat-pulsed at 42 °C for 45 seconds, returned to ice for 2 minutes and incubated with shaking for one hour at 37 °C, 250 rpm with 0.5 ml pre-heated LB media (42 °C) (Appendix A). The transformants were plated onto LB agar plates (Appendix A) containing ampicillin (50 µg/ml) and incubated at 37 °C overnight. To confirm the identity of the transformants, a single colony from the overnight plates was selected and incubated into 10 ml LB media

containing 100 µg/ml ampicillin overnight at 37 °C with vigorous shaking (250 rpm). Mutant DNA was isolated from the overnight cultures using the Qiagen mini-plasmid system following the manufacturer's instructions and using the buffers, resins and tubes provided.

### 7.1.3 Isolation of DNA

The mutant DNA was prepared using stationary phase culture. The culture (2 ml) was placed in a microcentrifuge tube and microcentrifuged for 1 minute. The supernatant was decanted and the tubes were inverted and placed on a paper towel to drain excess solution. The cell pellet was resuspended in pre-lysis buffer (50 µl). The tube was inverted to ensure mixing and alkaline lysis solution (100 µl) was added directly into the cell suspension. The cell suspension was mixed once again by inverting the tube and left standing at room temperature until the solution was clear and viscous. Neutralisation solution (75 µl) was added, mixed by brief vortexing and then microcentrifuged for 5 minutes. The top (aqueous) layer was removed and placed into a spin filter. Binding buffer (250 µl, containing silica gel matrix) was added and pipetted up and down to ensure mixing and microcentrifuged for one minute to allow collection of liquid in the bottom of the vial, which was then discarded. Wash solution (350 µl) was added to the spin filter and microcentrifuged for two minutes. The filter was then transferred to a new microcentrifuge tube. Sterile doubly deionised water (50 µl) was added to the spin filter, the solution vortexed briefly to resuspend the binding matrix/DNA, and then microcentrifuged for one minute. DNA was collected at the bottom of the microcentrifuge tube and stored at -20 °C. The DNA was analysed by 1% agarose gel electrophoresis.

### 7.1.4 Agarose Gel Electrophoresis

Agarose gels (1.0 % w/v) (5.5 cm × 8.5 cm) containing 0.6 µg/ml ethidium bromide were cast, and electrophoresis was performed in TBE buffer (Appendix A) at 100 V. Samples of isolated DNA (8 µl) were mixed with sample loading buffer (2 µl) (Appendix A) prior to being loading onto the gel. DNA markers (1 kb *Hind*III ladder, Pharmacia) were used to provide band sizes at 23130, 9416, 6557, 4361, 2322, 2027, 564, and 125 bp. Nucleic acids were visualised by exposing the gel to long wavelength UV radiation on a transilluminator.

### 7.1.5 DNA Sequencing

Sequencing of the entire recombinant mutant or rLb-coding gene was performed to ensure that no spurious mutations had arisen during the mutagenic reactions. Automated fluorescent sequencing was performed by the Protein and Nucleic Acid Chemistry Laboratory, University of Leicester, on an Applied Biosystems 373-Stretch machine and sequence data were analysed using the program SeqED (Applied Biosystems). The plasmid DNA sequencing was achieved using New England Biolabs PETFF and PETRR sequencing primers.

### 7.1.6 Transformation of the Recombinant DNA into Competent *E.Coli* Cells

The sequenced DNA (1  $\mu$ l) was added to filter-sterile deionised water (9  $\mu$ l), in prechilled Falcon® 2059 Propylene Tubes (15 ml). Competent cells (BL21(DE3), 50  $\mu$ l) were added, the reactions swirled to mix solutions and placed on ice for 40 minutes. A heat shock, of the solution at 42 °C, for 45 seconds, was followed by incubation with 450  $\mu$ l of LB media at 37 °C, shaking for 1 hour at 150 r.p.m. The cultures were then plated on LB ampicillin agar plates. A single colony from the overnight plate was selected and incubated into LB media (10 ml) containing 100  $\mu$ g/ml ampicillin overnight at 37 °C with vigorous shaking (250 rpm). DNA was isolated from the overnight cultures using the Qiagen mini-plasmid system and analysed as above using agarose electrophoresis and the DNA was re-sequenced to confirm mutation. Overnight cultures were also used to make glycerol stocks (700  $\mu$ l of overnight culture to 300  $\mu$ l of 50 % sterile glycerol, stored at –80 °C) as an inoculum for expression and isolation of variant proteins.

### 7.1.7 Expression of rLb and Variants in *E.Coli*

Large scale expression (8 litres) of rLb or variants was carried out using frozen glycerol stocks as starting inoculum for a LB plate containing 100  $\mu$ g/ml ampicillin. Single colonies were used to inoculate LB media (100 ml) containing 100  $\mu$ g/ml ampicillin, and the flask was incubated overnight at 37 °C with shaking (250 rpm). This culture (50 ml) was used to seed LB/ampicillin (1 l) in a 2 l flask, and was further incubated at 37 °C, 250 rpm, to an absorbance at 600 nm of 0.7-0.9, at which time the protein expression was induced with

isopropyl- $\beta$ -D-thiogalactopyranoside (final concentration 1 mM, (750  $\mu$ l of 0.1 M IPTG)) and incubated for a further 24 hours (225 rpm, 37 °C). Cells were harvested at 4 °C by centrifugation at 10,000 rpm and resuspended in cold lysis buffer (Appendix A). Lysozyme (100 mg) was added, and the cells gently shaken on ice for 60 minutes before freezing at -20 °C until required.

### 7.1.8 Isolation and Purification of rLb and Variants

All reaction steps were performed at 4 °C. The cells were thawed overnight and 5 mg deoxyribonuclease (DNase, Sigma) and 1 M MgCl<sub>2</sub> (5 ml) were added. The cells were then shaken gently on ice until the solution was no longer viscous. The mass of cells was centrifuged (10,000 rpm, 45 minutes) and the supernatant (pink/red for rLb and Glu63Leu and yellow (apo) for His61Ala/Tyr30Ala, His61Tyr, His61Lys and His61Arg) was collected and stored on ice. The pellet was resuspended in fresh lysis buffer (50-100 ml) the resulting solution re-centrifuged (10,000 rpm, 45 minutes) and the supernatant collected. This procedure was repeated until the pellet had no obvious colour. The first purification step was achieved by ammonium sulphate precipitation. The supernatant was brought to 50% saturation by gradual addition of solid (NH<sub>4</sub>)<sub>2</sub>SO<sub>4</sub> (28.3 g/100 ml) and left stirring at 4 °C for 1 hour. After centrifugation at 10,000 rpm (30 minutes), the colourless pellet was discarded and the supernatant (pink/red for rLb, Glu63Leu or yellow supernatant for His61Ala/Tyr30Ala, His61Tyr, His61Lys and His61Arg) was brought to 100% ammonium sulphate saturation by addition of a further 38.8 g/ 100 ml of (NH<sub>4</sub>)<sub>2</sub>SO<sub>4</sub> (stirring at 4 °C for 1 hour). The solution was centrifuged as before and the supernatant discarded. The pellet (pink/red for rLb and Glu63Leu and colourless for His61Ala/Tyr30Ala, His61Tyr, His61Lys and His61Arg) was resuspended in cold lysis buffer, loaded into dialysis membranes and dialysed against purified water (Elgastat) for 36 hours, changing the water every 12 hours. The protein was centrifuged for 1 hour (10,000 g) and applied to a 2.5 x 20 cm DE52 column (Whatman), previously equilibrated in 5 mM Tris/HCl, pH 9.2. The protein was eluted using a 5 mM Tris/HCl buffer containing 0.5 M NaCl, and concentrated to a volume of < 10 ml and then stored at -20 °C until the next step of purification.

The next step involved reconstitution of rLb and variant proteins with hemin chloride. A solution of haem was prepared from hemin chloride (10 mg, Sigma), dissolved in 0.1 M NaOH (1 ml). Haem was added in 20  $\mu$ l aliquots (and checked on and electronic absorption

spectrophotometer to check for incorporation of haem) to the solution of protein until a small excess had been added. An approximate 10-fold stoichiometric excess of potassium ferricyanide was added to ensure complete oxidation of the protein solution. Excess potassium ferricyanide was removed by exhaustive exchange with purified water (Elgastat) using an Amicon 10,000 MW cut off membrane and the protein solution stored at  $-20^{\circ}\text{C}$  until use.

A Sephadex G50 column equilibrated with 20 mM Tris/HCl buffer pH 8.0, was used to remove excess haem and any other impurities. Protein solution was applied to the G50 column and was allowed to run down the column gravitationally. Appearance of 2 bands was observed on the G50 column. The lower band was collected as one fraction and discarded and the upper band (containing the required protein) collected as 5 ml fractions and analysed over the range 270-700 nm on the electronic absorption spectrophotometer to ascertain an  $R_z$  value (where  $R_z$  is an expression of the purity of the protein). An SDS-PAGE gel was also carried out on the protein to verify purity (pure protein migrates as a single band, Figure 7.1 (see Section 7.1.9)). Fractions having  $R_z$  values  $> 3$  were considered pure, and were combined and concentrated by ultrafiltration, before storage at  $-80^{\circ}\text{C}$ .

### 7.1.9 SDS/Polyacrylamide Gel Electrophoresis of Proteins

All proteins were analysed on 15% discontinuous polyacrylamide gels containing SDS (0.1%) and polyacrylamide stacking gel (4%). Gels were prepared and run using Mini-Protean II gel systems (Bio-Rad), at a thickness of 0.75 mm. Protein samples were prepared for electrophoresis by the addition of an equal volume of reducing sample application buffer (Appendix A), followed by boiling for 5 minutes. Gels were run in SDS running buffer (Appendix A) at 50 V to load, and then 150 V until the dye-front reached the bottom of the gel. Gels were soaked in stain (Appendix A) for 30 minutes. The gel was destained by soaking in destain buffer (Appendix A). Figure 7.1 shows a SDS-PAGE gel of purification stages of rLb and variants and Figure 7.2 depicts the purified rLb and variants.

### 7.1.10 Preparation of Protein Samples for Analysis

Samples of the protein solutions used for analysis were oxidised using ferricyanide and were exhaustively exchanged in deionised water using a 10 ml centricon (Amicon) to

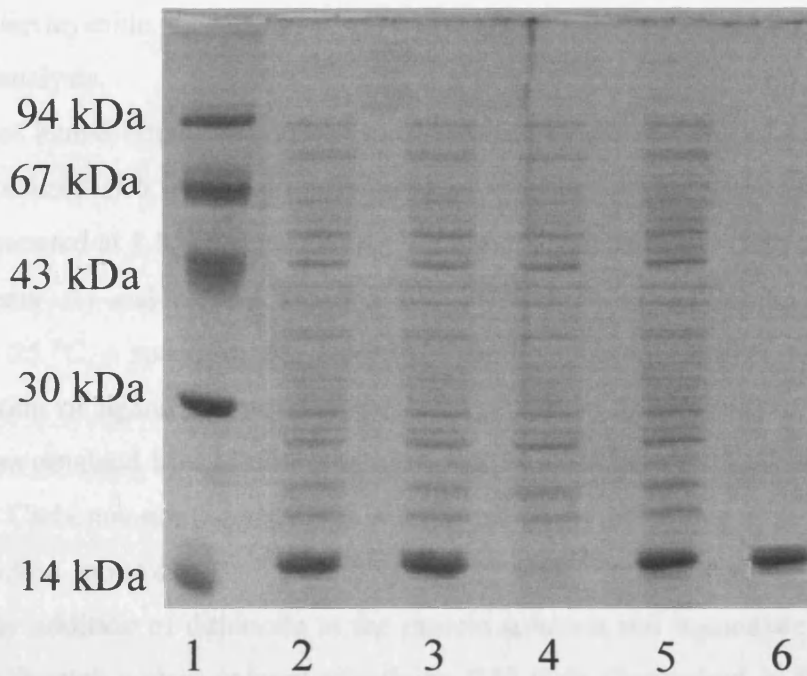


**Figure 7.1.** SDS-PAGE gel showing purification stages of rLb. Lane 1: molecular weight markers; Lane 2: supernatant after 50 % ammonium sulphate precipitation; Lane 3: pellet after 100 % ammonium sulphate precipitation; Lane 4: supernatant after 100 % ammonium sulphate precipitation; Lane 5: protein after reconstitution with haem and before application to a G50 column; Lane 6: purified rLb.

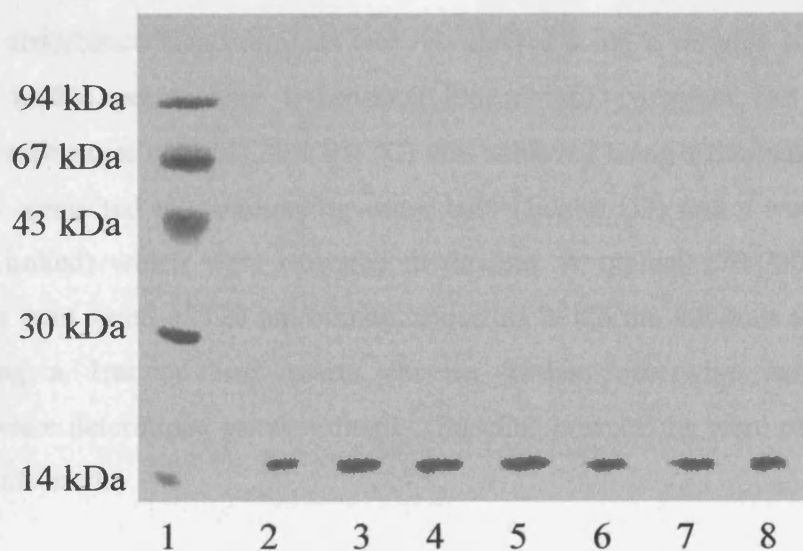


**Figure 7.2.** SDS-PAGE gel showing purified rLb and variants. Lane 1: Molecular weight marker; Lane 2: rLb; Lane 3: His61Ala/Tyr30Ala; Lane 4: Glu63Leu; Lane 5: His61Ala; Lane 6: His61Tyr; Lane 7: His61Lys; Lane 8: His61Arg.

remove excess ferricyanide. The samples were exchanged into the desired buffer needed for the experiment analysis.

Spectra of ligand-bound derivatives were obtained by the addition of a small excess of ligand to the oxidised rLb or variant. Samples of cyanide, azide, acetate, hydroxide and fluoride were prepared at 1 M concentrations. Sodium phosphate buffer (980  $\mu$ l,  $\mu$  = 0.10 M, pH 7.0, Appendix A) and protein solution (20  $\mu$ l) were weighed into a cuvette. After equilibration to 25 °C, a spectrum was recorded. The ligand solution (0.5  $\mu$ l) was added to ensure full ligation of ligand and another spectrum recorded. A spectrum of reduced ( $\text{Fe}^{2+}$ ) solution was also obtained by addition of a small excess of sodium dithionite to the oxidised ( $\text{Fe}^{3+}$ ) solution. Carbonmonoxy-derivatives were prepared by saturating a ferrous sample of protein with carbon monoxide and recording the spectrum immediately. Oxy-derivatives were obtained by addition of dithionite to the protein solution and immediate transfer of the reduced protein through a short column containing G25 resin (Sephadex) in Tris/HCl buffer, pH 8.0. The spectrum of the oxy-protein was recorded immediately.

## 7.2 Spectroscopic and Analytical Techniques

### 7.2.1 Electronic Absorption Spectroscopy

Routine absorbance measurements were conducted using a variable slit Perkin Elmer Lambda 14 UV-visible spectrometer, linked to an Exacta 466D computer, and an Epsom-LQ-1060 printer. Temperature control ( $25 \pm 0.1$  °C) was achieved using a thermally-jacketed cell holder that was connected to a circulating water bath (Julabo U3) and a water cooler (MK Refrigeration Limited) which were operated in tandem. A typical 270-700 nm scan was obtained using a scan speed of 120 nm/minute, acquiring at 0.5 nm intervals and with a 1 nm slit width using a 1ml or 3ml quartz cuvette. Unless otherwise indicated, sample concentrations were determined gravimetrically. Baseline corrections were made against the buffers or solvents used.

### 7.2.2 Determination of the Absorption Coefficient

The total haem content of a haem protein solution and therefore the absorption coefficient of the haem protein can be determined using the pyridine haemochromagen method according to the procedure of Antonini and Brunori.<sup>[1]</sup> An alkaline pyridine solution was prepared from the addition of pyridine (2 ml), 1 M NaOH (600  $\mu$ l) and distilled water to a final volume of 6 ml. A protein sample with an absorbance of 0.3 – 0.9 in the visible region was required to provide the most reliable data; thus, a spectrum was recorded on a gravimetrically determined sample drawn from the protein stock solution. Pyridine solution (1.5 ml) was added to the protein solution (500  $\mu$ l of known concentration) to form the pyridine-haem complex. The resulting solution (2 ml) of oxidised haemochromagen (yellow in colour) was divided into two 1 ml aliquots. After five minutes (to enable complete conversion to the haemochromagen), the electronic absorption spectrum was recorded using one of the oxidised aliquots. A single crystal of dithionite was added to the oxidised pyridine haemochromagen solution and the spectrum of the unstable reduced haemochromagen was recorded immediately over the wavelength range 450 – 650 nm. The complete transfer of haem from the protein to pyridine was checked by determining the absorbance at maximum ( $\lambda = 557$  nm) and minimum ( $\lambda = 540$  nm) wavelengths; a ratio of  $A_{557}/A_{540} = 3.5$  is found for protohaem. Absorption coefficients were then calculated knowing the absorption coefficient for the pyridine-protohaem complex ( $\epsilon_{557} = 32 \text{ mM}^{-1}\text{cm}^{-1}$ ) using Equation [7.1]: where  $A$  = absorbance of the stock solution,  $c$  = concentration of the protein,  $\epsilon$  = molar absorption coefficient and  $l$  is the pathlength of the cuvette.

$$A = \epsilon cl \quad [7.1]$$

The experiment was repeated on the other aliquot 24 hours later to check reproducibility. Figure 7.3 shows the pyridine haemochrome spectrum of rLb.

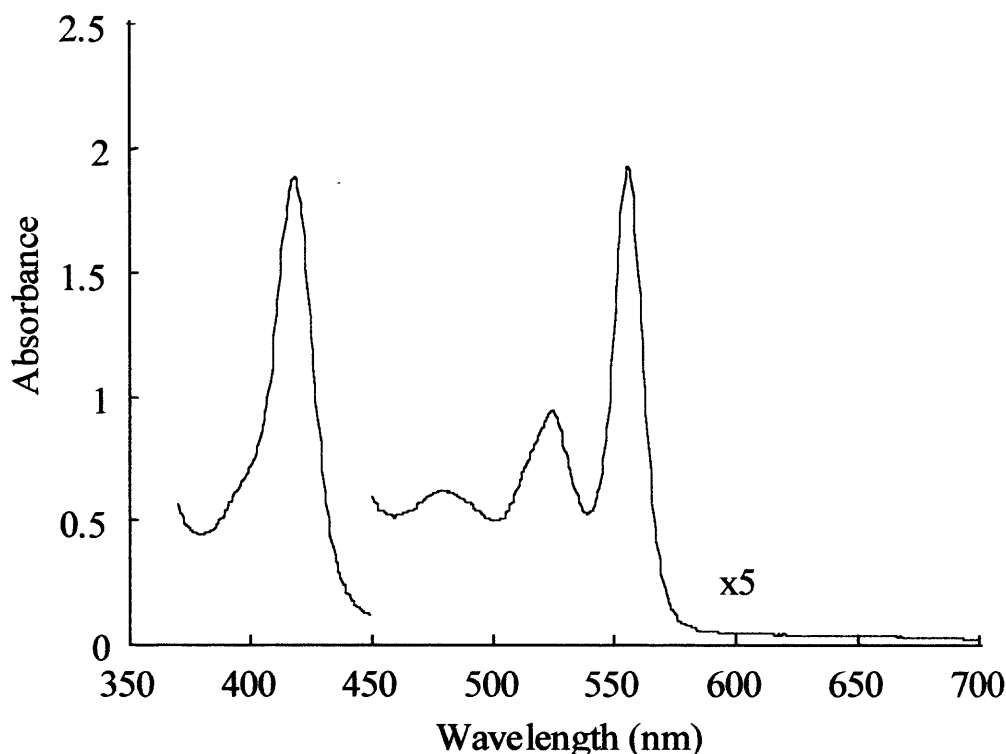
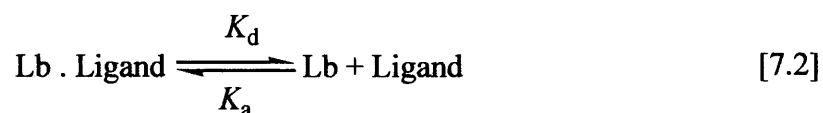


**Figure 7.3.** Electronic spectrum of the reduced pyridine haemochromagen of rLb. The visible region has been multiplied by a factor of five for clarity. The ratio of  $A_{557}/A_{540} = 3.5$ , and therefore indicates a protohaem structure for the protein. Conditions: sodium phosphate buffer, 25.0 °C.

### 7.2.3 Ligand Binding Equilibria

Determination of equilibrium dissociation constants,  $K_d$ , for the equilibrium [7.2]



was according to previously published procedures.<sup>[2]</sup>

The affinity of rLb and variants for ligand was measured by spectrophotometric titration. A known amount of ligand (10  $\mu\text{l}/1 \text{ ml}$ ) was added to the protein solution (the concentration of the proteins was determined using their calculated molar absorptivities) in a 1 ml cuvette and the decrease in intensity of the Soret band was measured. The volume of

added ligand was small (0.5 – 2.0  $\mu$ l) so that sample dilution was minimal. Each titration curve comprised 10 – 20 points.

The equilibrium dissociation constants for the rLb and variants with greater ligand binding affinity (smaller  $K_d$  values) were calculated according to Equation [7.3].

$$\bar{Y} = \frac{[\text{Ligand}]_{\text{free}}}{(K_d + [\text{Ligand}]_{\text{free}})} \quad [7.3]$$

Where [Ligand] refers to the concentration of the anionic ligand added, and  $\bar{Y}$ , the fractional saturation, which is calculated from the change in absorbance divided by the total change in absorbance, Equation [7.4],

$$\bar{Y} = \frac{(A_i - A_t)}{(A_i - A_f)} = \frac{[\text{Lb} \cdot \text{Ligand}]}{[\text{Lb}]_{\text{tot}}} \quad [7.4]$$

where  $A_i$  is the initial absorbance of the protein solution in the absence of ligand,  $A_f$  is the final absorbance at ligand saturation and  $A_t$  is the absorbance value at each intermediate point in the titration. The free ligand concentration,  $[\text{Ligand}]_{\text{free}}$ , is then defined by Equation [7.5].

$$[\text{Ligand}]_{\text{free}} = [\text{Ligand}]_{\text{tot}} - [\text{Lb} \cdot \text{Ligand}] \quad [7.5]$$

The variants with significantly lower ligand binding affinity (higher  $K_d$  values) were not titrated to saturation as concentration of ligand were required that would have resulted in significant increases in ionic strength. Assuming  $[\text{Ligand}]_{\text{free}} = [\text{Ligand}]_{\text{tot}}$ , an alternative equation, Equation [7.6], can be derived.

$$\text{Abs} = \frac{(K_d A_i + [\text{Ligand}]_{\text{tot}} A_f)}{(K_d + [\text{Ligand}]_{\text{tot}})} \quad [7.6]$$

Use of this relationship avoids the necessity of achieving complete saturation of the protein with ligand.

Nicotinate titrations were carried out in succinic acid buffer ( $\mu = 0.1$  M, 25.0 °C) for the acidic region (3.8 – 5.5) and sodium phosphate buffer ( $\mu = 0.1$  M, 25.0 °C) for the neutral to alkaline region (5.5 – 8.5) and CHES buffer for the alkaline region (8.0 – 10). Stock solutions of nicotinate were prepared in buffer of appropriate pH in 1, 10 and 100 mM concentrations (exact concentrations were determined gravimetrically), and used as appropriate during spectrophotometric titrations.

Buffered solutions of potassium cyanide (sodium phosphate buffer, pH 7.0, or succinic acid buffer, pH 4.0,  $\mu = 0.10$  M) were freshly prepared and stored in well-sealed vessels to prevent loss of HCN. Cyanide solutions were approximately 1, 10, 100, 1000, 2500, 5000 mM (exact concentrations were determined by mass), and were equilibrated prior to use. All binding experiments were carried out at  $25.0 \pm 0.1$  °C. Cuvettes were filled with solution and tightly sealed with a stopper to prevent the escape of HCN. Protein solutions were prepared in sodium phosphate buffer (pH 7.0,  $\mu = 0.10$  M) and succinic acid buffer (pH 4.0,  $\mu = 0.10$  M) and allowed to equilibrate for 10 minutes after each addition of cyanide before the spectrum was recorded.

Buffered solutions of sodium azide (sodium phosphate buffer, pH 7.0,  $\mu = 0.10$  M or succinic acid buffer (pH 4.0,  $\mu = 0.10$  M)) were freshly prepared. Azide solutions were approximately 1, 10, 100, 1000 and 2500 mM (exact concentrations were determined by mass), and were equilibrated prior to use. All binding experiments were carried out as for cyanide binding

Data were entered into an Excel spreadsheet and fitted to Equations [7.3] and [7.6] (Scientist v.4.03, Micromath) to determine the equilibrium dissociation constants for the strong and weak ligand binding, respectively. Reported values of  $K_d$  were an average of at least two independent measurements. For the pH-dependent nicotinate binding studies, a non-linear least squares fitting program (Scientist v.4.03, MicroMath) was used to fit the data (equilibrium dissociation constants) to the Henderson Hasselbach equation to a single proton process, Equation [7.7] (see Section 7.2.5).

#### **7.2.4 Haem Extraction from rLb, Glu63Leu and His61Ala and Reconstitution of the Apo-Proteins with Protoporphyrin IX Dimethyl Ester.**

Apo-rLb, Glu63Leu and His61Ala were prepared using the method of Teale at 4 °C.<sup>[3]</sup> Aqueous solutions of rLb, Glu63Leu and His61Ala were titrated with 1 M HCl to a pH of 1.5.

An equivalent volume of ice-cold 2-butanone was added with gentle, but continuous stirring. After a period of cooling on ice, two distinct layers were observed for each protein. The 2-butanone layer that contained the extracted haem was removed, and a further amount of 2-butanone was added to the aqueous layer to extract more haem. Several additions of 2-butanone were made to remove all of the haem. The resulting straw-coloured apo- rLb and Glu63Leu solutions were then dialysed against water (5 l) containing 0.6 mM sodium bicarbonate and (0.1 mM) EDTA, and then against water with 0.6 mM sodium bicarbonate. Reconstitution of the protein was carried out using freshly prepared solutions of protoporphyrin IX dimethyl ester (Sigma) in 0.1 M NaOH (10 mg/ml) in a 1:1 ratio.

Nicotinate binding experiments, using the protoporphyrin IX dimethyl ester-containing rLb, Glu63Leu and His61Ala proteins, in the acidic region, were carried out as described in Section 7.2.3.

### 7.2.5 pH Titrations of rLb and Variants

Titrations were conducted in mixed sulphonic acid buffer ( $\mu = 0.10$  M) and were carried out by cautious addition of 0.10 M NaOH ( $\sim 2$   $\mu$ l) to acquire intermediate pH values. Care was taken to avoid any excessive pH jump and protein precipitation. The pH was recorded before and after measurement of each spectrum and was monitored using a Russell pH-electrode attached to a digital pH-meter (Radiometer Copenhagen, model PHM93). A non-linear least squares fitting program (Scientist v.4.03, MicroMath) was used to fit the pH-dependent data to a single proton process, Equation [7.7]

$$Z = \frac{A + B \times 10^{(\text{pH} - \text{p}K_a)}}{1 + 10^{(\text{pH} - \text{p}K_a)}} \quad [7.7]$$

where  $Z$  is the absorbance and  $A$  and  $B$  are the absorbancies of the acidic and basic forms respectively. For a two-proton process, data were fitted to Equation [7.8]

$$Z = \frac{A + B \times 10^{(\text{pH} - \text{p}K_{a1})}}{1 + 10^{(\text{pH} - \text{p}K_{a1})}} - \frac{B - C \times 10^{(\text{pH} - \text{p}K_{a2})}}{1 + 10^{(\text{pH} - \text{p}K_{a2})}} \quad [7.8]$$

where  $A$  is the absorbance of the acidic form,  $B$  is the intermediate form and  $C$  is the basic form.

## 7.2.6 Paramagnetic $^1\text{H}$ NMR Spectroscopy

Data for rLb and Glu63Leu were collected on a Bruker AM300 NMR machine at an operating frequency of 300 MHz. Protein samples (~10 mg) were exhaustively exchanged into a solution of 50 mM deuterated phosphate buffer, pH 4.0. No account was made for the deuterium pH shift; measured pH is indicated as pH\*. The sample was concentrated to a volume of ~ 400  $\mu\text{l}$ , and loaded into a Youngs NMR tube.

### 7.2.6.1 $^1\text{H}$ -NMR of Nicotinate Derivatives

Samples of the nicotinate derivatives of rLb and Glu63Leu were prepared by adding a 4-fold excess of 100mM nicotinate (20-30  $\mu\text{l}$ ) prepared in deuterated buffer). The pH\* (initial pH of 4.0) was adjusted by careful addition of NaOD and measured using an Ingold micro-combination electrode and a Radiometer pH Meter; the readings in  $\text{D}_2\text{O}$  are uncorrected for isotope effects and designated pH\*. Proton NMR spectra were recorded on a Bruker AM300 NMR machine at an operating frequency of 300 MHz.

## 7.2.7 Spectroelectrochemistry

Potentiometric titrations were performed using an optically transparent, thin-layer electrode (OTTLE) cell as previously described.<sup>[4, 5]</sup> The OTTLE cell (prepared by Dr E. Raven) consisted of two quartz plates (Wilma) separated by two teflon spacers (Dilectrix Corp.), with a gold mesh (500 lines/inch, Buckbee Mears Co., Minneapolis, Minnesota) working electrode mounted onto a lucite frame. A 5 cm length of copper wire was attached by solder onto the bottom of the gold mesh and all the components were sealed using epoxy cement (Epoxy-Patch, The Dexter Corp.). Two ports were engineered into the top of the cell body, and a buffer-filled glass adaptor with a porous frit bottom was loaded into each. To complete the experimental set up, a saturated calomel electrode (SCE) was loaded into one of the frits, whilst a platinum wire counter electrode was loaded into the other. A representative cell is depicted in Figure 7.4. Control of the solution potential across the working electrode, was achieved by an EG&G Princeton Applied Research Model 362 potentiostat and monitored through a Thurlby 1503 digital multimeter (accurate to 0.1 mV) in conjunction with the reference electrode. All potentiometric titrations were performed at  $25 \pm 0.5$  °C.

The OTTLE cell solution (protein solution) was monitored using a Digital thermocouple, which was inserted into the OTTLE cell aperture.

Electronic absorption spectra in the range 700-340 nm were recorded using a Perkin-Elmer Lambda 14 spectrophotometer, linked to an Exacta 466D computer. The OTTLE cell was mounted onto a specially prepared jacketed cell holder (Chemistry Workshop, University of Leicester) connected to an Ecoline RE104 thermostatted water bath (Lauda, Germany), which was accurate to  $\pm 0.5$  °C. The temperature of the OTTLE cell itself was monitored using a Digitron 2751-K thermocouple which was inserted into a specially engineered aperture of the OTTLE cell.

The SCE was prepared at the University of Leicester using a mercury-platinum junction. A drop of mercury was placed at the platinum junction, a "paste" prepared from mercuric chloride and mercury was then added to pack the capillary and maintain a good contact between the platinum and mercury. Glass wool was used to plug the tube and the tube was jacketed in a saturated solution of KCl. The potential of the new electrode was determined by comparison against a commercially available SCE and was determined as + 242 mV *vs.* SHE.

#### 7.2.7.1 Preparation of Protein Samples

Samples of the protein solutions used for analysis were oxidised using ferricyanide, to ensure complete conversion to the ferric oxidation state, and were then exchanged using a 10 ml centricon (Amicon) to remove any excess ferricyanide. Ferric rLb or variant (120  $\mu$ M) proteins were prepared in sodium phosphate buffer, pH 7.0. Addition of  $[\text{Ru}(\text{NH}_3)_5^{3+}\text{Cl}_3]$  ( $E^\circ = 51$  mV *vs* SHE) mediator, at a tenth of the protein concentration, afforded mediated electrode transfer of the protein with the electrode surface. The mediator facilitates the electron transfer by efficiently equilibrating and exchanging electrons effectively with the electrode surface. This process then mediates the oxidation-reduction equilibrium of the protein to that of the electrode. Choice of mediator was selected by considering a number of factors. a) The mediator should not contribute to the electronic spectrum of the protein solution in the wavelength of interest. b) The mediator should not interact with or bind the protein in either oxidation state such that it influences the apparent mid-point potential. c) The mid-point potential of the mediator should be similar to that of the protein to ensure efficient equilibration at all potentials required during the potentiometric titration. Protein solutions

were made anaerobic by the use of *Rhus vernicifera* laccase (Sigma), which in the reduced form converts oxygen to water. Trace amounts of catalase were also present (Sigma type C-100): a 10:1 dilution of the semi-crystalline solution in the appropriate buffer was added to prevent the formation of a third species of the rLb (ferryl rLb) which could interfere with the ferric/ferrous equilibrium.

### 7.2.7.2 Data Collection and Analysis

The experimental procedure for determining reduction potentials was identical in all cases. The experiment proceeded with the application of a potential of -500 mV vs. SCE across the cell, to ensure that the protein was reduced completely to the deoxy state, and to activate the laccase. The protein was re-oxidised in stages, by applying potentials at ~ 50 mV intervals, with equilibration for one hour at each potential. Equilibration of the protein at each applied potential was determined by recording the absorbance at the Soret maxima; a constant absorbance value is observed when the protein is equilibrated. Re-oxidation of the protein was monitored by observing changes in the Soret maxima of the protein, complete oxidation of the protein was achieved by applying a potential of +200 mV vs SCE to the cell. A typical experiment consisted of a fully oxidised and reduced spectrum as well as six intermediate spectra illustrating varying ratios of oxidised and reduced protein.

Data were fitted to the Nernst equation, Equation [7.9].

$$E_a = E_m + (2.303 \times 10^{-3}) \frac{RT}{nF} \log \frac{A_{\text{red}} - A_i}{A_i - A_{\text{ox}}} \quad [7.9]$$

The terms  $A_{\text{red}}$ ,  $A_{\text{ox}}$  and  $A_i$  represent the absorbance values of the fully reduced, fully oxidised and mixed oxidation state, respectively, for rLb or variant protein at a given wavelength. Calculations are based on the change in absorbance at the Soret maxima of the protein, as the greatest change in absorbance is seen at this wavelength upon change in oxidation state. The terms  $E_a$  and  $E_m$  represent the applied potential (mV vs. SCE) and mid-point potential, respectively. The number  $2.303 \times 10^{-3}$  is a conversion factor used to adjust for the mV scale, and base 10 logarithm used in Equation [7.9]. The values of  $\log [(A_{\text{red}} - A_i) / (A_i - A_{\text{ox}})]$  were calculated and plotted versus the corresponding applied potentials to obtain a Nernst plot of the data. A linear regression analysis was used to fit the data and calculate the y-intercept and

slope. The calculated y-intercept represents the mid-point reduction potential (mV vs. SCE). Calculated potentials were adjusted to the standard hydrogen electrode (SHE) scale by the conversion  $\text{mV vs. SHE} = \text{mV vs. SCE} + 242 \text{ mV}$  at  $25 \text{ }^\circ\text{C}$ .

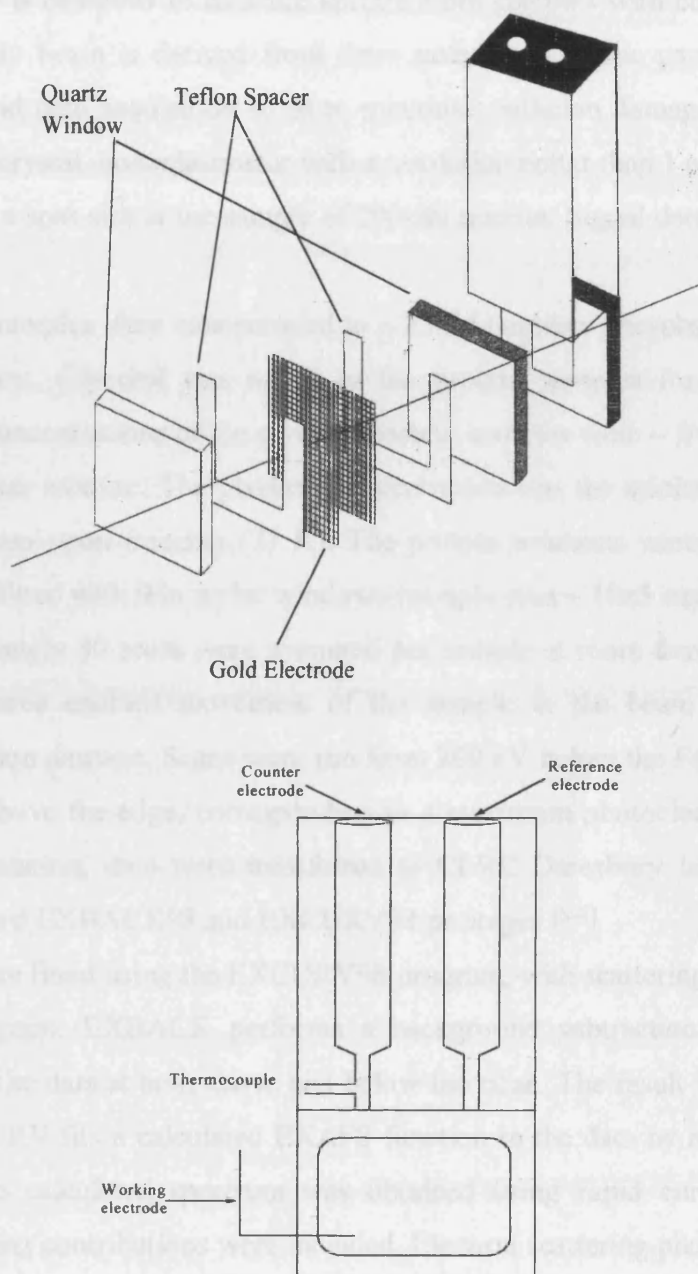


**Figure 7.4.** Top: OTTLE cell used for the spectroelectrochemistry experiments. Bottom: Experimental set up of OTTLE cell, showing electrode positions.

### 7.2.8 Extended X-ray Absorption Fine Structure (EXAFS)

X-ray absorption data were recorded in collaboration with Dr. S. Gurman and Dr. A. Svensson at the European Synchrotron Radiation Facility (Grenoble) using the ultra-dilute X-ray Absorption Spectroscopy (XAS) beamline ID26. The beamline has a spectral range of 3.2-30 keV and is designed to measure spectra from samples with concentrations below 10 mM. The X-ray beam is derived from three undulators whose gap may be continuously scanned for rapid data acquisition so as to minimise radiation damage to samples. It uses a Si(111) double-crystal monochromator with a resolution better than 1 eV at the iron edge. The focussing gives a spot size at the sample of 200x80 micron. Signal detection was by means of photodiodes.

Protein samples were concentrated to ~ 2 mM (sodium phosphate buffer) for the room temperature scans. Glycerol was added to the protein samples for the 77 K scans. The resulting final concentrations of the glycerol-protein samples were ~ 2 mM to produce a 30 % v/v glycerol/water mixture. The glycerol concentration was the minimum required to form a homogenous glass upon freezing (77 K). The protein solutions were syringed into perspex sample holders fitted with thin mylar windows (sample area ~ 10x5 mm; sample thickness ~ 1 mm). Approximately 30 scans were averaged per sample at room temperature and 77 K; the large window area enabled movement of the sample in the beam (~ every 4 scans) to minimise radiation damage. Scans were run from 200 eV below the Fe K-edge at 7112 eV to about 800 eV above the edge, corresponding to a maximum photoelectron wavevector of 13 Å<sup>-1</sup>. After summation, data were transferred to CLRC Daresbury laboratory and analysed using the standard EXBACK98 and EXCURV98 packages.<sup>[6-8]</sup>

Data were fitted using the EXCURV98 program, with scattering parameters calculated within the program. EXBACK performs a background subtraction by fitting low order polynomials to the data at both above and below the edge. The result is the standard EXAFS function. EXCURV fits a calculated EXAFS function to the data by non-linear least squares refinement. The calculated spectrum was obtained using rapid curved wave theory and multiple scattering contributions were included. Electron scattering phase shifts are calculated within the program using Hedin-Lundqvist potential, which includes inelastic processes. The structure of the sample is described within the program in terms of shells of atoms, a set of atoms of the same type at the same distance from the Fe atom, which absorbed the X-ray photon. The structural parameters varied in the fitted procedure were the interatomic

distances, the mean square deviations in these and the coordination numbers. The user could only vary the type of atom. Since the scattering parameters of atoms with similar atomic numbers are very similar, EXAFS can only distinguish between atoms whose atomic numbers differs by about 5 or more. Thus C, N and O are difficult to distinguish with certainty. Multiple scattering contributions were included for the porphyrin ring structure. The program used gave uncertainties in the fitting parameters as the  $2\sigma$  (95% confidence) level and also includes a check on statistical significance of added shells. The criterion of Joyner *et al.*<sup>[9]</sup> were used to establish whether the addition of an extra shell significantly improved the fit of the data. Only shells that significantly improved the fit were included in the results.

Data fitting was primarily carried out over the data range  $k = 2 - 10 \text{ \AA}^{-1}$  with the spectrum weighted by  $k^3$ . Further fits over the full data range,  $2 - 13.5 \text{ \AA}^{-1}$ , with both  $k^2$  and  $k^3$  weighting, were also made: the three results generally agreed in the structural data, to within their often considerable uncertainties. Most weight was placed on the short data range fit, since this included the least noise.

Fitting was carried out in several stages. The main porphyrin ring structure was fitted alone (including multiple scattering) to obtain a baseline fit index. The nearest neighbour structure was also fitted alone, to assess whether the six nearest-neighbour atoms were at the same or different distances. The MAP facility was used in this case, as suggested by Fonda *et al.*<sup>[10]</sup> A 4 + 2 split of the ligand distances usually showed the four porphyrin atoms to be close to  $2.05 \text{ \AA}$  with the remaining two atoms occupying a broad minimum between  $1.7$  and  $2.4 \text{ \AA}$ . Generally, a 4 + 1 + 1 split was found to lower the fit index by a (marginally) significant amount. Finally, a full fit, including the porphyrin ring atoms and the two axial ligands, was used to give the final structural data. The uncertainties quoted were fitting uncertainties given by the program, and did not include systematic uncertainties due to, for example, poor background subtraction or poor scattering parameters.

### 7.2.9 Resonance Raman Spectroscopy

Resonance Raman spectra were recorded by Dr. Pierre Moëgne-Loccoz at the Oregon Graduate Institute on a McPherson 2061/207 spectrograph (0.67m focal length, 1800-groove grating) using a Kaiser Optical notch or supernotch filters were used to attenuate Rayleigh scattering and equipped with a Princeton Instruments liquid N<sub>2</sub>-cooled (LN-1100PB) CCD detector. Excitation sources consisted of an Innova 302 krypton laser (413 nm) and a Liconix

4240NB He/Cd laser (442 nm). Spectra were collected in a 90°-scattering geometry on samples at room temperature with a collection time of a few minutes. Longer acquisition and a backscattering geometry were used for experiments performed on frozen samples. Frequencies were calibrated relative to indene and CCl<sub>4</sub> standards and are accurate to  $\pm 1 \text{ cm}^{-1}$ , CCl<sub>4</sub> was also used to check the polarisation conditions. The integrity of the samples before and after laser illumination was confirmed by optical absorption spectra of the Raman samples obtained on a Perkin-Elmer Lambda 9 spectrophotometer. Samples were prepared at neutral pH (pH 7.0, 100 mM sodium phosphate buffer).

### 7.2.10 Magnetic Circular Dichroism (MCD) Spectroscopy

MCD experiments for rLb and variants were conducted by Dr. M. R. Cheeseman, in the laboratory supervised by Prof. A. J. Thomson (University of East Anglia). Samples were prepared in deuterium oxide<sup>[11]</sup> to prevent interference in the 1400-2000 nm region from absorptions caused by vibrational overtones. Glycerol (50 % v/v) was added to protein samples<sup>[11]</sup> to obtain optical quality glasses on freezing for low temperature MCD measurements. MCD spectra were recorded using circular dichrographs (JASCO models J-500D and J-730 for the UV-visible and near-infrared regions, respectively). An Oxford Instruments superconducting solenoid with a 25 mm ambient temperature bore was used to generate a magnetic field of 6 Tesla for the room temperature MCD measurements. Low temperature MCD measurements were made using an Oxford Instruments SM4 split-coil superconducting solenoid generating a magnetic field of 5 Tesla. Low Temperature MCD intensities ( $\Delta\epsilon$ ) are plotted in units of  $\text{M}^{-1}\text{cm}^{-1}$  at a quoted magnetic field of 5 Tesla. At room temperature, MCD intensities are linearly dependent on magnetic field and are plotted normalised to magnetic field as  $\Delta\epsilon/H$  ( $\text{M}^{-1}\text{cm}^{-1}\text{T}^{-1}$ ).

### 7.2.11 Electronic Paramagnetic Resonance (EPR) Spectroscopy

The EPR studies were conducted in collaboration with Dr. M. R. Cheesman, in the laboratory supervised by Prof. A. J. Thomson (University of East Anglia). EPR spectra were recorded at 10 K using an ER-200D electromagnet and microwave bridge interfaced to an EMX control system (Bruker Spectrospin) and fitted with a liquid helium flow cryostat (ESR-9, Oxford Instruments) and dual-mode X-band cavity (Brüker, type ER4116CM). Unless otherwise stated, samples used were those prepared for the MCD spectra.

## 7.2.12 Haem Oxygenase Activity of rLb and His61Ala

### 7.2.12.1 Coupled Oxidation Assay

#### *Aerobic Coupled Oxidation*

Aerobic coupled oxidation assays of rLb (5 $\mu$ M) and His61Ala (5 $\mu$ M) with ascorbate (1mM, Sigma) were carried out in sodium phosphate buffer ( $\mu = 0.10$  M, pH 7.0) at 32 °C for 16 h and monitored spectrophotometrically (270 – 800 nm).

#### *Anaerobic Coupled Oxidation*

Preparation of protein solution for the anaerobic assays was performed in an oxygen free box, in the laboratory of Professor N. Scrutton, under the supervision of Dr. J. Basran (Department of Biochemistry, University of Leicester). All buffers and proteins were degassed with nitrogen and placed into the oxygen free box at least 12 hours prior to use to ensure that oxygen free solutions. The concentrated protein (His61Ala, 2.5 mM) was passed through a G25 column equilibrated with anaerobic sodium phosphate buffer. The protein solution was made up to the desired concentration (5 $\mu$ M) and volume (1ml) using anaerobic sodium phosphate buffer and the protein concentration determined spectrophotometrically using Equation [7.1]. The ascorbate was weighed gravimetrically to give the desired concentration (1  $\mu$ M) in 1ml of buffer and then added to the protein solution. The cuvette containing the protein and ascorbate was stoppered with a superseal and further sealed with Nesco film to ensure no exposure to air during the coupled oxidation process. The coupled oxidation process was monitored as for the aerobic process.

#### *Stoichiometric Addition of O<sub>2</sub> to the Coupled Oxidation Reaction*

The stoichiometric addition of oxygen to determine the coupled oxidation reaction mechanism and identify any intermediates was carried out as follows. The protein, ascorbate and some sodium phosphate buffer were made anaerobic as described above. The protein was made up to the required concentration (5  $\mu$ M) by addition aerobic buffer to the anaerobic

protein solution so that the concentration of oxygen in the protein solution was one equivalent to the haem concentration in the protein. Addition of two equivalents of oxygen to the protein solution was carried out in the same manner, however, in this case, aerobic buffer was added to the anaerobic protein solution so that the concentration of oxygen in the protein solution was two equivalents to the haem concentration in the protein. The saturated oxygen concentration in the buffer was taken to be 258  $\mu\text{M}$  at 25  $^{\circ}\text{C}$ .<sup>[12]</sup>

### 7.2.12.2. Kinetics of the Coupled Oxidation Reaction

The rate constants for the formation of the coupled oxidation intermediates and products were determined using equation [7.10] when fitting absorbance data to a single exponential process and equation [7.11] when fitting absorbance data to a double exponential process using the Grafit program.

$$A_t = A_o \exp(-k_1 t) + B \quad [7.10]$$

$$A_t = A_o \exp(-k_1 t) + A_o \exp(-k_2 t) + B \quad [7.11]$$

Where  $A_t$  is the absorbance change signal with time,  $A_o$  is the amplitude of the absorbance change,  $k_1$  and  $k_2$  are the first and second observed rate constants,  $t$  is the time in minutes, and  $B$  is the equilibrium absorbance signal or offset.

### 7.2.12.3 Biliverdin Extraction

For the analysis of coupled oxidation reaction products, His61Ala (10 mg His61Ala in 10 ml of sodium phosphate buffer (pH 7.0)) was reacted (37  $^{\circ}\text{C}$ ) with ascorbate (2 mg) for 7 hours. Cooling the reaction mixture on ice for 15 minutes stopped the reaction and the biliverdin products were extracted as follows. Glacial acetic acid (3 ml, Fischer Scientific) and 5 M hydrochloric acid (8 ml, Fischer Scientific) were added to the cooled mixture and the solution placed into a 100 ml separating funnel. The solution was extracted with diethyl ether (2x15 ml, Fischer Scientific) and the ether layer, which contained unreacted haem discarded. The aqueous layer, containing the coupled oxidation product, turquoise in colour, was

extracted with chloroform (1x5 ml, Fischer Scientific) to remove the biliverdin product and the chloroform removed subsequently by evaporation under a stream of argon. A fraction of the product as well as the biliverdin standard (Porphyrin Products) was dissolved in a minimum volume of Dimethylsulphoxide (DMSO) (Fischer Scientific) for HPLC analysis.

#### 7.2.12.4 Verdohaem Extraction

Analysis of the anaerobic coupled oxidation products was carried out as follows. The reaction product (800  $\mu$ l) was extracted with pyridine (100  $\mu$ l) and chloroform (1 ml). The chloroform phase was transferred to a test tube and dried with anhydrous sodium sulphate (Sigma). The resultant solution (the verdohaem-pyridine product) as well as the verdohaem standard (Porphyrin Products), which was made up as the pyridine-verdohaem complex, in chloroform were analysed by electronic absorption spectroscopy.

The identity of verdohaem was also conclusively demonstrated by Electrospray Ionisation Mass Spectrometric (ESI-MS) analysis of the reaction product obtained from the reaction mixtures containing the aforementioned concentrations of protein and ascorbate. The reaction (10 ml) was stopped after 10 hours by cooling to 4 °C dialysed against  $\text{NH}_4\text{HCO}_3$  (40 mM) at 4 °C, and concentrated to ~ 0.6 ml. An aliquot of the protein solution (100  $\mu$ l) was mixed with 10 mM ammonium acetate (100  $\mu$ l) and analysed by ESI-MS.

#### 7.2.12.5 HPLC Analysis of Haem Degradation Products

Haem degradation products were analysed chromatographically using a computer-controlled HPLC apparatus (Varian) equipped with a Prostar 310 UV/Vis detector. Samples were loaded onto a C-18 reverse phase column (4.6 mm x 25 cm, 10  $\mu$ M). All solvents were HPLC grade. Analysis of the biliverdin product was carried out in Solvent A, which consisted of 56 parts 0.10 M ammonium phosphate buffer (Fischer) and 44 parts methanol (Fischer). Prior to mixture, the ammonium sulphate buffer was adjusted to pH 3.5 by addition of phosphoric acid (Sigma). Solvent B was 100 % methanol. Solvents were filtered and degassed prior to use. The DMSO solutions of reaction products and standards were diluted into solvent A such that 100  $\mu$ l could be injected onto the column. Elution profiles were monitored at 400 nm.

#### 7.2.12.6 Reduction of Ferric His61Ala with Ascorbate

The rate constant for reduction of ferric His61Ala with ascorbate was determined using a SX.18 MV microvolume stopped-flow spectrofluorimeter (Applied Photophysics), with an arc lamp source and pbp SpectraKinetic Monochromator (Applied Photophysics), controlled by an Archimedes 410-1 microcomputer running SpectraKinetic software (Applied Photophysics). A photomultiplier detector was used for the single wavelength studies. A circulating water bath (Neslab, model RTE-200) ensured that the injection chamber and syringes were maintained at the required temperature, 32.0 °C.

Non-linear regression analysis of single wavelength kinetics was conducted using Applied Photophysics software, fitting to the appropriate model. Further data manipulation was performed using the Grafit software package (Version 3.0, Erithacus Software Ltd.).

Reduction of His61Ala was monitored and measured at 403 nm, close to the Soret maxima of His61Ala and is the wavelength where the most changes in absorbance occur. The final concentration of the protein sample in the mixing cell was 5 µM. The concentration of His61Ala was confirmed spectrophotometrically and freshly prepared reducing substrate (ascorbate) was prepared volumetrically from a concentrated stock of known molarity.

#### 7.2.12.7 Analysis of Regiospecificity of Coupled Oxidation

Determination of the resiospecificity of the coupled oxidation reaction was determined as follows: the biliverdin product isolated from the His61Ala coupled oxidation reaction (Section 7.2.12.2) and authentic biliverdin (Porphyrin Products) were treated with 5% HCl-methanol for 16 hours at 4°C. The resulting biliverdin dimethyl esters were extracted into chloroform after addition of 4 volumes of water. The chloroform was removed with N<sub>2</sub> and samples dissolved in acetonitrile:water (3:2, v/v) solvent to a volume of 200 µl prior to HPLC analysis. Samples (100 µl) were loaded onto a C-18 reverse phase column and eluted in the acetonitrile: water solvent and the elution profile monitored at 650 nm.

#### 7.2.12.8 Mass Spectrometry

The coupled oxidation reaction products were exchanged with highly purified water (Elgastat), using a centricon-10 concentrator (Amicon), to remove ascorbate and phosphate

from the reaction products, since high ascorbate and salt concentrations interfere with mass spectral analysis. The coupled oxidation products (10  $\mu$ l) were diluted ten-fold with methanol (Fischer Scientific) prior to injection into the mass spectrometer. Samples were provided to Dr. G. Eaton (Department of Chemistry, University of Leicester) for mass spectral analysis, which was carried out using a Micromass Quattro LC electrospray mass spectrometer. Horse heart myoglobin (Sigma) was prepared,  $\sim$ 2 mg/ml (20  $\mu$ l), and diluted ten-fold with methanol and used to calibrate the spectrophotometer in the range 500 to 700 m/z. The samples were introduced into the instrument via syringe infusion at a flow rate of 10 $\mu$ l/min and the mass spectral analysis conducted with a current voltage of 100 mV.

#### 7.2.12.9 $^{18}\text{O}_2$ Labelling

Coupled oxidation of His61Ala, under  $^{18}\text{O}_2$ , was carried out following the method of King and Brown.<sup>[13]</sup> After degassing and admission of labelled oxygen to the protein solution (5 $\mu$ M, 10 ml, sodium phosphate buffer, pH 7.0), a solution of ascorbate (1 mM, sodium phosphate buffer, pH 7.0) was added. Incubation of the coupled oxidation reaction mixture was allowed to proceed at 37 °C for 7 hours. At the end of the reaction, the flask was cooled in ice and biliverdin was extracted as described in Section 7.2.12.2. The biliverdin extract was evaporated to dryness under a stream of nitrogen and dissolved in 20  $\mu$ l methanol prior to ESI-MS analysis.

### 7.3 References

1. E. Antonini and M. Brunori, in *Hemoglobin and Myoglobin in Their Reactions with Ligands*, (North Holland, Amsterdam) 1971, pp. 10.
2. D. K. Jones, R. Badii, F. I. Rosell and E. Lloyd, *Biochem. J.* (1998) 330, 983.
3. F. W. J. Teale, *Biochim. Biophys. Acta* (1959) 35, 543.
4. W. R. Heineman, B. J. Norris and J. F. Goelz, *Anal. Chem.* (1975) 47, 79.
5. L. S. Reid, V. T. Taniguchi, H. B. Gray and A. G. Mauk, *J. Am. Chem. Soc.* (1982) 104, 7516.
6. J. R. W. Mosselmums, <http://srs.dl.ac.uk/xrs/index.html>.
7. A. J. Dent, <http://srs.dl.ac.uk/xrs/index.html>.
8. N. Binsted, <http://srs.dl.ac.uk/xrs/index.html>.
9. R. W. Joyner, K. J. Martin and P. Meehan, *J. Phys.* (1987) C20, 4005.
10. E. Fonda, A. Michalowicz, L. Randaccio, G. Tauzher and G. Vlaic, *Eur. J. Inorg. Chem.* (2001) 1269.
11. A. J. Thomson, M. R. Cheesman and S. J. George, *Meth. Enzymol.* (1993) 226, 199.
12. Y. Lui and P. R. Ortiz de Montellano, *J. Biol. Chem.* (2000) 275, 5297.
13. R. F. G. J. King and S. B. Brown, *Biochem. J.* (1978) 174, 103.

# Appendix

## Appendix A

### 10 × REACTION BUFFER

100 mM KCl, 100 mM (NH<sub>4</sub>)<sub>2</sub>SO<sub>4</sub>, 200 mM Tris-HCl, 20 mM MgSO<sub>4</sub>, 1 % Triton<sup>®</sup> X-100 and 1 mg/ml nuclease-free bovine serum albumin

### LB MEDIA

Per litre: tryptone (10 g), yeast extract (5 g), NaCl (5 g) and 0.2 % (w/v) glucose

### LB-AMPICILLIN AGAR PLATES

Per litre: NaCl (10 g), tryptone (10 g), yeast extract (5 g), agar (20 g) and water to 1 litre. Sterilised and supplemented with 100 µg/ml ampicillin

### 10 × TBE BUFFER

0.9 M Tris(hydroxymethyl)aminomethane (Tris) base, 0.9 M boric acid, 25 mM diaminoethanetetra-acetic-acid (EDTA)

### 5 × SAMPLE LOADING BUFFER

Sucrose (4 g), 2 M Tris-HCl (0.5 ml, pH 8), 0.5 M EDTA and bromophenol blue (4 mg), diluted to 10 ml with water

### LYSIS BUFFER

50 mM Tris, 1 mM EDTA adjusted to pH 8.0 with 2 M HCl

### SAMPLE BUFFER

Dithiothreitol (0.77 g), 10 % SDS (10 ml), 1 M Tris-HCl (1.25 ml, pH 6.8), glycerol (5 ml) and 0.5 % bromophenol blue in ethanol, diluted to 50 ml with water

### RUNNING BUFFER

192 mM glycine (14.4 g), 25 mM Tris-HCl, (3 g) and 0.1 % w/v SDS (0.5 g) diluted to 500 ml with water

**STAINING BUFFER**

30% (v/v) methanol, 12% (w/v) trichloroacetic acid, 0.01% (w/v) Coomassie Brilliant Blue R250, 10% (w/v) sulphosalicylic acid)

**DESTAINING BUFFER**

7.5% acetic acid and 5% methanol

**DEUTERATED BUFFER**

50 mM  $D_3PO_4$  (118.8 ml of  $D_3PO_4$  to a total of 20 ml  $D_2O$ ) adjust to required pH using NaOD and DCl

**MIXED SULPHONIC ACID BUFFER**

5 mM MOPS, 5 mM MES, 5 mM TAPS and 95 mM NaCl

**SODIUM PHOSPHATE BUFFER**

Sodium phosphate buffer was made using measurements according to Table A. All quantities were made to a final volume of 1 l.  $Na_2H$  is disodium hydrogen orthophosphate anhydrous (Sigma) and  $NaH_2$  is sodium dihydrogen orthophosphate anhydrous (Sigma).

**SUCCINIC ACID BUFFER**

Succinic acid buffer (Sigma) was made using measurements according to Table B. All quantities were made to a final volume of 100 ml.

**Table A**

Quantities of  $\text{Na}_2\text{H}$  and  $\text{NaH}_2$  required to make sodium phosphate buffer ( $\mu = 0.1 \text{ M}$ ) at the required pH

pH	$\text{NaH}_2$ (g/l)	$\text{Na}_2\text{H}$ (g/l)
5.5	12.23	0.53367
5.6	11.88	0.6581
5.7	11.46	0.8016
5.8	10.97	0.9681
5.9	10.42	1.159
6.0	9.798	1.372
6.1	9.114	1.606
6.2	8.376	1.860
6.3	7.602	2.125
6.4	6.808	2.397
6.5	6.014	2.670
6.6	5.247	2.932
6.7	4.521	3.182
6.8	3.849	3.412
6.9	3.243	3.620
7.0	2.714	3.801
7.1	2.246	3.962
7.2	1.846	4.099
7.3	1.507	4.215
7.4	1.224	4.312
7.5	0.9912	4.392
7.6	0.7994	4.458
7.7	0.6420	4.512
7.8	0.5144	4.556
7.9	0.4118	4.591
8.0	0.3290	4.619
8.1	0.2626	4.642
8.2	0.2089	4.660
8.3	0.1656	4.675
8.4	0.1314	4.687
8.5	0.1044	4.696

**Table B**

Quantities of Succinic acid and KOH required to make succinic acid buffer ( $\mu = 0.1$  M) at the required pH

<b>pH</b>	<b>0.1 M Succinic acid buffer (ml)</b>	<b>0.05 M KOH (ml)</b>
3.6	45.95	19.21
3.7	36.91	19.27
3.8	31.84	19.27
3.9	27.12	19.24
4.0	23.29	19.21
4.1	19.72	19.11
4.2	17.50	19.00
4.3	15.37	18.84
4.4	13.73	18.67
4.5	12.24	18.42
4.6	11.06	18.15
4.7	10.12	17.90
	<b>0.02 M Succinic acid buffer (ml)</b>	<b>0.05 M KOH (ml)</b>
4.8	46.04	17.57
4.9	41.62	17.15
5.0	38.12	16.80
5.1	35.01	16.42
5.2	32.15	16.02
5.3	29.88	15.68
5.4	27.70	15.34
5.5	25.89	15.05